

Neue Fanconi-Anämie-Gene als Wächter des Genoms

Dissertation

zur Erlangung des naturwissenschaftlichen Doktorgrades
der Julius-Maximilians-Universität Würzburg

Vorgelegt von

Kerstin Knies

Geboren in Würzburg



Würzburg 2017

Institut für Humangenetik

Eingereicht am:

Bei der Fakultät für Biologie an der Julius-Maximilians-Universität Würzburg

Mitglieder der Promotionskommission:

Vorsitzender: Prof. Dr.

Erstgutachter: Prof. Dr. Detlev Schindler (Institut für Humangenetik)

Zweitgutachter: Prof. Dr. Thomas Dandekar (Institut für Bioinformatik)

Tag des Promotionskolloquiums:

Doktorurkunde ausgehändigt am:

MEINEN ELTERN

Erklärungen nach §4 Abs. 3 Satz 3, 5, 8 der Promotionsordnung der Fakultät für Biologie

Affidavit

I hereby declare that my thesis entitled: „Neue Fanconi-Anämie-Gene als Wächter des Genoms“ is the result of my own work.

I did not receive any help or support from commercial consultants. All sources and / or materials applied are listed and specified in the thesis. In addition, the rules of good scientific practice of the University of Wuerzburg have been observed.

Furthermore I verify that the thesis has not been submitted as part of another examination process neither in identical nor in similar form.

Eidesstattliche Erklärung

Hiermit erkläre ich an Eides statt, die Dissertation: „Neue Fanconi-Anämie-Gene als Wächter des Genoms“, eigenständig, d. h. insbesondere selbstständig und ohne Hilfe eines kommerziellen Promotionsberaters, angefertigt und keine anderen, als die von mir angegebenen Quellen und Hilfsmittel verwendet zu haben. Des Weiteren wurden die Regeln der Universität Würzburg über gute wissenschaftliche Praxis eingehalten.

Ich erkläre außerdem, dass die Dissertation weder in gleicher noch in ähnlicher Form bereits in einem anderen Prüfungsverfahren vorgelegen hat.

_____, den _____

Unterschrift

INHALTSVERZEICHNIS

ZUSAMMENFASSUNG	1
SUMMARY.....	3
1 EINLEITUNG	5
1.1 FANCONI ANÄMIE	5
1.1.1 ENTDECKUNG UND ERSTBESCHREIBUNG.....	5
1.1.2 DER KLINISCHE UND ZELLULÄRE PHÄNOTYP	5
1.2 DIAGNOSTIK, GENOTYPISIERUNG UND THERAPIE	7
1.2.1 KLASSISCHE, DIAGNOSTISCHE METHODEN	7
1.2.2 KOMPLEMENTATIONSGRUPPENBESTIMMUNG	9
1.2.3 THERAPIEANSÄTZE	11
1.3 GENETISCHER UND MOLEKULARER HINTERGRUND	13
1.3.1 DIE FA-GENE	13
1.3.2 DIE FA-PROTEINE IN DER DNA-REPARATUR	16
1.3.3 DER FA/BRCA-SIGNALWEG.....	21
1.3.4 WEITERE ZELLULÄRE FA-MERKMALE	23
1.4 FANCONI ANÄMIE MAUSMODELLE	25
1.5 ZIEL DER ARBEIT	30
2 MATERIAL UND METHODEN	31
2.1 GENOTYPING OF FANCONI ANEMIA PATIENTS BY WHOLE EXOME SEQUENCING: ADVANTAGES AND CHALLENGES	31
2.2 WHOLE EXOME SEQUENCING REVEALS NOVEL MUTATIONS IN THE RECENTLY IDENTIFIED FANCONI ANEMIA GENE <i>FANCP</i>	31
2.3 MUTATIONS IN <i>ERCC4</i> , ENCODING THE DNA-REPAIR ENDONUCLEASE XPF, CAUSE FANCONI ANEMIA.....	31
2.4 BIALLELIC MUTATIONS IN THE UBIQUITIN LIGASE <i>RFWD3</i> CAUSE FANCONI ANEMIA.....	32
2.5 THE E3 LIGASE <i>RFWD3</i> PROMOTES TIMELY REMOVAL OF BOTH RPA AND RAD51 FROM DNA DAMAGE SITES TO FACILITATE HOMOLOGOUS RECOMBINATION.....	32
3 ERGEBNISSE	33
3.1 WHOLE EXOME SEQUENCING ALS NEUE METHODE DER GENOTYPISIERUNG	33
3.1.1 GENOTYPING OF FANCONI ANEMIA PATIENTS BY WHOLE EXOME SEQUENCING: ADVANTAGES AND CHALLENGES	33

3.1.2	WHOLE EXOME SEQUENCING REVEALS UNCOMMON MUTATIONS IN THE RECENTLY IDENTIFIED FANCONI ANEMIA GENE <i>SLX4/FANCP</i>	47
3.2	NEUE FANCONI ANÄMIE GENE UND DEREN CHARAKTERISIERUNG IM RAHMEN DES FA/BRCA-SIGNALWEGS	53
3.2.1	MUTATIONS IN <i>ERCC4</i> , ENCODING THE DNA-REPAIR ENDONUCLEASE XPF, CAUSE FANCONI ANEMIA	53
3.2.2	BIALLELIC MUTATIONS IN THE UBIQUITIN LIGASE <i>RFWD3</i> CAUSE FANCONI ANEMIA	67
3.2.3	THE E3 LIGASE RFWD3 PROMOTES TIMELY REMOVAL OF BOTH RPA AND RAD51 FROM DNA DAMAGE SITES TO FACILITATE HOMOLOGOUS RECOMBINATION	115
4	<u>DISKUSSION</u>	176
4.1	WHOLE EXOME SEQUENCING ALS SCHLÜSSELTECHNOLOGIE IN DER FA-KOMPLEMENTATIONSGRUPPENBESTIMMUNG	176
4.2	DIE ENTDECKUNG NEUER FANCONI ANÄMIE GENE UND DEREN CHARAKTERISIERUNG IM RAHMEN DES FA/BRCA-SIGNALWEGS	182
4.2.1	DIE STRUKTUR-SPEZIFISCHE ENDONUKLEASE XPF	182
4.2.2	DIE E3-UBIQUITIN LIGASE RFWD3	185
5	<u>REFERENZEN</u>	189
6	<u>ANHANG</u>	203
I.	LISTE DER ABKÜRZUNGEN	203
II.	EIGENE VERÖFFENTLICHUNGEN	207
III.	EIGENE BEITRÄGE ZU DEN ENTHALTENEN VERÖFFENTLICHUNGEN	208
IV.	LEBENS LAUF	215
V.	DANKSAGUNG	218

ZUSAMMENFASSUNG

Fanconi Anämie (FA) gehört zu den seltenen Chromosomeninstabilitäts-Syndromen. Ursächlich für die Erkrankung sind biallelische Mutationen mit autosomal rezessiver Vererbung in einem der bisher bekannten 21 Genen (*FANCA*, *-B*, *-C*, *-D1*, *-D2*, *-E*, *-F*, *-G*, *-I*, *-J*, *-L*, *-M*, *-N*, *-O*, *-P*, *-Q*, *-R*, *-S*, *-T*, *-U* und *-V*). Eine Ausnahme stellen *FANCB* und *FANCS* dar, die X-chromosomal rezessiv bzw. mit einem dominant negativen Effekt vererbt werden. Die Genprodukte sind als Teil des FA/BRCA-DNA-Reparatur Netzwerks bei der Beseitigung von DNA-Interstrang-Quervernetzungen (ICL) involviert. ICLs führen zu einer Stagnation der Replikationsgabel und blockieren somit wichtige zelluläre Prozesse wie Replikation und Transkription, sodass eine Aufrechterhaltung der Genomstabilität nicht mehr gewährleistet ist.

FA ist gekennzeichnet durch angeborene Fehlbildungen, fortschreitendes Knochenmarkversagen und eine erhöhte Prädisposition gegenüber Krebserkrankungen. Die Diagnose basiert auf phänotypischen Auffälligkeiten und wird auf zellulärer Ebene durch die Hypersensitivität gegenüber DNA-quervernetzenden Substanzen wie Mitomycin C (MMC) bestätigt. Da nicht jeder Patient einer bisher bekannten Komplementationsgruppe zugeordnet werden kann und herkömmliche molekulare Diagnostikverfahren mit der steigenden Anzahl an FA-Genen mühsam, zeitaufwändig und teuer geworden sind, war es nötig, neue molekulare Verfahren wie *Whole Exome Sequencing* (WES) zu etablieren. Im Rahmen dieser Arbeit wurde das Potential dieser Methode im Bezug auf die FA-Genotypisierung erforscht. Bei der Suche nach einer optimalen Anwendung des WES, untersuchten wir verschiedene Anreicherungs- und Sequenzieretechniken. Dennoch führen Fehler in den Datenbanken sowie Pseudogene zu falschen Dateninterpretationen und -darstellungen und stellen somit eine Herausforderung dar. Trotzdem zeigen unserer Daten, dass WES eine wertvolle Methode in der Molekulardiagnostik von FA ist. Dies bestätigte sich durch die Zuordnung mehrerer, vorher unklassifizierter FA-Patienten zu den bekannten Komplementationsgruppen und der Ergänzung eines siebten Patienten zum Subtyp FA-P, im Rahmen von zwei *Next Generation Sequencing* (NGS) Publikationen.

Außerdem wurden mit Hilfe von WES zwei neue FA-Gene (*FANCQ* und *FANCW*) im Rahmen dieser Arbeit gefunden, wobei *XPF* (*FANCQ*) das erste Gen überhaupt war, welches anhand von NGS detektiert wurde. ERCC4/XPF ist eine strukturspezifische Endonuklease, die durch ein Gen kodiert wird, welches bereits vorher mit den Krankheiten Xeroderma Pigmentosum (XP) und dem segmentalen XFE progeroid Syndrom in Verbindung gebracht wurde. Unsere Daten zeigen, dass abhängig von der Mutation in

XPF, Patienten eine der drei unterschiedlichen Funktionsstörungen aufweisen. Dies hebt die multifunktionale Stellung der XPF Endonuklease im Rahmen der Genomstabilität und von humanen Erkrankungen hervor. Das zweite Gen, das während dieser Arbeit entdeckt wurde, ist die WD40-Domäne tragende E3 Ubiquitin Ligase *RFWD3*, die kürzlich mit DNA-Reparatur und insbesondere HR verknüpft wurde. Wir konnten zeigen, dass eine *RFWD3* Mutation in der WD40-Domäne bei einem FA-Patienten mit der genetischen Erkrankung Fanconi Anämie assoziiert ist. Die HR ist in *RFWD3* (*FANCD3*) mutierten Zellen gestört, was auf einer verminderten Relokalisation von mutiertem *RFWD3* an das Chromatin und einer defekten Interaktion mit RPA beruht. Des Weiteren weisen *Rfwd3*-defiziente Mäuse typische Merkmale anderer FA-Mausmodelle auf, wie verminderte Fertilität, ovarielle und testikuläre Atrophie sowie eine reduzierte Lebenserwartung.

Insgesamt zeigt diese Arbeit, dass neue molekulare Ansätze wie NGS ein wertvolles Hilfsmittel in der FA-Diagnostik sind um bisher unklassifizierte Patienten einer Komplementationsgruppe zuordnen zu können. Zudem konnten mit Hilfe dieser Technik zwei neue Gene identifiziert werden. Deren Charakterisierung trägt zu einer Vervollständigung und weiteren Aufklärung des FA/BRCA-DNA-Reparatur-Netzwerks bei.

SUMMARY

Fanconi anemia (FA) is a rare genomic instability syndrome. Biallelic mutations are disease causing in any one of at least 21 genes (*FANCA*, *-B*, *-C*, *-D1*, *-D2*, *-E*, *-F*, *-G*, *-I*, *-J*, *-L*, *-M*, *-N*, *-O*, *-P*, *-Q*, *-R*, *-S*, *-T*, *-U* and *-V*). All are inherited in an autosomal recessive way, except *FANCB* and *FANCS*, which are inherited in a X-chromosomal recessive and a dominant negative way, respectively. The gene products are involved in the FA/BRCA DNA damage response pathway to remove interstrand-crosslinks (ICL). ICLs cause stalled replication forks and hence block crucial cellular processes like replication and transcription resulting in decreased maintenance of genome stability.

FA is characterized by congenital malformations, progressive bone marrow failure (BMF), and susceptibility to malignancies. Patients are diagnosed based upon phenotypical manifestations and the diagnosis of FA is confirmed by the hypersensitivity of cells to DNA interstrand crosslinking agents such as Mitomycin C (MMC). Since not every patient can be assigned to a complementation group and customary molecular diagnostics has become increasingly cumbersome, time-consuming and expensive the more FA genes have been identified new molecular approaches like Whole Exome Sequencing (WES) has been established. The potential of this method for FA genotyping has been investigated in the context of this thesis. By exploring different enrichment and sequencing techniques, we were able to identify the pathogenic mutations in each case using WES. However, database errors and pseudogenes pose challenges to interpret data correctly. Nevertheless our results show that WES is a valuable tool for molecular diagnosis of FA, since we were able to assign several previously unclassified FA patients to known complementation groups in the framework of two Next Generation Sequencing (NGS) studies.

In addition WES revealed two new FA-genes, *XPF* and *RFWD3*. Extraordinarily, *XPF* (*FANCC*) is the first gene to be detected with NGS. *ERCC4/XPF* is a structure-specific nuclease - encoding a gene previously connected to xeroderma pigmentosum (XP) and segmental XFE progeroid syndrome. Depending on the type of *ERCC4* mutation individuals present with one of the three clinically distinct disorders highlighting the multifunctional nature of the XPF endonuclease in genome stability and human disease. The second gene identified within this thesis is the WD40-containing E3 ubiquitin ligase *RFWD3*, which has been recently linked to the repair of DNA damage by Homologous Recombination (HR). Here, we show that an *RFWD3* mutation within the WD40 domain of a patient with typical FA malformations is connected to the genetic disease Fanconi anemia (FA). Disordered HR is the result of depleted relocation of mutant *RFWD3* to

chromatin and defective physical interaction with RPA. In addition, *Rfwd3* knockout mice show ovarian and testicular atrophy, a reduced life span and pups with sub-Mendelian birth ratios indicating embryonal-lethality. These features resemble other FA mouse models.

In summary, this work showed that new molecular approaches like WES are valuable tools for FA diagnosis. Additionally, this method is a useful medium to assign FA-patients to so far unknown complementation groups. Two novel genes have been identified and contribute to further completion of the FA/BRCA DNA repair network in the context of genome stability.

1 EINLEITUNG

1.1 FANCONI ANÄMIE

1.1.1 ENTDECKUNG UND ERSTBESCHREIBUNG

Vor 90 Jahren diagnostizierte der Schweizer Kinderarzt Guido Fanconi erstmals die Fanconi Anämie (FA). Er entdeckte die Krankheit bei einer Familie, in der drei von fünf Kindern bereits angeborene Fehlbildungen wie Mikrozephalie, Pigmentierungsstörungen, Hypoplasie der Hoden, Schieleffekte und Einblutungen der Haut aufwiesen. Die drei betroffenen Brüder starben im frühen Kindesalter an einer perniziösen Anämie, die sich durch macrozytäre Erythrozyten, verstärkter Hämolyse und einem Vitamin B₁₂ Mangel auszeichnet. (Fanconi, 1927) Ein ähnlicher Fall wurde im Jahre 1929 von Uehlinger beschrieben. (Uehlinger, 1929) Dadurch erkannte Fanconi, dass bei dieser Krankheit nicht nur die Erythropoese, sondern die gesamte Hämatopoese betroffen ist. (Fanconi, 1927; Lobitz and Velleuer, 2006)

1.1.2 DER KLINISCHE UND ZELLULÄRE PHÄNOTYP

Guido Fanconi ging davon aus, dass es sich bei FA um eine erbliche Erkrankung handelt. Dies konnte vor allem die Gruppe um Traute Schröder-Kurth 1964 weiter belegen und zeigen, dass FA-Patienten an einer spontanen Chromosomeninstabilität leiden. (Schroeder et al., 1964) In den Chromosomen der Patienten können Brüche, Lücken oder Tri- bzw. Quadriradialstrukturen, mittels DNA-quervernetzenden Substanzen wie Mitomycin C (MMC) oder Diepoxybutan (DEB) induziert werden. Diese Veränderungen sind nach Giemsa-Färbung im Lichtmikroskop sichtbar. (Auerbach, 2009) Den Schweregrad der Erkrankung, vor allem in Bezug auf die Wahrscheinlichkeit einen Tumor zu entwickeln, konnte Fanconi noch nicht anhand der Unterschiede in der Chromosomenstabilität korrelieren. (Fanconi, 1927)

Der vielfältige klinische Phänotyp der FA überlappt häufig mit anderen Syndromen wie Seckel, Nijmegen Breakage (NBS), Dubowitz, Holt-Oram, *Thrombocytopenia-Absent Radius Syndrome* (TAR), Townes-Brocks oder Saethre-Chotzen (TWIST1 Mutation). Deshalb kann eine eindeutige Diagnose für FA meist erst mit dem Eintreten hämatologischer Störungen gestellt werden. (Auerbach, 2009) Zwei Drittel aller FA-Patienten haben angeborene Fehlbildungen in verschiedenen Körperbereichen. Die Haut kann bspw. Café-au-lait-Flecken oder Hypopigmentierung aufweisen (bei ca. 40 %

der Patienten). Generell wird eine intrauterine und postnatale Wachstumsstörung beobachtet, die auch im weiteren Lebensverlauf nicht vollständig aufgeholt werden kann (ca. 40 % der Patienten betroffen). Des Weiteren zeigen sich bei etwa 35 % der Patienten Skelettanomalien wie Radius- bzw. Daumen A- und Hypoplasie, Skoliose oder Spina Bifida. Bei ca. 22 % der Betroffenen treten Hörstörungen, bis hin zur Taubheit, sowie Störungen des Sehapparats wie bspw. Mikrophthalmie auf. Etwa die Hälfte der FA-Patientinnen ist infertil. Das trifft auch auf einen großen Teil der FA-Patienten auf Grund genitaler Fehlbildungen (Mikropenis, fehlende Hoden) zu. Ebenfalls sind bei ca. 20 % der FA-Patienten renale Fehlbildungen wie eine Hufeisenniere oder das Fehlen einer bzw. beider Nieren zu beobachten. Außerdem sind FA-Patienten von gastrointestinalen und kardio-pulmonalen Störungen betroffen sowie von Auswirkungen auf das Zentralnervensystem (ZNS), die sich häufig in einem Mikrozephalus zeigen (<10 % der Betroffenen). Jedoch sind bis heute nur wenige Fälle von geistiger Behinderung bzw. Beeinträchtigung bekannt. 70 % aller FA-Patienten leiden zudem unter endokrinen Störungen, die neben Diabetes auch einen Mangel an Wachstumshormonen und Schilddrüsenhormonen beinhalten kann. (Auerbach, 2009; Tischkowitz and Hodgson, 2003)

Wie sich aus dem Namen der Erkrankung ableiten lässt, ist das Leitbild von hämatologischen Störungen geprägt, die auch schon Guido Fanconi in seiner Erstbeschreibung in Teilen erkannte. Das Durchschnittsalter für das Auftreten dieser Veränderungen im Blutbild beträgt bei FA-Patienten <7 Jahre bzw. für eine Leukämie 11,3 Jahre und steigt mit fortschreitendem Lebensalter dramatisch an, sodass 90 % aller 40-jährigen FA-Patienten an Knochenmarkversagen leiden. (Alter, 2014; Rosenberg et al., 2003) Anfangs lassen sich vor allem eine Macrozytose und eine Thrombozytopenie beobachten, welche schnell in eine Panzytopenie übergehen können. Durch Duplikationen und Triplikationen des langen Arms von Chromosom 1, Monosomie des Chromosom 7 oder dem Verlust des langen Arms von Chromosom 7, entstehen häufig eine akute myeloische Leukämie (AML) bzw. ein myelodysplastisches Syndrom (MDS), die wiederum mit klonalen zytogenetischen Aberrationen im Knochenmark einhergehen. (Neitzel et al., 2007) Chromosomale Instabilitäten sind auch eine Ursache für die in einigen Komplementationsgruppen auftretenden Krebserkrankungen. Häufig manifestieren sie sich bereits im jungen Erwachsenenalter und umfassen neben dem hämatoepoetischen System auch Plattenepithelkarzinome, vor allem im Kopf- und Nackenbereich, sowie weitere solide Tumore bspw. der Leber, WILMS Tumore oder im Genitalbereich. (Alter, 2014; Kutler et al., 2003)

Generell findet man diese Erkrankung in allen ethnischen Gruppen weltweit mit einer heterozygoten Frequenz von 1:181 in der US-Bevölkerung, wobei höhere Frequenzen von <1:100 bei den Ashkenasim oder den Gitanos bekannt sind. (Rosenberg et al., 2011; Tischkowitz and Hodgson, 2003) Die Prävalenz liegt zum heutigen Stand bei ca. 4-7 Betroffenen auf 1 Million Geburten, womit FA zu den seltenen genetischen Erkrankungen gehört. (Callen et al., 2005; Rosenberg et al., 2011)

1.2 DIAGNOSTIK, GENOTYPISIERUNG UND THERAPIE

1.2.1 KLASSISCHE, DIAGNOSTISCHE METHODEN

Da der klinische Phänotyp eine hohe Variabilität aufzeigt und sich dadurch FA in manchen Fällen schwer bzw. kaum diagnostizieren lässt, macht man sich die Hypersensitivität gegenüber DNA-quervernetzende Substanzen wie MMC und DEB zunutze, die bei ähnlichen Chromosomeninstabilitäts-Syndromen wie NBS, Ataxia teleangiectasia (AT), Diamond-Blackfan Anämie (DBA) oder TAR-Syndrom nicht zu finden ist. (Auerbach, 2009; Tischkowitz and Hodgson, 2003) Im Gegensatz dazu weisen FA-Zellen keine Sensitivität gegenüber ionisierender Strahlung oder ultraviolette (UV)-Strahlung auf, was wiederum der Fall bei NBS oder AT ist. (Kalb et al., 2004) Dadurch können auch Fälle ohne phänotypischen und hämatologischen Auffälligkeiten früh erkannt und diagnostiziert werden. Bei der Chromosomenbruchanalyse werden aus Blut oder aus Amnionzellen (daher eignet sich die Methode auch als Pränataldiagnostik) isolierte Lymphozyten mit unterschiedlichen Konzentrationen von MMC oder DEB versetzt und nach einer Aufarbeitung und Färbung im Lichtmikroskop betrachtet. Hierbei weisen Fanconi Anämie Patienten eine deutlich erhöhte Bruchrate im Vergleich zu gesunden Menschen auf (siehe Abbildung 1 A). Im Durchschnitt haben FA-Patienten eine Bruchrate von 0,65 Brüchen pro Zelle, gesunde Menschen hingegen eine durchschnittliche Bruchrate von kleiner als 0,09 pro Zelle. (Oostra et al., 2012)

Die Chromosomenbruchanalyse war lange der Goldstandard der FA-Diagnostik, wurde jedoch durch Zellzyklusanalysen ergänzt bzw. ersetzt, da diese weniger zeitaufwändig sind und keine zytogenetischen Kenntnisse erfordern. (Kitao and Takata, 2011; Tischkowitz and Hodgson, 2003) Erstmals wurde 1982 von Dutrillaux *et al.* eine verlängerte G2-Phase bei Kurzzeitkulturen von FA-Blutlymphozyten beobachtet. (Dutrillaux et al., 1982) Kubbies *et al.* konnte im Jahr 1985 diesen Versuch bestätigen und als diagnostische Methode mittels Durchflusszytometrie etablieren. (Kubbies et al., 1985) Auch hier werden die aus Blut isolierten Lymphozyten mit DNA-quervernetzenden Substanzen wie MMC oder Cisplatin versetzt um Unterschiede in der Länge des

Zellzyklus zu beobachten. FA-positive Zellen zeigen hier eine verlängerte G2/M-Phase im Zellzyklus, weswegen hier auch von einem Zellzyklus-Arrest gesprochen wird (siehe Abbildung 1 B). (Seyschab et al., 1995)

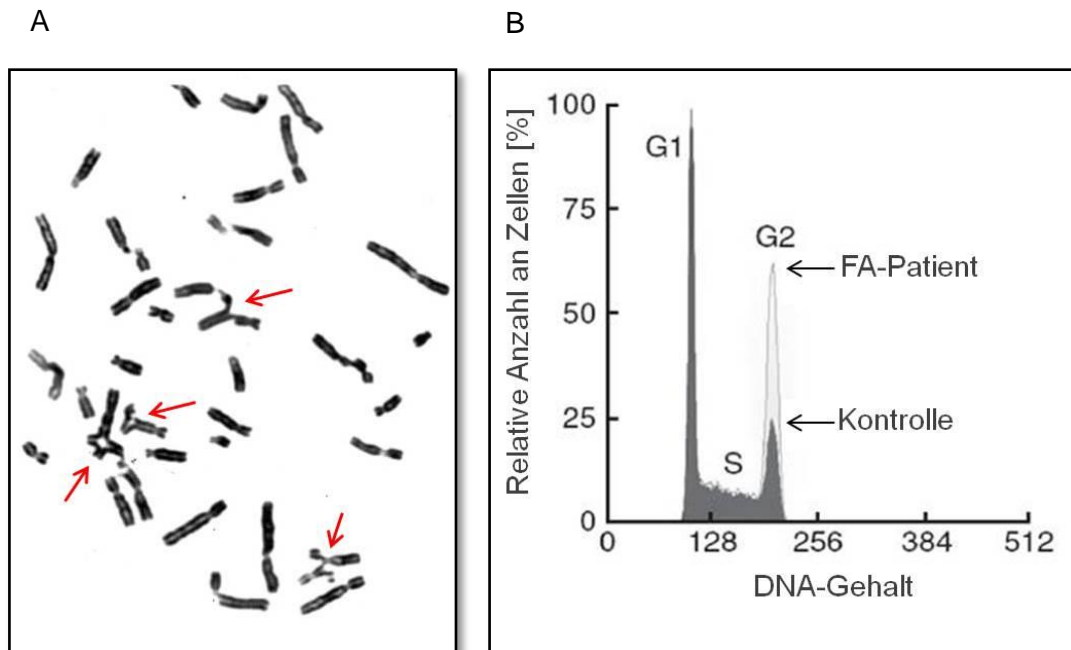


Abbildung 1: Exemplarische Darstellung der klassischen diagnostischen Methoden bei FA

A: Chromosomenbruchanalyse einer FA-Lymphozytenkultur nach DEB-Behandlung. Es sind für FA typische Tri- und Quadriradialfiguren sowie Brüche und Lücken erkennbar (rote Pfeile). Verändert nach Shimamura et al. (Shimamura, 2006) B: Zellzyklusanalyse von isolierten Blutlymphozyten eines FA-Patienten und einer Kontrolle. Der Patient zeigt einen typischen Anstieg an Zellen und den damit verbundenen G2-Phase Arrest nach MMC-Zugabe, wohingegen die Kontrolle keine erhöhte Anzahl an Zellen in der G2-Phase zeigt. In grau ist eine klassische Zellzyklusverteilung kultivierter Lymphozyten mit G1-, S- und G2-Phase dargestellt. Die erhöhte G2-Phase des FA-Patienten ist der erhöhte Peak mit weißem Hintergrund. Verändert nach Vaz et al. (Vaz et al., 2010) Für den Abdruck der Abbildung 1 B liegt die Erlaubnis der *Nature Publishing Group* vor.

Es gibt allerdings Limitierungen, vor allem wenn der Patient ein sog. „somatisches Mosaik“ aufweist (10-25 % der FA-Patienten sind hiervon betroffen). Hierbei ist ein Teil der Blutzellen rückmutiert bzw. hat eine kompensatorische „cis“ Mutation erlangt. Die revertierten Zellen weisen keine erkennbare Mutation mehr auf und zeigen auch keinen Zellzyklusarrest mehr. Des Weiteren ist bekannt, dass durch mitotische Rekombination beide Mutationen auf ein Allel gelangen können und somit das andere Allel wieder funktionsfähig ist. Die Zellen besitzen in diesem Fall einen Selektionsvorteil und reagieren weniger sensitiv auf DNA-quervernetzende Substanzen, da die DNA-Reparatur wieder funktionstüchtig ist. (Tischkowitz and Hodgson, 2003) Auch bei der Chromosomenbruchanalyse wird man hier eine andere Verteilung der Brüche beobachten können. In diesem Fall werden für eine eindeutige Diagnose Fibroblasten, gewonnen aus

einer Hautstanze, untersucht. Diese Zellen unterliegen nicht dem Selektionsdruck und so kann sich hier kein Mosaik entwickeln.

Beide Methoden lassen nur eine Klassifizierung in „FA-positiv“ oder „FA-negativ“ zu, geben jedoch keinen genauen Aufschluss über die vorliegende Mutation und das betroffene Gen bzw. erlauben keine Zuordnung in eine bestimmte Komplementationsgruppe. Hierfür sind molekulargenetische Analysen wie *Next Generation Sequencing* (NGS), Sanger Sequenzierung oder *Multiplex Ligation-dependent Probe Amplification* (MLPA)-Analyse unabdingbar, worauf im nächsten Abschnitt näher eingegangen wird.

1.2.2 KOMPLEMENTATIONSGRUPPENBESTIMMUNG

Obwohl zu diesem Zeitpunkt noch keine FA-Komplementationsgruppe bekannt war, wurde erstmals im Jahre 1980 eine sog. somatische Zellhybridisierung durchgeführt. Dazu wurden FA-Zellen mit einer nichtverwandten Patientenzelllinie fusioniert und im Anschluss auf die FA-typische Hypersensitivität gegenüber DNA-quervernetzenden Substanzen getestet. Bleibt diese Hypersensitivität nach der Fusionierung bestehen, gehören beide Zelllinien derselben Komplementationsgruppe an. Bei unterschiedlichen Komplementationsgruppen muss erneut eine Zellfusion durchgeführt werden, bis der zu Grunde liegende Defekt korrigiert ist. (Zakrzewski and Sperling, 1980) Später wurde dieses Verfahren durch die retrovirale Transduktion abgelöst. Darunter versteht man die Behandlung von Patientenzellen mittels retroviralen Vektoren, die das gewünschte Gen in der Wildtyp(wt)-Variante enthält. Die Zellen exprimieren das in den Vektoren enthaltene FA-Gen. Ein anschließender Test auf die FA-typische Hypersensitivität gegenüber DNA-Doppelstrangquervernetzenden Substanzen, wie bspw. MMC, zeigt ob diese aufgehoben ist oder nicht. Bei einer nicht mehr vorhandenen Hypersensitivität kann man den Patienten der Komplementationsgruppe zuordnen, die in dem lentiviralen Konstrukt enthalten war. (Hanenberg et al., 2002)

Seit 2012 hat sich die Methode der Hochdurchsatzsequenzierung in der FA-Komplementationsgruppenbestimmung immer weiter durchgesetzt. Sie erlaubt neben der Sequenzierung des gesamten Genoms (*Whole Genome Sequencing*, WGS) auch die Analyse des Exoms oder bestimmter Gene, die in einem sog. Panel zusammengefasst sind. 2005 wurde die erste Plattform von 454 Life Sciences eingeführt. (Margulies et al., 2005) Mit den Jahren kamen verschiedene andere Systeme wie SOLiD (*Sequencing by Oligonucleotide ligation and detection*) von Applied Biosystems und die Plattform von Illumina, die wie der Roche 454 auf der *Sequencing by synthesis*-Methode basiert, dazu. Bei dieser Methode erfolgt die Sequenzierung zyklusweise. In jedem Sequenzierzyklus

wird genau ein Nukleotid komplementär zu der Template-DNA eingebaut und die Bestimmung der Basenabfolge findet zeitgleich mit der Strangsynthese statt. Ein Vorteil der *Sequencing by synthesis*-Methode ist die Möglichkeit, eine sogenannte paired-end-Sequenzierung durchzuführen, die eine präzisere Analyse erlaubt. Mit einer vorher festgelegten Readlänge von 100-250 Basenpaaren (bp), werden die zu sequenzierenden DNA-Fragmente von jeder Seite sequenziert. (Fullwood et al., 2009; Mardis, 2008) Außerdem wurde der Zeit- und Kostenaufwand mit den Jahren immer geringer, um bspw. ein vollständiges Genom zu sequenzieren. Somit ist es für fast jeden Wissenschaftler eine lohnenswerte Investition, Sequenzier-Daten mittels dieser Methode bspw. über kommerzielle Anbieter generieren zu lassen. Daneben sind in den letzten Jahren auch Benchtop-Geräte entwickelt worden, die einen Einsatz von NGS in der Routinediagnostik ermöglichen. Hierbei ist jedoch zu beachten, dass eine nicht unerhebliche Datenmenge verarbeitet und ausgewertet werden muss. Des Weiteren konnten mit Hilfe dieser Methode zahlreiche neue Varianten in schon bekannten Genen detektiert oder neue krankheitsassoziierte Gene identifiziert werden, wie es im Rahmen dieser Arbeit bei *XPF* und *RFWD3* der Fall war. (Bogliolo et al., 2013; Majewski et al., 2011) Auch bei der Aufklärung von seltenen, monogenen Erkrankungen wie bspw. dem Miller-Syndrom spielt NGS, im Besonderen *Whole Exome Sequencing* (WES), eine wesentliche Rolle. (Bamshad et al., 2011; Ng et al., 2010) Daneben erleichtert es die Aufklärung der zugrunde liegenden Mutation bei Erkrankungen mit einer Vielzahl von Kandidatengenen wie z. B. bei mentaler Retardierung oder heterogenen Erkrankungen wie Retinitis Pigmentosum. (Bowne et al., 2011; Brett et al., 2014; Zuchner et al., 2011) Auch im Bereich der Krebsforschung ist NGS ein wertvolles Tool, um etwaige Mutationen aufzuklären, die für Familienangehörige ebenfalls ein erhöhtes Krebsrisiko darstellen oder um eine mögliche Chemoresistenz im Vorfeld zu untersuchen. Hierfür gibt es mittlerweile auch sog. Krebspanels, die auf bestimmte Krebsarten abgestimmt sind. (Majewski et al., 2011)

Dennoch ist NGS oder WES als Methode zur Komplementationsgruppenbestimmung *per se* oft nicht ausreichend. Großen Deletionen oder Duplikationen, wie sie bspw. häufig in *FANCA* zu finden sind, können mit Hilfe von WES nicht detektiert werden. Hierbei ist es hilfreich, eine MLPA durchzuführen, die jedoch bisher kommerziell nur für die Gene *FANCA* und *FANCC* zu erhalten ist. (Gille et al., 2012) Eine Validierung der kausalen Mutation sollte zudem immer mittels Sanger Sequenzierung erfolgen, da auch NGS kein fehlerfreies System darstellt und es zu falsch positiven Ergebnissen, wie z. B. bei Pseudogenen, kommen kann. (Ameziane et al., 2012; Knies et al., 2012) Außerdem dient die Sanger Sequenzierung zur Bestätigung oder dem Ausschluss einer bereits bekannten

Mutation bei einem Angehörigen eines FA-Patienten und in der Pränataldiagnostik. Hierfür ist es nötig, die Mutation des Index-Patienten bereits vorher zu kennen.

Oft ist es hilfreich eine vorausgehende Einordnung des mutierten Gens in „*downstream*“ oder „*upstream*“ bezüglich des FA/BRCA-Signalwegs durchzuführen. Hierbei nützt die Erstellung eines FANCD2-Immunblots. Da, wie in 1.3.3 beschrieben, der FA-Kernkomplex notwendig ist, um die Proteine FANCD2 und FANCI zu monoubiquitinieren, fehlt diese Monoubiquitinierung bei einer Variante in einem der Gene des Kernkomplex oder *FANCI*. Nach der Erstellung eines Westernblots mit Proteinlysaten, die aus MMC-behandelten Zellen generiert werden, fehlt die zweite Bande nach der Detektion mit einem FANCD2-Antikörper. Die nicht-ubiquitinierte Form von FANCD2 hat eine Größe von 155 kDa - wohingegen die monoubiquitinierte Form um 7 kDa größer ist. (Garcia-Higuera et al., 2001) Liegt ein Defekt im FANCD2 Protein vor, so ist kein bzw. nur ein sehr schwaches FANCD2 Protein im Westernblot nachweisbar. Bei einer Mutation in den *downstream* vom ID-Komplex gelegenen Genen, zeigen sich im Westernblot sowohl die nicht-ubiquitinierte als auch die monoubiquitinierte zweite Bande von FANCD2. Hierbei ist keine Unterscheidung zwischen einem gesunden Menschen und einem sog. „*downstream*“ Patienten möglich. (Shimamura et al., 2002) Vor allem bei möglichen „*downstream*“ Patienten lohnt es sich, im Anschluss RAD51-Foci zu untersuchen, da RAD51 als einer der Hauptfaktoren in der Koordination der homologen Rekombinationsreparatur (HRR) und seit 2015 auch als FA-Protein bekannt ist. (Ameziane et al., 2015; Wang et al., 2015). Hierbei werden die von RAD51 bei der HR gebildeten Nukleofilamente durch indirektes Anfärben mit einem Fluoreszenzantikörper sichtbar gemacht. Subtypen wie FANCD1, FANCN oder natürlich FANCR zeigen eine stark verminderte Anzahl (<10 % Foci-positive Zellen) an RAD51 Foci-positiven Zellen. (Ameziane et al., 2015; Godthelp et al., 2006; Reid et al., 2007; Wang et al., 2015) Als Foci-positiv bezeichnet man Zellen mit mehr als 10 sichtbaren Foci pro Zelle. Damit lässt sich anhand dieser Analyse ein Ausschluss bzw. eine Beteiligung an der HRR feststellen.

Gerade bei Erkrankungen wie FA, die keine Genotyp-Phänotyp Korrelation aufweisen, haben die letzten Jahre gezeigt, dass NGS im Zusammenspiel mit den beschriebenen Methoden die Suche nach einer ursächlichen Mutation bei bisher nicht zugeordneten Patienten erleichtert.

1.2.3 THERAPIEANSÄTZE

Da FA variabel im Phänotyp als auch im Genotyp ist, muss für jeden Patienten eine individuelle Therapiemaßnahme ergriffen werden. Trotzdem gibt es bis heute keine vollständige Heilung und die Therapie ist somit lediglich symptomatisch.

Des Weiteren muss zwischen der hämatologischen Seite der Erkrankung und der Krebserkrankung im Zusammenhang mit FA differenziert werden.

Bei beginnenden Auffälligkeiten im Blutbild kann eine Androgentherapie oder Bluttransfusion anfangs ein Fortschreiten der Erkrankung verlangsamen. Androgene, wie Oxymetholon, werden häufig verabreicht, da sie die Produktion von Erythropoetin und somit die Bildung roter Blutkörperchen steigern. Bei einem Therapieansprechen wird die Dosis über einen Zeitraum von drei Monaten langsam erhöht, um Nebenwirkungen wie eine Verschlechterung der Leberwerte bis hin zu Leberkrebs, Vermännlichung oder Akne zu vermeiden. (Tischkowitz and Hodgson, 2003)

Bei Knochenmarkversagen ist die Stammzelltransplantation von einem geeigneten Spender die einzige Therapiemöglichkeit. Idealerweise stimmen 10 von 10 HLA (*human leukocyte antigen*)-Marker überein. Dies wurde bereits 1989 von Eliane Gluckman mittels einer Stammzelltransplantation aus Nabelschnurblut bei einem FA-Patienten erfolgreich durchgeführt. (Gluckman et al., 1989) Hierbei ist jedoch zu beachten, dass durch die Hypersensitivität von FA-Zellen gegenüber Chemotherapeutika bzw. ionisierender Strahlung, eine Vorbereitung nach klassischen Regimen kontraindiziert ist. Fludarabin hat sich hier als ein geeignetes Mittel erwiesen, um ein mögliches Abstoßen der neuen Stammzellen zu vermeiden bzw. zu vermindern. (Alter BP, 1993-2015; Houghtaling et al., 2003) Dennoch kann nicht jeder FA-Patient mittels einer Stammzelltransplantation therapiert werden. Oft gibt es keinen geeigneten (Fremd)Spender und die Generierung eines gesunden Geschwisterkinds, mittels Präimplantationsdiagnostik und *in vitro* Fertilisation ist ethisch umstritten und die Erfolgsquote auf Grund des mendelschen Vererbungswegs niedrig (<5 %). (Trujillo and Surrallés, 2015) Deshalb richtete sich der Fokus in den letzten Jahren immer wieder auf die Gentherapie. Die anfänglichen Probleme bestanden vor allem in einer Ineffizienz bei der Transduktion mittels retroviralen Vektoren und der Schwierigkeit ausreichend Vorläuferzellen aus dem FA-Patienten zu gewinnen. Kürzlich konnte jedoch ein Fortschritt mit Hilfe von lentiviralen Vektoren erzielt werden. Außerdem ist es möglich, eine Gentherapie über Autotransplantation von korrigierten FA Hautfibroblasten durchzuführen. Hierbei werden aus Hautfibroblasten gesunde Vorläuferzellen hergestellt, die im Anschluss reprogrammiert werden und sich dann als sog. induzierte pluripotente Stammzelle (IPS) weiter differenzieren und dann einen Pool aus korrigierten hämatopoetischen Zellen liefert. Die Korrektur des fehlerhaften Gens, kann auch hier durch verschiedene Methoden stattfinden: Neben der bereits erwähnten ungerichteten Gentherapie mittels lentiviralen Vektoren, kann diese zielgerichtet mit Hilfe von genetischer Rekombination und eines adenoviralen Helfervektors oder dem CRISPR/Cas9 Endonuklease System erfolgen. (Bogliolo and

Surrallés, 2015) Dennoch sind hier noch weitere klinische Studien nötig, um diese Methoden in der Routine zu etablieren.

Entwickelt ein FA-Patient einen soliden Tumor, so ist auf Grund der bereits erwähnten Sensitivität der Zellen gegenüber Chemotherapeutika und ionisierenden Strahlen, die Operation das Mittel der Wahl. (Tischkowitz and Hodgson, 2003)

1.3 GENETISCHER UND MOLEKULARER HINTERGRUND

1.3.1 DIE FA-GENE

Entgegen Fanconis Annahme hat sich gezeigt, dass es sich bei FA um eine autosomal rezessive Erkrankung handelt. Ausnahmen stellen die Komplementationsgruppen FA-B, deren Genlocus sich auf dem X-Chromosom befindet und FA-R, dem ein dominant negativer Effekt zu Grunde liegt, dar. (Ameziane et al., 2015; Meetei et al., 2004; Wang et al., 2015)

Bis heute sind 21 FA-Gene bekannt (siehe Tabelle 1), die alle im FA/BRCA-Signalweg verwurzelt sind. Hierzu zählen *FANCA*, *-B*, *-C*, *-D1 (BRCA2)*, *-D2*, *-E*, *-F*, *-G*, *-I*, *-J (BRIP1)*, *-L*, *-M*, *-N (PALB2)*, *-O (RAD51C)*, *-P (SLX4)*, *-Q (XPF/ERCC4)*, *-R (RAD51)*, *-S (BRCA1)*, *-T (UBE2T)*, *-U (XRCC2)* und *-V (REV7)*. Im Rahmen dieser Arbeit konnte neben *XPF*, auch ein bisher nicht mit dem FA/BRCA-Signalweg assoziiertes Gen, *RFWD3*, als FA-Gen identifiziert und charakterisiert werden, welches wir mit dem Alias *FANCW* betiteln werden (siehe 3.2.2.). Trotz des variablen Phänotyps sind für die Krankheit nur eine homozygote bzw. zwei heterozygote Veränderungen in einem dieser Gene ausreichend. (Lobitz and Velleuer, 2006)

Sieben der 21 Gene sind auch als Prädispositionsgene für familiären Brust- und/oder Eierstockkrebs bekannt. Hierzu zählen *FANCD1*, *FANCM*, *FANCN*, *FANCI*, *FANCO*, *FANCS* und *FANCU*. Der Unterschied zu Fanconi Anämie ist, dass bereits eine Mutation in monoallelischer Form ausreicht, um ein erhöhtes Risiko für die o.g. Krebsarten zu tragen. Mit der Ausnahme von *FANCM*, sind die mit familiären Brust- und Eierstockkrebs assoziierten Gene alle an die homologe Rekombination (HR) gekoppelt (siehe 1.3.2.4 B). (Bogliolo and Surrallés, 2015; Mamrak et al., 2016)

Die Entdeckung des ersten FA-Gens, *FANCC*, liegt heute 24 Jahre zurück. (Strathdee et al., 1992a) Besonders eine Mutation in diesem Gen ist hier von Bedeutung, da sie vermehrt in Ashkenasim zu finden ist (c.345+4 A>T) und als sog. Founder Mutation gilt. 1996 wurde *FANCA* entdeckt, welches eines der größten FA-Gene ist und dem die meisten FA-Patienten zugeordnet werden können. (Apostolou S et al., 1996) Das Mutationsspektrum in *FANCA* ist äußerst heterogen. Neben Punktmutationen sind kleine

Duplikationen und Deletionen größerer Bereiche bekannt. (Tischkowitz and Hodgson, 2003) *FANCM* nimmt eine Sonderstellung in der Reihe der FA-Gene ein. Der zuvor der Komplementationsgruppe FA-M zugewiesene Patient wies auch biallelische Mutationen in *FANCA* auf. Nach einer Komplementation mit wildtypischen *FANCA* konnte zudem die zuvor fehlende Expression der monoubiquitinierten FANCD2-Bande mittels Westernblot detektiert werden, was nach einer Komplementation mit wildtypischen *FANCM* nicht der Fall war. Im Gegensatz dazu, blieb die Hypersensitivität gegenüber DNA-quervernetzenden Substanzen auch nach der Komplementation mit wt-*FANCM* bestehen. (Meetei et al., 2005; Singh et al., 2009) Somit ist der Patient der Komplementationsgruppe FA-A zuzuordnen. In einer weiteren Untersuchung, konnten finnische Forscher *FANCM* ebenfalls als FA-Gen ausschließen, nachdem sie mittels Exome Sequenzierung eine finnische Kohorte auf *loss-of-function* (lof) Founder Mutationen gescreent hatten. Dabei wiesen 7 Individuen sog. lof-Mutationen auf, ohne FA-typische Merkmale zu haben. (Lim et al., 2014) Die in den darauffolgenden Jahren entdeckten Gene haben mit ihrer Charakterisierung wesentlich zum Verständnis des FA/BRCA-Signalwegs und der damit verbundenen Entstehung von Fanconi Anämie beigetragen. Seit 2013 konnten mit Hilfe neuer Techniken - wie bspw. NGS - sechs neue Gene gefunden werden. (Bluteau et al., 2016; Bogliolo and Surrallés, 2015; Park et al., 2016; Shamseldin et al., 2012) So wurden auch im Rahmen dieser Arbeit mit dieser Methode zwei neue Gene identifiziert und charakterisiert (*XPF* und *RFWD3*). Bei den neu zugeordneten Genen gibt es meist nur einen bis wenige Patienten, die diesen Komplementationsgruppen angehören. Allerdings tragen v.a. die Entdeckungen dieser Gene wesentlich zur Aufklärung des molekularen Mechanismus von FA bei. In den kommenden Jahren ist damit zu rechnen, dass weitere Gene dem FA/BRCA-Signalweg als Fanconi-Gene zugeschrieben werden können, da es immer noch viele Patienten gibt, die bisher keiner Komplementationsgruppe zugeordnet werden können.

Eine Übersicht der 21 bekannten FA-Komplementationsgruppen, die dazugehörenden Gen-Aliase, deren chromosomale Lokalisation, sowie die Verteilung innerhalb der FA-Patienten und die Methode, mit welcher das Gen entdeckt wurde, sind in Tabelle 1 zusammengefasst.

Tabelle 1: Übersicht über alle bis dato bekannten FA-Gene

Neben der Komplementationsgruppe sind das dazugehörige Gen-Alias, die chromosomale Lokalisation und die Häufigkeit unter den FA-Patienten angegeben. Des Weiteren sind die Autoren der Erstbeschreibung genannt und die Methode, mit welcher das Gen im Zusammenhang mit FA entdeckt wurde. Die Häufigkeit ist aus der *Fanconi Anemia Mutation Database* (<http://www.rockefeller.edu/fanconi/>) entnommen.

Co-IP: Co-Immunopräzipitation; WES: Whole Exome Sequencing; WGS: Whole Genome Sequencing

Komplementationsgruppe	Gen-Alias	Lokalisation	Häufigkeit	Entdeckt von	Entdeckungsmethode
FA-A		16q24.3	63 %	(Apostolou S et al., 1996)	Expressions-/ Positionsklonierung
FA-B	<i>FAAP95</i>	Xp22.3	2 %	(Meetei et al., 2004)	Massenspektrometrie/ Co-IP
FA-C		9q22.3	12 %	(Strathdee et al., 1992b)	Expressionsklonierung
FA-D1	<i>BRCA2</i>	13q12.3	2 %	(Howlett et al., 2002)	Kandidatengenscreening
FA-D2		3p25.3	3 %	(Timmers et al., 2001)	Positionsklonierung
FA-E		6p22-p21	2 %	(Winter et al., 2000a)	Expressionsklonierung
FA-F		11p14.3	2 %	(Winter et al., 2000b)	Expressionsklonierung
FA-G	<i>XRCC9</i>	9p13.3	9 %	(de Winter et al., 1998)	Expressionsklonierung
FA-I	<i>KIAA1794</i>	15q25-q26	1 %	(Dorsman et al., 2007; Sims et al., 2007; Smogorzewska et al., 2007)	Kopplungsanalyse/ ATM und ATR Substratscreening/ bioinformatische Homologiesuche
FA-J	<i>BRIP1/ BACH1</i>	17q23.2	2 %	(Levitus et al., 2005; Levrant et al., 2005)	Genetisches Mapping/ Positionsklonierung
FA-L	<i>FAAP43</i>	2p16.1	0,5 %	(Meetei et al., 2003a)	Massenspektrometrie/ Co-IP
FA-M	<i>FAAP250</i>	14q21.3	0,1 %	(Meetei et al., 2005)	Massenspektrometrie/ Co-IP
FA-N	<i>PALB2</i>	16p12.2	0,6 %	(Reid et al., 2007; Xia et al., 2007)	Co-IP
FA-O	<i>RAD51C</i>	17q22	0,1 %	(Vaz et al., 2010)	Homozygosity Mapping
FA-P	<i>SLX4/ BTBD12</i>	16p13.3	0,5 %	(Kim et al., 2011; Stoepker et al., 2011)	Sanger Sequenzierung
FA-Q	<i>XPF/ ERCC4</i>	16p13.12	0,1 %	(Bogliolo et al., 2013)	WES /Sanger Sequenzierung
FA-R	<i>RAD51</i>	15q15.1	0,1 %	(Ameziane et al., 2015; Wang et al., 2015)	WGS/WES/Sanger Sequenzierung

Komplementationsgruppe	Gen-Alias	Lokalisation	Häufigkeit	Entdeckt von	Entdeckungsmethode
FA-S	<i>BRCA1</i>	17q21.31	0,1 %	(Sawyer et al., 2015)	WES
FA-T	<i>UBE2T</i>	1q32.1	0,1 %	(Hira et al., 2015; Rickman et al., 2015; Virts et al., 2015)	WES, Sanger Sequenzierung, RNA Sequenzierung, retrovirale Komplementation
FA-U	<i>XRCC2</i>	7q36.1	0,1 %	(Park et al., 2016)	WES
FA-V	<i>REV7/MAD2L2</i>	1p36.22	0,1 %	(Bluteau et al., 2016)	WES

1.3.2 DIE FA-PROTEINE IN DER DNA-REPARATUR

Auf Grund von exogenen (bspw. UV-Strahlen, radioaktive Strahlung oder chemischen Substanzen) oder endogenen Faktoren (bspw. fehlerhafte Replikation oder reaktive Sauerstoffspezies) entstehen in unserem Genom täglich eine Vielzahl an neuen Mutationen. Um diese Mutationen schnellstmöglich erfolgreich zu beseitigen, existieren in unserem Organismus verschiedene, spezifische DNA-Reparatursysteme. Sie erkennen bestimmte Mutationen und können diese beheben. Betrifft jedoch eine Mutation eines dieser Reparatursysteme, resultiert dies meist in einer schwerwiegenden Erkrankung. Im Folgenden soll auf verschiedene Reparaturmechanismen und die Beteiligung der FA-Proteine an diesen Mechanismen eingegangen werden.

1.3.2.1 NUCLEOTID-EXCISIONS-REPARATUR

Die Nukleotid-Excisions-Reparatur (NER) dient vor allem der Entfernung von DNA-Schäden, die auf Pyridindimeren oder 6,4 Photoprodukten basieren und auf Grund von UV-Strahlen entstanden sind. Vor allem bei Patienten mit Xeroderma Pigmentosum (XP) der Komplementationsgruppe F, ist eine genetisch bedingte, fehlerhafte NER bekannt. (Cleaver et al., 2009) Hier liegt eine Mutation im Gen *XPF/ERCC4* vor, welches zusammen mit *ERCC1* einen wichtigen Bestandteil der NER ausmacht. (Gregg et al., 2011) Die Patienten weisen vor allem eine erhöhte Sensitivität gegenüber UV-Strahlung und Pigmentierungsstörungen der Haut auf. Im Gegensatz dazu, haben FA-Patienten mit einem Defekt in *XPF* keine erhöhte Sensitivität gegenüber UV-Strahlung, jedoch gegenüber DNA-quervernetzenden Substanzen. Es wird vermutet, dass *XPF* an zwei unterschiedlichen Reparaturwegen beteiligt ist. (Bogliolo and Surrallés, 2015) Generell detektiert das Heterotrimer *XPC/hHR23B/centrin2* den DNA-Schaden und die DNA wird durch das Heterodimer *XPB* und *XPB* entwunden. *XPA* und *RPA* halten die entwundene

DNA in einem stabilen Zustand und rekrutieren weitere Enzyme wie den Endonuklease-Komplex ERCC1-ERCC4 und XPG. ERCC1-ERCC4 ist verantwortlich für das Ausschneiden des DNA-Schadens am 5'-Ende, wohingegen XPG den Einschnitt an der 3'-Stelle neben dem Schaden durchführt. Im Anschluss werden die fehlenden Basen mittels RFC, PCNA, Pol δ neu synthetisiert und die Lücke mit Hilfe der DNA-Ligase geschlossen. (Stauffer and Chazin, 2004)

1.3.2.2 BASENFEHLPAARUNGS-REPARATUR

Bei der Basenfehlpaarungs-Reparatur sind Fanconi Proteine nur indirekt beteiligt. MSH1 und MLH1 als Bindungspartner von FANCD2, regulieren im Wesentlichen diesen Reparaturweg. Außerdem ist bekannt, dass FANCD2 mit dem Komplex MutL α interagiert. In diesem hoch konservierten Reparaturweg werden Basenfehlpaarungen, wie Guanin mit Thymin, oder kleine Insertionen und Deletionen beseitigt. Im Menschen kennt man zwei Komplexe, die an der Erkennung und Bindung der Fehlpaarung beteiligt sind: MutS α und MutS β . MutS α besteht aus MSH2 und MSH6 und ist vornehmlich für die Detektion der Fehlpaarung bzw. kleiner Insertionen/Deletionen verantwortlich. MutS β , bestehend aus MSH2 und MSH3, erkennt und repariert hingegen Insertionen und Deletionen mit bis zu 16 Extrabasen. Nach der Detektion des Schadens rekrutieren die MutS-Komplexe MutL α , welcher wiederum aus MLH1 und PMS2 zusammengesetzt ist und die weiteren Schritte in der Basenfehlpaarungs-Reparatur regelt. Hierbei wird die Fehlpaarung mit Hilfe von Exonuklease 1 und PCNA entfernt, woraufhin die entfernten Nukleotide durch die Polymerase δ neu synthetisiert werden können. Im Anschluss wird der DNA-Strang mittels einer Ligase wieder verschlossen. (Williams et al., 2011)

Defekte in der MMR sind mit dem Hereditären Nicht-Polypösen Kolonkarzinom (HNPCC; *hereditary non-polyposis colon cancer*) assoziiert. (Muller and Fishel, 2002)

1.3.2.3 TRANSLÄSIONS-DNA-SYNTHESE

Die Transläsions DNA-Synthese ist ein Reparaturmechanismus, der die Eigenschaft hat, mittels verschiedener Polymerasen über chemisch modifizierte Basen bzw. abasische Stellen in der DNA hinweg zu synthetisieren. Dabei spielt v.a. die DNA-Polymerase ζ , bestehend aus den Untereinheiten REV1, REV3, REV7, POLD2 und POLD3, eine wichtige Rolle. Sie besitzt die Funktion, Nukleotide gegenüber geschädigter DNA, infolge von Addukten, abasischen Stellen und DNA-Quervernetzungen, einzubauen. Damit wird das Genom stabilisiert und die Replikation kann voranschreiten. (Sharma et al., 2013) Diese Art der Reparatur ist jedoch fehlerbehaftet und nimmt den Einbau von falschen Basen in Kauf, um ein Fortschreiten der Replikation zu garantieren.

1.3.2.4 REPARATUR VON DNA-DOPPELSTRANGBRÜCHEN

Hierbei wird vor allem die homologe Rekombination (HR) als Reparaturmechanismus zur Auflösung dieser Doppelstrangbrüche (DSB) verwendet. Alternativ kann bei einem fehlenden homologen Template die Reparatur mittels *Non-homologous-end-joining* (NHEJ) erfolgen.

A: *Non-homologous-end-joining* (NHEJ)

Non-homologous-end-joining dient wie die HR zur Reparatur von Doppelstrangbrüchen, ist aber im Gegensatz dazu fehlerbehaftet und kann in jeder Phase des Zellzyklus durchgeführt werden. Dieser Mechanismus lässt sich in zwei unterschiedliche Wege einteilen: Das klassische NHEJ (cNHEJ) und das alternative *End-Joining* (alt-EJ) (siehe Abbildung 2 A und C). Beim klassischen Weg bindet das Heterodimer des KU-Komplexes, bestehend aus KU70-KU80, an die offenen Enden des DSB um ihn zu stabilisieren und vor einer weiteren Prozessierung zu schützen. Dabei wird die katalytische Untereinheit der DNA-abhängigen Proteinkinase (*DNA-PKcs*) aktiviert. (Gottlieb and Jackson, 1993) Im Anschluss wird die DNA mit Hilfe des gebundenen MRN-Komplexes und der Exonuklease Artemis prozessiert, um 5' oder 3' des Bruchs einzelsträngige DNA zu entfernen. Die freien Enden werden mittels des DNA-Ligase-IV-XRCC4-Komplex und XLF direkt miteinander verknüpft, wobei kleine Insertionen oder Deletionen entstehen können. (Lieber et al., 2003) Das alt-EJ wurde an Hefen erforscht, die für den KU-Komplex oder Ligase-IV defizient sind. Es findet in kurzen Bereichen 5-25 bp von Mikrohomologien (MMEJ, *microhomology-mediated end-joining*) oder während der S und G2-Phase des Zellzyklus statt. Zu diesem Zeitpunkt ist das KU-Heterodimer weniger aktiv. Somit besteht ein geringerer Schutz für die offenen Enden, die leichter von Exonukleasen angegriffen werden können, wodurch auch größere Deletionen möglich sind. Nach der Bindung des MRN-Komplexes werden die Enden mittels der Exonuklease CtIP prozessiert und anschließend durch die DNA-Ligase III verbunden. (McVey and Lee, 2008) Das MMEJ ist eines der wenigen DNA-Reparatursysteme, das durch Überexpression der beteiligten Proteine zu Krebs führen kann, da es ein erhöhtes Fehlerpotenzial in der Reparatur hat. (Bernstein et al., 2013; Pettan-Brewer et al., 2012)

B: Homologe Rekombination (HR)

HR ist ein fehlerfreies Reparatursystem, welches sich in Form eines Schwesterchromatids ein homologes DNA-Template zur Vorlage nimmt, um einen Doppelstrangbruch zu reparieren. (Haber, 2000) HR findet jedoch nur in einer bestimmten Phase des Zellzyklus statt: in der späten S- und der G2-Phase. Zunächst binden die Nukleasen MRE11/RAD50/NBS1 (XRCC1) - auch als MRN-Komplex bezeichnet - an den DSB und

vermitteln dadurch die Aktivierung von ATM. (Williams and Tainer, 2007) Das 5'-Ende des DSB wird durch den MRN-Komplex mit Hilfe von BRCA1 prozessiert. Dies ist durch ATM und CtIP reguliert und wird durch EXO1 und BLM unterstützt. (Ciccia and Elledge, 2010) Dadurch entstehen freie 3'-Enden aus einzelsträngiger DNA (*single-stranded DNA*, ssDNA). An diese bindet RPA, welches durch RAD51 wieder verdrängt wird. Dieser Prozess ist durch BRCA2 reguliert. Im Falle von repetitiven Sequenzen, können die geschnittenen 3'-Enden mittels RAD52 direkt miteinander verknüpft werden. Diese Variante nennt man *single strand annealing* (SSA) und neben RAD52 sind auch die Endonukleasen XPF/ERRC1 daran beteiligt (siehe Abbildung 2 D). (Hartlerode and Scully, 2009; Motycka et al., 2004) Durch die Polymerisation von RAD51-Proteinen bilden sich RAD51-Nukleofilamenten an ssDNA. Sie vermitteln die Strang-Invasion, indem sie sich an den komplementären Bereich des homologen DNA-Strangs anlagern. (Stauffer and Chazin, 2004) Hierbei bildet sich eine sog. D-Loop-Struktur (*displacement-structure*) aus. Anschließend kann der 3'-Strang mittels DNA-Polymerasen erweitert werden, um sich dann an das prozessierte 5'-Ende anzulagern und die DNA wieder zu verschließen. Diese Variante des Signalwegs bezeichnet man als SDSA (*synthesis-dependent strand annealing*) und wird vor allem durch die Helikase RTEL1 begünstigt. Hierbei entstehen in der Regel *Non-Crossover*-Produkte. (Barber et al., 2008) Als Alternative zum SDSA können sich aus der D-Loop Struktur doppelte *Holliday Junction* Strukturen (dHJs) ausbilden. Diese können entweder durch den BLM/TOPOIII Komplex aufgelöst oder von den Nukleasen GEN1, MUS81/EME1 oder SLX1/SLX4 geschnitten werden. Daraus resultieren *Non-Crossover* oder *Crossover*-Produkte. (Ciccia and Elledge, 2010) Eine schematische Darstellung der HR findet sich in Abbildung 2 B.

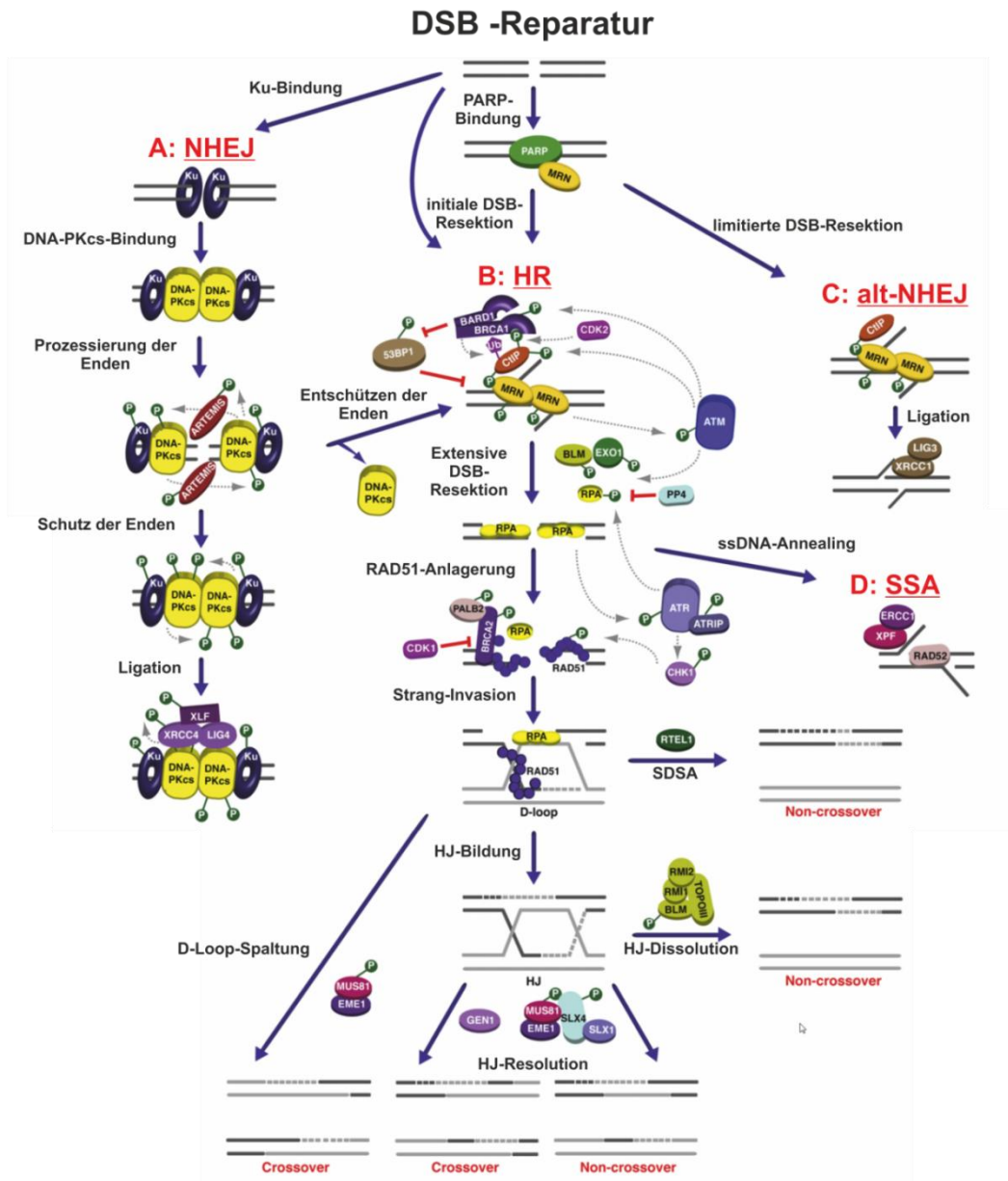


Abbildung 2: Schematische Darstellung der Doppelstrangbruch-Reparatursysteme

A: cNHEJ → Durch die Bindung des Ku-Komplexes und den DNA-PKcs entsteht eine aktive Proteinkinase. Nach der Anlagerung der Exonuklease Artemis werden die Enden prozessiert und Artemis wird phosphoryliert. Die freien Enden werden mittels des DNA-Ligase-IV-XRCC4-Komplex und XLF direkt miteinander verknüpft. B: HR → Die initiale Resektion findet durch Bindung des MRN-Komplexes statt. Die Prozessierung der 5'-Enden erfolgt mit Hilfe von BRCA1. Die Regulation findet mit Hilfe von CtIP und ATM statt. BLM und EXO1 fördern die Resektion sowie die Anlagerung von RPA an die DNA. Nach Bindung von BRCA2 kommt es zur ATR-abhängigen Anlagerung von RAD51-Filamenten sowie zur Stranginvasion in homologe Sequenzbereiche. Ausbildung von D-Loop-Strukturen, die direkt über MUS81/EME1 gespalten oder durch RTEL1 während SDSA aufgelöst werden. Holliday Junctions (HJ) können auch über den BLM/TOPOIII-Komplex oder durch die Nukleasen GEN1 sowie MUS81/EME1-SLX1/SLX4 aufgelöst werden. C: alt-NHEJ → Beim Vorliegen kurzer, homologer Abschnitte nahe des DSBs. Bindung des MRN-Komplex und der Exonuklease CtIP, die die Enden prozessiert. Ligation der Enden mit Hilfe von XRCC1 und Lig3. D: SSA → Im Falle von repetitiven Sequenzen werden die geschnittenen 3'-ssDNA-Enden mittels RAD52 direkt miteinander verknüpft. Weitere beteiligte Endonukleasen sind XPF und ERCC1.

cNHEJ: klassisches *Non-homologous-end-joining*; HR: homologe Rekombination; alt-NHEJ: alternatives *Non-homologous-end-joining*

Verändert nach Ciccia et al. (Ciccia and Elledge, 2010). Für den Abdruck der Abbildung liegt die Erlaubnis von Elsevier vor.

1.3.3 DER FA/BRCA-SIGNALWEG

Die 21, bisher bekannten, FA-Gene lassen sich in unterschiedliche Gruppen und Bereiche des FA/BRCA-Signalwegs einordnen, abhängig von ihrer Funktion und der Interaktion mit anderen Genprodukten. Die Hauptfunktion des FA/BRCA-Signalwegs besteht in der Auflösung von DNA-Interstrang-Quervernetzungen. Diese bewirken ein Anhalten der Replikationsgabel, das im schlimmsten Fall zu einem Doppelstrangbruch führen kann. Somit kann eine Aufrechterhaltung des Genoms nicht mehr gewährleistet werden. Als Folge von blockierten Replikationsgabeln wird der Replikations-Kontrollpunkt des Zellzyklus durch die ATR-Kinase aktiviert. Daraufhin erfolgt die Aktivierung des FA/BRCA-Signalwegs, wodurch der Schaden behoben werden kann.

Im Allgemeinen lässt sich die Behebung eines DNA-Schadens, der durch DNA-quervernetzende Substanzen induziert wurde, in drei Phasen einteilen. Die erste Phase dient der Schadenserkenkung und wird bestimmt durch die Proteine des Fanconi-Kernkomplexes. Dieser besteht aus den Proteinen FANCA, FANCB, FANCC, FANCE, FANCF, FANCG, FANCL und FANCM. Ferner zählen die assoziierten Proteine FAAP20 und FAAP100, sowie MHF1, MHF2, FAAP24 und HES1 (*hairy enhance of split 1*) dazu. Erst vor kurzem wurde entdeckt, dass der eigentliche Kernkomplex vermutlich in drei weitere Subkomplexe unterteilt werden kann: FANCA-FANCG-FAAP20 (AG20), FANCB-FANCL-FAAP100 (BL100) und FANCC-FANCE-FANCF (CEF). (Huang et al., 2014; Rajendra et al., 2014) Über den FANCA-FANCG-FAAP20 Komplex ist noch wenig bekannt, von FANCC-FANCE-FANCF weiß man hingegen, dass es als Adapter-Protein die Interaktion von FANCD2 und anderen Kernkomplexproteinen steuert und in zweifacher Ausführung an die gegenüberliegenden Seiten des BL100 Komplexes bindet. (Swuec and Costa, 2016; Swuec et al., 2016) Von Bedeutung ist vor allem der, als symmetrischer Heterotrimer vorkommender, Subkomplex FANCB-FANCL-FAAP100, der als E3 Ubiquitin Ligase agiert. Diese wird nach der Detektion von stagnierten Replikationsgabeln aktiviert. Die E3 Ubiquitin Ligase Aktivität liegt in der PHD (*plant homeodomain*)-Finger-Domäne von FANCL. FANCB und FAAP100 dienen in diesem Homodimer aus BL100 vor allem dazu, die beiden PHD-Finger Proteine korrekt zu positionieren, um einen Übertrag des Ubiquitins von der E2 auf das Substrat zu ermöglichen. (Meetei et al., 2003a; Swuec et al., 2016)

Nach der Schadensdetektion mittels des Kernkomplexes und dessen Bindung an das Chromatin wird mit Hilfe des E2 konjugierenden Enzyms FANCT/UBE2T der sog. ID-Komplex, bestehend aus FANCD2 und FANCI, monoubiquitiniert. (Garcia-Higuera et al., 2001; Machida et al., 2006; Smogorzewska et al., 2007) Dies ist die zweite Phase der DNA-Schadensbehebung. Hervorzuheben ist auch die Rolle von FANCM: Als ein

Homolog der archealen DNA-Helikase bzw. -Nuklease HEF, hat FANCM DNA-Helikasemotive und eine degenerierte Nuklease. FANCM bindet zusammen mit FAAP24, MHF1 und MHF2 bevorzugt an einzelsträngige und verzweigte DNA und rekrutiert den restlichen Kernkomplex an das Chromatin um einen DNA-Schaden zu erkennen und die Kaskade zur Behebung dieses Schadens in Gang zu setzen. Dieser Vorgang ist, wie bei einigen anderen FA-Proteinen auch, mittels der Kinase ATR reguliert. (Collis et al., 2008) Neben seiner Funktion als Ubiquitin Ligase bildet der FA-Kernkomplex im Zusammenspiel mit BLM, RPA und der Topoisomerase III α einen weiteren, größeren Komplex (BRAFT), welcher mit dem Bloom Syndrom assoziiert ist. (Meetei et al., 2003b)

Das monoubiquitinierte Heterodimer des ID-Komplexes bindet an das Chromatin, wo es die vom ID-Komplex *downstream* gelegenen Genprodukte von *FANCP* (SLX4) und -Q (XPF) rekrutiert und aktiviert. Hierbei spielen auch FAN1 und BRCA1 eine Rolle. Die struktur-spezifische Endonuklease FAN1 bindet mittels ihrer *ubiquitin-binding zinc finger* (UBZ)-Domäne an geschädigte DNA, indem sie mit monoubiquitiniertem FANCD2 interagiert. (Liu et al., 2010) Trotz der wichtigen Funktion im FA/BRCA-Signalweg konnte *FAN1* bisher als kausales FA-Gen ausgeschlossen werden, da bis heute noch kein Patient mit Mutationen in diesem Gen gefunden wurde, der den klinischen und zellulären FA-Phänotyp aufweist. (Trujillo et al., 2012) Mit Hilfe von FANCP (SLX4) und -Q (XPF) erfolgt 3' und 5' des DNA-Schadens ein Einschnitt an der DNA um den Schaden zu entfernen. (Douwel et al., 2014; Liu et al., 2010) Daran sind neben XPF und SLX4 noch weitere Endonukleasen (ERCC1, MUS81, EME1, SLX1) beteiligt, die unter anderem auch an der Auflösung von *Holliday Junction* Strukturen mitwirken. Vor allem SLX4 trägt hierbei zur Organisation der spezifischen Nukleasen bei. Im Folgenden werden die Transläsionspolymerasen REV1, POL ζ und REV7 aktiviert, die mittels Transläsionssynthese (TLS) den geschädigten DNA-Strang verlängern, um ein Ausgangsprodukt für die anschließende HR herzustellen. (Bogliolo and Surrallés, 2015) In der dritten und finalen Phase der DNA-Reparatur werden die FA-Proteine FANCD1, FANCI, FANCD2, FANCD3, FANCD4, FANCD5, FANCD6, FANCD7, FANCD8, FANCD9, FANCD10, FANCD11, FANCD12, FANCD13, FANCD14, FANCD15, FANCD16, FANCD17, FANCD18, FANCD19, FANCD20, FANCD21, FANCD22, FANCD23, FANCD24, FANCD25, FANCD26, FANCD27, FANCD28, FANCD29, FANCD30, FANCD31, FANCD32, FANCD33, FANCD34, FANCD35, FANCD36, FANCD37, FANCD38, FANCD39, FANCD40, FANCD41, FANCD42, FANCD43, FANCD44, FANCD45, FANCD46, FANCD47, FANCD48, FANCD49, FANCD50, FANCD51, FANCD52, FANCD53, FANCD54, FANCD55, FANCD56, FANCD57, FANCD58, FANCD59, FANCD60, FANCD61, FANCD62, FANCD63, FANCD64, FANCD65, FANCD66, FANCD67, FANCD68, FANCD69, FANCD70, FANCD71, FANCD72, FANCD73, FANCD74, FANCD75, FANCD76, FANCD77, FANCD78, FANCD79, FANCD80, FANCD81, FANCD82, FANCD83, FANCD84, FANCD85, FANCD86, FANCD87, FANCD88, FANCD89, FANCD90, FANCD91, FANCD92, FANCD93, FANCD94, FANCD95, FANCD96, FANCD97, FANCD98, FANCD99, FANCD100, FANCD101, FANCD102, FANCD103, FANCD104, FANCD105, FANCD106, FANCD107, FANCD108, FANCD109, FANCD110, FANCD111, FANCD112, FANCD113, FANCD114, FANCD115, FANCD116, FANCD117, FANCD118, FANCD119, FANCD120, FANCD121, FANCD122, FANCD123, FANCD124, FANCD125, FANCD126, FANCD127, FANCD128, FANCD129, FANCD130, FANCD131, FANCD132, FANCD133, FANCD134, FANCD135, FANCD136, FANCD137, FANCD138, FANCD139, FANCD140, FANCD141, FANCD142, FANCD143, FANCD144, FANCD145, FANCD146, FANCD147, FANCD148, FANCD149, FANCD150, FANCD151, FANCD152, FANCD153, FANCD154, FANCD155, FANCD156, FANCD157, FANCD158, FANCD159, FANCD160, FANCD161, FANCD162, FANCD163, FANCD164, FANCD165, FANCD166, FANCD167, FANCD168, FANCD169, FANCD170, FANCD171, FANCD172, FANCD173, FANCD174, FANCD175, FANCD176, FANCD177, FANCD178, FANCD179, FANCD180, FANCD181, FANCD182, FANCD183, FANCD184, FANCD185, FANCD186, FANCD187, FANCD188, FANCD189, FANCD190, FANCD191, FANCD192, FANCD193, FANCD194, FANCD195, FANCD196, FANCD197, FANCD198, FANCD199, FANCD200, FANCD201, FANCD202, FANCD203, FANCD204, FANCD205, FANCD206, FANCD207, FANCD208, FANCD209, FANCD210, FANCD211, FANCD212, FANCD213, FANCD214, FANCD215, FANCD216, FANCD217, FANCD218, FANCD219, FANCD220, FANCD221, FANCD222, FANCD223, FANCD224, FANCD225, FANCD226, FANCD227, FANCD228, FANCD229, FANCD230, FANCD231, FANCD232, FANCD233, FANCD234, FANCD235, FANCD236, FANCD237, FANCD238, FANCD239, FANCD240, FANCD241, FANCD242, FANCD243, FANCD244, FANCD245, FANCD246, FANCD247, FANCD248, FANCD249, FANCD250, FANCD251, FANCD252, FANCD253, FANCD254, FANCD255, FANCD256, FANCD257, FANCD258, FANCD259, FANCD260, FANCD261, FANCD262, FANCD263, FANCD264, FANCD265, FANCD266, FANCD267, FANCD268, FANCD269, FANCD270, FANCD271, FANCD272, FANCD273, FANCD274, FANCD275, FANCD276, FANCD277, FANCD278, FANCD279, FANCD280, FANCD281, FANCD282, FANCD283, FANCD284, FANCD285, FANCD286, FANCD287, FANCD288, FANCD289, FANCD290, FANCD291, FANCD292, FANCD293, FANCD294, FANCD295, FANCD296, FANCD297, FANCD298, FANCD299, FANCD300, FANCD301, FANCD302, FANCD303, FANCD304, FANCD305, FANCD306, FANCD307, FANCD308, FANCD309, FANCD310, FANCD311, FANCD312, FANCD313, FANCD314, FANCD315, FANCD316, FANCD317, FANCD318, FANCD319, FANCD320, FANCD321, FANCD322, FANCD323, FANCD324, FANCD325, FANCD326, FANCD327, FANCD328, FANCD329, FANCD330, FANCD331, FANCD332, FANCD333, FANCD334, FANCD335, FANCD336, FANCD337, FANCD338, FANCD339, FANCD340, FANCD341, FANCD342, FANCD343, FANCD344, FANCD345, FANCD346, FANCD347, FANCD348, FANCD349, FANCD350, FANCD351, FANCD352, FANCD353, FANCD354, FANCD355, FANCD356, FANCD357, FANCD358, FANCD359, FANCD360, FANCD361, FANCD362, FANCD363, FANCD364, FANCD365, FANCD366, FANCD367, FANCD368, FANCD369, FANCD370, FANCD371, FANCD372, FANCD373, FANCD374, FANCD375, FANCD376, FANCD377, FANCD378, FANCD379, FANCD380, FANCD381, FANCD382, FANCD383, FANCD384, FANCD385, FANCD386, FANCD387, FANCD388, FANCD389, FANCD390, FANCD391, FANCD392, FANCD393, FANCD394, FANCD395, FANCD396, FANCD397, FANCD398, FANCD399, FANCD400, FANCD401, FANCD402, FANCD403, FANCD404, FANCD405, FANCD406, FANCD407, FANCD408, FANCD409, FANCD410, FANCD411, FANCD412, FANCD413, FANCD414, FANCD415, FANCD416, FANCD417, FANCD418, FANCD419, FANCD420, FANCD421, FANCD422, FANCD423, FANCD424, FANCD425, FANCD426, FANCD427, FANCD428, FANCD429, FANCD430, FANCD431, FANCD432, FANCD433, FANCD434, FANCD435, FANCD436, FANCD437, FANCD438, FANCD439, FANCD440, FANCD441, FANCD442, FANCD443, FANCD444, FANCD445, FANCD446, FANCD447, FANCD448, FANCD449, FANCD450, FANCD451, FANCD452, FANCD453, FANCD454, FANCD455, FANCD456, FANCD457, FANCD458, FANCD459, FANCD460, FANCD461, FANCD462, FANCD463, FANCD464, FANCD465, FANCD466, FANCD467, FANCD468, FANCD469, FANCD470, FANCD471, FANCD472, FANCD473, FANCD474, FANCD475, FANCD476, FANCD477, FANCD478, FANCD479, FANCD480, FANCD481, FANCD482, FANCD483, FANCD484, FANCD485, FANCD486, FANCD487, FANCD488, FANCD489, FANCD490, FANCD491, FANCD492, FANCD493, FANCD494, FANCD495, FANCD496, FANCD497, FANCD498, FANCD499, FANCD500, FANCD501, FANCD502, FANCD503, FANCD504, FANCD505, FANCD506, FANCD507, FANCD508, FANCD509, FANCD510, FANCD511, FANCD512, FANCD513, FANCD514, FANCD515, FANCD516, FANCD517, FANCD518, FANCD519, FANCD520, FANCD521, FANCD522, FANCD523, FANCD524, FANCD525, FANCD526, FANCD527, FANCD528, FANCD529, FANCD530, FANCD531, FANCD532, FANCD533, FANCD534, FANCD535, FANCD536, FANCD537, FANCD538, FANCD539, FANCD540, FANCD541, FANCD542, FANCD543, FANCD544, FANCD545, FANCD546, FANCD547, FANCD548, FANCD549, FANCD550, FANCD551, FANCD552, FANCD553, FANCD554, FANCD555, FANCD556, FANCD557, FANCD558, FANCD559, FANCD560, FANCD561, FANCD562, FANCD563, FANCD564, FANCD565, FANCD566, FANCD567, FANCD568, FANCD569, FANCD570, FANCD571, FANCD572, FANCD573, FANCD574, FANCD575, FANCD576, FANCD577, FANCD578, FANCD579, FANCD580, FANCD581, FANCD582, FANCD583, FANCD584, FANCD585, FANCD586, FANCD587, FANCD588, FANCD589, FANCD590, FANCD591, FANCD592, FANCD593, FANCD594, FANCD595, FANCD596, FANCD597, FANCD598, FANCD599, FANCD600, FANCD601, FANCD602, FANCD603, FANCD604, FANCD605, FANCD606, FANCD607, FANCD608, FANCD609, FANCD610, FANCD611, FANCD612, FANCD613, FANCD614, FANCD615, FANCD616, FANCD617, FANCD618, FANCD619, FANCD620, FANCD621, FANCD622, FANCD623, FANCD624, FANCD625, FANCD626, FANCD627, FANCD628, FANCD629, FANCD630, FANCD631, FANCD632, FANCD633, FANCD634, FANCD635, FANCD636, FANCD637, FANCD638, FANCD639, FANCD640, FANCD641, FANCD642, FANCD643, FANCD644, FANCD645, FANCD646, FANCD647, FANCD648, FANCD649, FANCD650, FANCD651, FANCD652, FANCD653, FANCD654, FANCD655, FANCD656, FANCD657, FANCD658, FANCD659, FANCD660, FANCD661, FANCD662, FANCD663, FANCD664, FANCD665, FANCD666, FANCD667, FANCD668, FANCD669, FANCD670, FANCD671, FANCD672, FANCD673, FANCD674, FANCD675, FANCD676, FANCD677, FANCD678, FANCD679, FANCD680, FANCD681, FANCD682, FANCD683, FANCD684, FANCD685, FANCD686, FANCD687, FANCD688, FANCD689, FANCD690, FANCD691, FANCD692, FANCD693, FANCD694, FANCD695, FANCD696, FANCD697, FANCD698, FANCD699, FANCD700, FANCD701, FANCD702, FANCD703, FANCD704, FANCD705, FANCD706, FANCD707, FANCD708, FANCD709, FANCD710, FANCD711, FANCD712, FANCD713, FANCD714, FANCD715, FANCD716, FANCD717, FANCD718, FANCD719, FANCD720, FANCD721, FANCD722, FANCD723, FANCD724, FANCD725, FANCD726, FANCD727, FANCD728, FANCD729, FANCD730, FANCD731, FANCD732, FANCD733, FANCD734, FANCD735, FANCD736, FANCD737, FANCD738, FANCD739, FANCD740, FANCD741, FANCD742, FANCD743, FANCD744, FANCD745, FANCD746, FANCD747, FANCD748, FANCD749, FANCD750, FANCD751, FANCD752, FANCD753, FANCD754, FANCD755, FANCD756, FANCD757, FANCD758, FANCD759, FANCD760, FANCD761, FANCD762, FANCD763, FANCD764, FANCD765, FANCD766, FANCD767, FANCD768, FANCD769, FANCD770, FANCD771, FANCD772, FANCD773, FANCD774, FANCD775, FANCD776, FANCD777, FANCD778, FANCD779, FANCD780, FANCD781, FANCD782, FANCD783, FANCD784, FANCD785, FANCD786, FANCD787, FANCD788, FANCD789, FANCD790, FANCD791, FANCD792, FANCD793, FANCD794, FANCD795, FANCD796, FANCD797, FANCD798, FANCD799, FANCD800, FANCD801, FANCD802, FANCD803, FANCD804, FANCD805, FANCD806, FANCD807, FANCD808, FANCD809, FANCD810, FANCD811, FANCD812, FANCD813, FANCD814, FANCD815, FANCD816, FANCD817, FANCD818, FANCD819, FANCD820, FANCD821, FANCD822, FANCD823, FANCD824, FANCD825, FANCD826, FANCD827, FANCD828, FANCD829, FANCD830, FANCD831, FANCD832, FANCD833, FANCD834, FANCD835, FANCD836, FANCD837, FANCD838, FANCD839, FANCD840, FANCD841, FANCD842, FANCD843, FANCD844, FANCD845, FANCD846, FANCD847, FANCD848, FANCD849, FANCD850, FANCD851, FANCD852, FANCD853, FANCD854, FANCD855, FANCD856, FANCD857, FANCD858, FANCD859, FANCD860, FANCD861, FANCD862, FANCD863, FANCD864, FANCD865, FANCD866, FANCD867, FANCD868, FANCD869, FANCD870, FANCD871, FANCD872, FANCD873, FANCD874, FANCD875, FANCD876, FANCD877, FANCD878, FANCD879, FANCD880, FANCD881, FANCD882, FANCD883, FANCD884, FANCD885, FANCD886, FANCD887, FANCD888, FANCD889, FANCD890, FANCD891, FANCD892, FANCD893, FANCD894, FANCD895, FANCD896, FANCD897, FANCD898, FANCD899, FANCD900, FANCD901, FANCD902, FANCD903, FANCD904, FANCD905, FANCD906, FANCD907, FANCD908, FANCD909, FANCD910, FANCD911, FANCD912, FANCD913, FANCD914, FANCD915, FANCD916, FANCD917, FANCD918, FANCD919, FANCD920, FANCD921, FANCD922, FANCD923, FANCD924, FANCD925, FANCD926, FANCD927, FANCD928, FANCD929, FANCD930, FANCD931, FANCD932, FANCD933, FANCD934, FANCD935, FANCD936, FANCD937, FANCD938, FANCD939, FANCD940, FANCD941, FANCD942, FANCD943, FANCD944, FANCD945, FANCD946, FANCD947, FANCD948, FANCD949, FANCD950, FANCD951, FANCD952, FANCD953, FANCD954, FANCD955, FANCD956, FANCD957, FANCD958, FANCD959, FANCD960, FANCD961, FANCD962, FANCD963, FANCD964, FANCD965, FANCD966, FANCD967, FANCD968, FANCD969, FANCD970, FANCD971, FANCD972, FANCD973, FANCD974, FANCD975, FANCD976, FANCD977, FANCD978, FANCD979, FANCD980, FANCD981, FANCD982, FANCD983, FANCD984, FANCD985, FANCD986, FANCD987, FANCD988, FANCD989, FANCD990, FANCD991, FANCD992, FANCD993, FANCD994, FANCD995, FANCD996, FANCD997, FANCD998, FANCD999, FANCD1000, FANCD1001, FANCD1002, FANCD1003, FANCD1004, FANCD1005, FANCD1006, FANCD1007, FANCD1008, FANCD1009, FANCD1010, FANCD1011, FANCD1012, FANCD1013, FANCD1014, FANCD1015, FANCD1016, FANCD1017, FANCD1018, FANCD1019, FANCD1020, FANCD1021, FANCD1022, FANCD1023, FANCD1024, FANCD1025, FANCD1026, FANCD1027, FANCD1028, FANCD1029, FANCD1030, FANCD1031, FANCD1032, FANCD1033, FANCD1034, FANCD1035, FANCD1036, FANCD1037, FANCD1038, FANCD1039, FANCD1040, FANCD1041, FANCD1042, FANCD1043, FANCD1044, FANCD1045, FANCD1046, FANCD1047, FANCD1048, FANCD1049, FANCD1050, FANCD1051, FANCD1052, FANCD1053, FANCD1054, FANCD1055, FANCD1056, FANCD1057, FANCD1058, FANCD1059, FANCD1060, FANCD1061, FANCD1062, FANCD1063, FANCD1064, FANCD1065, FANCD1066, FANCD1067, FANCD1068, FANCD1069, FANCD1070, FANCD1071, FANCD1072, FANCD1073, FANCD1074, FANCD1075, FANCD1076, FANCD1077, FANCD1078, FANCD1079, FANCD1080, FANCD1081, FANCD1082, FANCD1083, FANCD1084, FANCD1085, FANCD1086, FANCD1087, FANCD1088, FANCD1089, FANCD1090, FANCD1091, FANCD1092, FANCD1093, FANCD1094, FANCD1095, FANCD1096, FANCD1097, FANCD1098, FANCD1099, FANCD1100, FANCD1101, FANCD1102, FANCD1103, FANCD1104, FANCD1105, FANCD1106, FANCD1107, FANCD1108, FANCD1109, FANCD1110, FANCD1111, FANCD1112, FANCD1113, FANCD1114, FANCD1115, FANCD1116, FANCD1117, FANCD1118, FANCD1119, FANCD1120, FANCD1121, FANCD1122, FANCD1123, FANCD1124, FANCD1125, FANCD1126, FANCD1127, FANCD1128, FANCD1129, FANCD1130, FANCD1131, FANCD1132, FANCD1133, FANCD1134, FANCD1135, FANCD1136, FANCD1137, FANCD1138, FANCD1139, FANCD1140, FANCD1141, FANCD1142, FANCD1143, FANCD1144, FANCD1145, FANCD1146, FANCD1147, FANCD1148, FANCD1149, FANCD1150, FANCD1151, FANCD1152, FANCD1153, FANCD1154, FANCD1155, FANCD1156, FANCD1157, FANCD1158, FANCD1159, FANCD1160, FANCD1161, FANCD1162, FANCD1163, FANCD1164, FANCD1165, FANCD1166, FANCD1167, FANCD1168, FANCD1169, FANCD1170, FANCD1171, FANCD1172, FANCD1173, FANCD1174, FANCD1175, FANCD1176, FANCD1177, FANCD1178, FANCD1179, FANCD1180, FANCD1181, FANCD1182, FANCD1183, FANCD1184, FANCD1185, FANCD1186, FANCD1187, FANCD1188, FANCD1189, FANCD1190, FANCD1191, FANCD1192, FANCD1193, FANCD1194, FANCD1195, FANCD1196, FANCD1197, FANCD1198, FANCD1199, FANCD1200, FANCD1201, FANCD1202, FANCD1203, FANCD1204, FANCD1205, FANCD1206, FANCD1207, FANCD1208, FANCD1209, FANCD1210, FANCD1211, FANCD1212, FANCD1213, FANCD1214, FANCD1215, FANCD1216, FANCD1217, FANCD1218, FANCD1219, FANCD1220, FANCD1221, FANCD1222, FANCD1223, FANCD1224, FANCD1225, FANCD1226, FANCD1227, FANCD1228, FANCD1229, FANCD1230, FANCD1231, FANCD1232, FANCD1233, FANCD1234, FANCD1235, FANCD1236, FANCD1237, FANCD1238, FANCD1239, FANCD1240, FANCD1241, FANCD1242, FANCD1243, FANCD1244, FANCD1245, FANCD1246, FANCD1247, FANCD1248, FANCD1249, FANCD1250, FANCD1251, FANCD1252, FANCD1253, FANCD1254, FANCD1255, FANCD1256, FANCD1257, FANCD1258, FANCD1259, FANCD1260, FANCD1261, FANCD1262, FANCD1263, FANCD1264, FANCD1265, FANCD1266, FANCD1267, FANCD1268, FANCD1269, FANCD1270, FANCD1271, FANCD1272, FANCD1273, FANCD1274, FANCD1275, FANCD1276, FANCD1277, FANCD1278, FANCD1279, FANCD1280, FANCD1281, FANCD1282, FANCD1283, FANCD1284, FANCD1285, FANCD1286, FANCD1287, FANCD1288, FANCD1289, FANCD1290, FANCD1291, FANCD1292, FANCD1293, FANCD1294, FANCD1295, FANCD1296, FANCD1297, FANCD1298, FANCD1299, FANCD1300, FANCD1301, FANCD1302, FANCD1303, FANCD1304, FANCD1305, FANCD1306, FANCD1307, FANCD1308, FANCD1309, FANCD1310, FANCD1311, FANCD1312, FANCD1313, FANCD1314, FANCD1315, FANCD1316, FANCD1317, FANCD1318, FANCD1319, FANCD1320, FANCD1321, FANCD1322, FANCD1323, FANCD1324, FANCD1325, FANCD1326, FANCD1327, FANCD1328, FANCD1329, FANCD1330, FANCD1331, FANCD1332, FANCD1333, FANCD1334, FANCD1335, FANCD1336, FANCD1337, FANCD1338, FANCD1339, FANCD1340, FANCD1341, FANCD1342, FANCD1343, FANCD1344, FANCD1345, FANCD1346, FANCD1347, FANCD1348, FANCD1349, FANCD1350, FANCD1351, FANCD1352, FANCD1353, FANCD1354, FANCD1355, FANCD1356, FANCD1357, FANCD1358, FANCD1359, FANCD1360, FANCD1361, FANCD1362, FANCD1363, FANCD1364, FANCD1365, FANCD1366, FANCD1367, FANCD1368, FANCD1369, FANCD1370, FANCD1371, FANCD1372, FANCD1373, FANCD1374, FANCD1375, FANCD1376, FANCD1377, FANCD1378, FANCD1379, FANCD1380, FANCD1381, FANCD1382, FANCD1383, FANCD1384, FANCD1385, FANCD1386, FANCD1387, FANCD1388, FANCD1389, FANCD1390, FANCD1391, FANCD1392, FANCD1393, FANCD1394, FANCD1395, FANCD1396, FANCD1397, FANCD1398, FANCD1399, FANCD1400, FANCD1401, FANCD1402, FANCD1403, FANCD1404, FANCD1405, FANCD1406, FANCD1407, FANCD1408, FANCD1409, FANCD1410, FANCD1411, FANCD1412, FANCD1413, FANCD1414, FANCD1415, FANCD1416, FANCD1417, FANCD1418, FANCD1419, FANCD1420, FANCD1421, FANCD1422, FANCD1423, FANCD1424, FANCD1425, FANCD1426, FANCD1427, FANCD1428, FANCD1429, FANCD1430, FANCD1431, FANCD1432, FANCD1433, FANCD1434, FANCD1435, FANCD1436, FANCD1437, FANCD1438, FANCD1439, FANCD1440, FANCD1441, FANCD1442, FANCD1443, FANCD1444, FANCD1445, FANCD1446, FANCD1447, FANCD1448, FANCD1449, FANCD1450, FANCD1451, FANCD1452, FANCD1453, FANCD1454, FANCD1455, FANCD1456, FANCD1457, FANCD1458, FANCD1459, FANCD1460, FANCD1461, FANCD1462, FANCD1463, FANCD1464, FANCD1465, FANCD1466, FANCD1467, FANCD1468, FANCD1469, FANCD1470, FANCD1471, FANCD1472, FANCD1473, FANCD1474, FANCD1475, FANCD1476, FANCD1477, FANCD1478, FANCD1479, FANCD1480, FANCD1481, FANCD1482, FANCD1483, FANCD1484, FANCD1485, FANCD1486, FANCD1487, FANCD1488, FANCD1489, FANCD1490, FANCD1491, FANCD1492, FANCD1493, FANCD1494, FANCD1495, FANCD1496, FANCD1497, FANCD1498, FANCD1499, FANCD1500, FANCD1501, FANCD1502, FANCD1503, FANCD1504, FANCD1505, FANCD1506, FANCD1507, FANCD1508, FANCD1509, FANCD1510, FANCD1511, FANCD1512, FANCD1513, FANCD1514, FANCD1515, FANCD1516, FANCD1517, FANCD1518, FANCD1519, FANCD1520, FANCD1521, FANCD1522, FANCD1523, FANCD1524, FANCD1525, FANCD1526, FANCD1527, FANCD1528, FANCD1529, FANCD1530, FANCD1531, FANCD1532, FANCD1533, FANCD1534, FANCD1535, FANCD1536, FANCD1537, FANCD1538, FANCD1539, FANCD1540, FANCD1541, FANCD1542, FANCD1543, FANCD1544, FANCD1545, FANCD1546, FANCD1547, FANCD1548, FANCD1549, FANCD1550, FANCD1551, FANCD1552, FANCD1553, FANCD1554, FANCD1555, FANCD1556, FANCD1557, FANCD1558, FANCD1559, FANCD1560, FANCD1561, FANCD1562, FANCD1563, FANCD1564, FANCD1565, FANCD1566, FANCD1567, FANCD1568, FANCD1569, FANCD1570, FANCD1571, FANCD1572, FANCD1573, FANCD1574, FANCD1575, FANCD1576, FANCD1577, FANCD1578, FANCD1579, FANCD1580, FANCD1581, FANCD1582, FANCD1583, FANCD1584, FANCD1585, FANCD1586, FANCD

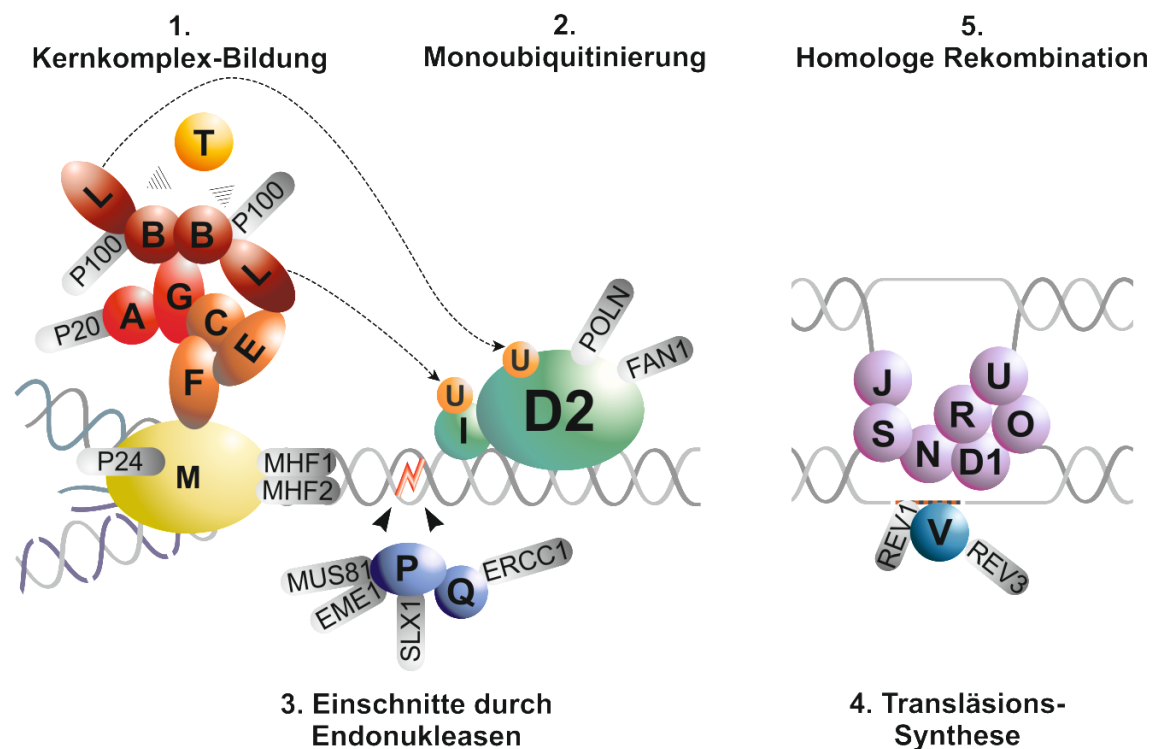


Abbildung 3: Schematische Darstellung des FA/BRCA-Signalweges.

Nach einem DNA-Schaden in Form einer DNA-Quervernetzung (roter Blitz innerhalb der DNA) wird der FA/BRCA-Signalweg aktiviert. (1) Der Kernkomplex (rote und orangefarbene Proteine) bindet nach der Erkennung des Schadens durch FANCM (gelb) an das Chromatin. Durch die E3-Ligase-Aktivität von FANCL wird das vom Ubiquitin-konjugierenden Enzym UBE2T/FANCT (gold-gelb) bereitgestellte Ubiquitin auf den ID-Komplex (grün) übertragen. (2) Der ID-Komplex ist ebenfalls am Chromatin lokalisiert. Mit Hilfe des aktiven, monoubiquitinierten ID-Komplexes werden weitere Proteine zur Schadensbehebung rekrutiert. (3) Die Endonukleasen (blau) schneiden den Schaden aus der DNA (Pfeilspitzen). (4) Die Lücke wird mittels Transläsions-Synthese aufgefüllt (türkis). (5) Die endgültige Reparatur erfolgt durch die Komponenten der Homologen Rekombination (violett). Alle assoziierten Proteine sind in grau dargestellt. Verändert nach Schindler *et al.* (Schindler *et al.*, 2012) Für den Abdruck der Abbildung liegt die Erlaubnis des Springer Verlags vor.

1.3.4 WEITERE ZELLULÄRE FA-MERKMALE

Die Wesentlichen, von Guido Fanconi entdeckten, zellulären FA-Merkmale wurden bereits in 1.1.2 beschrieben. Dennoch gibt es weitere zelluläre Dysfunktionen und -regulationen, die ebenfalls zum klinischen Phänotyp der FA beitragen.

Bei FA-Zellen kommt es zu einem Arrest in der G2/M-Phase im Zellzyklus, die man sich auch in der Diagnostik zunutze macht (siehe 1.2.1). Der G2/M Checkpoint spielt im Zellzyklus in der Aufrechterhaltung der Genomstabilität eine wichtige Rolle. Während dieser gewollten Pause findet die DNA-Reparatur statt, bevor die Zellen anschließend in die Mitose eintreten. Da bei FA-Patienten diese DNA-Reparatur nicht stattfinden kann, arretieren FA-Zellen in der G2/M-Phase. (Tischkowitz and Hodgson, 2003)

Mehrere Studien haben bestätigt, dass FA-Zellen eine erhöhte Sensitivität gegenüber reaktiven Sauerstoffspezies (ROS) und Aldehyden aufweisen. Die Gruppe um Joenje *et al.* konnte zeigen, dass die chromosomale Bruchrate in FA-Zellen unter niedrigen Sauerstoffbedingungen verringert ist. (Joenje *et al.*, 1981) Außerdem wachsen in Kultur gehaltene FA-Fibroblasten unter hypoxischen (5 % O₂) Bedingungen besser als in atmosphärischen Bedingungen (20 % O₂). (Schindler and Hoehn, 1988) Viele Substanzen - wie auch MMC - bilden ROS, woraus die Hypersensitivität gegenüber diesen DNA-quervernetzenden Substanzen resultieren kann. (Clarke *et al.*, 1997) Der oxidative Stress, dem die Zelle durch ein Ungleichgewicht zwischen der Produktion von reaktiven Sauerstoffspezies und der antioxidativen Bekämpfung ausgesetzt ist (mitochondriale Dysfunktion), bringt vor allem hämatopoetische Stammzellen bzw. Vorläuferzellen dazu, vorzeitig in Apoptose zu gehen. Die gestörte Hämatopoese führt letztlich zu Knochenmarkversagen und Leukämie. (Du *et al.*, 2008; Pagano *et al.*, 2013; Tischkowitz and Hodgson, 2003) Das Labor von KJ Patel konnte in mehreren Studien an FA-Mäusen nachweisen, dass neben ROS auch endogene Aldehyde in FA-Zellen erheblich zum zellulären Phänotyp beitragen. (Garaycochea and Patel, 2014) Nicht nur bei Aldh2-defizienten FA-Mäusen (siehe 1.4), stellt die endogene Toxizität von Acetaldehyd ein Problem dar, vor allem auch für die japanisch-asiatische Bevölkerung, von denen 40 % ein dominant-negatives Allel für *ALDH2* tragen. Sie besitzen zudem, im Falle einer zusätzlichen Mutation in einem Fanconi Anämie Gen, ein deutlich erhöhtes Risiko schon in jungen Jahren ein Knochenmarkversagen zu entwickeln. Außerdem zeigen betroffene Japaner erhöhte Raten an FA-abhängigen Geburtsdefekten. (Hira *et al.*, 2013)

Die erhöhte Apoptoserate im Vergleich zu gesunden Zellen kann ebenfalls auf dem zugrunde liegenden DNA-Reparatur Defekt oder an einer fehlenden bzw. fehlerhaften Interaktion mit anderen, Apoptose-assoziierten Proteinen manifestiert sein. (Cumming *et al.*, 2001; Pang *et al.*, 2001) Des Weiteren besteht bei FA-Patienten häufig ein Ungleichgewicht an pro-apoptotischen Wachstumsfaktoren, wie Interferon- γ (INF- γ) oder Tumornekrosefaktor- α (TNF- α). (Du *et al.*, 2008)

Mehrere Studien haben gezeigt, dass FA-Zellen, vor allem Lymphozyten, eine erhöhte Rate an verkürzten Telemoren haben bzw. diese sich schneller verkürzen als in Kontrollzellen. (Neveling *et al.*, 2009) Damit assoziiert ist auch eine 10-fach erhöhte Rate von einer Chromosomenendfusion. (Callen and Surrallés, 2004)

Generell gilt, dass letztendlich das Zusammenspiel aller zellulären Dysfunktionen zu FA führt.

1.4 FANCONI ANÄMIE MAUSMODELLE

Die Maus wird seit Jahrzehnten in der Forschung als Modellorganismus eingesetzt. Durch ihre kurze Generationszeit, die hohe Zahl an Nachkommen und der großen Homologie des Mausgenoms mit dem des Menschen, eignet sich die Maus hervorragend um *in vivo* Studien verschiedenster Erkrankungen oder Therapieansätze durchzuführen. Mittlerweile gibt es verschiedene knockout Mäuse für die einzelnen FA-Gene (siehe Tabelle 2). Im Durchschnitt haben die bisher bekannten FA-Mausproteine eine 50-85 % Sequenzhomologie mit den humanen Orthologen. (Dong et al., 2015) Dennoch zeigen nur wenige FA-Mäuse einen, mit dem von FA-Patienten vergleichbaren, klinischen Phänotyp. Dieser beschränkt sich vor allem auf eine über alle Komplementationsgruppen verteilte In- bzw. Subfertilität mit Hypogonadismus und ovarieller Dysfunktion. Der humane, zelluläre Phänotyp spiegelt sich hingegen in embryonalen Mausfibroblasten wider. Sie zeigen ebenfalls eine Hypersensitivität gegenüber DNA-quervernetzenden Substanzen, ein verlangsamtes Zellwachstum und eine erhöhte Chromosomenbruchrate. Generell kann man beobachten, dass knockout Mäuse mit Defekten in den Kernkomplex Genen einen milderen Phänotyp aufweisen, als Mäuse mit einem Defekt im ID-Komplex oder den „downstream“ Genen. Des Weiteren scheint auch der genetische Hintergrund der Maus eine Rolle zu spielen. So sind Mäuse mit einem C57BL/6J Hintergrund stärker betroffen, als bspw. Mäuse mit einem 129SV oder 129S4 Hintergrund. Man geht hier davon aus, dass sog. „modifier“ Gene diese erhöhte Penetranz auslösen. (Parmar et al., 2009)

Den schwersten Phänotyp weisen *Fancd1* defiziente Mäuse auf. Sie sind embryonal lethal. Lediglich eine homozygote Deletion von Exon 27 ist lebensfähig, zeigt jedoch eine spontane Chromosomeninstabilität und eine erhöhte MMC-Sensitivität im Vergleich zu *Fanca*^{-/-} Mäusen. Des Weiteren bilden diese Mäuse keine RAD51-Foci nach Bestrahlung oder Behandlung mit DNA-quervernetzenden Substanzen aus. Auffällig ist jedoch, dass diese Mäuse keine verminderte Fertilität aufweisen – ein Merkmal, das alle anderen FA-Mäuse gemeinsam haben. (Atanassov et al., 2005; McAllister et al., 2006)

Ein weiterer Vorteil eines Mausmodells ist die Untersuchung von Doppelmutanten. Mittels Kreuzung zweier FA-knockout Mäuse bekommt man eine Doppelmutante für beide Gene. So gibt es Doppelmutanten für *Fanca*^{-/-}/*Fancc*^{-/-}, *Fancc*^{-/-}/*Sod1*^{-/-}, *Fancc*^{-/-}/*p53*^{-/-}, *Fancd2*^{-/-}/*p53*^{+/-}, *Fancd2*^{-/-}/*Fancj*^{-/-} und *Fancd2*^{-/-}/*Aldh2*^{-/-}. (Langevin et al., 2011; Matsuzaki et al., 2015; Parmar et al., 2009) Vor allem Doppelmutanten mit *p53*-Defizienz geben Aufschluss über die Entstehung von Tumoren und die Möglichkeit, eine Strategie zu entwickeln, um diese Tumore bei FA-Patienten in Zukunft vermeiden zu können bzw. mittels Chemotherapie erfolgreich behandeln zu können. (Freie et al., 2003; Houghtaling et al., 2005)

Vergleichbar mit FA-Zellen, zeigen auch *mouse-embryonic-fibroblasts* (MEFs) eine erhöhte Sensitivität gegenüber Acetaldehyd und reaktiven Sauerstoffspezies. Homozygote Doppelmutanten von *Fancd2*^{-/-} und *Aldh2*^{-/-} sind nicht lebensfähig, insofern das Muttertier *Aldh2*^{-/-} ist. Selbst wenn das Muttertier heterozygot für *Aldh2* ist, sterben die Nachkommen innerhalb von 3-6 Monaten an akuter lymphatischer Leukämie (ALL). (Langevin et al., 2011) Jedoch ist dieses Phänomen bisher nur bei *Fancd2* defizienten Mäusen zu erkennen. (Noda et al., 2011) Dies steht im Gegensatz zu einer Studie von Yabe *et al.*, die japanische FA-Patienten und ihre Mütter bezüglich ihres ALDH2 Status untersuchten. Hierbei scheint ein normales, maternales ALDH2-Allel nicht nötig zu sein, um eine normale fetale Entwicklung zu fördern. Alle Kinder von ALDH2 defizienten Müttern sind lebensfähig. Dennoch entwickeln alle FA-Patienten mit einer homozygot oder heterozygot defizienten ALDH2-Mutter schon früh ein Knochenmarkversagen oder myelodysplastisches Syndrom. (Yabe et al., 2016)

Den abweichenden Phänotyp von FA-Mäusen im Vergleich zu FA-Patienten, vor allem in Bezug auf die Entwicklung von Knochenmarkversagen und Krebsentwicklung, lässt sich zum einen durch die verkürzte Lebensdauer einer Maus (ca. 3 Jahre) und zum anderen mit den sterilen Bedingungen, unter denen Labortiere gehalten werden, erklären. Sie sind in dieser Umgebung keinen exogenen Noxen ausgesetzt, die auch im endogenen System somit nicht zu bspw. ROS oder Acetaldehyd metabolisiert werden. Dies sollte ein Hinweis für FA-Patienten sein, sich – wenn möglich – dem Einfluss von exogenen Noxen zu entziehen. (Bakker et al., 2013)

Tabelle 2: Übersicht über die aktuellen FA-Mausmodelle.

Neben dem deletierten Gen, den phänotypischen Auffälligkeiten und den zellulären FA-Merkmalen, sind die Publikation mit der Erstbeschreibung eines jeden Mausmodells, angegeben. Des Weiteren ist der genetische Hintergrund des Mausstammes angegeben, auf dem der Knockout basiert.

Gen	Phänotyp	Zelluläre FA-Merkmale	Genetischer Hintergrund	Erstbeschreibung
<i>Fanca</i>	Hypogonadismus, verminderte Fertilität, Mikrozephalie, Thrombozytopenie, Lymphome, Sarkome und Eierstocktumore	Hypersensitivität gegenüber MMC	129/Ola und C57BL/6 Deletion Exon 4-7	(Cheng et al., 2000)
<i>Fancb</i>	Testikuläre Atrophie	Hypersensitivität gegenüber MMC	C57BL/6J Deletion Exon 2	(Kato et al., 2015)
<i>Fancc</i>	Hypogonadismus, verminderte Fertilität, Mikrophthalmie und nicht-mendelsche Geburtenrate, Sarkome, Adenokarzinome (bei Mäusen >1 Jahr)	Hypersensitivität gegenüber MMC und DEB, erhöhte Chromosomenbruchrate	129/Sv und C57BL/6J Deletion Exon 8	(Chen et al., 1996)
<i>Fancd1</i>	Embryonal lethal Fancd1 ^{Δ27/Δ27} Karzinome	Hypersensitivität gegenüber MMC und IR	C57BL/6J Deletion Exon 10-11 bzw. 27	(Suzuki et al., 1997)
<i>Fancd2</i>	Prä- und postnatale Wachstumsstörung, Hypogonadismus, verminderte Fertilität, Adenome und Karzinome; nicht-mendelsche Geburtenrate und Mikrophthalmie (bei C57BL/6J Hintergrund)	Hypersensitivität gegenüber MMC, schwach sensitiv gegenüber IR	129/S4 und C57BL/6J Deletion Exon 26/27	(Houghtaling et al., 2003)
<i>Fance</i>	Verminderte Fertilität	Nicht getestet	FVB/N Insertion Intron 8	(Fu et al., 2016)
<i>Fancf</i>	Erhöhte Rate an ovariellen Tumoren, Hypogonadismus	Hypersensitivität gegenüber MMC,	129/Ola und FVB Deletion Exon 1	(Bakker et al., 2012)

Gen	Phänotyp	Zelluläre FA-Merkmale	Genetischer Hintergrund	Erstbeschreibung
<i>Fancg</i>	Hypogonadismus, verminderte Fertilität, Wachstumsverzögerung, Mikrozephalie, Mikrophthalmie,	Hypersensitivität gegenüber MMC und DEB, erhöhte Chromosomenbruchrate	129/Sv und C57BL/6 Deletion Exon 2-9	(Yang et al., 2001)
<i>Fancf</i>	Verringertes Geburtsgewicht, embryonal lethal bei 129/Sv oder C57BL/6 Hintergrund, jedoch lebensfähig bei C57BL/6xFVB Hintergrund	Nicht getestet	129/Sv und C57BL/6 150kb große Deletion auf Chromosom 11 (umfasst Exon 4-14)	(AgoulNIK et al., 2002)
<i>Fancm</i>	Verkürzte Lebensdauer, erhöhte Krebsrate, verminderte Rate an homozygoten Weibchen	Hypersensitivität gegenüber DNA- quervernetzenden Substanzen	FVB und C57BL/6 Deletion Exon 2	(Bakker et al., 2009)
<i>Fancn</i>	Homozygote Tiere sind embryonal lethal, heterozygote ohne Auffälligkeiten	Nicht getestet	129/Ola und C57BL/6N Ersatz von Exon 1 durch β -geo	(Rantakari et al., 2010)
<i>Fanco</i>	Homozygote Tiere sind embryonal lethal, Hypomorphes Allel zeigt keine Auffälligkeiten	Nicht getestet	129/5v und C57BL/6J Deletion Exon 2/3	(Kuznetsov et al., 2007)
<i>Fancp</i>	Mikrophthalmie, erniedrigte Zahl an Blutplättchen und Lymphozyten, nicht- mendelsche Geburtenrate, kleiner, verminderte Fertilität, Entwicklungsstörung im Gehirn, Störungen im Zuckerhaushalt	Hypersensitivität gegenüber DNA- quervernetzenden Substanzen	C57BL/6N Deletion Exon 3	(Crossan et al., 2011)
<i>Fancq</i>	Postnataler Minderwuchs, verkürzte Lebenszeit	Hypersensitivität gegenüber MMC und UV-Strahlen	Genetischer Hintergrund nicht bekannt Deletion Exon 8	(Tian et al., 2004)
<i>Fancr</i>	Embryonal lethal, heterozygote Tiere zeigen keine Auffälligkeiten	Hypersensitivität gegenüber IR	C57BL/6 Deletion Exon 5	(Lim and Hasty, 1996)
<i>Fancs</i>	Embryonal lethal, Tumorgenese abhängig von Mutation	Hypersensitivität gegenüber DNA- quervernetzenden Substanzen	C57BL/6 Deletion Exon 1-3	(Hakem et al., 1998)

Gen	Phänotyp	Zelluläre FA-Merkmale	Genetischer Hintergrund	Erstbeschreibung
<i>Fancu</i>	Embryonal lethal	Hypersensitivität gegenüber γ -Strahlen	C57BL/6 Deletion Exon 3	(Deans et al., 2000)
<i>Fancv</i>	Wachstumsverzögerung, Infertilität, teilweise embryonal lethal	Nicht getestet	C57BL6J/129SvJ Deletion Exon 1 und 2	(Watanabe et al., 2013)

1.5 ZIEL DER ARBEIT

Diese Arbeit ist in zwei große Abschnitte gegliedert. Im ersten Teil wird die Methode *Whole Exome Sequencing* als neues diagnostisches Werkzeug im Zusammenhang mit Fanconi Anämie etabliert. Dadurch können nicht klassifizierte Patienten einer Komplementationsgruppe zugeordnet und gleichzeitig eine genaue Mutationsanalyse durchgeführt werden. Die hierfür nötigen Vorarbeiten, die sich im Wesentlichen auf die Eingruppierung in „*Upstream*“ oder „*Downstream*“ im Sinne des FA/BRCA-Signalwegs beziehen und mit Hilfe von FANCD2-Westernblots oder RAD51-Foci erfolgten, werden ebenfalls in Teilen im Rahmen dieser Arbeit, geleistet.

Der zweite Bereich beinhaltet die Entdeckung und Erforschung neuer FA-Gene und deren Zusammenhang im FA/BRCA-Netzwerk. Hierzu dient ebenfalls das WES, das mittels nachfolgender *in silico* Analysen eine weitere Eingrenzung der Kandidatengene und einen Ausschluss der bereits bekannten FA-Gene zulässt. Anhand anschließender funktioneller Studien, wurden während dieser Arbeit zwei neue Fanconi Anämie Gene bestätigt, die zur weiteren Aufklärung dieser seltenen Erkrankung beitragen. Im Vordergrund steht hier vor allem *RFWD3*, das bisher nicht mit dem FA/BRCA-Netzwerk in Verbindung gebracht wurde. Eine detaillierte Charakterisierung des Gens und der molekulare Zusammenhang mit dem zellulären FA-Phänotyp findet mittels verschiedener *RFWD3*-defizienter Zelllinien statt. Als ein weiteres *in vivo* Modell neben der Patientin, diente ein neu designtes knockout Maus-Modell, das *RFWD3* als neues FA-Gen zusätzlich bestätigt.

2 MATERIAL UND METHODEN

Alle verwendeten Materialien und Methoden sind in den einzelnen Abschnitten der enthaltenen Publikationen explizit dargestellt und erklärt.

2.1 GENOTYPING OF FANCONI ANEMIA PATIENTS BY WHOLE EXOME SEQUENCING: ADVANTAGES AND CHALLENGES

Details zu den verwendeten Materialien und den Methoden der Veröffentlichung „Genotyping of Fanconi Anemia Patients by Whole Exome Sequencing: Advantages and Challenges“ (siehe 3.1.1) befinden sich auf den Seiten 35-40. Explizit beschrieben sind die Durchführung des WES, die Datenanalyse und Filterstrategie. Des Weiteren werden Details zu Sanger Sequenzierung, Westernblot und „Homozygosity Mapping“ zur Validierung der Daten angegeben.

2.2 WHOLE EXOME SEQUENCING REVEALS NOVEL MUTATIONS IN THE RECENTLY IDENTIFIED FANCONI ANEMIA GENE *FANCP*

Die detaillierten Materialien und Methoden der Veröffentlichung “Whole Exome Sequencing reveals novel mutations in the recently identified Fanconi Anemia gene *FANCP*“ (siehe 3.1.2) sind auf den Seiten 49-51 enthalten und im gesamten Text integriert. Sie beschreiben die Analyse der WES Daten und die Mutationsvalidierung mittels Sanger Sequenzierung auf gDNA und cDNA Ebene. Die proteinanalytischen Methoden wie Zellfraktionierungen, Westernblot und Immunopräzipitation, sowie Zellzyklusanalyse sind detailliert im Abschnitt 3.2.2 auf den Seiten 86-90 dargestellt. Details zur Durchführung von Immunofluoreszenz Versuchen finden sich ebenfalls im Abschnitt 3.2.2 auf Seite 88-89.

2.3 MUTATIONS IN *ERCC4*, ENCODING THE DNA-REPAIR ENDONUCLEASE XPF, CAUSE FANCONI ANEMIA

Nähere Angaben zu den verwendeten Materialien und Methoden in der Veröffentlichung „Mutations in *ERCC4*, Encoding the DNA-Repair Endonuclease XPF, Cause Fanconi Anemia“ (siehe 3.2.1) sind in den jeweiligen Bildunterschriften der einzelnen Abbildungen angegeben (siehe Seiten 54-57). Beschrieben sind die Sequenzanalyse nach Sanger und die Auswertung der WES Daten, sowie Wachstumskurven in Abhängigkeit von verschiedenen DNA-quervernetzenden Substanzen oder UV-Strahlung von den Patientenzelllinien, den komplementierten Linien, Referenzzelllinien und MEFs. Des

Weiteren werden Chromosomenbruchanalysen nach MMC oder DEB Schadensinduktion näher beschrieben. Material und Methoden zur Durchführung der NER-Tests finden sich unter Abbildung 3 auf Seite 56. Proteinanalytische Methoden zur Validierung der Nuklease-Aktivität finden sich unter der Abbildung 4 auf Seite 57.

Weitere Validierungsexperimente sind in den *Supplements* dieser Veröffentlichung angegeben und befinden sich auf den Seiten 61-64.

2.4 BIALLELIC MUTATIONS IN THE UBIQUITIN LIGASE RFWD3 CAUSE FANCONI ANEMIA

Die detaillierten Materialien und Methoden der Veröffentlichung „Biallelic mutations in the ubiquitin ligase RFWD3 cause Fanconi anemia“ (siehe 3.2.2) sind auf den Seiten 84-92 explizit dargestellt. Die beschriebenen Methoden umfassen molekulargenetische Arbeitsweisen wie DNA-Extraktion, PCR, die Sequenzanalyse nach Sanger und die Auswertung der WES-Daten. Des Weiteren wurden Chromosomenbruchanalysen unterschiedlicher Zelllinien, sowie Wachstumskurven in Abhängigkeit von verschiedenen DNA-quervernetzenden Substanzen durchgeführt. Außerdem sind die Herstellung komplementierter Zelllinien, DT40 Zelllinien, CRISPR/Cas9 Zelllinien und die genaue Beschreibung der Mausgenerierung enthalten. Zudem werden die proteinanalytischen Untersuchungen mittels Westernblot, Proteinfractionierung, Immunfluoreszenz und Ko-Immunopräzipitation detailliert beschrieben. Die verwendeten Primer, Antikörper und Southernblot-Sonden erscheinen in den *Supplemental Data* auf Seite 110-114.

2.5 THE E3 LIGASE RFWD3 PROMOTES TIMELY REMOVAL OF BOTH RPA AND RAD51 FROM DNA DAMAGE SITES TO FACILITATE HOMOLOGOUS RECOMBINATION

Alle Details zu den verwendeten Materialien und den Methoden der Veröffentlichung “The E3 Ligase RFWD3 promotes timely removal of both RPA and RAD51 from DNA damage sites to facilitate homologous recombination” (siehe 3.2.3) sind auf den Seiten 136 und 167-173 (im Rahmen der *Supplemental Data*) zu finden.

3 ERGEBNISSE

Die folgenden Arbeiten sind von den jeweiligen Journalen zur Veröffentlichung im Rahmen dieser Dissertation als (Co-)Autor genehmigt.

3.1 WHOLE EXOME SEQUENCING ALS NEUE METHODE DER GENOTYPISIERUNG

3.1.1 GENOTYPING OF FANCONI ANEMIA PATIENTS BY WHOLE EXOME SEQUENCING: ADVANTAGES AND CHALLENGES

Genotyping of Fanconi Anemia Patients by Whole Exome Sequencing: Advantages and Challenges

Kerstin Knies^{1*}, Beatrice Schuster^{1*}, Najim Ameziane², Martin Rooimans², Thomas Bettecken³, Johan de Winter², Detlev Schindler¹

¹ Department of Human Genetics, University of Wuerzburg, Wuerzburg, Germany, ² Department of Clinical Genetics, Vrije Universiteit (VU) Medical Center, Amsterdam, The Netherlands, ³ Center for Applied Genotyping Munich, Max-Planck-Institut für Psychiatrie, Munich, Germany

Abstract

Fanconi anemia (FA) is a rare genomic instability syndrome. Disease-causing are biallelic mutations in any one of at least 15 genes encoding members of the FA/BRCA pathway of DNA-interstrand crosslink repair. Patients are diagnosed based upon phenotypical manifestations and the diagnosis of FA is confirmed by the hypersensitivity of cells to DNA interstrand crosslinking agents. Customary molecular diagnostics has become increasingly cumbersome, time-consuming and expensive the more FA genes have been identified. We performed Whole Exome Sequencing (WES) in four FA patients in order to investigate the potential of this method for FA genotyping. In search of an optimal WES methodology we explored different enrichment and sequencing techniques. In each case we were able to identify the pathogenic mutations so that WES provided both, complementation group assignment and mutation detection in a single approach. The mutations included homozygous and heterozygous single base pair substitutions and a two-base-pair duplication in *FANCF*, *-D1*, or *-D2*. Different WES strategies had no critical influence on the individual outcome. However, database errors and in particular pseudogenes impose obstacles that may prevent correct data perception and interpretation, and thus cause pitfalls. With these difficulties in mind, our results show that WES is a valuable tool for the molecular diagnosis of FA and a sufficiently safe technique, capable of engaging increasingly in competition with classical genetic approaches.

Citation: Knies K, Schuster B, Ameziane N, Rooimans M, Bettecken T, et al. (2012) Genotyping of Fanconi Anemia Patients by Whole Exome Sequencing: Advantages and Challenges. PLoS ONE 7(12): e52648. doi:10.1371/journal.pone.0052648

Editor: Markus Schuelke, Charité Universitätsmedizin Berlin, NeuroCure Clinical Research Center, Germany

Received: July 22, 2012; **Accepted:** November 20, 2012; **Published:** December 20, 2012

Copyright: © 2012 Knies et al. This is an open-access article distributed under the terms of the Creative Commons Attribution License, which permits unrestricted use, distribution, and reproduction in any medium, provided the original author and source are credited.

Funding: This publication was funded by the German Research Foundation (DFG) and the University of Wuerzburg in the funding programme Open Access Publishing. The funders had no role in study design, data collection and analysis, decision to publish, or preparation of the manuscript.

Competing Interests: The authors have declared that no competing interests exist.

* E-mail: kerstin.knies@uni-wuerzburg.de (KK); beatrice.schuster@biozentrum.uni-wuerzburg.de (BS)

† These authors contributed equally to this work.

Introduction

Fanconi anemia (FA) is an autosomal or X-chromosomal recessive disorder characterized by variable yet typical developmental malformations, bone marrow failure and predisposition to leukemia and solid tumors. As much as 15 genes define corresponding complementation groups designated as FA-A, -B, -C, -D1, -D2, -E, -F, -G, -I, -J, -L, -M, -N, -O and -P. Biallelic or in the case of FA-B hemizygous mutations in any one of the underlying genes lead to FA, while monoallelic mutations in *FANCD1* (*BRCA2*), *FANCF* (*BRIP1*), *FANCN* (*PALB2*) or *FANCO* (*RAD51C*) increase the risk of carriers for developing breast and ovarian cancer [1]. FA patients commonly suffer from physical abnormalities like short stature, abnormal skin pigmentation, radial ray defects and malformations of the ears, eyes and inner organs. More than 80% of FA patients develop progressive bone marrow failure which makes pancytopenia a highly suggestive clinical feature [2–4]. In addition, FA patients show not only greatly elevated frequencies of myelodysplastic syndrome and acute myeloid leukemia in childhood, but there is also markedly increased prevalence of non-hematologic malignancies. They experience an up to 700-fold higher risk of squamous cell carcinomas especially of the head and neck or anogenital region [3,5]. Other solid tumors are less frequent among FA patients but

a variety of them are still extraordinarily common compared to the general population [5]. The reason for the overall increased cancer risk may be due to the DNA repair defect that characterizes the cellular phenotype [6]. FA cells show elevated rates of chromosomal breakage and typical radial rearrangement figures. These features occur spontaneously but are exaggerated following exposure of cultured cells to DNA crosslinking agents such as diepoxybutane (DEB) or mitomycin C (MMC) [7–9]. Since this hypersensitivity is typical for FA cells, chromosomal breakage analysis is used as a diagnostic tool. Alternatively, cell cycle studies or cellular survival assays using flow cytometric methods are utilized for diagnosis because FA cells are hindered to pass the G2 checkpoint control, accumulate in G2 phase of the cell cycle and show increased death rates after DNA damage induction [10,11]. On the molecular level diagnosis is more complicated. Even though about 60% of FA patients carry mutations in *FANCA* [3], 14 other FA and several associated genes remain that may contain disease-causing defects. While there is so far no cure for FA, knowledge of the individual complementation group and the specific mutations of patients may be important for differential, prenatal or preimplantation diagnosis, prognosis or upcoming gene therapy trials. Biallelic mutations of *FANCD1*, for example, are associated with early-onset acute myelogenous leukemia and blastomas [12,13]. Subtyping of FA patients can be performed by

cell fusion experiments, retroviral complementation analysis or in some cases by Western blotting, but the specific mutations have to be analyzed by Sanger sequencing. Because of the high number of FA and FA-associated genes and because some of these genes have more than 40 exons, DNA sequencing by Sanger technique is becoming increasingly tedious, time-consuming and costly.

Recently, an efficient and reliable technique, Next Generation Sequencing (NGS), emerged to improve and accelerate conventional methods of molecular diagnostics. In the present study we demonstrate the versatility of Whole Exome Sequencing (WES) in four independent projects. The four patients involved had previously been confirmed to be afflicted with FA by non-molecular procedures but were not assigned to any complemen-

tation group and thus lacking accountable mutations. Using WES we genotyped each patient by the identification of their disease-causing mutations in one of three different FA genes. Thus we consider WES an efficient tool to compete with traditional approaches for the molecular diagnosis of FA.

Materials and Methods

Study design

The study scope, patient information and consent form were approved by the Ethical Review Committee of the Medical Faculty of the University of Wuerzburg.

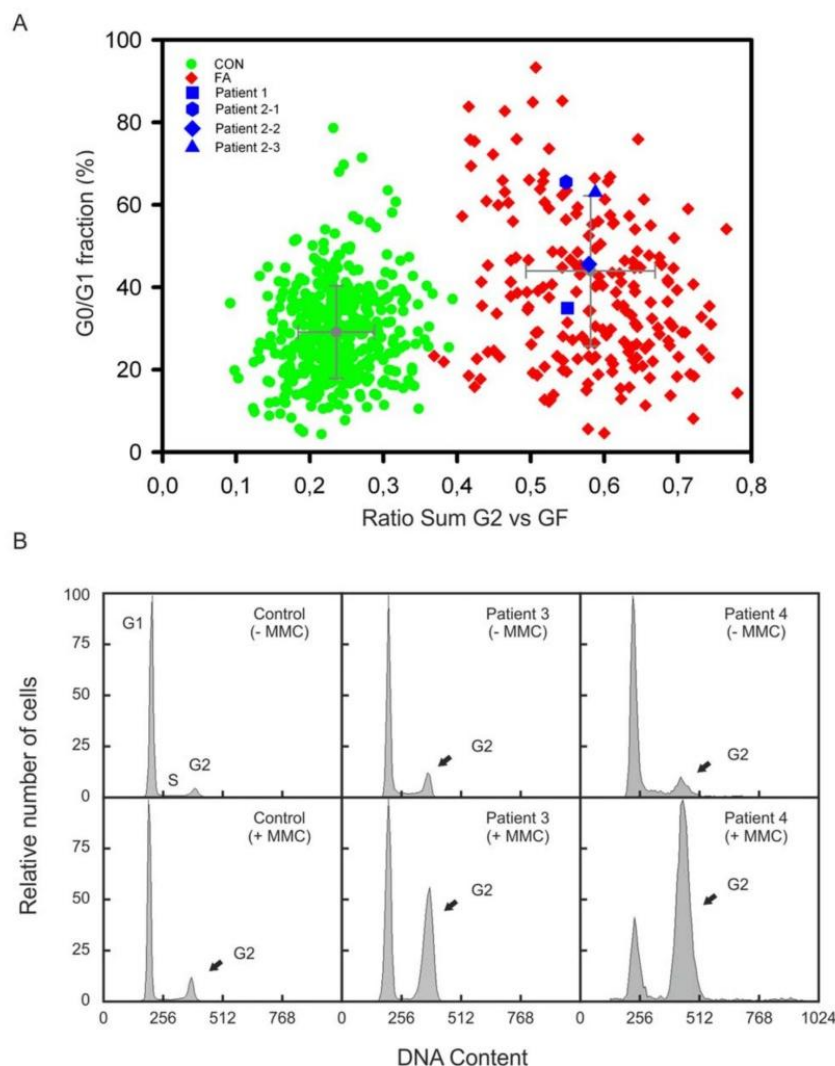


Figure 1. Cell cycle analysis. (A) Graphic presentation of the results of flow cytometric cell cycle analysis. Peripheral blood lymphocytes were exposed to MMC. The ratio “sum of all G2 phases vs. growth fraction” was calculated from individual cultures and plotted against the G0/G1 phase compartment. Cells from patient 1 and the siblings 2–1, 2–2 and 2–3 show high $\sum G2/GF$ ratios (blue squares) similar to those from other persons with FA (red diamonds), but were distinct of normal controls (green dots). (B) Flow histograms of fibroblast cultures from patients 3 and 4 show increased G2 arrest after exposure to MMC, in contrast to a control cell line (arrows). doi:10.1371/journal.pone.0052648.g001

Table 1. Summary of statistical data from four independent WES projects.

	Project 1	Project 2	Project 3	Project 4
Total read number	33,661,920	121,791,357	152,961,886	27,371,419
Average read length	86bp	45bp	40bp	72bp
Reads passing QC	32,251,042	82,558,019	117,526,556	27,371,419
Reads on target (whole exome)	29,837,615 (93%)	67,361,646 (82%)	83,597,787 (71%)	20,707,708 (76%)
Reads on target (FA genes)	17,518	93,806	76,257	31,925
Average exome coverage	22x	77x	71x	36x
Average coverage of FA genes	21x	56x	53x	31x
Total number of variants	20,065	13,466	14,978	18,885
Known SNPs/MNPs	15,213	9,846	13,563	15,469
UV in cs	4,652	3,567	1,386	3,281
UV at ess	200	46	29	136
Homozygous UV (cs+ess)	107	201	44	30
Heterozygous UV (cs+ess)	4,745	3,419	1,371	3,387
Silent UV (cs)	1,012 het	73 hom	286 het	884
Missense UV (cs)	2,736 het	102 hom	920 het	2,289
Nonsense UV (cs)	113 het	1 hom	44 het	23
Unknown InDels (cs+ess)	766 het	24 hom	101 het	77
Multiply heterozygous mutated genes	683	-	207	411
Homozygous mutated genes	-	102	-	-

QC, quality control; UV, unknown variants; cs, coding sequence; ess, essential splice sites; SNP, single nucleotide polymorphism; MNP, multiple nucleotide polymorphism.

The initial number of genes with homozygous or double heterozygous mutations was counted without filtering for low mutation scores or benign sequence changes. doi:10.1371/journal.pone.0052648.t001

Cell cycle analysis

For confirmation or exclusion of FA we used flow cytometric cell cycle analysis as described earlier [11,14].

DNA sample preparation

Genomic DNA was isolated from patient-derived fibroblasts (patients 1, 3 and 4) using the *GeneJetTM* Genomic DNA Purification Kit (Fermentas, patients 1 and 3) or the QIAamp DNA isolation kit (Qiagen, patient 4) following the manufacturer's instructions. For isolation of gDNA from peripheral blood of patient 2-1, his siblings 2-2 and 2-3 and their parents we used a salting-out technique.

Whole Exome Sequencing

Enrichment and sequencing of the exomes of projects 1 to 3 were commissioned to different service providers on an exclusively commercial basis. Sample 1 was enriched by means of the *NimbleGen SeqCap E₂ Human Exome Library v2.0* and sequenced on an *Illumina HiSeq2000*. For sample 2 the *Agilent SureSelect Human All Exon 38 Mb Kit* (hg18) was used together with the *SOLiD* sequencing technology by *Applied Biosystems*. In project 3 WES was performed with *SOLiD4* technology after enrichment using the *Agilent SureSelect Human All Exon 50 Mb Kit* (hg19). Raw data from *Illumina* sequencing were provided in *fq* format. *SOLiD* raw data were provided in *csfasta* format along with *qual* files containing corresponding quality information. For project 4 we used the *SureSelect Human All Exon Kit* (Agilent) targeting approximately 38 Mb, following the manufacturer's instructions. The enriched sample was sequenced on one lane of the *Illumina GAIIx* instrument using a paired-end sequencing protocol, which is available upon request.

Data analysis

Analysis of the WES data of projects 1 to 3 was performed using the alignment and analysis software *NextGENTM* v2.18 by *Softgenetics*. The raw data were filtered for low quality reads before alignment. Based on the enrichment kits being used, reads that passed the quality filter were aligned to the whole human genome hg18 in project 2 and hg19 in projects 1 and 3. The average exome coverage was determined using a complete list of human exons generated by the *UCSC Table Browser*. The same procedure was performed for FA gene coverage. The following analytical steps were performed only with reads that matched exonic regions including exon-intron-boundaries. SNP and insertion/deletion (indels) analysis was done by different filtering steps depending on whether consanguinity was suspected or not. In patient 2-1 of consanguineous descent only homo-/hemizygous variants were taken into account. In patients 1 and 3 with non-consanguineous background genes with at least two heterozygous changes in the DNA sequence were considered to be most likely disease-causing, even though homozygous variants were not completely withdrawn.

For sample 4 we used a data analysis pipeline for the evaluation of single nucleotide variants and small indels, which was comprised of tools freely available on the web. The paired-end reads were mapped by the Burrows-Wheeler Aligner (BWA) [15] to the reference genome built according to NCBI hg19. Subsequently, SNPs and small indels were called using Samtools [16] and Varscan [17]. The resulting list of variants was annotated with Annovar [18] that summons and utilizes information from external databases to assess implications and consequences of a given sequence alteration, such as an ensuing amino acid change, location within a canonical splice site, and information from

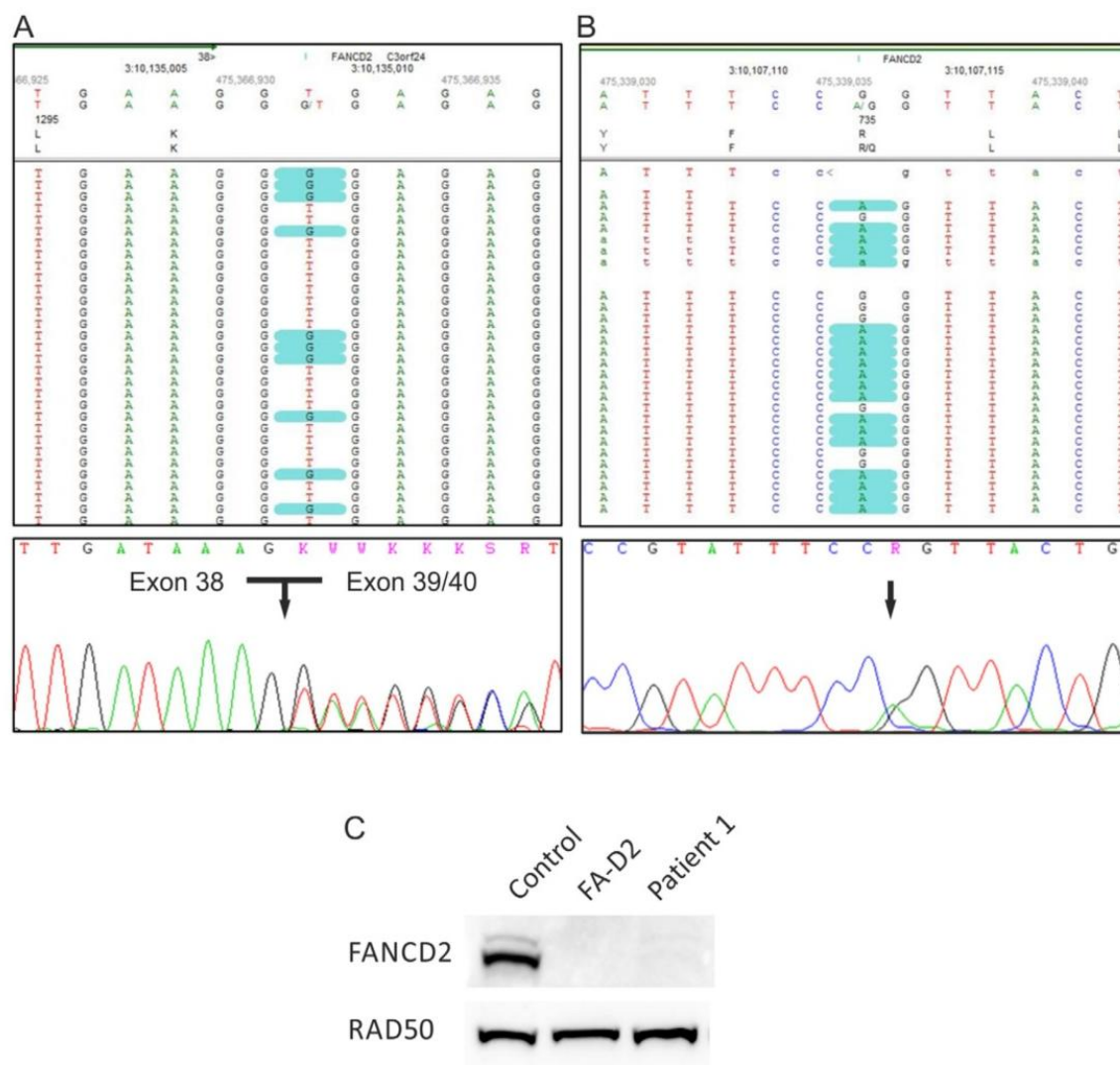


Figure 2. Genotyping of patient 1. (A) The heterozygous *FANCD2* splice site mutation c.3888+2T>G in patient 1. The upper panel demonstrates mutation calling in NGS data format. The lower panel shows an electropherogram of Sanger cDNA sequencing depicting heterozygous skipping of exon 39. (B) The heterozygous *FANCD2* missense mutation c.2204G>A. The upper panel demonstrates the substitution in NGS data format, while the lower panel shows the confirmation by Sanger sequencing of gDNA. (C) An immunoblot shows very faint *FANCD2*-S and -L bands after exposure of fibroblasts from patients 1 to MMC (lane 3). This was similar to other FA-D2 patients (example on lane 2) but contrasted markedly to normal controls (example on lane 1). RAD50 was used as loading control. doi:10.1371/journal.pone.0052648.g002

dbSNP along with the SNP frequency if available. Finally, a manual filtering step was carried out to prioritize relevant mutations.

Filtering strategy

Holding for all samples, the variant detection frequency was set at a minimum of 20% of the reads covering any aberration. A minimum coverage by 10 reads was set as threshold for any variant to be considered a real mutation. In each case all variants listed in the most recent version of the NCBI (National Center for Biotechnology Information) dbSNP database were excluded as well as silent mutations. Low frequency frameshift and truncating

mutations in any FA gene were considered pathogenic. Unreported non-synonymous amino acid variants were analyzed *in silico* by Align-GVGD (data not shown), MutationTaster (<http://www.mutationtaster.org>), Polyphen-2 (<http://genetics.bwh.harvard.edu/pph2>) and SIFT (<http://sift.jcvi.org>) to assess any potentially damaging effect. Variants passing these filtering steps were considered to be most likely disease-causing and forwarded to validation process by Sanger sequencing and other techniques.

Genotyping FA Patients by Whole Exome Sequencing

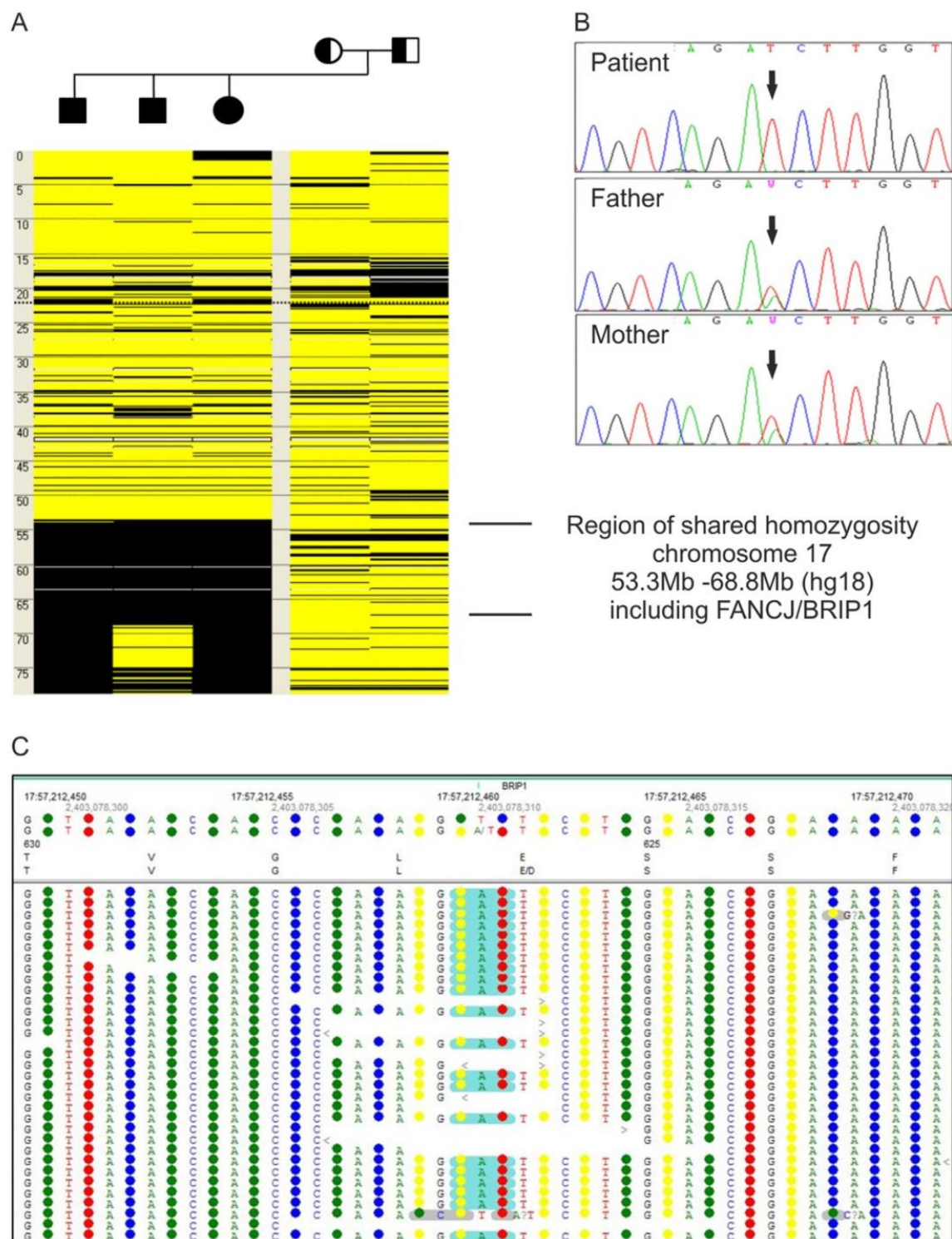


Figure 3. Genotyping of patient 2. (A) Homozygous mutation call c.1878A>T in *FANCF* detected in NGS data of patient 2-1. (B) Autozygosity mapping with SNP data of the family of project 2. The figure schematically presents chromosome 17 (positions in Mb) of each family member. Heterozygous SNP calls are displayed in yellow, homozygous calls in black. The three affected siblings share a homozygous region between 53.3 Mb

and 68.8 Mb. (C) Confirmation of homozygosity of the mutation in patient 2-1 and heterozygosity in his parents by Sanger sequencing electropherograms, consistent with Mendelian segregation.
doi:10.1371/journal.pone.0052648.g003

Sanger sequencing

Potential mutations were verified by Sanger sequencing generally using an *Applied Biosystems 3130xl* instrument. Primer sequences and PCR conditions are available upon request.

Immunoblotting

FANCD2 expression analysis was performed with whole protein extracts isolated from patient-derived fibroblasts. Cell lines were treated with hydroxyurea or MMC before analysis. We used primary antibodies including mouse monoclonal anti-FANCD2 (sc20022, Santa Cruz Biotechnology), mouse monoclonal anti-RAD50 (GTX70228, GeneTex), rabbit polyclonal anti-RAD51 (ab63801, Abcam), rabbit polyclonal anti-FANCI (NB 100-416A, Novus) and mouse monoclonal anti-Vinculin (sc-25336, Santa Cruz Biotechnology). Secondary antibodies included Alexa Fluor 594 goat anti-rabbit IgG (H+L) (A11012, Invitrogen), Goat pAb to

rabbit IgG (HRP) (ab97200, Abcam), Donkey pAb to mouse IgG (HRP) (ab98665, Abcam).

Autozygosity mapping

Autozygosity mapping was performed with SNP data generated with the Illumina SNP array HumanHap300v2. Genotypes were analyzed using AutoSNPa software [19].

Results

Confirmation of the FA diagnosis

In each project the clinical diagnosis was confirmed by flow-cytometric cell cycle analysis. In patients 1 and 2 FA was evident from studies of peripheral blood lymphocyte cultures. After 72 h incubation with 10 ng/ml MMC the ratio "sum of all G2 phases vs. growth fraction" was above 0.4 which is characteristic of FA patients (Fig. 1A) [20]. Patients 3 and 4 showed distinct cell accumulations in the G2 phase (>20%) in fibroblast cultures

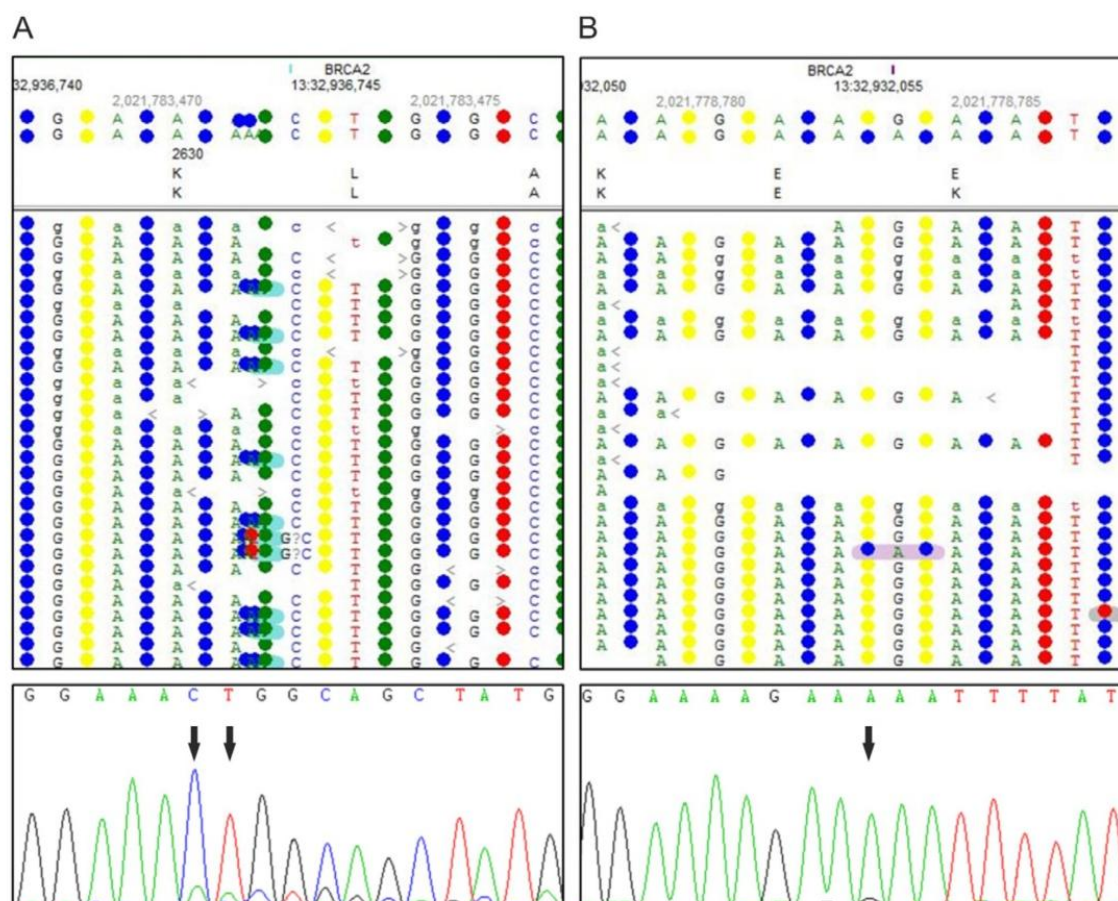


Figure 4. Genotyping of patient 3. (A) NGS data in the upper panel show the insertion c.7890_7891insAA in *FANCD1* detected in patient 3. The electropherogram in the lower panel demonstrates corresponding validation by Sanger sequencing. (B) The upper panel misleadingly displays the single-bp substitution c.7795G>A in the NGS data of patient 3 as a SNP, highlighted in pink. Confirmation by Sanger sequencing is shown below.
doi:10.1371/journal.pone.0052648.g004

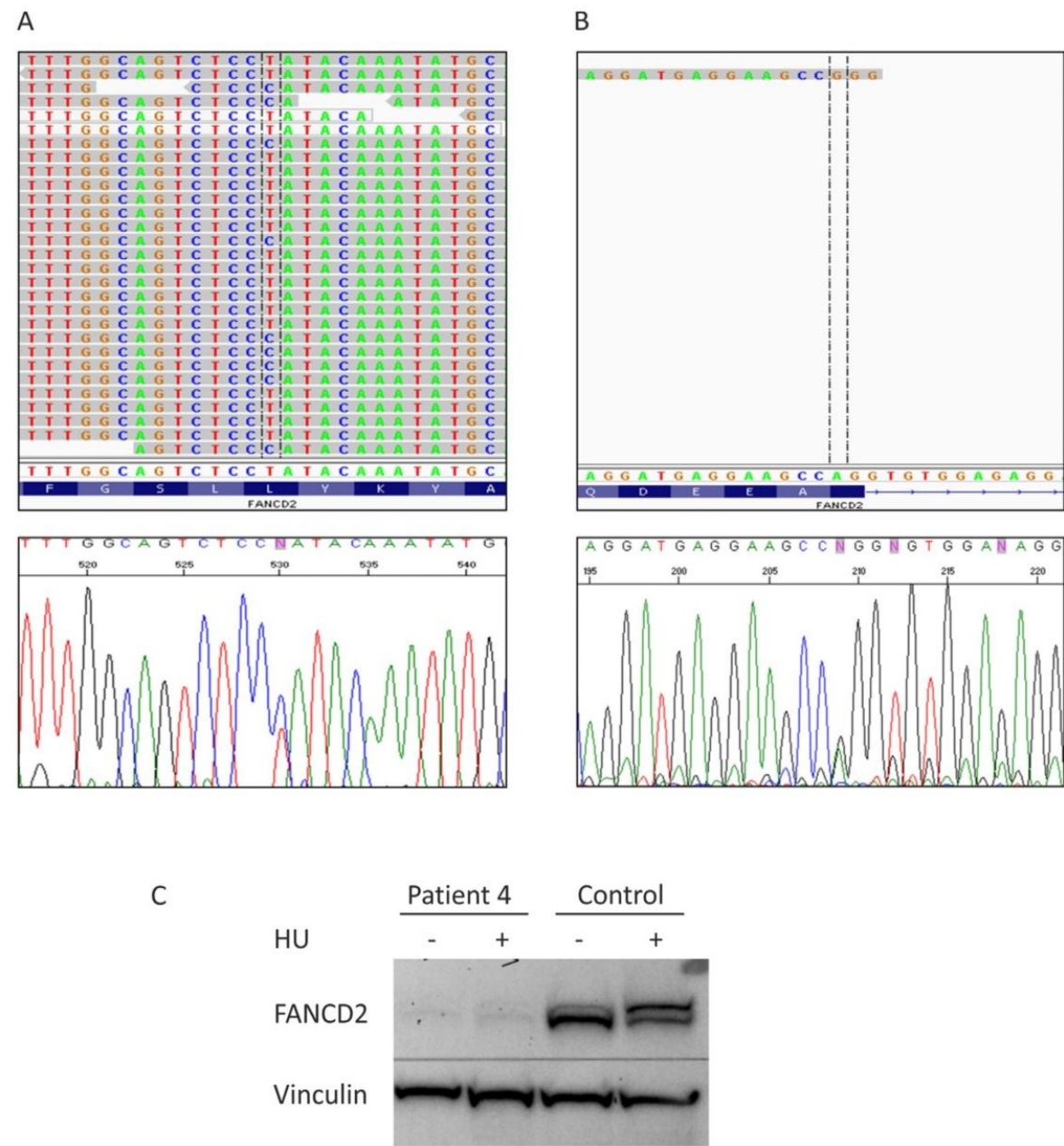


Figure 5. Genotyping of patient 4. (A) Displayed is the *FANCD2* mutation c.1370T>C in patient 4 in NGS data as well as validated by Sanger sequencing. (B) The upper panel shows NGS data with low coverage of *FANCD2* exon 5 containing the substitution c.376A>G. The electropherogram in the lower panel depicts validation by Sanger sequencing. (C) Hydroxyurea (HU) treated (+) and untreated (–) fibroblasts of patient 4 show very low levels of both the S and L species of residual *FANCD2* protein. Vinculin was used as loading control.
doi:10.1371/journal.pone.0052648.g005

exposed to 12 ng/ml MMC for 48 h, likewise consistent with other FA patients (Fig. 1B).

Mutation detection by WES and validating experiments

Statistical data of each WES project are summarized in Table 1 and Table S2. The exome was covered on average between 22x

and 77x. The FA and FA-associated genes with homozygous or at least two potentially heterozygous mutations were first assessed. Assignment of the mutations to different alleles and screening for their pathogenicity revealed the following results.

Project 1. We employed 3 µg gDNA isolated from cultured fibroblasts of patient 1 to enrich the whole exome. WES revealed

two heterozygous mutations with a score ≥ 10 (probability 1:100 for being false positive) exclusively in *FANCD2*. They included the single-base substitution c.2314G>T, resulting in a premature stop codon at amino acid position p.772, and the canonical splice site change c.3888+2T>G in exon 38. Sanger sequencing confirmed the splice site alteration in gDNA and showed an *in frame* skipping of exon 39 at the cDNA level (Fig. 2A). Because of the pseudogene *FANCD2-P2*, containing an incomplete copy of the active gene region [21], validation of the nonsense mutation by Sanger sequencing was performed on long range PCR product (exon 22 to exon 26). Re-sequencing of this super-amplicon did not confirm the substitution c.2314G>T (Fig. S1A). Thus we concluded that this variant had occurred in the pseudogene and therefore could not be causative of FA in that patient. By decreasing the filter settings we additionally detected the missense substitution c.2204G>A in exon 24 resulting in the amino acid change p.R735Q. Even though this base is also present in the pseudogene sequence, its assessment by gene-specific super-amplification rendered it an authentic *FANCD2* mutation (Fig. 2B). We confirmed the maternal segregation of p.R735Q, whereas the splice site change was not present in maternal gDNA and may have occurred *de novo* or was, more likely, inherited from the father, of whom no material was available. Finally, decreased abundance of FANCD2 protein in the patient's cells confirmed our DNA sequencing results (Fig. 2C).

Project 2. Parallel to WES we performed a genome-wide SNP study in patient 2–1, his two affected siblings (2–2, 2–3) and their parents. Autozygosity mapping using these data revealed a large homozygous region on chromosome 17 (Fig. 3A). The whole exome was enriched from 3 μ g gDNA, isolated from peripheral blood of patient 2–1. Analysis of the color-spaced *SOLID4* sequencing data revealed the homozygous single base substitution c.1878A>T in exon 13 of *FANCF* (Fig. 3B) compatible with the outcome of the disease gene mapping. This point mutation results in the amino acid change p.E626D (Fig. 3B) that is predicted to be pathogenic (Table S1). Sanger sequencing confirmed the homozygous mutation of the patient (Fig. 3C) and his siblings (data not shown). These results and the heterozygous detection of the mutation in both parents (Fig. 3C) were consistent with Mendelian segregation. Additionally we could detect reduced FANCF protein levels by Western blot analysis of whole protein extracts from patient derived-cell lines (data not shown).

Project 3. 3 μ g gDNA of patient 3 were isolated from fibroblasts. Initial analysis of the WES data failed to show FA or FA-associated genes with biallelic mutations. Re-examination of all unknown variants and listed SNPs resulted in the identification of a 2-bp insertion c.7890_7891dupAA in exon 17 of *BRCA2/FANCD1* (Fig. 4A) with the effect p.L2631Nfs16X. Three additional variants were found in the same gene, of which only c.7795G>A was predicted to be pathogenic (Fig. 4B, Table S1). The SNP rs80359682 listed at this position is a deletion of three bases (c.7795_7797delGAA) in exon 16, which is of unknown pathogenicity, whereas our detected single-bp substitution results in the probably damaging missense mutation p.E2599K. We confirmed both mutations of patient 3 by Sanger sequencing, even though the allele carrying the insertion was detectable only at a very low level (Fig. 4A). In accordance with those results we detected proficient FANCD2 monoubiquitination and impaired RAD51 foci formation in the patient derived fibroblastic cell line (data not shown).

Project 4. In contrast to projects 1 to 3, where data have been analyzed by means of the alignment and analysis software *NextGENe*TM v2.18 by *Softgenetics*, we used for project 4 an in-house variation detection pipeline to score sequence variants [21].

We focused on rare variants within the coding and splice site regions of all known FA genes. Only one already reported heterozygous base substitution was detected in *FANCD2* exon 16, c.1370T>C (p.L457P), which had previously been recognized to be pathogenic [22]. Initially we failed to detect a second mutation in *FANCD2*. After visual inspection of the mapped reads in the IGV browser, *FANCD2* exon 5 was shown to be covered by a single read. Therefore, the data appeared unreliable for mutation detection. Subsequent Sanger sequencing of that exon demonstrated a c.376A>G base substitution resulting in another missense mutation p.S126G, that had previously been shown to be pathogenic and affects splicing [23] (Fig. 5A). Western blotting revealed distinct deficiency of the FANCD2 protein (Fig. 5B).

Discussion

The present study proposes the application of WES for the molecular diagnosis of FA. Major concerns with WES are ethical issues, less its performance. Potentially, WES data could be used to analyze any gene, or even all genes, for any purpose. In our projects the patients had given informed consent for FA diagnostics. We addressed and resolved the discrepancy to WES in the way that we used the whole body of data only for quality control, statistical analyses, and to apply general filtering settings. For mutation screening we solely regarded FA and FA-associated genes.

We performed four independent sequencing projects with disparate exome enrichment and sequencing technologies. Although the performances differed slightly, we were able to identify the disease causing mutations in all index patients. Except for the mutations in patient 4, all of the detected pathogenic variants had not yet been listed in the *Fanconi Anemia Mutation Database* (<http://www.rockefeller.edu/fanconi/>) such that we consider the identification of missense, nonsense and splice site mutations as well as a 2-bp insertion in *FANCD1*, *FANCD2* and *FANCF* by WES a challenging task and major accomplishment. The successful outcome led us to conclude that WES generally is a reliable tool for the molecular diagnosis of FA. It also proved to be efficient in time and adequate in expense. Including sample quality control, target enrichment, sequencing and basic bioinformatics each of our projects was brought to completion within two to three months. Alignment and mutation calling afforded another few days, followed by validation processes. The cost of each of the four projects was highly variable and ranged from 800\$ to 4500\$, but decreased in tendency over time. Sanger sequencing of all FA genes would have exceeded the projects' current term and cost several times. Sanger sequencing of the 43 FANCA exons only would be comparable to the price of exome sequencing but would fail to detect the mutation in more than 40% of cases. Enrichment of the FA gene regions followed by NGS would be an effective alternative, because it could increase the locus-specific coverage and decrease cost and sequencing time. Although this approach has been published recently [21], so far this application is not commercially available for the FA genes. In some instances WES holds some advantages compared to a target enrichment approach, because there are still FA patients who cannot be assigned to any of the reported complementation groups. In agreement with the patient WES data can be used for further screenings not only including FA-associated genes such as FAAP100, but also of other candidate genes. An additional agreement between patient and the diagnostic lab addressing this issue is required.

In all presented cases we found point mutations or small insertions to be disease-causing. Therefore we can safely assume

that those patients do not carry additional large insertions or deletions, which would have been difficult to identify by WES. In the case of large and complex variations this technical drawback can, however, be avoided if WES is combined with MLPA or microarray techniques. Additionally a recent report by Ameiziane et al. (2012) detected large deletions after NGS of enriched FA gene regions by evaluating the Log2 ratio of the local read depth divided by a read depth reference [21]. None of the FA patients in our four projects had mosaicism in the hematopoietic system as shown by diagnostic procedures preceding WES. If there was indication for such a situation it would have been appropriate to use fibroblast DNA for WES. Deep intronic mutations, which could affect splicing, might be the only kind of sequence changes that are not detectable by WES. However those mutations are rare in FA and would anyway be difficult to identify by classical approaches. Our study also raised technical issues and revealed methodical difficulties that should be addressed. For each project we analyzed the exome coverage and in particular the coverage of the FA genes (Table 1). Even though the average exome coverage in the *SureSelect* enrichment projects clearly exceeded the coverage in the *NimbleGen* project, we found coverage of the FA gene regions in the latter to be more consistent and complete (Table S2). A similar observation was reported by Clark et al. (2011) for the whole exome in general. Most of the entirely unsequenced exons in our study had a high GC or high AT content leading to the conclusion that excess GC content is still a limiting factor for efficient hybridization and amplification during target enrichment [24]. In project 4 initially only one pathogenic mutation was detected, while the other mutation was missed because of insufficient coverage. In this case the GC and AT content of *FANCD2* exon 5, where the second mutation later was identified, is balanced with 44% and 56%, but probably the high AT content of the adjacent intron regions that were included in enrichment may explain the low coverage. Nevertheless, the identification of the first mutation led to close examination of that gene and subsequent identification of the second mutation. On the other hand it is a rare but recurrent experience that a single heterozygous mutation in one FA gene may accompany compound heterozygous, disease-causing mutations in another FA gene.

We observed a lower rate of sequencing errors in *SOLiD* data. The two-base-encoding technology leads to lower rates of false positive or false negative base calls and facilitates the discrimination of sequencing errors from authentic mutations [25,26]. Incomplete or even contradictory gene databases can complicate the validation process and can cause confusion by wrong and incomplete or misleading mutation calling. In project 3 we experienced a problem even with SNP databases. A truly pathogenic mutation was designated as a SNP because there was a known polymorphism that included the mutated base pair. To avoid such pitfalls as far as possible and because mutation screening becomes easier the more polymorphisms are excluded, we recommend using always the latest version of the dbSNP database in combination with minor allele frequencies and information from other sources such as the 1000 Genomes project.

Another issue to consider during *in silico* pathogenicity assessment is the choice of mutation prediction software. For the mutations described in this study we compared the performance of three different mutation prediction tools (*SIFT*, *PolyPhen-2* and *MutationTaster*). While *SIFT* and *PolyPhen-2* often failed to ascertain the pathogenic effect of the mutations, *MutationTaster* generally was able to provide a reliable prognosis for all genes and every type of mutations.

Finally, in this and other NGS studies we noticed that the existence of pseudogene sequences can complicate the detection of

genuine mutations residing in functional genes and thus may result in false positives. In project 1 re-sequencing showed that the c.2314G>T mutation call in *FANCD2* was due to incorrect mapping of the variant containing reads, which should have mapped to the pseudogene, *FANCD2-P2*. The missense mutation c.2204G>A likewise represented *FANCD2-P2* pseudogene sequence. In this case it proved to be a true *FANCD2* mutation at the same time. In that same exon we identified two more base substitutions representing pseudogene sequence but the corresponding reads were misleadingly mapped to *FANCD2*. Only gene-specific re-sequencing resolved the correct sequence (data not shown). We recognized this problem not only in FA genes. For example, another project had revealed a hemizygous deletion including the *CDC27* locus, but WES unexpectedly showed heterozygous base variants of that gene. On closer inspection we found three related pseudogenes, containing the complete cDNA sequence of *CDC27* from exon 3 to 14. This led us to re-check the putative gene variants by Sanger sequencing. All of them turned out to be false positives attributable to pseudogene sequences (data not shown). We suggest that this problem may be due to the short read length produced by *SOLiD* and *Illumina* NGS and ambiguous mapping during alignment with the genome. Pseudogenes are characterized by high sequence similarity with their corresponding functional genes and therefore ambivalent mapping in the analysis of NGS data cannot always be avoided. In terms of FA genes, special attention needs to be paid to *FANCD2* for which only *FANCD2-P1* LOC100421239 is listed in the NCBI database but not the other reported pseudogene, *FANCD2-P2* [22]. For *FANCL* and the FA-associated gene *MHFI* at least partial copies have been disclosed.

Notwithstanding the challenges with WES data analysis, we would recommend it as a valuable tool for FA genotyping. In our opinion, WES, if carefully applied, is able to compete with classical molecular approaches in diagnostics and research not only for FA but generally for other disorders with locus heterogeneity.

Supporting Information

Figure S1 Validation by Sanger technique. (A) Sanger sequencing of cDNA revealed a false positive result of c.2314 G>T in *FANCD2* being a mutation of patient 1 due to interference with the pseudogene *FANCD2-P2*. (B) Confirmation of Mendelian segregation of c.2204 G>A and c.3888+2 T>G. The missense mutation is inherited from the mother. The healthy sister is a heterozygous mutation carrier. The canonical splice site change must have occurred *de novo* or been inherited from the father whose DNA was not available. It was not detectable in other family members. (DOCX)

Table S1 Predicted effect of the mutations detected in *FANCD1*, *FANCD2* and *FANCF*. (DOCX)

Table S2 Coverage of FA genes. (DOCX)

Acknowledgments

We thank Richard Friedl and Birgit Gottwald, Wuerzburg, for excellent technical assistance.

Author Contributions

Conceived and designed the experiments: BS NA DS JW. Performed the experiments: BS KK NA. Analyzed the data: BS KK NA. Contributed reagents/materials/analysis tools: TB MR DS JW. Wrote the paper: BS KK DS.

References

1. Vuorela M, Pykäs K, Hartikainen JM, Sundfeldt K, Lindblom A, et al. (2011) Further evidence for the contribution of the RAD51C gene in hereditary breast and ovarian cancer susceptibility. *Breast Cancer Res Treat* 130: 1003–1010.
2. Alter BP, Kupfer G (1993) Fanconi Anemia. In: Pagon RA, Bird TD, Dolan CR, Stephens K, editors. *GeneReviews*. Seattle (WA).
3. Auerbach AD (2009) Fanconi anemia and its diagnosis. *Mutat Res* 668: 4–10.
4. Seif AE (2011) Pediatric leukemia predisposition syndromes: clues to understanding leukemogenesis. *Cancer Genet* 204: 227–244.
5. Rosenberg PS, Greene MH, Alter BP (2003) Cancer incidence in persons with Fanconi anemia. *Blood* 101: 822–826.
6. Deans AJ, West SC (2011) DNA interstrand crosslink repair and cancer. *Nat Rev Cancer* 11: 467–480.
7. Auerbach AD (1993) Fanconi anemia diagnosis and the diepoxybutane (DEB) test. *Exp Hematol* 21: 731–733.
8. Cervenka J, Arthur D, Yasis C (1981) Mitomycin C test for diagnostic differentiation of idiopathic aplastic anemia and Fanconi anemia. *Pediatrics* 67: 119–127.
9. Schroeder TM, Anschutz F, Knopp A (1964) [Spontaneous chromosome aberrations in familial panmyelopathy]. *Humangenetik* 1: 194–196.
10. Schindler D, Kubies M, Hoehn H, Schinzel A, Rabinovitch PS (1987) Confirmation of Fanconi's anemia and detection of a chromosomal aberration (1Q12-32 triplication) via BrdU/Hoechst flow cytometry. *Am J Pediatr Hematol Oncol* 9: 172–177.
11. Seyschab H, Friedl R, Sun Y, Schindler D, Hoehn H, et al. (1995) Comparative evaluation of diepoxybutane sensitivity and cell cycle blockage in the diagnosis of Fanconi anemia. *Blood* 85: 2233–2237.
12. Wagner JE, Tolar J, Levran O, Scholl T, Deffenbaugh A, et al. (2004) Germline mutations in BRCA2: shared genetic susceptibility to breast cancer, early onset leukemia, and Fanconi anemia. *Blood* 103: 3226–3229.
13. Hirsch B, Shimamura A, Moreau L, Baldinger S, Hag-alshiekh M, et al. (2004) Association of biallelic BRCA2/FANCD1 mutations with spontaneous chromosomal instability and solid tumors of childhood. *Blood* 103: 2554–2559.
14. Vaz F, Hanenberg H, Schuster B, Barker K, Wick C, et al. (2010) Mutation of the RAD51C gene in a Fanconi anemia-like disorder. *Nat Genet* 42: 406–409.
15. Li H, Durbin R (2009) Fast and accurate short read alignment with Burrows-Wheeler transform. *Bioinformatics* 25: 1754–1760.
16. Li H, Handsaker B, Wysoker A, Fennell T, Ruan J, et al. (2009) The Sequence Alignment/Map format and SAMtools. *Bioinformatics* 25: 2078–2079.
17. Koboldt DC, Chen K, Wylie T, Larson DE, McLellan MD, et al. (2009) VarScan: variant detection in massively parallel sequencing of individual and pooled samples. *Bioinformatics* 25: 2283–2285.
18. Wang K, Li M, Hakonarson H (2010) ANNOVAR: functional annotation of genetic variants from high-throughput sequencing data. *Nucleic Acids Res* 38: e164.
19. Carr IM, Flintoff KJ, Taylor GR, Markham AF, Bonthron DT (2006) Interactive visual analysis of SNP data for rapid autozygosity mapping in consanguineous families. *Hum Mutat* 27: 1041–1046.
20. Schindler D, Friedl R, Gavvovidis I, Kalb R, Neveling K, et al. (2007) Applications of Cell Cycle testing in Fanconi Anemia. In: Schindler D, H H, editors. *Fanconi Anemia – A Paradigmatic disease for the understanding of cancer and aging*. Basel: Karger. 110–130.
21. Ameiziane N, Sie D, Dentre S, Ariyurek Y, Kerkhoven L, et al. (2012) Diagnosis of fanconi anemia: mutation analysis by next-generation sequencing. *Anemia* 2012: 132856.
22. Kalb R, Neveling K, Hoehn H, Schneider H, Linka Y, et al. (2007) Hypomorphic mutations in the gene encoding a key Fanconi anemia protein, FANCD2, sustain a significant group of FA-D2 patients with severe phenotype. *Am J Hum Genet* 80: 895–910.
23. Timmers C, Taniguchi T, Hejna J, Reifsteck C, Lucas L, et al. (2001) Positional cloning of a novel Fanconi anemia gene, FANCD2. *Mol Cell* 7: 241–248.
24. Clark MJ, Chen R, Lam HY, Karczewski KJ, Euskirchen G, et al. (2011) Performance comparison of exome DNA sequencing technologies. *Nat Biotechnol* 29: 908–914.
25. Shendure J, Ji H (2008) Next-generation DNA sequencing. *Nat Biotechnol* 26: 1135–1145.
26. Mardis ER (2008) The impact of next-generation sequencing technology on genetics. *Trends Genet* 24: 133–141.

Supporting information

Table S1. Predicted effect of the mutations detected in *FANCD1*, *FANCD2* and *FANCI*

	Mutation Taster	Poly-Phen 2	SIFT
FANCD2 c.2204G>A	55 % disease causing	100 % probably damaging	damaging, score 0.01
FANCD2 c.3888+2T>G	72 % Polymorphism, Splice Site Change	-	-
FANCD2 c.1370T>C	86 % Polymorphism	100 % probably damaging	damaging, score 0
FANCD2 c.376A>G	74 % Polymorphism	100 % probably damaging	damaging, score 0.02
FANCI c.1878A>T	71 % disease causing	100 % probably damaging	-
FANCD1 c.7890insAA	100 % disease causing, NMD, FS	-	-
FANCD1 c.7795G>A	83 % disease causing, rs80359682	-	damaging, score 0.01 rs 80359682

The percentages denominate probability of being pathogenic.

Supporting information

Table S2. Coverage of FA genes.

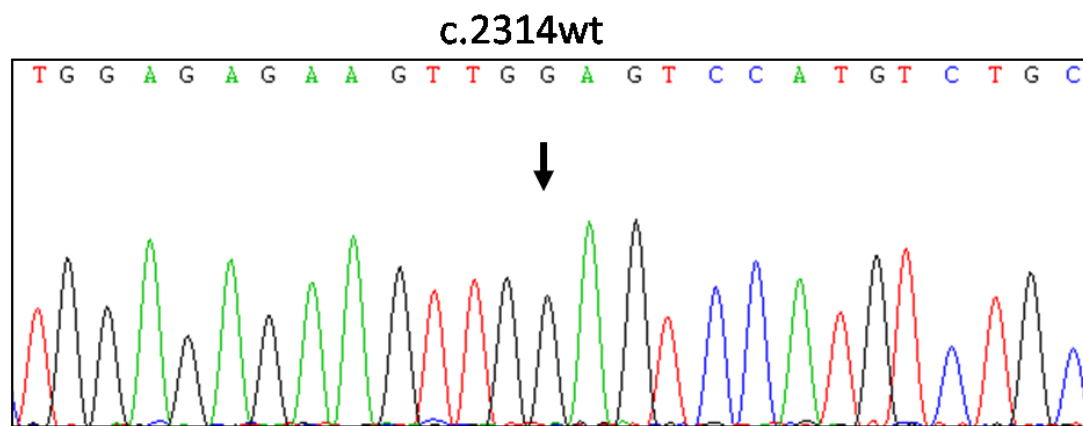
	Project 1	Project 2	Project 3	Project 4
FANCA	1 (79 %)	1 (79 %)	1 (79 %)	1 (79 %), 22 (63 %)
FANCB				
FANCC				
FANCD1		12 (31 %)		
FANCD2				5 (44 %)
FANCE	1 (76 %)	1 (76 %)	1 (76 %)	1 (76 %)
FANCF				
FANCG				
FANCI		23 (36 %)		23 (36 %)
FANCI				
FANCL				
FANCM				
FANCN				
FANCO				
FANCP				8 (72 %)

Listed are the completely unsequenced exons of 15 FA genes in the four independent WES projects. Corresponding GC contents are given in percent.

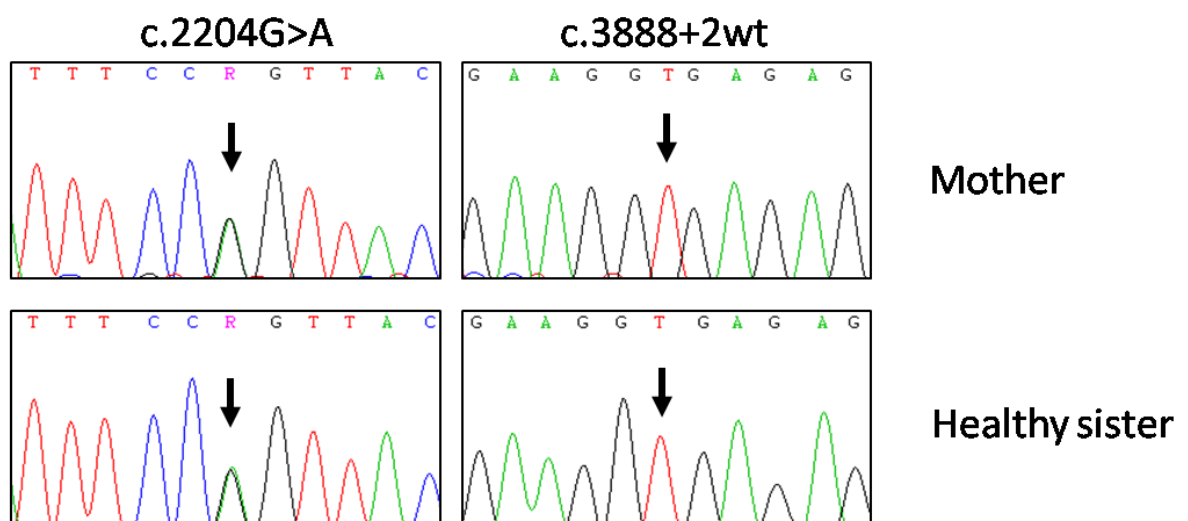
Supporting information

Figure S1

A



B



3.1.2 WHOLE EXOME SEQUENCING REVEALS UNCOMMON MUTATIONS IN THE RECENTLY IDENTIFIED FANCONI ANEMIA GENE *SLX4/FANCP*

BRIEF REPORT

Human Mutation



Whole Exome Sequencing Reveals Uncommon Mutations in the Recently Identified Fanconi Anemia Gene *SLX4/FANCP*

Beatrice Schuster,^{1*} Kerstin Knies,^{1†} Chantal Stoecker,² Eunike Velleuer,³ Richard Friedl,¹ Birgit Gottwald-Mühlhauser,¹ Johan P. de Winter,² and Detlev Schindler¹

¹Department of Human Genetics, University of Wuerzburg, Wuerzburg, Germany; ²Department of Clinical Genetics, Vrije Universiteit (VU) Medical Center, Amsterdam, The Netherlands; ³Department of Pediatric Hematology, Oncology and Clinical Immunology, University of Duesseldorf School of Medicine, Duesseldorf, Germany

Communicated by Georgia Chenevix-Trench

Received 6 June 2012; accepted revised manuscript 7 September 2012.

Published online 3 October 2012 in Wiley Online Library (www.wiley.com/humanmutation). DOI: 10.1002/humu.22221

ABSTRACT: Fanconi anemia (FA) is a rare genetic disorder characterized by congenital malformations, progressive bone marrow failure (BMF), and susceptibility to malignancies. FA is caused by biallelic or hemizygous mutations in one of 15 known FA genes, whose products are involved in the FA/BRCA DNA damage response pathway. Here, we report on a patient with previously unknown mutations of the most recently identified FA gene, *SLX4/FANCP*. Whole exome sequencing (WES) revealed a nonsense mutation and an unusual splice site mutation resulting in the partial replacement of exonic with intronic bases, thereby removing a nuclear localization signal. Immunoblotting detected no residual *SLX4* protein, which was consistent with abrogated interactions with XPF/ERCC1 and MUS81/EME1. This cellular finding did not result in a more severe clinical phenotype than that of previously reported FA-P patients. Our study additionally exemplifies the versatility of WES for the detection of mutations in heterogenic disorders such as FA.

Hum Mutat 34:93–96, 2013. © 2012 Wiley Periodicals, Inc.

KEY WORDS: Fanconi anemia; *FANCP*, *SLX4*; nuclear localization signal

Fanconi anemia (FA; MIM# 227650) is an autosomal or X-chromosomal recessive disorder first described in 1927 by the Swiss pediatrician Guido Fanconi [Lobitz and Velleuer, 2006]. Recently, the carrier frequency in the United States was estimated to be 1:181, corresponding to an incidence of FA of less than 1:100,000 [Rosenberg et al., 2011]. Higher rates have been reported for certain ethnicities or due to isolation or founder effects [Callen et al., 2005]. The clinical manifestations of FA are variable yet characteristic. Typical congenital malformations include short

stature, skin hyper- or hypopigmentations, radial ray defects, and malformations of ears, eyes, and inner organs. Most FA patients develop progressive bone marrow failure in childhood. Furthermore, they have an increased risk of myelodysplastic syndrome (MDS) and hematological malignancies, in particular acute myelogenous leukemia [Alter and Kupfer, 1993; Rosenberg et al., 2003; Seif, 2011]. In addition, they are predisposed for solid tumors occurring in young adulthood. FA patients have an up to 700-fold increased risk for squamous cell carcinomas, which arise most frequently in the mucosa of the head and neck or genital regions [Rosenberg et al., 2008, 2011]. The reasons for the increased susceptibility of FA patients to neoplasms are not fully understood. Most likely, this is due to a DNA repair defect and genomic instability that characterize the cellular phenotype [Deans and West, 2011]. FA cells show highly increased rates of chromosomal breakage especially after exposure to DNA-crosslinking agents, accumulate in the G2 phase of the cell cycle, and encounter diminished survival [Auerbach, 1993; Schindler et al., 1987; Schroeder et al., 1964]. Like the clinical phenotype, the genetic background of FA is very heterogeneous. To date, 15 complementation groups (FA-A, -B, -C, -D1, -D2, -E, -F, -G, -I, -J, -L, -M, -N, -O, and -P) have been delineated. The first identified FA gene, *FANCC* (MIM# 613899), was reported in 1992 [Strathdee et al., 1992]. Since 2000, nearly every year a new FA gene has been added, most recently *FANCP* (MIM# 613951), encoded by the gene *SLX4/BTBD12* (approved symbol *SLX4*; MIM# 613278) [Kim et al., 2011; Stoecker et al., 2011]. Its product interacts with different structure-specific endonucleases such as XPF/ERCC1 (MIM#s 133520, 126380), MUS81/EME1 (MIM#s 606591, 610885) and the Holliday junction resolvase *SLX1*, by coordinating their activity in DNA repair and recombination [Andersen et al., 2009]. *FANCP* is involved in the FA/BRCA pathway and the network of DNA interstrand crosslink (ICL) repair. A key step in this pathway is *FANCD2* (MIM# 613984) and *FANCI* (MIM# 611360) monoubiquitination through the FA core complex following DNA damage and replication fork stalling. *FANCP* acts downstream of these protein modifications, similar to *FANCD1* (MIM# 600185), *FANCI* (MIM# 605882), *FANCN* (MIM# 610355), and *FANCO* (MIM# 602774). *FANCP*-mutated cells are proficient of RAD51 foci formation, unlike FA-D1- or FA-O cells. Given these facts, a role in the coordination of DNA incision for ICL unhooking seems more likely than one in Holliday junction resolution, even though the precise function of *FANCP* in the FA/BRCA pathway remains elusive [Crossan et al., 2011; Stoecker et al., 2011]. Four families with a total of six affected children have been assigned to

Additional Supporting Information may be found in the online version of this article.

[†]Both authors contributed equally to this work.

*Correspondence to: Beatrice Schuster, Department of Human Genetics, University of Wuerzburg, Biozentrum, Am Hubland, D-97074 Wuerzburg, Germany. E-mail: beatrice.schuster@biozentrum.uni-wuerzburg.de

Contract grant sponsors: Schroeder-Kurth Fund at the University of Wuerzburg.

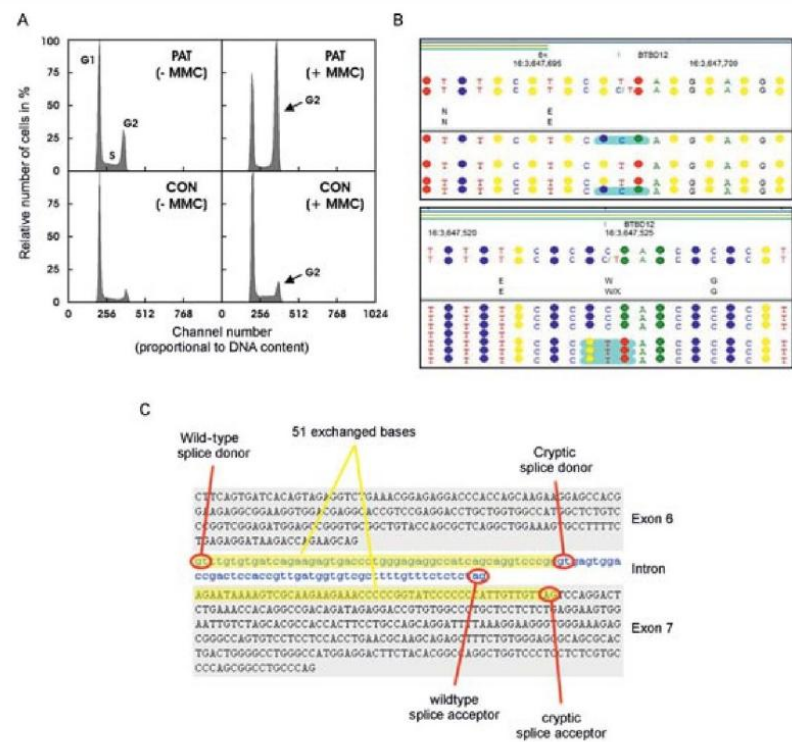


Figure 1. See figure legend on next page.

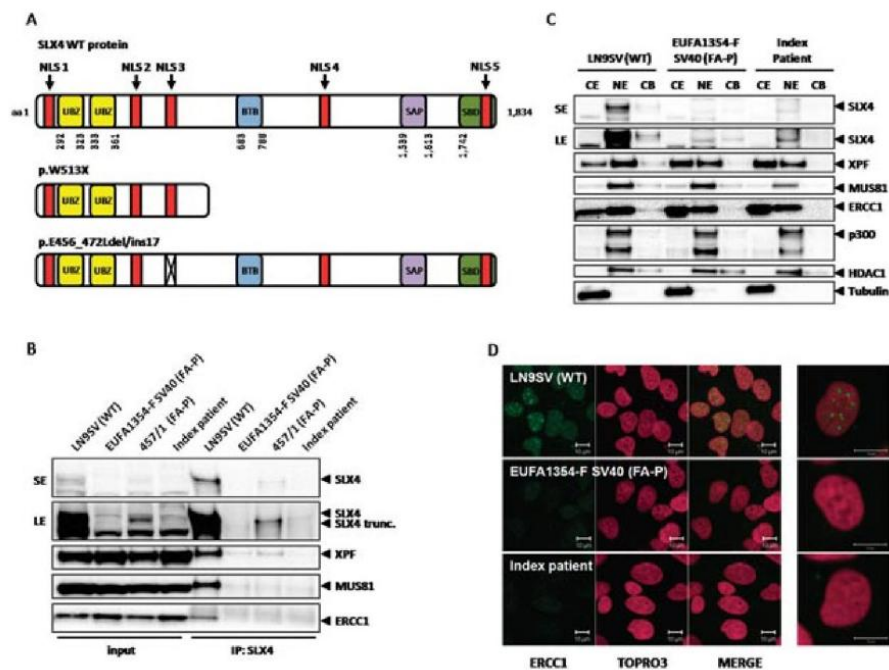


Figure 2. See figure legend on next page.

Figure 1. G2-phase arrest and *SLX4/FANCP* mutation. **A:** Cell cycle distribution of patient-derived lymphoblastoid cells shows increased G2 arrest without (21.4% of cells in G2) and especially after exposure of cultures to 15 ng/ μ l MMC (55.4% of cells in G2) compared to a control cell line (0 MMC: 9.1% of cells in G2, 15 ng/ μ l MMC: 10.9% of cells in G2). **B:** The graphic chart shows the splice site mutation c.1367-2A>G (upper panel) and the nonsense mutation c.1538G>A (lower panel) by color-space WES data according to NextGENe™ software presentation. The cutout displays from top to bottom the number of the coding exon and the gene name, the chromosomal position, followed by the reference and the patient consensus nucleotide sequences, the corresponding amino acids and, below the horizontal line, the original WES reads. Since *FANCP* (*BTBD12*) is encoded on the minus-strand of gDNA, the sequences and base changes are displayed in reverse complementary manner. **C:** Depicted is an excerpt from exon 6 to 7 of the *Ensembl* gDNA sequence of *SLX4/FANCP* (ENSG00000188827). Red circles indicate the wild-type and cryptic splice sites. The 51 bases of exon 7 which are interchanged with the same number of bases of intron 6 are highlighted in yellow.

Figure 2. Mutant *SLX4/FANCP* expression and function. **A:** Ideograms of the *SLX4/FANCP* domain structure (modified after Svendsen et al., 2009). Wild-type (WT) protein (top) contains in addition to reported domains (UBZ, yellow; BTB, blue; SAP, purple; and SBD, green) five potential nuclear localization signals (NLS, red) predicted by the Web tool <http://psort.hgc.jp/form2.html>, spanning amino acid (aa) positions 109_124 (NLS 1), 397_412 (NLS 2), 460_464 (NLS 3), 1079_1085 (NLS 4), and 1814_1830 (NLS 5). The ideograms below (middle and bottom) show the predicted protein effect of the *SLX4/FANCP* mutations in the present patient. c.1538G>A leads to protein truncation at p.W513X, whereas c.1367-2A>G leads to p.E456_472Ldelins17 and the loss of NLS 3. **B:** Immunoprecipitation and Western blot analysis shows *SLX4/FANCP* deficiency in fibroblasts of the patient compared to WT and FA-P controls. There is no co-precipitation of XPF, MUS81 and ERCC1 with the mutant protein. SE and LE indicate short and long exposure of the blot, respectively. **C:** Subcellular fractionation of patient's fibroblasts fails to demonstrate *SLX4/FANCP* protein in any fraction. Chromatin loading of XPF and MUS81 were not detected. Tubulin, p300 and HDAC1 served as loading controls for the cytoplasmic fraction (CE), nuclear extract (NE), and chromatin fraction (CB). The faint band observed in NE slightly below *SLX4/FANCP* is unspecific. **D:** Formation of nuclear ERCC1 foci is abolished in patient's fibroblasts as in other FA-P cells (EUFA1354) in contrast to the wild-type control line (LN9SV). The ERCC1 antibody FL297 was used for immunofluorescence and TOPRO3 as a nuclear counterstain.

complementation group FA-P. Their underlying *SLX4* mutations result in protein truncation and degradation. The presence of residual protein, retained function, and other factors may explain the variable severity of clinical FA manifestations [Andersen et al., 2009; Kim et al., 2011; Stoepker et al., 2011].

In this study, we report on an additional FA-P patient who was assigned to that complementation group due to *SLX4* mutations identified by whole exome sequencing (WES). *SLX4* proved to be the only FA gene carrying compound heterozygous pathogenic sequence changes that were confirmed by Sanger sequencing. A nonsense and a splice site mutation followed Mendelian segregation in the family of the patient.

The 21-year-old girl of German descent was diagnosed with FA at the age of 5 years, showing FA-typical features including prenatal dystrophy, short stature, hypoplasia of the right thumb, microcephaly, speckles of skin hyperpigmentation at the arms and legs, minor café-au-lait and vitiligo spots, trivial mitral valve prolapse, and hypothyroidism. Apart from the platelets (reduced since age 5, lowest number about 20,000/ μ l) her blood counts were relatively stable until she developed MDS at 19 years of age. She was successfully transplanted with hematopoietic stem cells from a 10/10 matched unrelated donor. The patient has not developed malignancies up to her current age of 21; nor does she have a strong family history of cancer.

Initially, the clinical suspicion of FA was confirmed by elevated spontaneous and mitomycin C-induced chromosome breakage rates (data not shown) and G2-phase accumulation in lymphocyte, lymphoblastoid (Fig. 1A), and fibroblast cultures, which was shown by flow cytometric cell cycle analysis as described in Vaz et al. (2010).

We isolated genomic DNA from fibroblasts using the GeneJet™ Genomic DNA Purification Kit (Fermentas, St. Leon-Rot, Germany). For isolation of RNA, we employed the Quick-RNA™ MiniPrep Kit (Zymo Research, Freiburg, Germany). Translation into cDNA was performed by SuperScript® II Reverse Transcriptase (Invitrogen, Darmstadt, Germany).

Because the patient was among those who remained without detected mutation or assignment to a distinct subtype, we got interested in the significance of WES for molecular diagnostics of FA. We commissioned enrichment and sequencing of the patient's exome to a service provider. Target enrichment was achieved by means of the SureSelect Human All Exon 50 Mb Kit (Agilent, Boeblingen, Germany) and was followed by

next-generation sequencing on a *SOLID5500xl* instrument (Applied Biosystems, Darmstadt, Germany). Afterward we performed *in house* analysis of the WES data using NextGENe™ v2.18 software (Softgenetics, State College, PA, USA). The data revealed a total of 103,222,641 reads (Supp. Table S1). Sixty-one percent of these mapped on target and resulted in an 87-fold average coverage of the exome. Altogether we detected 32,013 variants, including novel mutations as well as listed SNPs. Because of the patient's nonconsanguineous descent, we restricted our search to compound heterozygous changes and detected 14,715 unknown (excluding reported polymorphisms) heterozygous variants in coding sequences and adjacent intron portions. In particular, 15 base substitutions were detected in 21 FA and FA-associated genes (91% of exons covered by ≥ 5 reads). *SLX4* (NM_032444.2) carried two bona fide pathogenic variants. Even though WES could have missed pathogenic mutations in other FA genes, the compound heterozygous finding in *SLX4* makes this most unlikely. The mutated positions were covered by 6 and 15 reads, respectively. We observed the nonsense mutation c.1538G>A in exon 7 resulting in a premature stop codon with the predicted effect of protein truncation, p.W513X, and the splice acceptor mutation c.1367-2A>G in intron 6 (Fig. 1B). Mutation nomenclature is based on cDNA sequence of *SLX4* transcript ENST00000294008 and nucleotide numbering reflects cDNA numbering with +1 corresponding to the A of ATG initiation codon.

Mutation validation was performed by Sanger technique on a 3130xl instrument (Applied Biosystems, Darmstadt, Germany). The primers for gDNA sequencing included *FANCP*_exon7_for 5'-CCAGAAGCAGGTTTGTGTGA-3' and *FANCP*_exon7_rev 5'-CCTTCCTGGACTTCCATCA-3'. We resequenced the corresponding regions of *SLX4* in the patient and additionally confirmed the biallelic mutation status and Mendelian segregation of the mutations by sequencing genomic DNA from both parents. The results showed that the splice site mutation was paternally inherited, whereas the nonsense mutation was transmitted maternally (Supp. Fig. S1A).

We analyzed the consequences of c.1367-2A>G by Sanger sequencing of patient's cDNA using the primers *FANCP*_c.1-65_for 5'-CAGTACTTTTGTTCATTGTGCAAACTC-3' and *FANCP*_c.1570_rev 5'-CACAGAAAGCTCTGCTTGCGTTC-3'. This analysis demonstrated that a cryptic splice acceptor in exon 7 at position c.1417_1418 is used instead of the mutated in intron 6, as it was

predicted by in silico analysis. Splice site score calculation using the Web tool http://rulai.cshl.edu/new_alt_exon_db2/HTML/score.html revealed a score of 1.2 of the cryptic splice acceptor at positions c.1417_1418 and a score of -1.7 of the mutated one. Of note, this change of the splice acceptor altered the usage of the unaffected wild-type splice donor of intron 6 (score 5.4) to that of a cryptic splice donor at position c.1366+52_1366+53 (score 10). This fact is indicated by the substitution of the 5'-terminal 51 bases of exon 7 with the 5'-terminal 51 bases of intron 6. The electropherogram of cDNA sequencing demonstrates this finding by the superposition of exactly 51 bases starting at cDNA position 1,367 and ending at 1,417 (Fig. 1C and Supp. Fig. S1B), designated as r.1367_1417delins gttgtgtgatcagaagagtgcacctggagagccatcagcaggtcccgg. The length of the open reading frame does not differ as a result of this aberrant splicing pattern. Other in silico analyses revealed that the deduced wild-type amino acids at positions p.456_472, ENKSRKKKP-PVSPPLL, are predicted to include at positions p.460_464 one of five potential SLX4/FANCP nuclear localization signals (NLS) (<http://psort.hgc.jp/form2.html>) (Fig. 2A). The mutation, denoted p.E456_L4772delinsGLCDQKSDPGRGHQV, results in the loss of that potential NLS.

Further experiments similar to those described by Stoepker et al. (2011) showed that no residual protein is present. Neither by immunoprecipitation (Fig. 2B), nor in a cell fractionation assay (Fig. 2) SLX4/FANCP was detected on Western blots. We conclude that the allele carrying the stop mutation gives rise to a truncated protein that is unstable and rapidly degraded. Similarly, the allele with the splice mutation does not express a stable protein, which could locate to the nucleus. Therefore, it is not surprising that interactions with the structure-specific nucleases XPF/ERCC1 and EME1/MUS81 are disrupted (Fig. 2B) and that ERCC1 is not able to form nuclear foci (Fig. 2D), as described for other FA-P patients [Stoepker et al., 2011].

In summary, our study adds a seventh patient to the most recently described FA subtype, FA-P. Neither of her compound heterozygous mutations has previously been reported. They extend the mutation spectrum of the latest member of the FA gene family, *FANCP*, and have been added to the Fanconi Anemia Mutation Database (<http://www.rockefeller.edu/fanconi/>). In contrast to the FA-P patients reported so far, cells derived from the present patient do not seem to be able to express any SLX4/FANCP protein [Kim et al., 2011; Stoepker et al., 2011]. The failure of coordination of structure-specific nucleases in ICL unhooking due to the absence of SLX4/FANCP does not result in a more severe phenotype as that of other FA-P patients previously reported, which is not comparable to the cancer-prone phenotype of subtypes FA-D1 or -N, but falls into the clinical spectrum of the other FA groups. These insights were facilitated by WES that proved a valuable tool for molecular diagnostics of FA, as of other heterogeneous diseases, by the identification of disease-causing genes so that it may increasingly replace classical genetic approaches.

Acknowledgments

We are grateful to Helmut Hanenberg (Indianapolis) and Kornelia Neveling (Nijmegen) for earlier pre-classifications of patient's cells; Ralf Diet-

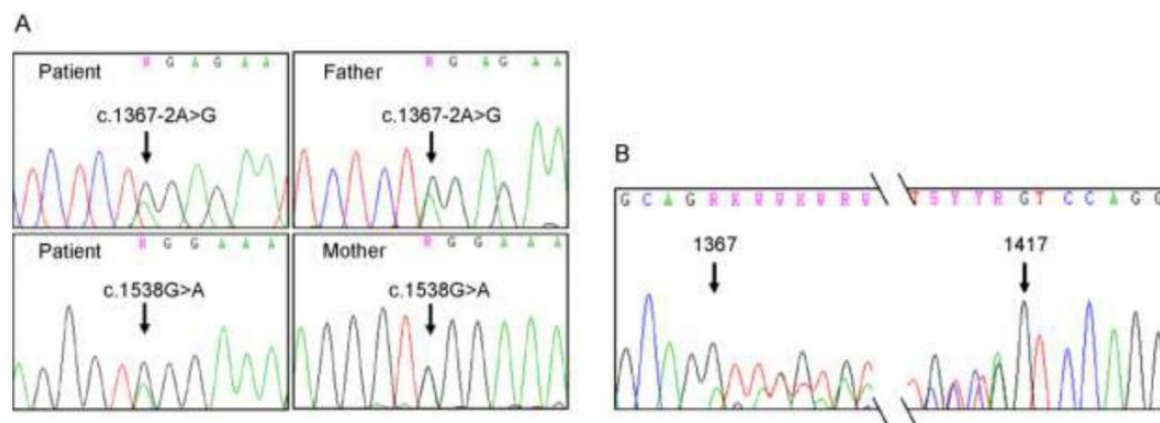
rich, executive director of the German FA support association "Deutsche Fanconi-Anämie-Hilfe e. V.," for facilitating contact to the family. The patient and her parents generously provided information on the disease course.

Authors' contribution: B.S. and K.K. designed and performed experiments, generated data, and wrote the manuscript; C.S. performed experiments and contributed data; E.V. contributed vital materials; R.F. and B.M.-G. performed experiments; J.P.deW. and D.S. contributed data, directed experiments, and revised the manuscript.

Disclosure statement: The authors declare no financial conflict of interest.

References

- Alter BP, Kupfer G. 1993. Fanconi anemia. In: Pagon RA, Bird TD, Dolan CR, Stephens K, Adam MP, editors. *GeneReviews*TM [Internet]. Seattle, WA: University of Washington, Seattle; 1993–2002 Feb 14 [updated 2012 Sep 06].
- Andersen SL, Bergstralh DT, Kohl KP, LaRocque JR, Moore CB, Sekelsky J. 2009. Drosophila MUS312 and the vertebrate ortholog BTBD12 interact with DNA structure-specific endonucleases in DNA repair and recombination. *Mol Cell* 35:128–135.
- Auerbach AD. 1993. Fanconi anemia diagnosis and the diepoxybutane (DEB) test. *Exp Hematol* 21:731–733.
- Callen E, Casado JA, Tischkowitz MD, Bueren JA, Creus A, Marcos R, Dasi A, Estella JM, Munoz A, Ortega JJ, deWinter J, Joenje H, et al. 2005. A common founder mutation in *FANCA* underlies the world's highest prevalence of Fanconi anemia in Gypsy families from Spain. *Blood* 105:1946–1949.
- Crossan GP, van der Weyden L, Rosado IV, Langevin F, Gaillard PH, McIntyre RE, Gallagher F, Kettunen MI, Lewis DY, Brindle K, Arends MJ, Adams DJ, et al. 2011. Disruption of mouse Slx4, a regulator of structure-specific nucleases, phenocopies Fanconi anemia. *Nat Genet* 43:147–152.
- Deans AJ, West SC. 2011. DNA interstrand crosslink repair and cancer. *Nat Rev Cancer* 11:467–480.
- Kim Y, Lach FP, Desetty R, Hanenberg H, Auerbach AD, Smogorzewska A. 2011. Mutations of the *SLX4* gene in Fanconi anemia. *Nat Genet* 43:142–146.
- Lobitz S, Velleuer E. 2006. Guido Fanconi (1892–1979): a jack of all trades. *Nat Rev Cancer* 6:893–898.
- Rosenberg PS, Alter BP, Ebell W. 2008. Cancer risks in Fanconi anemia: findings from the German Fanconi Anemia Registry. *Haematologica* 93:511–517.
- Rosenberg PS, Greene MH, Alter BP. 2003. Cancer incidence in persons with Fanconi anemia. *Blood* 101:822–826.
- Rosenberg PS, Tamary H, Alter BP. 2011. How high are carrier frequencies of rare recessive syndromes? Contemporary estimates for Fanconi anemia in the United States and Israel. *Am J Med Genet A* 155A:1877–1883.
- Schindler D, Kubbies M, Hoehn H, Schinzel A, Rabinovitch PS. 1987. Confirmation of Fanconi's anemia and detection of a chromosomal aberration (1Q12-32 triplication) via BrdU/Hoechst flow cytometry. *Am J Pediatr Hematol Oncol* 9:172–177.
- Schroeder TM, Anschutz F, Knopp A. 1964. Spontaneous chromosome aberrations in familial panmyelopathy. *Humangenetik* 1:194–196.
- Seif AE. 2011. Pediatric leukemia predisposition syndromes: clues to understanding leukemogenesis. *Cancer Genet* 204:227–244.
- Stoepker C, Hain K, Schuster B, Hilhorst-Hofstee Y, Rooimans MA, Steltenpool J, Oostra AB, Eirich K, Korthof ET, Nieuwint AW, Jaspers NG, Bettecken T, et al. 2011. SLX4, a coordinator of structure-specific endonucleases, is mutated in a new Fanconi anemia subtype. *Nat Genet* 43:138–141.
- Strathdee CA, Duncan AM, Buchwald M. 1992. Evidence for at least four Fanconi anaemia genes including FACC on chromosome 9. *Nat Genet* 1:196–198.
- Svendsen JM, Smogorzewska A, Sowa ME, O'Connell BC, Gygi SP, Elledge SJ, Harper JW. 2009. Mammalian BTBD12/SLX4 assembles a Holliday junction resolvase and is required for DNA repair. *Cell* 138:63–77.
- Vaz F, Hanenberg H, Schuster B, Barker K, Wiek C, Erven V, Neveling K, Endt D, Kesterton I, Autore F, Fraternali F, Freund M, et al. 2012. Mutation of the RAD51C gene in a Fanconi anemia-like disorder. *Nat Genet* 42:406–409.



Supp. Figure S1. Validation of Whole Exome Sequencing results by Sanger resequencing. **(A)** Mendelian segregation of the *FANCP* mutations in the patient's family. The splice site change c.1367-2A>G was inherited from the father, while the nonsense mutation c.1538G>A is of maternal origin. **(B)** Consequence of c.1367-2A>G on transcript level. Sequencing the patient's cDNA revealed the replacement of exactly 51 exonic bases starting at cDNA position 1367 and ending at 1417 by the first 51 bases of the following intron.

Supp. Table S1. Statistical summary of WES results including read counts and detected variants

Total read number	109,637,890
Reads passing QC	103,222,641
Reads on target	62,868,844 (61%)
Average exome coverage	87x
Total number of variants	32,013
Known SNPs/MNPs	17,194
Unknown variants in coding sequence	13,519
Unknown variants at canonical splice sites	377
Unknown homozygous variants	91
Unknown heterozygous variants	14,715
Unknown silent variants	2,983
Unknown missense variants	9,629
Unknown nonsense variants	510
Unknown insertions/deletions	468
Genes with heterozygous variants (≥ 2 altered bases)	131
Heterozygous variants in FA and FA associated genes	15

QC: quality control; SNP: single nucleotide polymorphism; MNP: multiple nucleotide polymorphism

3.2 NEUE FANCONI ANÄMIE GENE UND DEREN CHARAKTERISIERUNG IM RAHMEN DES FA/BRCA-SIGNALWEGS

3.2.1 MUTATIONS IN *ERCC4*, ENCODING THE DNA-REPAIR ENDONUCLEASE XPF, CAUSE FANCONI ANEMIA

REPORT

Mutations in *ERCC4*, Encoding the DNA-Repair Endonuclease XPF, Cause Fanconi Anemia

Massimo Bogliolo,^{1,2,10} Beatrice Schuster,^{3,10} Chantal Stoecker,⁴ Burak Derkunt,⁵ Yan Su,⁵ Anja Raams,⁶ Juan P. Trujillo,¹ Jordi Minguiñón,¹ María J. Ramírez,^{1,2} Roser Pujol,^{1,2} José A. Casado,^{2,7} Rocío Baños,^{2,7} Paula Rio,^{2,7} Kerstin Knies,³ Sheila Zúñiga,⁸ Javier Benítez,^{2,9} Juan A. Bueren,^{2,7} Nicolaas G.J. Jaspers,⁶ Orlando D. Schärer,⁵ Johan P. de Winter,⁴ Detlev Schindler,^{3,*} and Jordi Surralés^{1,2,*}

Fanconi anemia (FA) is a rare genomic instability disorder characterized by progressive bone marrow failure and predisposition to cancer. FA-associated gene products are involved in the repair of DNA interstrand crosslinks (ICLs). Fifteen FA-associated genes have been identified, but the genetic basis in some individuals still remains unresolved. Here, we used whole-exome and Sanger sequencing on DNA of unclassified FA individuals and discovered biallelic germline mutations in *ERCC4* (*XPF*), a structure-specific nuclease-encoding gene previously connected to xeroderma pigmentosum and segmental XFE progeroid syndrome. Genetic reversion and wild-type *ERCC4* cDNA complemented the phenotype of the FA cell lines, providing genetic evidence that mutations in *ERCC4* cause this FA subtype. Further biochemical and functional analysis demonstrated that the identified FA-causing *ERCC4* mutations strongly disrupt the function of XPF in DNA ICL repair without severely compromising nucleotide excision repair. Our data show that depending on the type of *ERCC4* mutation and the resulting balance between both DNA repair activities, individuals present with one of the three clinically distinct disorders, highlighting the multifunctional nature of the XPF endonuclease in genome stability and human disease.

Fanconi anemia (FA) is characterized by bone marrow failure (BMF), congenital malformations, hypersensitivity to DNA interstrand crosslink (ICL)-inducing agents, chromosome fragility, and a high susceptibility to cancer. Since the discovery of the first FA-associated gene 20 years ago, all together, 15 genes associated with FA have been identified; these include *FANCA*, *FANCB*, *FANCC*, *FANCD1* (*BRCA2*), *FANCD2*, *FANCE*, *FANCF*, *FANCG* (*XRCC9*), *FANCI*, *FANCL* (*BRIP1*), *FANCL* (*PHF9*), *FANCM*, *FANCN* (*PALB2*), *FANCO* (*RAD51C*), and *FANCP* (*SLX4*)^{1,2} (MIM 227650, 300514, 227645, 605724, 227646, 600901, 603467, 614082, 609053, 609054, 614083, 614087, 610832, 613390, and 613951, respectively). Studies to unravel the genetic basis of this rare disorder uncovered a genome-maintenance pathway that protects dividing cells against replication-blocking DNA lesions. To identify additional FA-associated genes, we used the SOLiD 4 platform for whole-exome sequencing on peripheral-blood DNA from a Spanish FA individual (FA104) who was previously excluded from all known FA complementation groups (this study was approved by the Institutional Committee on Ethical Research in Human Samples, and proper informed consent was obtained). FA104 was born to unrelated parents and was diagnosed neonatally with a malformative syndrome suggestive of FA, the symptoms of which included bilateral absent thumbs, microsomia, esophageal atresia, a ventrally translocated anus, and dysplastic and

low-set ears. She did not show any dermatological abnormality such as skin hyperpigmentation, photosensitivity, sunlight-induced scarring, or atrophy. FA104 developed BMF at the age of 2 years and died as a result of a hemorrhagic shock after bone marrow transplantation at the age of 4 years. A positive chromosome-breakage test unambiguously confirmed the FA diagnosis: 92% of the cells showed on average 4.4 diepoxbutane (DEB)-induced breaks. Lymphoblasts from this individual were hypersensitive to mitomycin-C (MMC) and melphalan but were insensitive to the topoisomerase I inhibitor camptothecin and the PARP inhibitor KU58948 (data not shown) and showed normal FANCD2 monoubiquitination and RAD51 focus formation.³ This suggests a defect downstream within the FA pathway, which does not involve homologous recombination. On the basis of a recessive mode of inheritance, exome sequencing identified 17 candidate disease genes for FA104 (Table S1, available online); of these, *ERCC4* (MIM 133520; also known as *XPF*) immediately caught our attention given the involvement of the XPF-ERCC1-structure-specific nuclease in ICL repair.⁴ Both *ERCC4* mutations were predicted to be pathogenic: a 5 bp deletion in exon 8 (c.1484_1488delCTCAA) was predicted to lead to a frameshift and a premature stop codon (p.Thr495Asnfs*6), and a missense mutation in exon 11 (c.2065C>A [p.Arg689Ser]; RefSeq accession numbers NG_011442.1, NM_005236.2, and NP_005227.1) was

¹Genome Instability and DNA Repair Group, Department of Genetics and Microbiology, Universitat Autònoma de Barcelona, Bellaterra, 08193 Barcelona, Spain; ²Centre for Biomedical Network Research on Rare Diseases, Instituto de Salud Carlos III, Bellaterra, 08193 Barcelona, Spain; ³Department of Human Genetics, University of Würzburg, D-97074 Würzburg, Germany; ⁴Department of Clinical Genetics, VU University Medical Center, 1081 BT Amsterdam, the Netherlands; ⁵Department of Pharmacological Sciences and Chemistry, Stony Brook University, Stony Brook, NY 11794-3400, USA; ⁶Department of Genetics, Erasmus University Medical Center, 3015 GE Rotterdam, the Netherlands; ⁷Hematopoiesis and Gene Therapy Division, Centro de Investigaciones Energéticas, Medioambientales y Tecnológicas, 28040 Madrid, Spain; ⁸Department of Bioinformatics, Sistemas Genómicos SL, 46980 Valencia, Spain; ⁹Human Genetics Group, Spanish National Cancer Center, Centro Nacional de Investigaciones Oncológicas, E-28029 Madrid, Spain

¹⁰These authors contributed equally to this work

*Correspondence: jordi.surrales@uab.es (J.S.), schindler@biozentrum.uni-wuerzburg.de (D.S.)

http://dx.doi.org/10.1016/j.ajhg.2013.04.002. ©2013 by The American Society of Human Genetics. All rights reserved.

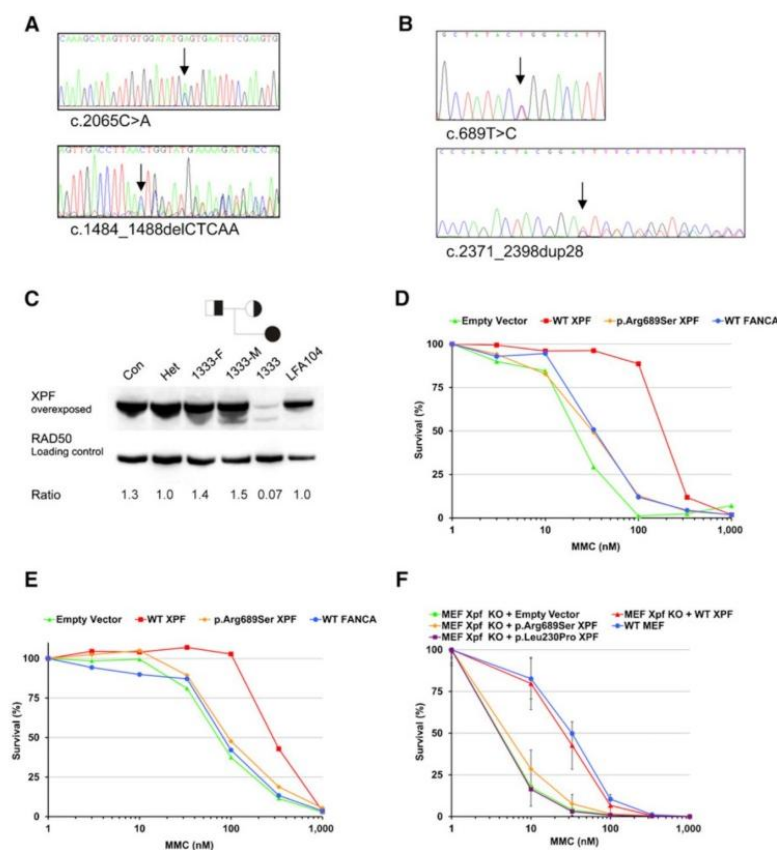


Figure 1. *ERCC4* Mutations and XPF Deficiency in FA Individuals

(A) Sequence analysis of blood DNA from FA104 revealed a missense mutation in exon 11 (c.2065C>A [p. Arg689Ser]) (upper panel) and a 5 bp deletion in exon 8 leading to a frameshift and premature termination of translation (c.1484_1488delCTCAA [p. Thr495Asnfs*6]) (lower panel).

(B) Sequence analysis of blood DNA from 1333 revealed a missense mutation in exon 4 (c.689T>C [p. Leu230Pro]) (upper panel) and a 28 bp duplication in exon 11 (lower panel) leading to a frameshift and a premature stop codon (c.2371_2398dup28 [p. Ile800Thrfs*24]).

(C) Immunoblot analysis showing XPF expression in lymphoblasts from 1333 and FA104. Lymphoblasts from a healthy individual (Con), the parents of 1333 (1333-F and 1333-M), and an unrelated *ERCC4* mutation carrier (Het) were used as controls. XPF levels are expressed as a ratio relative to the loading control (RAD50).

(D) Genetic complementation of MMC sensitivity in FA104 lymphoblasts by wild-type XPF, but not by p.Arg689Ser altered XPF. Site-directed mutagenesis was used for introducing point mutations into the pWPXL-XPF hemagglutinin (HA)-tagged plasmid with the QuickChange method (Stratagene) as described.⁵ Lentiviral supernatant production and transduction were done as previously described,⁶ and cells were grown for 10 days in the presence of MMC. Data represent a typical result of at least three independent experiments.

(E) Genetic complementation of MMC sensitivity of 1333 lymphoblasts by wild-type XPF (experiments were performed as in D).

(F) MMC-induced growth inhibition of *Ercc4*-knockout MEFs transduced with lentiviral particles coding for GFP (negative control vector), wild-type XPF, and p.Arg689Ser and p.Leu230Pro altered XPF. Data represent means and SD of at least three independent experiments.

predicted to change a highly conserved arginine within the nuclease active site of XPF. Sanger sequencing on blood DNA confirmed these mutations (Figure 1A) and their correct segregation (data not shown). In MMC-resistant FA104 lymphoblasts (FA104R) obtained after long-term exposure to a low dose of MMC, we detected a mutation that restored the *ERCC4* reading frame (Figure S1A), supporting the notion that MMC sensitivity is due to *ERCC4* mutations. Consistently, XPF levels were reduced in FA104 lymphoblasts but were normalized in the reverted FA104R lymphoblasts (Figure S1B). Immunoblotting did not detect a truncated XPF, indicating that only the p.Arg689Ser altered XPF was present in the FA104 cell line.

Sanger sequencing on 18 unclassified FA individuals from Germany revealed biallelic *ERCC4* mutations in another individual (1333). Individual 1333 was born in 2002 and was unambiguously diagnosed with FA at the age of 5 years as a result of multiple FA-related features, such as perinatal growth retardation, short stature, pronounced microcephaly, café-au-lait spots, an ostium-primum defect, biliary atresia with fibrosis of the liver, BMF,

and a positive chromosome-fragility test (0.2, 6.7, and 9.4 breaks per cell at 0, 50, and 100 ng/ml MMC, respectively). Individual 1333 is redheaded and has pale skin color, but no spontaneous or UV-light-induced skin lesions were reported at the age of 10 years. Similar to those of FA104, lymphoblasts from individual 1333 were normal with regard to FANCD2 monoubiquitination and RAD51 focus formation and were sensitive to MMC and melphalan but insensitive to the topoisomerase I inhibitor camptothecin and to the PARP inhibitor KU58948 (data not shown). Individual 1333 carries a 28 bp duplication in exon 11 of the maternal allele (c.2371_2398dup28 [p. Ile800Thrfs*24]; Figure 1B), and this duplication is predicted to result in a truncated XPF that lacks the double helix-hairpin-helix (HhH₂) domain involved in heterodimerization with ERCC1 and DNA binding.⁷ The paternal allele contains a missense mutation that changes a highly conserved amino acid residue within the helicase-like domain (c.689T>C [p. Leu230Pro]; Figure 1B). Immunoblot analysis showed that a missense altered XPF and a truncated 90–95 kDa XPF are present at very low levels

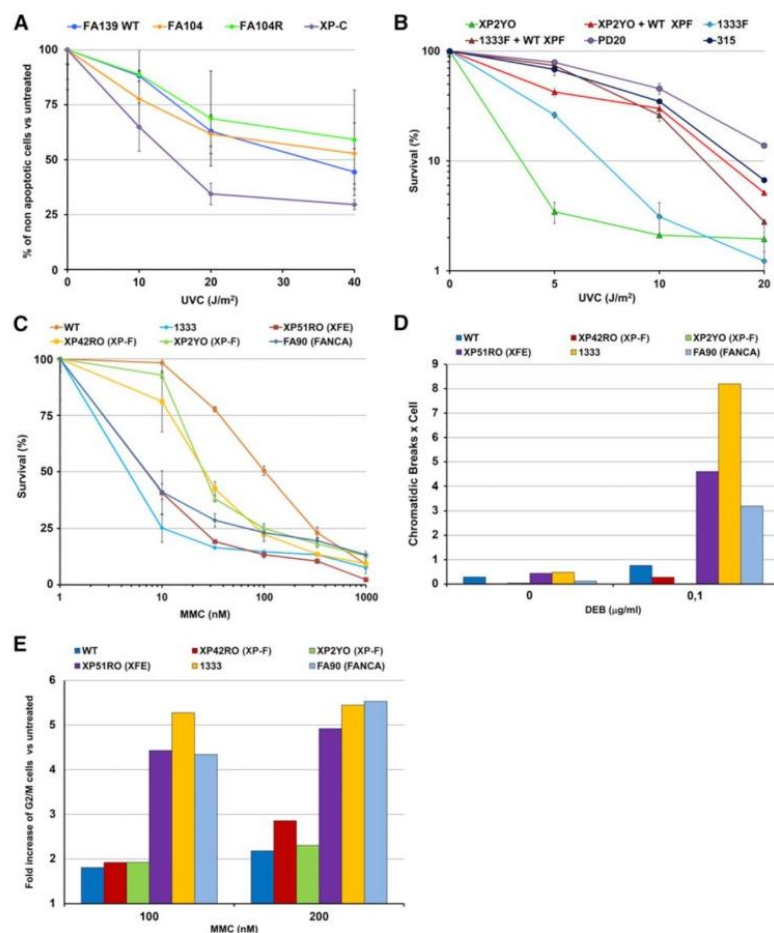


Figure 2. UV-Light and ICL Sensitivities of ERCC4 Mutants Leading to FA

(A) UVC-light-induced apoptosis in FA104 lymphoblasts. Cells were analyzed for UVC-light-induced apoptosis 24 hr after irradiation with the use of the Annexin-V-FLUOS Staining Kit (Roche). Data represent means and SD of at least three independent experiments.

(B) UVC-light-induced growth inhibition of human ERCC4-deficient immortal fibroblast cell lines (from XP individual XP2YO and FA individual 1333) transduced with lentiviral particles carrying cDNA coding for wild-type XPF. The results are expressed as a percentage of viable UVC-light-treated cells relative to untreated controls. Data represent means and SD of two independent experiments.

(C) MMC sensitivity of human ERCC4-deficient primary fibroblasts from XP, FA, and XFE individuals (XP42RO, 1333, and XP51RO, respectively). Data represent means and SD of two independent experiments.

(D) DEB-induced chromosome-fragility test in human ERCC4-deficient primary fibroblasts from XP, FA, and XFE individuals (XP42RO, 1333, and XP51RO, respectively).

(E) MMC-induced G2/M cell-cycle arrest in the same cells as in (D). Experiments presented in (D) and (E) were performed as reported earlier.¹⁰

ERCC4 missense mutations found in both FA individuals inactivate XPF. The genetic and functional data show that mutations in ERCC4 cause FA in two unrelated nonconsanguineous individuals. Because mutations in ERCC4 cause an additional FA subtype (FA-Q), we propose FANCA as an alias for ERCC4.

ERCC4 mutations have been linked to the skin-photo-sensitive and nucleotide excision repair (NER)-deficient disorders xeroderma pigmentosum (XP [MIM 278700, 610651, 278720, 278730, 278740, 278760, 278780, and 278750])⁸ and XFE progeroid syndrome (MIM 610965),⁹ and we therefore tried to understand why the identified ERCC4 variants specifically lead to FA. We hypothesized that these mutants cause an FA phenotype because of a strong deficiency in ICL repair but have sufficient NER activity to prevent clinically relevant skin photosensitivity and other NER-related features. Compared to an XP complementation group C (XP-C) lymphoblast line, FA104 lymphoblasts were indeed not sensitive to UVC light (Figure 2A). Given that UV-light survival experiments are challenging in lymphoblastoid cell lines, we studied skin fibroblasts from individual 1333 (FA104 fibroblasts were not available) and found that the UV-light sensitivity in FA individual 1333 was milder than that in XP complementation group F (XP-F) individual XP2YO (Figure 2B).

(Figure 1C). As expected, the truncated XPF was undetectable with an antibody against the C-terminal HhH2 domain of XPF (amino acids 866–916, data not shown). Interestingly, the truncated XPF was absent in a MMC-resistant lymphoblastoid cell line (1333R) generated by long-term exposure to MMC, and near-normal XPF levels were detected in this reverted cell line (Figure S1C). PCR amplification and sequence analysis revealed that the 28 bp duplication had disappeared in 1333R (Figure S1D) and had thus restored the wild-type sequence. Both the inherited duplication and the somatic reversion might have been triggered by an inverted 5 bp repeat flanking the region.

Genetic complementation of MMC sensitivity in lymphoblasts from both FA individuals was achieved by lentiviral transduction of wild-type ERCC4 cDNA (Figures 1D and 1E). In addition, we expressed wild-type and mutant human ERCC4 cDNAs in embryonic fibroblasts (MEFs) from Ercc4 (Xpf)-null mice. We found that ectopic expression of ERCC4 mutants encoding p.Leu230Pro and p.Arg689Ser did not complement MMC sensitivity of these MEFs (Figure 1F), providing additional evidence that the

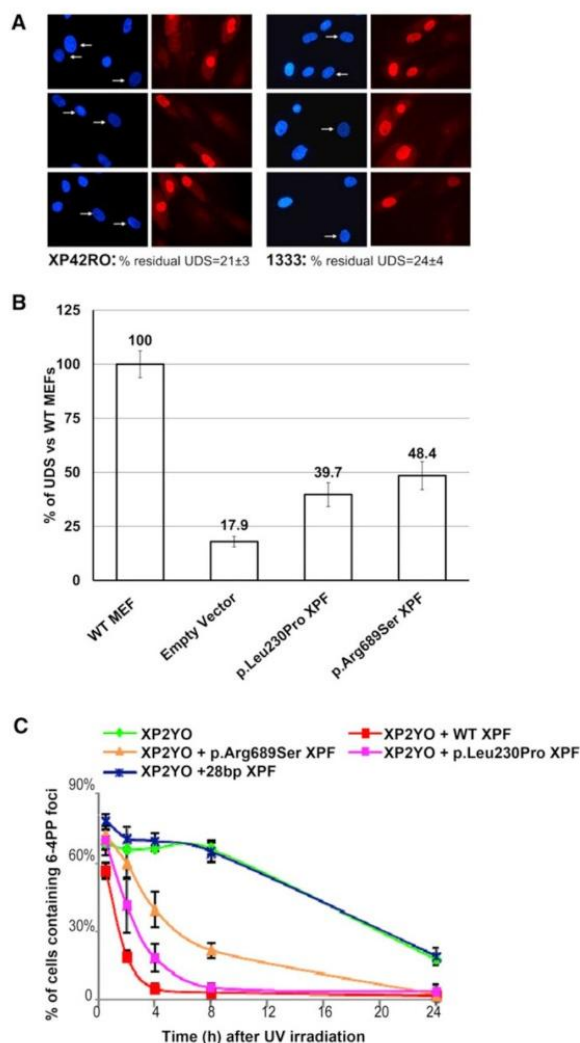


Figure 3. NER Analysis of *ERCC4* Mutants In Vivo
 (A and B) In primary fibroblasts, unscheduled DNA synthesis (UDS) representing global NER activity was measured with 5-ethynyl-deoxyuridine grossly as previously described.¹²
 (A) XP-F (XP42RO) and FA (1333) cells (arrows) were compared to mixed-in normal fibroblasts preloaded with polystyrene microbeads (no arrows), used as an internal control. UDS signal was quantified from 20–40 random XP-F or FA G1/G2 nuclei and expressed as a percentage of control wild-type cells.
 (B) UDS signals in *Ercc4*^{-/-} MEFs measured as in (A) are expressed as a percentage of control wild-type MEFs. *Ercc4*^{-/-} cells were stably expressing an empty vector or one of various *ERCC4* cDNAs (wild-type or encoding p.Leu230Pro or p.Arg689Ser).
 (C) Repair kinetics of UV-light-induced DNA damage by FA-specific *ERCC4* mutants in *ERCC4*- and NER-deficient human cells (XP2YO). Cells expressing wild-type XPF, p.Arg689Ser or p.Leu230Pro altered XPF, or XPF resulting from the 28 bp duplication were locally irradiated with UV light, cultured for the indicated times, fixed and stained for 6-4 PPs, and tagged with HA with the use of specific antibodies. Data represent the percentage of cells with 6-4 PP spots at various time points; means and SD of at least two independent experiments are shown. For each experiment, 100 cells were counted.

In addition, the FA-specific XPF alterations p.Leu230Pro and p.Arg689Ser rescued 100% of the UVC sensitivity of XP2YO fibroblasts (Figure S2A) and approximately 80% of the UVC-light sensitivity of *Ercc4*-null MEFs (Figure S2B) but were both unable to complement MMC sensitivity (Figure 1F). Furthermore, XFE and 1333 fibroblasts responded typically like FA cells upon MMC-induced survival (Figure 2C), DEB-induced chromosome breakage (Figure 2D), and MMC-induced G2-phase arrest (Figure 2E), whereas XP-F cells showed milder MMC sensitivity and lacked DEB-induced chromosome fragility and MMC-induced cell-cycle arrest (Figure 2C–2E). Previous experiments in Chinese hamster ovary cells also demonstrated that the XFE-specific p.Arg153Pro altered XPF does not rescue MMC or UV-light sensitivity.¹¹ Therefore, we conclude that XP, XFE, and FA cells with *ERCC4* mutations clearly have a distinct response to UV light and MMC (Table S2).

To further investigate the extent of NER deficiency in the FA-affected individuals, we measured UV-light-induced unscheduled DNA synthesis (UDS) in primary skin fibroblasts from individual 1333 and from an XP-F individual (XP42RO) with mild clinical UV-light sensitivity and found $24 \pm 4\%$ and $21 \pm 3\%$ residual UDS activity, respectively (Figure 3A). We also determined UDS in *Ercc4*-null MEFs expressing the FA-specific XPF alterations p.Leu230Pro or p.Arg689Ser. The levels of UDS activity were 39.7% and 48.4% of the normal mean for p.Leu230Pro and p.Arg689Ser altered XPF, respectively (Figure 3B), enough to complement 80% of UVC-light sensitivity of these MEFs (Figure S2B). In XPF-deficient human XP2YO fibroblasts, p.Leu230Pro and p.Arg689Ser altered XPF rather efficiently corrected the defective removal of 6-4 photo-products (PPs) at sites of local UV damage (Figure 3C). In contrast, XP2YO cells expressing the *ERCC4* mutant with the 28 bp duplication were completely deficient in NER activity, as predicted from the disruption of the ERCC1- and DNA-binding domain of this truncated protein. The studies presented in Figures 2 and 3 demonstrate that FA cells with *ERCC4* mutations are fully deficient in ICL repair but retain significant levels of NER activity.

Cell lines from XP-F individuals show a characteristic failure of the altered XPF to properly translocate to the nucleus through aggregation of the protein in the cytoplasm.¹¹ This feature is evident for XP-causing mutations and accentuated in cells from the individual with XFE syndrome. However, FA-causing XPF missense altered proteins can actually translocate to the nucleus, where they are recruited to sites of active NER (Figures S3A and S3B) and can interact with SLX4 and ERCC1 (Figures S3C and S3D). These results might be functionally important, given that a recent article reports that SLX4 interaction with XPF is crucial for ICL repair and that SLX4-knockout mice phenocopy FA.¹³ Using *Xenopus* extracts, J.C. Walter's group reported that the FA upstream pathway genes are required to regulate a nuclease that makes DNA incisions near the ICL.¹⁴ Given that FA-specific altered XPF proteins can

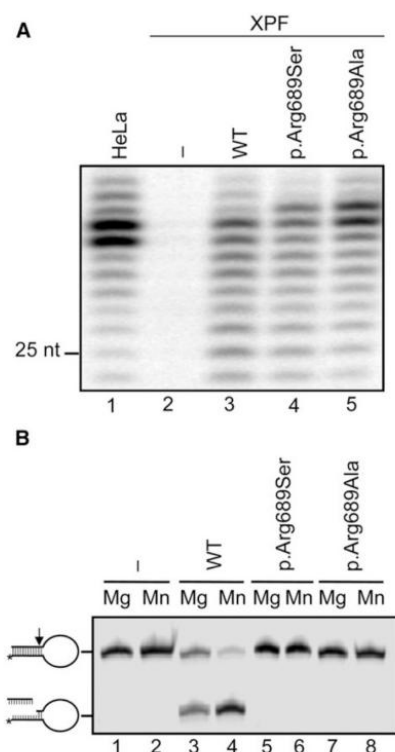


Figure 4. Nuclease Activity of Altered XPF
(A) NER activity of wild-type and altered ERCC1-XPF dimer. A plasmid containing a site-specific 1,3-intrastrand cis-Pt DNA crosslink was incubated with whole-cell extracts from HeLa cells or XPF-deficient cells (XP2YO) complemented with recombinant ERCC1-XPF purified from Sf9 insect cells as reported.¹³ The excised DNA fragments of 24–32 nucleotides are shown. The position of a 25-mer is indicated.
(B) Incision of a stem-loop substrate with wild-type and altered XPF. The 3' Cy5-labeled substrate was incubated with recombinant ERCC1-XPF in the presence of 2 mM MgCl₂ or 0.4 mM MnCl₂, and the products were analyzed by denaturing PAGE. The incision reaction was performed essentially as described earlier.^{5,11}

reach the site of damage, we then investigated their ability to cleave DNA. For this aim, the p.Arg689Ser altered XPF was purified as a heterodimer with ERCC1 as previously described.⁵ Subsequently, NER reactions were performed with the purified altered protein, extracts from XPF-deficient XP2YO cells, and a plasmid containing an NER substrate (1,3-cisplatin intrastrand crosslink).¹⁵ Consistent with the functional data above, the purified heterodimer composed of ERCC1 and p.Arg689Ser XPF is proficient in the excision step of NER similarly to wild-type XPF, given that it restored the ability to cleave and remove the site-specific intrastrand crosslink from the plasmid in XP2YO cell extracts (Figure 4A). Nevertheless, the excision reaction is not perfect given that the excised fragments are, on average, 1 nucleotide longer than expected from a normal reaction with wild-type-XPF-ERCC1 dimer (Figure 4A, lane 4). We also performed in vitro nuclease

activity assays with purified ERCC1-p.Arg689Ser-XPF and ERCC1-p.Arg689Ala-XPF on a stem-loop model DNA substrate. Unlike wild-type XPF and altered XPF proteins causing XP (p.Arg799Trp) or XFE progeroid syndrome (p.Arg153Pro),¹¹ p.Arg689Ser XPF is unable to cleave such a substrate (Figure 4B), indicating that the nuclease-type activity of p.Arg689Ser XPF is grossly abnormal. Unfortunately, we could not perform these biochemical experiments with the p.Leu230Pro altered XPF because we were unable to express and purify ERCC1-p.Leu230Pro-XPF as a result of its low stability and tendency to aggregate. We finally checked whether the FA-specific altered XPF proteins ectopically expressed in *Ercc4*-null MEFs can perform the incision step of ICL repair. Both p.Leu230Pro and p.Arg689Ser altered XPF completely restored the incision defect of *Ercc4*-null MEFs, as measured by the COMET assay (data not shown), but the cells remained hypersensitive to ICLs (Figure 1F). Although additional biochemical experiments are required, our results suggest that the ICL sensitivity of individuals FA104 and 1333 is not directly linked to the absence of XPF nuclease activity. It seems unlikely that the defect is a downstream step of homologous recombination because FA104 and 1333 cells are not sensitive to PARP inhibitors and are normal in Rad51 focus formation. Given that the nuclease activity of the FA-specific p.Arg689Ser altered XPF is grossly abnormal, it is tempting to speculate that the ICL-unhooking step in these FA cells leaves an intermediate aberrant substrate that is irreparable by subsequent ICL-repair factors.

Our genetic, biochemical, and functional studies, along with the characterization of previous *ERCC4* mutations causing XP-F and XFE, provide a model for the mechanistic understanding of how mutations in *ERCC4* lead to three distinct diseases (Table S2). Most of the presently known XP-F individuals suffer from a relatively mild form of XP.¹⁶ Cells from these individuals have a reduced level of XPF in the nucleus because the altered XPF has a tendency to aggregate in the cytoplasm.¹¹ This reduced level of nuclear XPF is insufficient to mediate complete NER, but it still has enough ICL-repair-specific functions to prevent chromosome fragility, cell-cycle arrest, and subsequent FA clinical manifestations. A second set of *ERCC4* mutations, characterized in this study, allow localization of the protein to the nucleus, where they exert a certain level of NER activity but are fully deficient in ICL repair. p.Arg689Ser XPF is a stable and NER-proficient protein with an active site structure that prevents it from properly processing ICL-repair intermediates. p.Leu230Pro XPF is more similar to the products of previously described *ERCC4* mutations in that it is less stable and might have a tendency to aggregate in the cytoplasm. However, sufficient amounts of the protein are properly folded and reach chromatin, where it appears to have some activity in the removal of 6-4 PPs. Residual NER activity in the skin tissue of individual 1333 in vivo might explain why this individual has no clinically relevant skin photosensitivity,

although we cannot exclude that dermatological problems will arise later in life. A final category of *ERCC4* mutations is associated with XFE progeroid syndrome, which is characterized by very low levels of nuclear XPF, apparently insufficient to support either NER or ICL repair. Importantly, the only XFE-affected individual described suffered from both skin photosensitivity and anemia^{9,16} and shared some cellular features with XP (NER defect and UV-light sensitivity) and FA (extreme ICL sensitivity, DEB-induced chromosome fragility, and MMC-induced cell-cycle arrest), suggesting that XFE syndrome is characterized by a combination of XP and FA manifestations (Table S2). Exhaustion of hematopoietic stem cells is also an attribute of *ERCC1*-XPF hypomorphic mice that mimic XFE (Laura Niedernhofer, personal communication). Microsomy, microcephaly, and liver fibrosis were likewise observed in FA individual 1333, in *Ercc1*- and *Ercc4*-deficient mice, and in the unique *ERCC1*-deficient individual, who all lack ICL-repair functions.^{17–21}

In a broader sense, this study demonstrates that depending on the type of *ERCC4* mutation and the balance between NER and ICL-repair activities, affected individuals present with one of three clinically distinct disorders. This resembles the case of *XPD*, which is involved in XP complementation group D, trichothiodystrophy (MIM 601675), or Cockayne syndrome (MIM 216400) depending on the type of mutation,²² and highlights the value of characterizing rare genetic disorders for gaining insight into the mechanisms of genome maintenance and human disease. XPF has a central role in preventing genome instability, cancer, BMF, developmental abnormalities, and premature aging. Like those of other breast and ovarian cancer susceptibility genes mutated in FA,^{23,24} the product of *ERCC4* also acts downstream of FANCD2 monoubiquitination. Therefore, it is important to study *FANCD2* as a candidate gene in hereditary breast and ovarian cancer.

Supplemental Data

Supplemental Data include three figures and two tables and can be found with this article online at <http://www.cell.com/AJHG>.

Acknowledgments

The use of *FANCD2* as an alias for *ERCC4* was approved by the HUGO Gene Nomenclature Committee. We would like to thank the families affected by Fanconi anemia and their clinicians for providing samples and clinical data, as well as María A. Blasco (Centro Nacional de Investigaciones Oncológicas, Madrid) for providing *Ercc4*-deficient mouse embryonic fibroblasts. The J.A.B. laboratory is funded by grants from European Program “7FWP, Health” (PERSIST; agreement 222878), the Spanish Ministry of Science and Innovation (Refs110-90.1 and SAF 2009-07164), Programa RETICS-RD06/0010/0015 ISCIII, and Fundación Botín. O.D.S. acknowledges funding from the National Institutes of Health (GM080454 and CA092584). C.S. is funded by CCA/V-ICI Amsterdam. D.S. and B.S. received grants from the Deutsche Fanconi-Anaemie-Hilfe, Aktionskreis Fanconi-Anaemie, and the Schroeder-Kurth Fund. J.S.’s laboratory is funded by the

Generalitat de Catalunya (SGR0489-2009), the ICREA-Academia award, the Spanish Ministry of Science and Innovation (Centre for Biomedical Network Research on Rare Diseases [CIBERER] CB06/07/0023, SAF2009-11936, and SAF2012-31881), and the European Regional Development FEDER Funds. CIBERER is an initiative of the Instituto de Salud Carlos III, Spain.

Received: November 13, 2012

Revised: March 5, 2013

Accepted: April 5, 2013

Published: April 25, 2013

Web Resources

The URLs for data presented herein are as follows:

Online Mendelian Inheritance in Man (OMIM), <http://www.omim.org>

RefSeq, <http://www.ncbi.nlm.nih.gov/RefSeq>

References

1. Stoepker, C., Hain, K., Schuster, B., Hilhorst-Hofstee, Y., Roovers, M.A., Steltenpool, J., Oostra, A.B., Eirich, K., Korthof, E.T., Nieuwint, A.W., et al. (2011). SLX4, a coordinator of structure-specific endonucleases, is mutated in a new Fanconi anemia subtype. *Nat. Genet.* 43, 138–141.
2. Kim, Y., Lach, F.P., Desetty, R., Hanenberg, H., Auerbach, A.D., and Smogorzewska, A. (2011). Mutations of the SLX4 gene in Fanconi anemia. *Nat. Genet.* 43, 142–146.
3. Antonio Casado, J., Callén, E., Jacome, A., Río, P., Castella, M., Lobitz, S., Ferro, T., Muñoz, A., Sevilla, J., Cantalejo, A., et al. (2007). A comprehensive strategy for the subtyping of patients with Fanconi anaemia: conclusions from the Spanish Fanconi Anemia Research Network. *J. Med. Genet.* 44, 241–249.
4. Deans, A.J., and West, S.C. (2009). FANCD2 connects the genome instability disorders Bloom’s Syndrome and Fanconi Anemia. *Mol. Cell* 36, 943–953.
5. Enzlin, J.H., and Schärer, O.D. (2002). The active site of the DNA repair endonuclease XPF-ERCC1 forms a highly conserved nuclease motif. *EMBO J.* 21, 2045–2053.
6. Almaraz, E., Río, P., Meza, N.W., Aldea, M., Agirre, X., Guenechea, G., Segovia, J.C., and Bueren, J.A. (2007). Characteristics of lentiviral vectors harboring the proximal promoter of the *vav* proto-oncogene: a weak and efficient promoter for gene therapy. *Mol. Ther.* 15, 1487–1494.
7. de Laat, W.L., Sijbers, A.M., Odijk, H., Jaspers, N.G., and Hoeijmakers, J.H. (1998). Mapping of interaction domains between human repair proteins ERCC1 and XPF. *Nucleic Acids Res.* 26, 4146–4152.
8. Sijbers, A.M., de Laat, W.L., Ariza, R.R., Biggerstaff, M., Wei, Y.F., Moggs, J.G., Carter, K.C., Shell, B.K., Evans, E., de Jong, M.C., et al. (1996). Xeroderma pigmentosum group F caused by a defect in a structure-specific DNA repair endonuclease. *Cell* 86, 811–822.
9. Niedernhofer, L.J., Garinis, G.A., Raams, A., Lalai, A.S., Robinson, A.R., Appeldoorn, E., Odijk, H., Oostendorp, R., Ahmad, A., van Leeuwen, W., et al. (2006). A new progeroid syndrome reveals that genotoxic stress suppresses the somatotrophic axis. *Nature* 444, 1038–1043.
10. Trujillo, J.P., Mina, L.B., Pujol, R., Bogliolo, M., Andrieux, J., Holder, M., Schuster, B., Schindler, D., and Surrallés, J.

- (2012). On the role of FAN1 in Fanconi anemia. *Blood* 120, 86–89.
11. Ahmad, A., Enzlin, J.H., Bhagwat, N.R., Wijgers, N., Raams, A., Appeldoorn, E., Theil, A.F., J. Hoeijmakers, J.H., Vermeulen, W., J. Jaspers, N.G., et al. (2010). Mislocalization of XPF-ERCC1 nuclease contributes to reduced DNA repair in XP-F patients. *PLoS Genet.* 6, e1000871.
 12. Limsirichaikul, S., Niimi, A., Fawcett, H., Lehmann, A., Yamashita, S., and Ogi, T. (2009). A rapid non-radioactive technique for measurement of repair synthesis in primary human fibroblasts by incorporation of ethynyl deoxyuridine (EdU). *Nucleic Acids Res.* 37, e31.
 13. Crossan, G.P., van der Weyden, L., Rosado, I.V., Langevin, F., Gaillard, P.H., McIntyre, R.E., Gallagher, F., Kettunen, M.I., Lewis, D.Y., Brindle, K., et al.; Sanger Mouse Genetics Project. (2011). Disruption of mouse Slx4, a regulator of structure-specific nucleases, phenocopies Fanconi anemia. *Nat. Genet.* 43, 147–152.
 14. Knipscheer, P., Räsche, M., Smogorzewska, A., Enoiu, M., Ho, T.V., Schärer, O.D., Elledge, S.J., and Walter, J.C. (2009). The Fanconi anemia pathway promotes replication-dependent DNA interstrand cross-link repair. *Science* 326, 1698–1701.
 15. Moggs, J.G., Yarema, K.J., Essigmann, J.M., and Wood, R.D. (1996). Analysis of incision sites produced by human cell extracts and purified proteins during nucleotide excision repair of a 1,3-intrastrand d(GpTpG)-cisplatin adduct. *J. Biol. Chem.* 271, 7177–7186.
 16. Gregg, S.Q., Robinson, A.R., and Niedernhofer, L.J. (2011). Physiological consequences of defects in ERCC1-XPF DNA repair endonuclease. *DNA Repair (Amst.)* 10, 781–791.
 17. Weeda, G., Donker, I., de Wit, J., Morreau, H., Janssens, R., Vissers, C.J., Nigg, A., van Steeg, H., Bootsma, D., and Hoeijmakers, J.H. (1997). Disruption of mouse ERCC1 results in a novel repair syndrome with growth failure, nuclear abnormalities and senescence. *Curr. Biol.* 7, 427–439.
 18. McWhir, J., Selfridge, J., Harrison, D.J., Squires, S., and Melton, D.W. (1993). Mice with DNA repair gene (ERCC-1) deficiency have elevated levels of p53, liver nuclear abnormalities and die before weaning. *Nat. Genet.* 5, 217–224.
 19. Tian, M., Shinkura, R., Shinkura, N., and Alt, F.W. (2004). Growth retardation, early death, and DNA repair defects in mice deficient for the nucleotide excision repair enzyme XPF. *Mol. Cell. Biol.* 24, 1200–1205.
 20. Jaspers, N.G., Raams, A., Silengo, M.C., Wijgers, N., Niedernhofer, L.J., Robinson, A.R., Giglia-Mari, G., Hoogstraten, D., Kleijer, W.J., Hoeijmakers, J.H., and Vermeulen, W. (2007). First reported patient with human ERCC1 deficiency has cerebro-oculo-facio-skeletal syndrome with a mild defect in nucleotide excision repair and severe developmental failure. *Am. J. Hum. Genet.* 80, 457–466.
 21. Gregg, S.Q., Gutiérrez, V., Robinson, A.R., Woodell, T., Nakao, A., Ross, M.A., Michalopoulos, G.K., Rigatti, L., Rothermel, C.E., Kamileri, I., et al. (2012). A mouse model of accelerated liver aging caused by a defect in DNA repair. *Hepatology* 55, 609–621.
 22. Cleaver, J.E., Lam, E.T., and Revet, I. (2009). Disorders of nucleotide excision repair: the genetic and molecular basis of heterogeneity. *Nat. Rev. Genet.* 10, 756–768.
 23. Meindl, A., Hellebrand, H., Wiek, C., Erven, V., Wappenschmidt, B., Niederacher, D., Freund, M., Lichtner, P., Hartmann, L., Schaal, H., et al. (2010). Germline mutations in breast and ovarian cancer pedigrees establish RAD51C as a human cancer susceptibility gene. *Nat. Genet.* 42, 410–414.
 24. Levy-Lahad, E. (2010). Fanconi anemia and breast cancer susceptibility meet again. *Nat. Genet.* 42, 368–369.

The American Journal of Human Genetics, Volume 92

Supplemental Data

Mutations in *ERCC4*, Encoding the DNA-Repair

Endonuclease XPF, Cause Fanconi Anemia

Massimo Bogliolo, Beatrice Schuster, Chantal Stoeper, Burak Derkunt, Yan Su, Anja Raams, Juan P. Trujillo, Jordi Minguillón, María J. Ramírez, Roser Pujol, José A. Casado, Rocío Baños, Paula Río, Kerstin Knies, Sheila Zuñiga, Javier Benítez, Juan A. Bueren, Nicolaas G.J. Jaspers, Orlando D. Schärer, Johan P. de Winter, Detlev Schindler, and Jordi Surralles

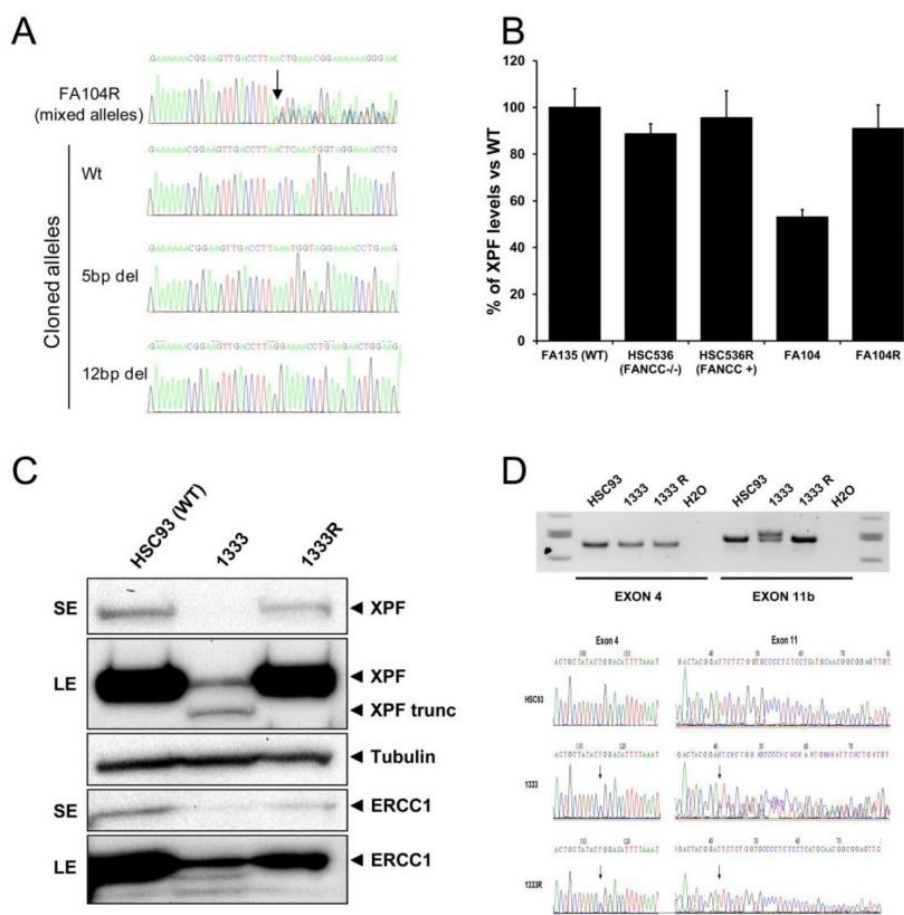


Figure S1. Genetic Analysis of Back Mutations in *ERCC4* in Reverted MMC-Resistant FA Cell Lines

(A) Sequence analysis of individual exon 8 alleles cloned from the FA104R cell line. Exons 8 was amplified from FA104R DNA and the PCR products were cloned with the Topo TA Cloning kit (Invitrogen) and transfected into Library Efficiency DH5alpha Competent Cells (Invitrogen). The plasmids from single bacterial colonies were prepared with the NucleoSpin® Plasmid QuickPure Kit (Macherey-Nagel). Sequencing of single bacterial clones revealed the presence of a 12 bp deletion in exon 8 encompassing the pathogenic 5 bp deletion and restoring the reading frame of the *ERCC4* gene.

(B) Quantification of XPF expression by immunoblot in lymphoblasts from FA104, FA104R, HSC536 (FA-C), HSC536R (HSC536 reverted to wt) and FA139 (wt). XPF levels are expressed as a ratio of the loading control (vinculin). Further details on antibodies used can be obtained upon request. The histogram represents XPF levels in the different cell lines normalized to the levels of the loading control. Means and SEM of at least three independent experiments are shown.

(C) Immunoblot analysis showing low levels of two XPF proteins in 1333 and a normal size XPF protein in the reverted cell line 1333R.

(D) Absence of the 28 bp duplication in *ERCC4* exon 11 in 1333R eliminating the longer *ERCC4* mutant allele with the 28 bp duplication (upper panel) and restoring the wt sequence in exon 11 (lower panel).

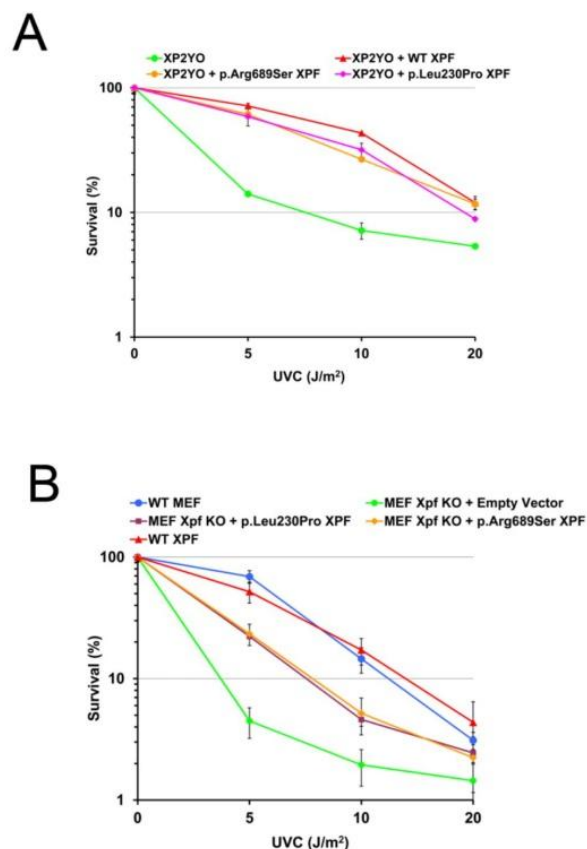


Figure S2. XPF Mutants Leading to FA Restore UVC Resistance of NER-Deficient Human and Mouse Fibroblasts

(A) UVC-induced growth inhibition of human XPF-deficient immortal cell lines from XP and FA individuals (XP2YO and 1333, respectively) transduced with lentiviral particles carrying cDNAs coding for XPF-WT, XPF-p.Arg689Ser and XPF-p.Leu230Pro. Data represent means and SD of two independent experiments.

(B) UV-induced growth inhibition of *Ercc4* KO MEFs transduced with lentiviral particles expressing GFP (negative control vector), wild type XPF, XPF-p.Arg689Ser and XPF-p.Leu230Pro. Data represent means and SD of at least four independent experiments. Lentivirus mediated cDNA transduction and survival analysis were performed as shown in Fig. 1 and 2 (main text).

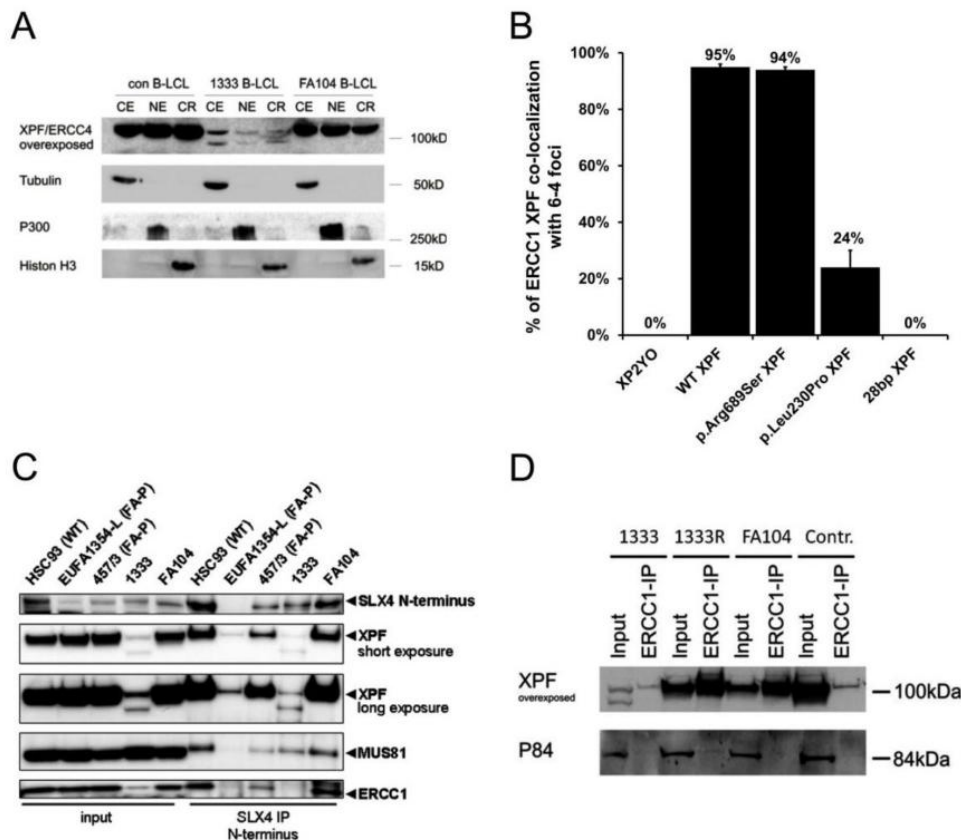


Figure S3. XPF Relocation to DNA Damage and Protein-Protein Interactions

(A) Immunoblot analysis of XPF protein in cytoplasmic (CE), nucleoplasmic (NE) and chromatin (CR) fractions from wild type, 1333 and FA104 lymphoblast cell lines. FA104 and FA104 show an abundance and a distribution of XPF between the cytoplasmic, nuclear and chromatin compartments comparable to a normal control, whereas 1333 reveals reduced abundance and two species of that protein with sizes predicted by its mutations but, of note, XPF is still detected in the nucleus and on chromatin with grossly unaffected ratios to the cytoplasmic fraction. Specificity of the separation of extracts from lymphoblasts is confirmed by the compartment-specific marker proteins tubulin, p300 and histone H3. Subcellular Protein Fractionation Kit from Pierce (Thermo Scientific) following the manufacturer's instructions. Further details on antibodies used and subfractioning conditions can be obtained upon request.

(B) Graphical representation of the percent co-localization of XPF with (6-4)PP in XP2YO cells expressing various forms of XPF. XP2YO cells were transduced with HA-tagged wild type XPF, XPF-p.Arg689Ser, XPF-p.Leu230Pro, or XPF-28bp dup, irradiated with UVC (120 J m^{-2}) through a polycarbonate filter with $5 \mu\text{m}$ pores, incubated for 0.5 h, fixed and stained with antibodies to (6-4)PP and antibodies to HA. Data represent the average of at least 3 independent experiments \pm the SD. For each experiment 100 cells were counted.

(C) Normal SLX4 interactions in XPF-deficient FA individuals. SLX4 was immunoprecipitated with a polyclonal antibody raised against the first 300 amino acids of SLX4 (SLX4 N-terminus; gift from J. Rouse, Dundee). Precipitated proteins were visualized by immunoblotting with antibodies to SLX4 N-terminus, XPF, ERCC1 and MUS81. Reduced XPF and ERCC1 protein expression was found in lymphoblasts of individual 1333. In these cells, full-length and truncated XPF and MUS81 were coprecipitated with SLX4, whereas ERCC1 is barely detectable. In lymphoblasts of individual FA104, the interaction between SLX4 and its binding partners XPF-ERCC1 and MUS81 is normal. Wild type lymphoblasts (HSC93) and lymphoblasts of FA-P individuals (EUFA1354-L and 457/3) were used as controls.

(D) Normal ERCC1-XPF interactions in FA104 and 1333 lymphoblast cell lines. ERCC1 was immunoprecipitated with a polyclonal antibody against ERCC1 and the precipitated proteins were visualized by immunoblotting with antibodies against XPF and P83 as internal control. Further technical details on co-immunoprecipitation conditions and antibodies used can be obtained upon request.

Table S1. List of Candidate Genes with Biallelic Mutations after Whole-Exome Sequencing

Chrom	Pos	Ref	Alt	Ensembl pred	AA change	GN	NRR	SNV Q	GT Q
1	169489751	A	W	SS	-	<i>F5</i>	42	171	171
1	169525877	T	Y	SS	-	<i>F5</i>	52	36	36
2	73675227	-	CTC	NFC	S/SP	<i>ALMS1</i>	16	N/A	N/A
2	73678183	G	R	NSC	G1509D	<i>ALMS1</i>	156	120	120
3	49094490	G	S	NSC	N381K	<i>QRICH1</i>	122	228	228
3	49095011	C	S	NSC	G208R	<i>QRICH1</i>	109	43	43
4	126238305	C	M	NSC	P247T	<i>FAT4</i>	52	178	178
4	126355484	C	M	NSC	A2368E	<i>FAT4</i>	56	190	190
5	156479444	TTG	-	NFC	TS/S	<i>HAVCR1</i>	61	N/A	N/A
5	156479568	-	GTT	NFC	T/TT	<i>HAVCR1</i>	106	N/A	N/A
6	31238942	G	W	NSC	A176V	<i>HLA-C</i>	23	61	39
6	31239577	A	C	NSC	S48A	<i>HLA-C</i>	21	90	90
6	32709309	A	R	SS	-	<i>HLA-DQA2</i>	29	84	84
6	32713044	C	Y	NSC	T64M	<i>HLA-DQA2</i>	192	228	228
6	32713188	C	Y	SS	-	<i>HLA-DQA2</i>	126	228	228
6	38840915	A	R	NSC	I2479V	<i>DNAH8</i>	72	216	216
6	38879340	A	T	NSC	E3267D	<i>DNAH8</i>	12	34	34
7	100686777	C	Y	NSC	T4027M	<i>MUC17</i>	323	228	228
7	100687107	G	R	SS	-	<i>MUC17</i>	66	79	79
8	30700598	T	Y	NSC	N1979S	<i>TEX15</i>	33	97	97
8	30701995	A	M	NSC	D1513E	<i>TEX15</i>	141	228	228
10	69682773	T	Y	NSC	D920G	<i>HERC4</i>	64	69	69
10	69785435	-	A	SS	-	<i>HERC4</i>	9	N/A	N/A
16	14029271	AACTC	-	FC	-	<i>ERCC4</i>	22	N/A	N/A
16	14041518	C	M	NSC	R689S	<i>ERCC4</i>	121	228	228
16	72137553	C	S	NSC	Q564E	<i>DHX38</i>	56	85	85
16	72142141	A	R	NSC	S994G	<i>DHX38</i>	52	106	106
17	74272839	C	Y	NSC	V1593M	<i>QRICH2</i>	54	33	33
17	74277009	T	Y	NSC	Q1264R	<i>QRICH2</i>	23	81	81
18	14105016	C	M	NSC	R508I	<i>ZNF519</i>	136	228	228
18	14105853	C	M	NSC	R229I	<i>ZNF519</i>	23	51	51
19	51918360	A	R	NSC	S445P	<i>SIGLEC12</i>	43	39	39
19	52004795	G	CT	FC	-	<i>SIGLEC12</i>	19	N/A	N/A
X	53561632	A	W	NSC	F4226I	<i>HUWE1</i>	42	53	53
X	53642759	C	M	NSC	E665D	<i>HUWE1</i>	16	33	33

Chrom: chromosome number; Pos: genomic position (GRCh37/hg19); Ref: reference allele; Alt: sample allele; Ensembl pred: consequence prediction of variants on transcript according to Ensembl v59. This column contains one of the following values: SS=splice site, NSC=non-synonymous coding, FC=frameshift coding, NFC=non-frameshift coding; AA change: amino acid change in the affected protein; GN: Gene name; NRR: Number of non-redundant reads; SNV Q: the phred-scaled likelihood that the genotype is identical to the reference; GT Q: Phred-scaled likelihood that the genotype is wrong.

Table S2. Comparative Summary of Clinical and Cellular/Molecular Features of XP, XFE, and FA Individuals with Mutations in *ERCC4*

Clinical/Cellular Features	XPF	XFE	FA
Skin photosensitivity	mild	severe	no
Atrophic epidermis	variable	yes	no
Neurologic features	rare	yes	no
Hematology	normal	anemia ^a	anemia, BMF
Growth retardation ^b	no	yes	yes
Premature death	no	16yo	4yo (FA104). 1333 alive at age 10
UV sensitivity	mild	severe ^c	none (FA104) ^d , mild (1333)
UDS defect	mild	severe ^c	mild (1333), ND in (FA104) ^d
MMC sensitivity	mild	severe	severe
DEB-test	negative	positive	positive
MMC induced G2/M arrest	negative	positive	positive
Nuclease activity on stem loop substrates	yes ^e	yes ^e	no

^aIt is not known whether anemia evolved to BMF in the XFE individual (Laura Niedernhofer, personal communication).

^bInclude microsomy in 1333, FA104 and XFE and microcephaly in XFE and 1333.

^cReported in Niedernhofer et al., 2005.

^dUDS assay was not done in FA104 due to the lack of skin fibroblasts but FA104 lymphoblasts were resistant to UV.

^eReported in Ahmad et al., 2010 for XP mutation p.Arg799Trp and XFE mutation p.Arg153Pro. Typically XP and FA features are marked in yellow and green, respectively.

3.2.2 BIALLELIC MUTATIONS IN THE UBIQUITIN LIGASE *RFWD3* CAUSE FANCONI ANEMIA

Biallelic mutations in the ubiquitin ligase *RFWD3* cause Fanconi anemia

Kerstin Knies,¹ Shojiro Inano,^{2,3} María J. Ramírez,⁴ Masamichi Ishiai,² Jordi Surallés,^{4,5} Minoru Takata,² and Detlev Schindler¹

¹Department of Human Genetics, Biozentrum, University of Würzburg, Würzburg, Germany.

²Laboratory of DNA Damage Signaling, Department of Late Effects Studies, Radiation Biology Center, Kyoto University, Kyoto, Japan.

³Department of Hematology and Oncology, Graduate School of Medicine, Kyoto University, Kyoto, Japan.

⁴Department of Genetics and Microbiology, Universitat Autònoma de Barcelona, Bellaterra (Barcelona), Spain.

⁵Center for Biomedical Network Research on Rare Diseases (CIBERER), Carrer d'Alvaro de Bazan 10, València, Spain.

Conflict of interest: The authors have declared that no conflict of interest exists.

Abstract

The WD40-containing E3 ubiquitin ligase RFWD3 has been recently linked to the repair of DNA damage by Homologous Recombination (HR). Here we show that an *RFWD3* mutation within the WD40 domain is connected to the genetic disease Fanconi anemia (FA). An individual revealed congenital abnormalities characteristic for FA. Cells from the patient, carrying the compound heterozygous mutations c.204_205dupCC and c.1916T>A in *RFWD3*, show increased sensitivity to DNA interstrand cross-linking agents in terms of increased chromosomal breakage, reduced survival and cell cycle arrest in G2 phase. The cellular phenotype is mirrored in genetically engineered human and avian cells by inactivation of RFWD3 or by introduction of the patient-derived missense mutation, and is rescued by expression of wildtype RFWD3 protein. HR is disrupted in *RFWD3* mutant cells, caused by impaired relocation of mutant RFWD3 to chromatin and defective physical interaction with RPA. *Rfwd3* knockout mice exhibit increased embryonic lethality, are sub-fertile, show ovarian and testicular atrophy and have a reduced life span in which they resemble other FA mouse models. Although mutation was detected in a single child with FA yet, we propose *RFWD3* as a novel FA gene, *FANCW*, supported by cellular paradigm systems and an animal model.

Introduction

Safeguarding of the genome is essential for the suppression of oncogenesis and for stem cell maintenance in many organisms and is warranted by DNA repair mechanisms. If they fail on a genetic basis, DNA repair disorders occur. Fanconi anemia (FA) is such a rare human genomic instability disease. While variability occurs, recurrent features include developmental anomalies and malformations, most commonly growth retardation, cutaneous pigment displacement and radial ray defects. Other frequent aspects of FA comprise early-onset bone marrow failure and cancer predisposition, specifically for acute myelogenous leukemia and head and neck squamous cell carcinoma (1-4). FA results from faults in the FA/BRCA pathway for DNA interstrand crosslink (ICL) repair, in which proteins encoded by thus far 21 reported FA genes alias with the prefix *FANCL*- and serial letters of the alphabet, *FANCA* to *FANCV*, and associated proteins interact (5-9). Germline inactivation of any one of the FA genes causes classical FA or variant (FA-like) disease lacking single clinical core features of FA. Common to all subtypes is cellular sensitivity to endogenously or exogenously produced ICLs, implicating spontaneous and induced chromosomal breakage, reduced cell survival and arrest in G2 phase of the cell cycle (2). The FA/BRCA pathway orchestrates the action of other DNA repair proteins such as nucleases, translesion polymerases and effectors of Homologous Recombination (HR), with all of which it interfaces and shares components. New elements of the FA/BRCA pathway continue to be identified in ways that keep our understanding of the FA/BRCA pathway evolving (5, 8-10).

Many of the FA proteins undergo secondary modification. Ubiquitination has become an important issue of ICL repair including ubiquitin donors and acceptors (7). Ubiquitin transfer is facilitated by the coordinate action of three different types of enzymes, E1 for activation, E2 for conjugation and E3 for ligation (11). The monoubiquitination of FANCD2 and FANCI by the E3 ligase FANCL and the E2 ligase UBE2T/FANCT are key steps of the FA/BRCA pathway (7). Compromised function of FANCD2, FANCI, FANCL or FANCT due to defective ubiquitin transfer can abrogate the FA/BRCA pathway (9). In the opposite direction, the deubiquitinating enzyme complex USP1-UAF1 critically regulates ICL repair by the FA

pathway through its deubiquitination activity towards FANCD2-Ub. It has been recognized that the USP1/UAF1 complex also promotes HR (12). This occurs, at least in part, by UAF1-stimulated RAD51AP1 activity (13).

HR has emerged as the most important mechanism for the error-free repair of DNA double-strand lesions. Notably, certain proteins have been acknowledged as both, late-acting components of the FA/BRCA pathway and actors in HR, including BRCA2, PALB2, RAD51C, RAD51, BRCA1 and RAD51B, also known as FANCD1, -N, -O, -R, -S and -U, respectively. One of the major proteins early in HR, replication protein A (RPA), not a known component of the FA/BRCA pathway, is polyubiquitinated by the RING-type E3 ubiquitin ligase RFWD3 on multiple lysine residues in response to DNA damage (14). Primarily described as an ATM and ATR phosphorylation substrate, RFWD3 accumulates at stalled replication forks as part of the DNA damage response (15). At these sites RFWD3 co-localizes with RPA and binds via its WD40 domain at the C-terminus to replication protein A2 (RPA2). RFWD3 functions in replication checkpoint signaling under replication stress and promotes replication fork restart after HR (14, 16-18). Recent work shows that RFWD3 ubiquitinates RPA which is essential for productive HR (14). The formation of an RPA-ssDNA complex and the recruitment of RAD51 alias FANCR, one of the most versatile factors in HR, advance the process (19, 20).

Here we report on a 12-year-old German individual with typical FA phenotype and compound heterozygous mutations in the E3 ubiquitin ligase *RFWD3* [GenBank: NM_018124.3]. Based on our findings we conclude that biallelic germline mutations in *RFWD3* result in FA.

Results

Undefined subtype of a child with classical FA. The individual, referred to as 1143, offspring of unrelated parents of German descent, was born preterm (35 GW) and small for date (1850 g). She presented with duodenal atresia, small midface and bilateral radial ray malformations including left radius hypoplasia and absent thumb on either side. Ultrasonography revealed enlarged lateral cerebral ventricles, a hypoplastic left kidney and polysplenia. Growth retardation with length and weight below the 3rd percentiles and microcephaly continued postnatally. Hypothalamic partial growth hormone deficiency gave cause for hormone replacement therapy starting as of 2 y, resulting in catch-up growth along the 3rd percentiles for height and weight to date. MRI at age 2 y demonstrated rarefied periventricular white matter, a narrowed corpus callosum, downscaled anterior pituitary, ectopic position of the posterior pituitary in the hypothalamic region and Chiari malformation type 1. These changes did not cause neurological deficits or intellectual disability such that she attends regular classes. This is consistent with the observation that minor brain malformations with little, if any clinical manifestation are relatively frequent in FA patients (21). As from age 10 her bone marrow was cytopenic with reduced hematopoiesis and increased fatty tissue. There were mild dysplastic features including dysmyelopoiesis (hypogranularity) and dysmegakaryopoiesis (abnormal lobulation) while erythropoiesis was slightly megaloblastoid. MDS was excluded on several occasions. Cytopenia is restricted to bone marrow; up to her present age of 12 y peripheral blood counts remain stable at a normal level. The clinical diagnosis of FA based on the indicated findings was confirmed by cellular hypersensitivity of cultured lymphocytes and fibroblasts to DNA-crosslinking agents (Supplemental Figure 1, A and B). She was classified to belong to a post-D2 FA subtype owing to intact cellular FANCD2 monoubiquitination (Supplemental Figure 1C). Proper RAD51 foci formation effectively ruled out groups FA-D1, -N and -O, -R, -S and -U (Supplemental Figure 1D). Sanger sequencing of the remaining downstream FA genes failed to detect any mutation.

Whole exome sequencing (WES) identifies biallelic mutations of RFWF3. Assuming a yet unreported FA subgroup, WES was performed on fibroblast DNA. Statistical results of the

data analysis are summarized in Supplemental Table 1. After exclusion of non-authentic variants and formally inconsistent mutations, data mining left only two meaningful heterozygous mutations in the gene *RFWD3* (Supplemental Table 2) that had been reported to be involved in the DNA damage response mediated by p53 and RPA2 (14, 22, 23). The two detected mutations, a 2-bp-duplication resulting in premature termination of translation (c.204_205dupCC; p.L69Pfs*12) and a missense mutation (c.1916T>A; p.I639K) at a highly conserved position (Figure 1A), were confirmed by Sanger sequencing. They are located on different parental alleles and segregate in the family consistent with an autosomal recessive disorder (Figure 1B). Both variants are rare. They have not been reported in the 1000 Genomes Project (27,478 samples, February 2017) or in the Exome Aggregation Consortium (ExAC) database (60,706 samples, February 2017). Both variants were classified as probably damaging by several in silico prediction software tools. c.204_205dupCC (p.L69Pfs*12) is located in the N-terminal region of RFWD3 that is characterized by LQP-SSQ repeats of hitherto unknown function (23), whereas c.1916T>A (p.I639K) is situated in the WD40 domain responsible for RPA2 binding.

Wildtype (WT)-RFWD3 reverses genomic instability and deficient HR of 1143 cells. While there is little doubt that c.204_205dupCC represents a functional null allele, reasonable concern was raised about the pathogenic nature of the missense variant p.I639K. To address this question, 1143 and control cultured fibroblasts were transduced with WT-RFWD3 and control vectors. Susceptibility of cultured 1143 cells to specified chemical agents allowed for sensitivity testing. On cell cycle studies, FA-typical G2-phase accumulation following exposure to MMC or DEB was restored to normal control levels in 1143 cells expressing ectopic WT-RFWD3, but not in mock-transduced 1143 cells (Supplemental Figure 1, E and F). Chromosomal breakage analysis showed accumulation of metaphases with ≥ 10 breaks per nucleus including frequent radial figures (that reflect misdirected break repair by error-prone homology-directed pathways when HR is compromised) following exposure to MMC of non-transduced cells, or of those that were transduced with mock vector or vector containing the patient mutation, RFWD3-I639K cDNA

(Figure 1C). In contrast, 1143 fibroblasts ectopically expressing WT-RFWD3 showed very few metaphases with high breakage rates. Moreover, survival of 1143 fibroblasts exposed to MMC was rescued after transduction with WT-RFWD3, whereas untreated 1143 cells, 1143 transduced with mock virus or FA fibroblasts of subtype Q (FA-Q) showed significantly reduced survival in a dose-dependent manner (Figure 1D). 1143 fibroblasts were also hypersensitive to cisplatin (CDDP) to an extent that is comparable with FA-B or FA-Q fibroblasts (Figure 1E).

Similar to FA-D1 (biallelic *BRCA2*-mutant) cells with impaired HR, 1143 fibroblasts reveal sensitivity to the topoisomerase-1 inhibitor camptothecin (CPT). Decreased survival compared to non-FA control was rescued when 1143 cells were transduced with WT-RFWD3 (Figure 1F). Lastly, 1143 fibroblasts and those transduced with mock or I639K-mutant vector were sensitive to the poly-ADP ribose polymerase 1/2 (PARP) inhibitor olaparib. This sensitivity was distinct but not as pronounced as that of FA-D1 cells. Once again, this sensitivity was rescued by ectopic expression of WT-RFWD3 (Figure 1G). Poly-ADP ribose mediates the *BRCA2*-dependent early DNA damage response (24). Since RFWD3 deficiency impairs that mechanism, as indicated by cellular olaparib sensitivity, the latter results suggest the involvement of RFWD3 in HR in a *BRCA2*-dependent manner.

Consequences of RFWD3 deprivation. RFWD3 deficiency provides a means to infer normal protein functions from malfunction. The I-SceI-induced HR assay has become widely accepted as an indicator for a protein to influence the HR mechanism (25, 26). In this assay, inactivation by RNA interference of either *BRCA2* or RFWD3 resulted in a highly significant loss of HR function relative to mock siLUC transfection, confirming that RFWD3 is involved in the HR pathway (Figure 2A, left panel). Similarly, HR activity of FA-D1 (biallelic *BRCA2*-mutant) fibroblasts and of 1143 cells was compared with human normal control fibroblasts. RFWD3 deficiency down-regulated HR activity substantially, resembling *BRCA2* deficiency (Figure 2A, middle panel). Untreated, mock or RFWD3-I639K cDNA-transduced 1134 fibroblasts were impaired in HR in contrast to 1143 fibroblasts after WT-RFWD3

transduction, confirming in a isogenic system that the RFWD3-I639K mutation of 1143 cells is responsible for the loss of HR activity (Figure 2A, right panel).

Further experiments aimed at understanding in which way the 1143 mutations exert their effects. Western blot analysis of 1143 lymphoblasts showed that mutant RFWD3 of normal size is expressed whereas any truncated protein was undetectable (Figure 2B). The full-length mutant protein may be slightly less stable in cytoplasm, as cellular fractionation studies suggested, but is strikingly less relocated to the nucleus and to chromatin (Figure 2C). Paucity of mutant RFWD3-I639K in chromatin, leave alone impaired function, resulted in a longer persistence of RPA and RAD51 nuclear foci in 1143 fibroblasts. After an initial pulse of 8 h exposure to MMC the proportion of 1143 cells that scored positive for RPA foci was increased at early times (24 h and 48 h; Figure 2D, left and middle panel) and the proportion of RAD51 foci-positive cells was elevated at later times (72 h and 96 h; Figure 2D, right panel). At other times (RPA foci-positive cells after 48 h and RAD51 foci-positive cells before 72 h) there was no significant difference of foci-positive 1143 cells compared with 1143+WT complemented and normal control fibroblasts. These data extend the idea that RFWD3 normally promotes HR induced by ICLs, and HR is delayed when RFWD3 is mutated.

Three different cellular model systems recapitulate RFWD3 mutation. Using the CRISPR/Cas9 system we generated an *RFWD3*-mutant clone of U2OS cells, designated CR21F5, owning the homozygous 6-bp deletion c.1941_1947delICGGCAC. The deletion results in the in frame loss of 2 aa, p.R648_H649del, located in the RPA2-binding WD40 domain. CR21F5 cells displayed increased sensitivity to MMC on survival and cell cycle studies (Figure 2, E and F) and to CPT (Supplemental Figure 1G), mimicking 1143 fibroblasts, but contrasting parental U2OS cell and 1143 WT-*RFWD3*-complemented fibroblasts.

A second *RFWD3*-deficient cellular model represent HAP1 cells harboring a 13-bp deletion in *RFWD3* exon 3, c.566_578del, predicted to result in the largely mutated and truncated protein RFWD3 p.P189Lfs*174. Consistently, these cells also displayed MMC sensitivity on survival and cell cycle studies (Figure 2, E and G). Unfortunately, HAP1 cells

tend to duplicate chromosomes, which limits their use for chromosome breakage studies. *RFWD3*-mutated HAP1 cells were complemented by transduction with WT-*RFWD3*, demonstrated by rescue from MMC sensitivity in terms of G2 arrest (Figure 2G). Third, we generated Δ *RFWD3* DT40 cells by targeted disruption of the chicken *RFWD3* locus (Supplemental Figure 2, A and B). The cells were deduced to be functionally null for two reasons, the CxxC motif in the RING finger was deleted and no *RFWD3* transcript was detected by RT-PCR (Supplemental Figure 2C). Δ *RFWD3* DT40 cells grew slower in culture than non-targeted DT40 cells (Supplemental Figure 2D). The gene targeting frequency at the *OVALBUMIN* and *KU70* loci in Δ *RFWD3* DT40 cells was determined by disruption constructs as previously described (27). Targeting events were greatly reduced in two independently produced Δ *RFWD3* vs. parental DT40 cell lines (Figure 3A).

Defective HR in Δ *RFWD3* DT40 cells was further examined by a modified I-SceI induced HR assay. The recombination substrate SCneo (two tandem non-functional *neo* cassettes that can be repaired by HR) was integrated at the *OVALBUMIN* locus. In DT40 cells, transient transfection of I-SceI expression vector resulted in an increase of more than three orders of magnitude of neo-resistant cells compared to cells transfected with control vector (Figure 3B). Δ *RFWD3* DT40 cells achieved HR events with approximately one order of magnitude less efficiency, which was not improved when they were transfected with ch*RFWD3*-C267A. This mutation disrupts the RING domain, inactivating the *RFWD3* E3 ligase function as has been described for the human equivalent mutation C315A in U2OS cells (23). Expression of WT-ch*RFWD3* rescued the frequency to some extent, while transfection with ch*RFWD3*-I615K, the chicken counterpart of the human I639K mutation, did not. We also determined the ratios of short and long tract gene conversion events (STGC and LTGC, Supplemental Figure 2E) in the HR repair product of SCneo by isolating *neo*-resistant colonies following I-SceI transduction. STGC and LTGC occurred at indistinguishable rates in non-targeted and Δ *RFWD3* DT40 cells, suggesting that loss of *RFWD3* affects efficiency, but not the tract length, of HR induced by DNA double-strand breaks (Supplemental Figure 2F).

Δ RFWD3 DT40 cells proved hypersensitive to MMC or cisplatin in terms of survival, compared with parental DT40 cells (Figure 3, C and D). Δ RFWD3 DT40 cells were rescued by stable expression of WT-chRFWD3, but not of chRFWD3-C267A. Transfection with chRFWD3-I615K resulted in intermediate sensitivity. Chromosomal studies revealed increased breakage in the form of chromatid and chromosome type lesions in Δ RFWD3 DT40, compared to parental DT40 cells, when exposed to MMC (Figure 3E), resembling Δ FANCD2 or Δ XRCC3 DT40 cells (28). Again, stable expression of WT-chRFWD3 restored the breakage rate to normal, whereas transfection with chRFWD3-C267A had virtually no effect and expression of chRFWD3-I615K resulted in intermediate rates. These results show that cells with the chI615K (equivalent to human I639K) mutant are impaired in HR, in the maintenance of challenged chromosomal integrity, and in MMC and cisplatin tolerance.

Collectively, these three different cellular models, all lacking RFWD3 on a different genetic background, support the notion that *RFWD3* functions in the FA pathway and HR.

RFWD3-I639 is necessary for RFWD3 focus formation. In order to examine how the chicken I615K mutation (equivalent human I639K) affects functions of the RFWD3 protein in cells, Δ RFWD3 DT40 cells were transiently transfected with mock vector, vector containing GFP-tagged chRFWD3-C267A or the double mutant GFP-chRFWD3-C267A/I615K. The expression of GFP-chRFWD3-C267A showed RFWD3 protein that was relocated to the nucleus and induced RFWD3 focus formation (Figure 3F). By contrast, expression of the GFP-chRFWD3-C267A/I615K double mutant prevented the translocation of RFWD3 to the nucleus and focus formation. In this experiment, the percentage of GFP-positive cells was comparable between cells expressing GFP-chRFWD3-C267A and GFP-chRFWD3-C267A/I615K (Figure 3G, upper panel), indicating that expression levels were similar. However, GFP foci-positive cells were much decreased in the C267A/I615K double mutant relative to the C267A mutant (Figure 3G, middle panel). Even stronger reduced was the number of foci in individual GFP-RFWD3 foci-positive cells (Figure 3G, lower panel). Immunoblotting confirmed that GFP-WT-chRFWD3 is able to access chromatin whereas the level of GFP-chRFWD3-I615K in chromatin was much less (Figure 3H), paralleling our

findings in human *RFWD3*-mutant 1134 cells. Reduced amounts of FLAG-*RFWD3*-I639K in chromatin compared with FLAG-WT-*RFWD3* were also observed on immunoblots when U2OS cells were transiently transfected with corresponding vectors and exposed to MMC (Figure 4A). This notion was underscored by the reduction of *RFWD3* foci-positive cells, but not RPA2 foci-positive cells, when the I639K mutant was transfected (Figure 4B). Quantification confirmed that there was a highly significant difference in the number of FLAG-*RFWD3* foci in individual FLAG-*RFWD3* foci-positive cells (Figure 4C, upper panel), but there was no difference in the proportion of RPA foci-positive U2OS cells after exposure to MMC (Figure 4C, lower panel). Co-immunoprecipitation of human FLAG-*RFWD3*-I639K with RPA2 displayed a largely decreased physical interaction in U2OS cells after exposure to MMC which was in contrast to the transfection with FLAG-WT-*RFWD3* (Figure 4D). Pull-down studies between GFP-*RFWD3* containing the RING mutation C315A, or the RING mutation plus the patient's WD40 mutation (I639K), and human his-*RFWD3*-C315A showed that neither mutation affects *RFWD3*-*RFWD3* dimerization (Figure 4E). However, the RING mutation C315A abrogated *RFWD3* auto-ubiquitination whereas the WD40 mutation I639K did not when U2OS cells were transiently transfected with FLAG-*RFWD3*-WT, FLAG-*RFWD3*-I639K or FLAG-*RFWD3*-C315A and exposed to the proteasome inhibitor MG132 (Figure 4F).

Thus we conclude that *RFWD3*-I639 or its chicken equivalent *chRFWD3*-I615 is an absolute requirement for chromatin translocation, physical interaction with RPA, and ICL repair/HR functions of *RFWD3*.

In U2OS cells FLAG-*RFWD3* and FANCD2 foci occur in overlapping or immediate adjacent positions in a majority of cells after exposure to MMC, suggesting temporary cooperation of the proteins in HR (Figure 4G and Supplemental Figure 2G). This is similar to observations that, following DNA damage induction, a majority of GFP-FancD2 and Rad51 foci co-localized although Rad51 and FancD2 foci formation are independent events (29), and that monoubiquitinated FANCD2 and BRCA2/FANCD1 co-localize in DNA damage-

inducible foci (30). Together these data indicate that FANCD2 and RFWD3, RAD51 and BRCA2/FANCD1 converge and accumulate at the same DNA damage sites.

We depleted FANCD2 in HAP1 *RFWD3*-knockout cells and confirmed that by immunoblotting (Supplemental Figure 2H). An MMC dose-response curve demonstrates that FANCD2 knockdown has a small but significant additive effect to RFWD3 deficiency such that both defects can be designated as non-epistatic in terms of ICL repair (Figure 4H). A similar observation has been made in DT40 cells that were double-mutant for *FANCC* whole gene deletion and *BRCA2* C-terminal deletion. Such *fancc/brca2* Δ CTD double-mutant cells showed a more severe level of sensitivity to cisplatin and MMC compared with either of the single mutants (29). The additive sensitivity indicates that FANCD2 and RFWD3, or FANCC and BRCA2 have non-overlapping functions in ICL repair.

An Rfwd3^{-/-} mouse model resembles other FA mouse models. Using gene targeting in ES cells of C57BL/6 mice, *Rfwd3* exon 3 was disrupted (Supplemental Figure 3A). Southern blot analysis was used to genotype the offspring (Supplemental Figure 3B). RT-PCR analysis of normalized relative *Rfwd3* mRNA expression in *Rfwd3^{-/-}* and *Rfwd3^{+/+}* mice confirmed *Rfwd3* silencing in *Rfwd3^{-/-}* mice (Supplemental Figure 3C). An initial characterization of *Rfwd3^{-/-}* mice demonstrated that they are viable and do not show overt phenotypic abnormalities. Heterozygous and homozygous offspring was born at approximately 1:1 sex ratio (Figures 5A). However, *Rfwd3^{+/+}* heterozygous mating resulted in a sub-Mendelian proportion of *Rfwd3^{-/-}* homozygous pups, consistent with the notion of embryonic lethality. Subfertility was an additional finding. Mating of homozygous *Rfwd3^{-/-}* mice failed nine times including three attempts of mating KO males and KO females, three attempts of mating WT males and KO females, and three attempts of mating KO males and WT females. That way, six females (23.1% of 26 KO mice) and 3 males (11.5% of 26 KO mice) proved infertile. We refer to this observation as subfertility since not all *Rfwd3^{-/-}* mice were mated. Histological examination of *Rfwd3^{-/-}* mice detected testicular and ovarian atrophy. In males, seminiferous tubules were largely retained. There was a patchy change where few showed only small amounts of spermatogenesis but most appeared empty with little evidence of any active cell

divisions (Figure 5B). Female *Rfwd3*^{-/-} mice displayed small ovaries with predominance of luteal cells and inactive epithelium on the surface. No follicular differentiation or development was detected (Figure 5C). As a preliminary observation, some *Rfwd3*^{-/-} offspring lived a shortened lifespan for unknown reasons.

Rfwd3^{-/-} MEFs proved hypersensitive to DNA crosslinking agents. When exposed to MMC they showed increased G2 phase accumulation compared with *Rfwd3*^{+/+} MEFs (Figure 5D). Chromosomal breakage analysis of *Rfwd3*^{-/-} MEFs revealed increased numbers of lesions with a distribution typical for FA, in contrast to *Rfwd3*^{+/+} mice that showed unremarkable rates and distribution (Figure 5E). Breaks were mostly of the chromatid type and included characteristic radial figures (Figure 5F). *Rfwd3*^{-/-} MEFs also showed reduced dose-dependent survival when exposed to MMC compared with *Rfwd3*^{+/+} MEFs, and they were rescued by prior transduction with human WT-RFWD3 (Figure 5G).

Discussion

This study presents a new FA subtype resulting from biallelic mutations in the E3 ubiquitin ligase gene *RFWD3*. Two compound heterozygous mutations have been identified using WES. The paternally derived allele shows a duplication of the cytosine residues at positions c.204_205 leading to premature termination of translation. Because we did not detect truncated RFWD3 protein and the mutation is N-terminally located, it is safe to assume that the transcript is subject to nonsense-mediated RNA decay. The maternal allele produced a relatively stable RFWD3 protein with the missense substitution p.I639K. This is located in the predicted WD40 domain (23). We showed it to be pathogenic in different systems as it prevents RFWD3 relocation to chromatin and impairs several of its functions.

Elia et al. (14) recently reported, in a context independent of FA, that RFWD3 ubiquitinates RPA. Our work shows a disrupted physical interaction of mutant RFWD3 and RPA. This RFWD3-RPA malfunction adds a mechanistic insight primarily from a human system and another missing piece of the jigsaw regarding the pathogenesis of FA. One possibility is that the RFWD3 I639K mutation abrogates the E3 ligase function towards RPA2, since the RPA2 interaction domain is located at the C-terminus of the RFWD3 protein (22) that includes the I639 residue. Further studies will elucidate the exact mechanisms. It also remains to be seen if other interactors or processes are involved. Since RPA is involved in HR, our studies were aimed at the demonstration that this holds also for RFWD3. Two experimental results supported this view. The results of the I-SceI induced HR assay in human and chicken cells globally indicated impaired homology-directed recombination upon *RFWD3* mutation. Prolonged retention of RPA1 and RPA2 foci in cells with the I639K substitution suggested delayed HR. The finding that RAD51 foci also were longer persisting as in controls may indicate an indirect effect on, or could mean a direct implication of RAD51.

HR is a hierarchical process with master players such as the BRCA1-PALB2-BRCA2 complex and RAD51, and it is also a linear pathway that proceeds sequentially step by step. Impaired HR can result in an FA phenotype as has been demonstrated by mutations of genes contributing to HR which are also FA genes (31). Including *RFWD3*, the number of

reported FA genes involved in HR amounts to a total of remarkable seven, which act at different stages of HR. While the BRCA1, PALB2 and BRCA2 proteins function at the level of orchestration, RFW3 works at an early step of ssDNA marking whereas RAD51, RAD51C and XRCC2 have been associated with strand invasion, D-loop formation and Holliday junction resolution (32). This leads us to conclude that the FA/BRCA pathway converges on HR. Of note, it has not been the frequently mutated FA genes whose products are among those that form the FA core complex, which have most contributed to recognize the association of FA and HR for genomic stability in man including cancer prevention and longevity. This has rather been achieved by the more recent observation of inactivation of newly identified downstream or late FA genes with immediate involvement in the excision of ICLs, in TLS or in HR. These less frequently affected FA genes have all been reported initially with few or single patients and hypomorphic mutations because other constellations may be nonviable. Nevertheless, this way we have learned more of the FA/BRCA pathway with than was discovered over a long period with the upstream or early FA genes.

The proposed patient demonstrates that RFW3 deficiency does not necessarily result in early tumorigenesis, partly perhaps because the p.L639K mutation is not fully penetrant. On the other hand 1143 patient cells do clearly show impaired HR activity which evidently does not drive forth early-onset embryonal tumors or AML. Pronounced early cancer proneness has been reported only for FA due to biallelic mutations of *BRCA2* (FA-D1) (33) and of the direct *BRCA2* interactor *PALB2* (FA-N) (34). Our study of RFW3 deficiency extends observations in FA subtypes FA-O (*RAD51C/FANCO*-mutant) and FA-U (*XRCC2/FANCU*-mutant) whose cells are deficient in HR, too, but patients have not been described with early embryonal tumors (35-37). Moreover, distinct early tumorigenesis has not been associated with FA-R (*RAD51/FANCR*-mutant) or FA-S (*BRCA1/FANCS*-mutant) FA patients (19, 20, 38) whose affected genes likewise are involved in HR. We suggest that *BRCA2*-specific rather than FA/BRCA pathway functions facilitate the extreme proneness to malignancies of FA groups FA-D1 and FA-N, which is much greater than and different from the tumor disposition inherent to other FA subtypes (1, 4).

This is different from the concept of synthetic lethality that affects all cells with deficient HR. Such synthetic lethality occurs when there is a potent and lethal synergy between two otherwise nonlethal events: here, one element is camptothecin, a highly specific type 1 DNA polymerase inhibitor that prevents the ligation of DNA single-strand breaks, or olaparib, a PARP inhibitor that also interferes with single-strand break repair. Unrepaired single-strand breaks are converted to double-strand breaks upon replication. The other component of synthetic lethality in our study is *RFWD3* deficiency that leads to the loss of HR function necessary to repair double-strand breaks. As they cannot be properly repaired HR-deficient cells become selectively and exceptionally sensitive to compounds that exploit their Achilles heel. Apart from *RFWD3* deficiency, increased sensitivity to this type of chemicals is shared with cells with biallelic mutations of one of the other six FA genes acting upon HR.

We generated an *Rfwd3* KO mouse model that serves as a direct support of the pathogenicity of mutant *RFWD3* in the human disease of FA. It may also serve as a future basis for a better understanding of patient-independent in vivo functions of *RFWD3*. The fact that *Rfwd3*^{-/-} mice fail to show a recognizable pattern of phenotypical anomalies that resemble FA patients (39-41) is compatible with this view as it is mirrored in other FA knock-out mouse models (42). In contrast, subfertility and embryonic lethality are features frequently seen in other FA mouse models (39). Notably, *Rfwd3*^{-/-} mice are not completely sterile, a trait in which they are more similar to recently reported *Fancp*^{-/-} mice than to most other FA mouse models (39, 41). *Rfwd3*^{-/-} mice may serve for studies of attrition of hematopoietic stem cells in FA, for transplantation studies, for sensitivity testing of aldehydes and oxygen, for drug screens, and for cancer studies. However, long-term survival observations are still necessary for *Rfwd3*^{-/-} mice as regards the occurrence of malignancies.

In conclusion, we identified biallelic mutations in *RFWD3* in an individual presenting with classical FA. As an E3 ubiquitin ligase that promotes HR via ubiquitination of RPA it finds its position late in the FA/BRCA pathway, downstream of *BRCA2/FANCD1*. Since HR is hampered when *RFWD3* is mutated, *RFWD3* seems to be one of the key players in the

regulation of HR. In recognition of its function as a FA gene we propose to assign RFWD3 the alias FANCW. Further clinical studies will reveal if it is also a susceptibility gene for familial cancer such as the Hereditary Breast and Ovarian Cancer disorder (HBOC) when mutated on only one allele, as it holds true for many downstream FA genes (43).

Methods

Cell lines. All cells except DT40 were cultured in complete DMEM supplemented with 15% FBS at 37 °C in incubators with 5% CO₂. Exceptions are indicated where applicable. Cells were immortalized using standard protocols. RFWD3⁻-HAP1 cells were obtained from Horizon Genomics (HZGHC002532c010), revealed a 13-bp deletion in exon 3 of *RFWD3* (c.566_578del; p.P189Lfs*174), and were maintained according to the manufacturer's instructions.

DNA sample preparation, PCR and Sanger sequencing. Genomic DNA was isolated using the GeneJet™ Genomic DNA Purification Kit (Fermentas) and the Quick-gDNA MiniPrep Kit (Zymo Research). Mutation validation, segregation analysis and screens for off-target events were performed by Sanger Sequencing using Bio-X-Act DNA short polymerase (Bioline) according to manufacturer's protocol on an Applied Biosystems 3130xl sequencer. Primer sequences for genomic sequencing are listed in Supplemental Table 3. Primer design and mutational nomenclature are based on transcript ENST00000361070.8. PCR conditions are available upon request.

Whole exome sequencing. Target enrichment was performed with the Agilent SureSelect Human All Exon 50Mb Kit and followed by Next Generation Sequencing on a HighSeq2000 instrument (Illumina). Processing of WES data using NextGENe™ software v2.18 (Softgenetics) and in silico analysis were performed as described before (44).

Transfection and viral transduction. Generation of stable oncoretroviral producer lines and transduction of adherent cells were performed following the instructions in the Lenti-X Lentiviral Expression System User Manual of Takara Clontech. The control vector pLVX-EF1α, expressing an IRES-*puro* cassette, and the RFWD3 vector pLVX-EF1α+WT, expressing additionally human wildtype RFWD3 cDNA, were constructed using classical cloning methods (primer sequences for cloning are listed in Supplemental Table 4). Because of inappropriate restriction sites in the MCS, we generated convenient restrictions sites using gBlocks (IDT, Integrated DNA Technologies; sequences available upon request). The missense mutation encoding the I639K substitution was introduced using the Q5 Site-

Directed Mutagenesis Kit (New England Biolabs) according to the manufacturer's instructions. Transduced cells were selected in puromycin for 7–14 d, and challenged with MMC. We analyzed transduced fibroblasts and other cells by cell cycle analysis as described, did survival assays or used other readout systems.

DT40 gene targeting. Δ RFWD3 DT40 cells were generated by gene targeting as described (45). Briefly, a targeting vector with a histidinol or puromycin resistance cassette was used to substitute a ~1.2kb genomic segment between chRFWD3 exons 2 and 3, similarly as described elsewhere (27). The strategy is shown in Supplemental Figure 2A. Gene targeting replaced a ~9.3 kb wild-type genomic with a ~4.5kb targeted SacI fragment on Southern blots. chRFWD3 cDNA was amplified from DT40 total RNA, cloned into pENTR plasmids and transferred to expression plasmids using the Gateway system (Thermo Fisher Scientific). Generation of chRFWD3 mutants were performed by QuikChange Site-Directed Mutagenesis Kit (Agilent Technologies) according to manufacturer's instructions. To obtain stably expressing clones, chRFWD3-IRES-GFP or GFP-chRFWD3 expressing plasmids were transfected into DT40 Δ RFWD3 cells. Clones were selected by measuring GFP expression levels on a FACS Calibur (Becton Dickinson) flow cytometer (27, 46). DT40 cells were cultured as described (45).

Cell cycle, cell survival and chromosomal studies. Flow cytometric cell cycle analysis was deployed as described after exposure of fibroblasts to 30 nM (10 ng/ml) MMC or to 116 nM (10 ng/ml) DEB for 48 h (47, 48). For cell survival assays we adopted protocols reported by Kim et al. (49). Human fibroblasts were exposed to 20–100 nM MMC or 0.1–16 μ M cisplatin for 8 d. In knockdown studies, HAP1 cells were treated with FANCD2 siRNA and exposed to the indicated concentrations of MMC for 16 h. After 8 h of recovery, cells were plated with serial dilution and colonies were counted after 7 d. To study MMC sensitivity of DT40 cells, they were serially diluted, exposed to an MMC pulse of 1 h and plated into medium containing 1.5% methylcellulose. Colonies were counted after incubation for 1–2 weeks. Cell numbers were determined using a Nucleo Counter NC-250 (Chemometec). Assays were performed according to the manufacturer's protocols. To assess cisplatin

sensitivity, DT40 cells were treated with the indicated concentration for 48 h, and cell viability was assessed in solution using a FACS Calibur instrument after propidium iodide staining (45). For the PARP-inhibitor assay the commercially available PARP-inhibitor olaparib (Selleckchem) was used.

Chromosome preparations were made by the air drying method. Solid (Giemsa)-stained metaphases were examined for chromatid and chromosome type damage. Whole-blood cultures were stimulated by phytohemagglutinin. They were exposed to MMC at final concentrations of 0, 50 or 100 ng/ml for 72 h. Mitotic cells were arrested in metaphase using colcemid for 45 min. 0.075 M KCl was used as hypotonic treatment. Metaphase spreads were solid-stained with 5% Giemsa solution. Slides were analyzed on an Axioskop Imager A1 (Zeiss) and scored for chromosomal instability. Cultured fibroblasts were processed similarly but exposure to MMC was for 48 h, exposure to colcemid for 2.5 h and 0.8 M sodium citrate dihydrate was used as hypotonic treatment. Analysis of chromosome aberrations in DT40 cells was performed as previously described (27).

Protein fractionation and immunoblotting. Protein fractionation was achieved using the Subcellular Protein Fractionation Kit (Thermo Fisher Scientific) for cultured cells according to the manufacturer's instructions. Whole protein lysates of lymphoblasts or fibroblasts were obtained using Pierce IP Lysis Buffer (Thermo Fisher Scientific). Aliquots equaling 40 µg of protein were prepared in 4x LDS Sample Buffer (Invitrogen). 10x Sample Reducing Agent (Invitrogen) was added. Samples were heated to 70 °C for 10 min and separated on 7%, 4-12% or 3-8% gels by SDS-PAGE (Invitrogen). Proteins were transferred to a nitrocellulose membrane using the iBlot2 system (Invitrogen). After blocking of unspecific binding sites by 5% skim milk in phosphate buffered saline (PBS) containing 0.1% Tween20 for 1 h, antibodies listed in Supplemental Table 5 were applied. After four rounds of washing with PBS-T for 15 min, membranes were overlayed with Immobilon Western Chemiluminescent HRP Substrate (Millipore) and analyzed using the MicroChemi System (Berthold).

To isolate the chromatin fraction, DT40 cells were lysed in buffer A (10 mM HEPES, 10 mM KCl, 1.5 mM MgCl₂, 0.34 M Sucrose, 10% Glycerol, 0.1% tritonX-100 containing 1

mM DTT, 1mM Na₃VO₄, and protease inhibitor cocktail (Roche)). After incubation on ice for 30 min samples were centrifuged at 1,700 x g for 5 min. The pellets were washed with buffer A once. Cells were lysed in buffer B (3 mM EDTA, 0.3 mM EGTA, containing 1 mM DTT, 1 mM Na₃VO₄ and protease inhibitor cocktail) and incubated on ice for 30 min. After centrifugation at 5,000 x g for 5 min, pellets contained the chromatin fraction. Proteins were separated by SDS-PAGE and detected by immunoblotting using anti-GFP (MBL), anti-Histone H3 (Active Motif) and the ECL prime kit.

CRISPR/Cas9 gene targeting. U2OS cells seeded in 6-well plates with 70-80% confluency were transfected with pSPCas9(BB)-2A-Puro (PX459, Addgene) using Lipofectamine 3000 (Life Technologies) according to user's manual. Each transfection contained three different sgRNA's, generated by using <http://crispr.mit.edu/guides> (50). sgRNAs for targeting the *RFWD3* gene were as follows: CR1, GGCAGTGTCTTGTGACCTACAG; CR2, GCACTGTCTTGTGACCTACA; CR3, GGGGGCTGCATAGACTTTCA. All three sgRNAs are directed to exon 11, one of them covers even position c.1916 of the missense mutation. In addition the same experiment was performed by co-transfecting U2OS cells with one of the sgRNA's and a template vector (pBlueScript II SK(+), Addgene) containing *RFWD3* cDNA with c.1916T>A. This vector was generated by classical cloning via the restriction sites SacI-HF and EcoRI-HF. 72 h after transfection, the medium was changed and selection with puromycin was launched for 4 d. Single cells were seeded in 96-well plates and expanded until sufficient cells were available for DNA isolation. Clones were analyzed by Sanger Sequencing.

Immunofluorescence. Cells were grown on glass slides. Sub-confluent cultures were exposed to 40 ng/ml of MMC and analyzed after indicated intervals as described (35). For U2OS experiments, cells were fixed with PBS containing 3% paraformaldehyde, 2% sucrose and 0.5% Triton-X-100 on ice for 30 min, and were then permeabilized with 0.5% Triton-X-100/PBS for 5 min. After blocking with 2% BSA/PBS, samples were stained with antibodies diluted in 2% BSA/PBS for 1 h at room temperature. The secondary antibodies used were Alexa Fluor 488-conjugated anti-mouse IgG or Alexa Fluor 594-conjugated anti-rabbit IgG

(Molecular Probes). For DT40 experiments, cells were exposed to 500 ng/ml MMC for 8 h. DT40 cells were immobilized on glass slides using a Cytospin (Thermo Fisher Scientific) centrifuge, and were fixed with 4% paraformaldehyde for 30 min. Cells were permeabilized with PBS containing 0.5% Triton-X for 5 min and incubated with anti-GFP monoclonal antibody (MBL) or other antibodies at 37 °C for 30 min. Nuclei were counterstained with DAPI, and slides were analyzed on a BIOREVO BZ-9000 microscope (Keyence).

Plasmid transfection. For adherent cells, Lipofectamine 3000 (Invitrogen) was used according to the manufacturer's instructions. For DT40 cells, electroporation by Neon (Invitrogen) at 1,500 V, 20 msec, 1 pulse, was used.

RNA interference. Cells were transfected with siRNA using Lipofectamine RNAiMAX (Invitrogen) according to the manufacturer's instructions. Briefly, a dilution containing siRNA (10nM) and lipofectamine was premade using OPTI-MEM I 1x (GIBCO) and then added to the cells. Four hours later the medium was replaced with fresh medium. Cells were allowed to grow for 24 h before siRNA transfection was repeated. The following siRNAs were used: Luciferase (5'-CGUACGCGGAUACUUCGA-3'), BRCA2 (5'-GGAUUUAUACAUAUUUCGCA-3'), RFWD3 (5'-GGACCUACUUGCAAACUAU-3'/ 5'-AUAGUUUGCAAGUAGGUCC-3') and FANCD2 (5'-UAGAGAGUGAAGCAAACUCUG-3'). siLuciferase was used as a negative control in the RNA interference assays.

I-SceI-induced HR assay. Immortalized patient fibroblasts (cell line 1143) were stably transfected with a plasmid containing a wild type copy of RFWD3 full length cDNA (1143+WT), an empty vector (1143+mock) or a plasmid containing RFWD3 with the patient mutation (1143+I639K). The HR assay was performed in these cell lines by transient transfection of the pDR-GFP plasmid. Two days later, the cells were co-transfected with an I-SceI endonuclease expression vector (pCBASce), with an empty vector (pCAGGS) or with a plasmid constitutively expressing GFP (pNZE-GFP). In U2OS cells, the HR assay was performed as previously described (24). Briefly, U2OS cells stably transfected with a vector containing a single copy of the DR-GFP construct and were transduced with specific siRNAs against luciferase, BRCA2 or RFWD3. Two days later, the cells were transfected with

pCBASce, pCAGGS or pNZE-GFP. In all cases, 2 µg of plasmid was added in 6 well plates. 48 h after transfection, cells were trypsinized and resuspended in a buffer containing sodium citrate (3.4 mM), triton (0.1%), RNAase (200 µg/mL) and FBS (20%). The number of green-fluorescent cells was counted in a flow cytometer. Cells were finally stained with propidium iodide (50 µg/mL) and the cell cycle distribution was determined by flow cytometry. The level of HR was quantified as the proportion of green fluorescent cells corrected by transfection rate and size of S phase.

The same assay was performed in DT40 cells as previously described (27). We generated WT-DT40 WT, Δ RFWD3-DT40, and chRFWD3-complemented Δ RFWD3-DT40 cell lines in which the SCneo construct with an I-SceI recognition site was targeted into the *Ovalbumin* locus. To determine the nature of repair events, G418-selected colonies from WT and Δ RFWD3 cells were expanded and genomic DNA was analyzed by long range PCR as shown in Supplemental Figure 2E.

Co-immunoprecipitation. Cells were washed once with PBS, lysed in NETN buffer (150 mM NaCl, 0.5 mM EDTA, 20 mM Tris-HCl pH 8.0, 0.5% NP-40) supplemented with protease inhibitor cocktail, 25 U/ml benzonase (Millipore), and 1 mM Na_3VO_4 on ice for 30 min, and centrifuged at 14,000 rpm for 10 min. The pellet was discarded. Dynabeads Protein G (Invitrogen) was incubated with an appropriate primary antibody before it was added to the supernatant, following the manufacturer's instructions. To capture his-tagged or FLAG-tagged proteins, Complete His-Tag Purification Resin (Roche) or anti-FLAG M2 Agarose Affinity Gel (Sigma) was used, respectively. Captured proteins were washed and analyzed by immunoblotting. Samples were separated by SDS-PAGE and transferred to a PVDF membrane (Millipore). Proteins were detected as described previously (51).

Generation of $Rfwd3^{-/-}$ mice and analysis of embryonic fibroblasts (MEFs). A replacement vector for targeting of *Rfwd3* exon 3 was generated by assembly of three fragments using sequential cloning. The final recipient vector contained the FRT-flanked neomycin selection (neo) cassette and the 3'-loxP site. PCR primers used to amplify the fragments included all

the restriction enzyme sites required to join them together and to ligate them into the Surf2 vector backbone (Ozgene). The first fragment encompassed the 4.8 kb 5'-homology arm. The second fragment comprised the 0.7 kb region of exon 3 and was amplified using a sense primer (1589_42) that contained the 5' loxP site. The third fragment encompassed the 3.6 kb 3'-homology arm. All of the fragments were amplified from BACs RP23-55G21 and RP23-297L3. For sequence information of the primers see Supplemental Table 6. The final targeting vector 1589_pTV contained the 5'-homology arm, exon 3 of *Rfwd3*, a neo cassette and the 3'-homology arm (Supplemental Figure 3A). A PshAI and a Scal site to be used for screening were inserted immediately 5' of the 5' loxP site and immediately 3' of the 3' loxP site, respectively. The FRT sites for conditional KO were not used. 1589_pTV was linearized by digestion with PmeI prior to electroporation into C57Bl/6 Bruce4 ES cells (52). Neo-resistant ES cell clones were screened by Southern hybridization to identify potentially targeted clones, using a probe downstream of the 3'-homology arm (P3). The WT allele showed a 6.5-kb band and the correctly targeted allele a 4.1-kb band when genomic DNA was digested with Scal. Correct 5'-integration was confirmed using a probe upstream of the 5'-homology arm (5Pi). The WT allele showed an 11.8-kb band and the correctly targeted allele a 5.3-kb band when genomic DNA was digested with PshAI. The possibility of additional random targeting events was precluded by using a probe to the neo cassette (NeoP). Correctly targeted alleles showed a band size of 8.3 kb when genomic DNA was digested with PshAI. The KO allele was distinguished by Southern hybridization using probe P3. The WT allele showed a band size of 11.8 kb, the targeted allele of 8.3 kb and the KO allele 5.9 kb when genomic DNA was digested with PshAI. *Rfwd3*^{-/-} ES cells were injected into goGermline blastocysts (53). Male chimeric mice were obtained and crossed to a ubiquitous Cre mouse line to remove the loxP-flanked exon 3. 8- to 10-week-old *Rfwd3*^{-/-} mice were generated from heterozygous breeding. All strains were backcrossed on a C57BL/6 background for more than 3 generations. Mouse embryonic fibroblasts (MEFs) were obtained from embryos of *Rfwd3*^{-/-} male mice crossed with *Rfwd3*^{+/+} females. Genotyping of the pups confirmed their *Rfwd3* status (Supplemental Figure 3B).

Phenotypical analyses of homozygous *Rfwd3*^{-/-} mice were performed at Ozgene by a veterinarian and according to ethical guidelines of Australia. Blood analyses were done by cutting the tail vein. MEFs were cultured in DMEM (Sigma Aldrich) with 10% FBS (Sigma Aldrich), 0.2% β -mercaptoethanol (Life Technologies) and 2 mM GlutaMax (Gibco). Survival assays, chromosomal breakage and flow-cytometric cell cycle analyses were performed similarly to experiments with other cell types. All experiments in mice were performed in accordance with protocols approved by the Ozgene Animal Ethics Committee under the proposal 150602_PHEN, project 1589_Cajun.

Real-time (RT)-PCR analysis of Rfwd3 mRNA expression. Liver samples were harvested, snap frozen in liquid nitrogen and stored at -80 °C. mRNA was extracted from frozen tissue using the PureLink RNA Mini Kit (Thermo Fisher Scientific) as per manufacturer protocol. Extracted mRNA was reverse transcribed using the High-Capacity cDNA Reverse Transcription Kit (Thermo Fisher Scientific) as per manufacturer protocol. Real-time (RT)-PCR was performed using the CFX Connect Real-Time PCR Detection System (Bio-Rad). Each duplex PCR reaction consisted of 0.5 μ l 40x Beta Actin qPCR assay, 1 μ l 20x Rfwd3 qPCR assay, 1 μ l cDNA, 7.5 μ l H₂O, and 10 μ l 2x PrimeTime Gene Expression Master Mix (Integrated DNA Technologies) in a 20 μ l reaction as per IDT assay protocols. This resulted in a final 1x concentration of 250 nM for each of the probes, and 500 nM of each primer set. Sequence information of the *Rfwd3* primers used is shown in Supplemental Table 6. Amplification conditions were: 95 °C for 3 minutes followed by 40 cycles of 15 s at 95 °C and 1 min at 62 °C. All qPCR reactions on cDNA were carried out in triplicate with "no template" and "no reverse transcriptase" control samples. Data was analyzed using CFX Manager Software, version 3.1 (Bio-Rad).

Statistics. For the siRNA or other transfection assays in U2OS or DT40 cells and immunofluorescence analysis of 1143, 1143 WT-RFWD3-complemented and non-FA cells, 3 independent experiments each were done and Student's T-test was used to compare the results. With patient-derived fibroblasts, 5 independent experiments were done and the

Student's T-test or the Mann-Whitney test was performed depending on whether or not the data were normally distributed. Statistical analyses were performed using SPSS software.

Study approval. The parents of the patient gave their informed consent to patient-related studies. Genetic work on FA was approved by the Institutional Review Board of the Faculty of Medicine at the University of Wurzburg.

Author contributions

K.K. designed and performed experiments, analyzed data, prepared the figures and wrote the draft. S.I. designed and performed DT40 and HAP1 cell studies with M.I., analyzed DT40 data, contributed results and wrote parts of the draft. M.J.R. and J.S. performed the I-SceI-induced HR assay with human cell lines, analyzed the data, contributed results and wrote parts of the draft. M.T. and D.S. conceived the experiments, analyzed data, contributed results, supervised the study and wrote the manuscript.

Supplemental Data

Supplemental data include three figures and six tables, and can be found with this article online.

Acknowledgments

We are grateful to the patient and her family for providing information on the disease course and agreeing to publication in an anonymized manner. We thank the attending pediatrician, A. Gnekow, for medical information and great cooperation. We deeply appreciate expert technical contributions by R. Friedl. Plasmids for the I-SceI-induced HR assay were kindly provided by M. Jasin. We also express our gratitude to J. Jardine for sharing mouse histology data and to R. Kalb for discussions and critically reading of the manuscript. This work was supported, in part, by a grant from the Schroeder-Kurth Fund (to K.K. and D.S.) and by JSPS KAKENHI Grant Numbers JP23114010 (to M.T.), JP26550026 (to M.T.), JP15H01738 (to M.T.), JP26281021 (to M.I.). Radiation Biology Center is a Joint Usage

Research Center supported by the Ministry of Education, Culture, Sports, Science and Technology (MEXT) of Japan.

Address correspondence to: Detlev Schindler, University of Wurzburg, Dept. of Human Genetics, Biozentrum, Am Hubland, D-97074 Wurzburg, Germany. Phone: +49 931 318 4089; Fax: +49 931 318 4069; Email: schindler@biozentrum.uni-wuerzburg.de.

References

1. Kutler, D.I., Auerbach, A.D., Satagopan, J., Giampietro, P.F., Batish, S.D., Huvos, A.G., Goberdhan, A., Shah, J.P., and Singh, B. 2003. High incidence of head and neck squamous cell carcinoma in patients with Fanconi anemia. *Arch Otolaryngol Head Neck Surg* 129:106-112.
2. Auerbach, A.D. 2009. Fanconi anemia and its diagnosis. *Mutat Res* 668:4-10.
3. Kutler, D.I., Patel, K.R., Auerbach, A.D., Kennedy, J., Lach, F.P., Sanborn, E., Cohen, M.A., Kuhel, W.I., and Smogorzewska, A. 2016. Natural history and management of Fanconi anemia patients with head and neck cancer: A 10-year follow-up. *Laryngoscope* 126:870-879.
4. Alter, B.P. 2014. Fanconi anemia and the development of leukemia. *Best Pract Res Clin Haematol* 27.
5. Kottemann, M.C., and Smogorzewska, A. 2013. Fanconi anaemia and the repair of Watson and Crick DNA crosslinks. *Nature* 493:356-363.
6. Wang, A.T., and Smogorzewska, A. 2015. SnapShot: Fanconi Anemia and Associated Proteins. *Cell* 160:354-354.e351.
7. Schwertman, P., Bekker-Jensen, S., and Mailand, N. 2016. Regulation of DNA double-strand break repair by ubiquitin and ubiquitin-like modifiers. *Nat Rev Mol Cell Biol* 17:379-394.
8. Bluteau, D., Masliah-Planchon, J., Clairmont, C., Rousseau, A., Ceccaldi, R., Dubois d'Enghien, C., Bluteau, O., Cuccuini, W., Gachet, S., Peffault de Latour, R., et al. 2016. Biallelic inactivation of REV7 is associated with Fanconi anemia. *J Clin Invest* 126.
9. Ceccaldi, R., Sarangi, P., and D'Andrea, A.D. 2016. The Fanconi anaemia pathway: new players and new functions. *Nat Rev Mol Cell Biol* 17:337-349.
10. Moldovan, G.L., and D'Andrea, A.D. 2009. How the fanconi anemia pathway guards the genome. *Annu Rev Genet* 43:223-249.
11. Herskho, A., and Ciechanover, A. 1998. THE UBIQUITIN SYSTEM. *Annual Review of Biochemistry* 67:425-479.
12. Murai, J., Yang, K., Dejsuphong, D., Hirota, K., Takeda, S., and D'Andrea, A.D. 2011. The USP1/UAF1 complex promotes double-strand break repair through homologous recombination. *Mol Cell Biol* 31:2462-2469.
13. Paquin, K.L., Vierra, D.A., and Howlett, N.G. 2016. A DUB-less step? Tighten up D-loop. *Cell Cycle*:1-2.
14. Elia, Andrew E.H., Wang, David C., Willis, Nicholas A., Boardman, Alexander P., Hajdu, I., Adeyemi, Richard O., Lowry, E., Gygi, Steven P., Scully, R., and Elledge,

- Stephen J. 2015. RFWD3-Dependent Ubiquitination of RPA Regulates Repair at Stalled Replication Forks. *Mol Cell* 60:280-293.
15. Matsuoka, S., Ballif, B.A., Smogorzewska, A., McDonald, E.R., 3rd, Hurov, K.E., Luo, J., Bakalarski, C.E., Zhao, Z., Solimini, N., Lerenthal, Y., et al. 2007. ATM and ATR substrate analysis reveals extensive protein networks responsive to DNA damage. *Science* 316:1160-1166.
16. Fu, X., Yucer, N., Liu, S., Li, M., Yi, P., Mu, J.-J., Yang, T., Chu, J., Jung, S.Y., O'Malley, B.W., et al. 2010. RFWD3-Mdm2 ubiquitin ligase complex positively regulates p53 stability in response to DNA damage. *Proceedings of the National Academy of Sciences* 107:4579-4584.
17. Liu, S., Chu, J., Yucer, N., Leng, M., Wang, S.-Y., Chen, B.P.C., Hittelman, W.N., and Wang, Y. 2011. RING Finger and WD Repeat Domain 3 (RFWD3) Associates with Replication Protein A (RPA) and Facilitates RPA-mediated DNA Damage Response. *Journal of Biological Chemistry* 286:22314-22322.
18. Gong, Z., and Chen, J. 2011. E3 Ligase RFWD3 Participates in Replication Checkpoint Control. *Journal of Biological Chemistry* 286:22308-22313.
19. Wang, A.T., Kim, T., Wagner, J.E., Conti, B.A., Lach, F.P., and Huang, A.L. 2015. A dominant mutation in human RAD51 reveals its function in DNA interstrand crosslink repair independent of homologous recombination. *Mol Cell* 59.
20. Ameziane, N., May, P., Haitjema, A., van de Vrugt, H.J., van Rossum-Fikkert, S.E., Ristic, D., Williams, G.J., Balk, J., Rockx, D., Li, H., et al. 2015. A novel Fanconi anaemia subtype associated with a dominant-negative mutation in RAD51. *Nat Commun* 6.
21. Stivaros, S.M., Alston, R., Wright, N.B., Chandler, K., Bonney, D., Wynn, R.F., Will, A.M., Punekar, M., Loughran, S., Kilday, J.P., et al. 2015. Central nervous system abnormalities in Fanconi anaemia: patterns and frequency on magnetic resonance imaging. *Br J Radiol* 88:20150088.
22. Gong, Z., and Chen, J. 2011. E3 ligase RFWD3 participates in replication checkpoint control. *J Biol Chem* 286:22308-22313.
23. Liu, S., Chu, J., Yucer, N., Leng, M., Wang, S.-Y., Chen, B.P., Hittelman, W.N., and Wang, Y. 2011. RING finger and WD repeat domain 3 (RFWD3) associates with replication protein A (RPA) and facilitates RPA-mediated DNA damage response. *J Biol Chem* 286:22314-22322.
24. Zhang, F., Shi, J., Bian, C., and Yu, X. 2015. Poly(ADP-Ribose) Mediates the BRCA2-Dependent Early DNA Damage Response. *Cell Rep* 13:678-689.
25. Jasin, M., and Rothstein, R. 2013. Repair of strand breaks by homologous recombination. *Cold Spring Harb Perspect Biol* 5.

26. Pierce, A.J., Johnson, R.D., Thompson, L.H., and Jasin, M. 1999. XRCC3 promotes homology-directed repair of DNA damage in mammalian cells. *Genes Dev* 13:2633-2638.
27. Yamamoto, K., Ishiai, M., Matsushita, N., Arakawa, H., Lamerdin, J.E., Buerstedde, J.-M., Tanimoto, M., Harada, M., Thompson, L.H., and Takata, M. 2003. Fanconi Anemia FANCG Protein in Mitigating Radiation- and Enzyme-Induced DNA Double-Strand Breaks by Homologous Recombination in Vertebrate Cells. *Mol Cell Biol* 23:5421-5430.
28. Takata, M., Sasaki, M.S., Tachiiri, S., Fukushima, T., Sonoda, E., Schild, D., Thompson, L.H., and Takeda, S. 2001. Chromosome Instability and Defective Recombinational Repair in Knockout Mutants of the Five Rad51 Paralogs. *Mol Cell Biol* 21:2858-2866.
29. Kitao, H., Yamamoto, K., Matsushita, N., Ohzeki, M., Ishiai, M., and Takata, M. 2006. Functional interplay between BRCA2/FancD1 and FancC in DNA repair. *J Biol Chem* 281:21312-21320.
30. Wang, X., Andreassen, P.R., and D'Andrea, A.D. 2004. Functional interaction of monoubiquitinated FANCD2 and BRCA2/FANCD1 in chromatin. *Mol Cell Biol* 24:5850-5862.
31. Park, J.-Y., Virts, E.L., Jankowska, A., Wiek, C., Othman, M., Chakraborty, S.C., Vance, G.H., Alkuraya, F.S., Hanenberg, H., and Andreassen, P.R. 2016. Complementation of hypersensitivity to DNA interstrand crosslinking agents demonstrates that XRCC2 is a Fanconi anaemia gene. *J Med Genet*.
32. Yokoyama, H., Sarai, N., Kagawa, W., Enomoto, R., Shibata, T., Kurumizaka, H., and Yokoyama, S. 2004. Preferential binding to branched DNA strands and strand-annealing activity of the human Rad51B, Rad51C, Rad51D and Xrcc2 protein complex. *Nucleic Acids Res* 32:2556-2565.
33. Howlett, N.G., Taniguchi, T., Olson, S., Cox, B., Waisfisz, Q., De Die-Smulders, C., Persky, N., Grompe, M., Joenje, H., Pals, G., et al. 2002. Biallelic inactivation of BRCA2 in Fanconi anemia. *Science* 297:606-609.
34. Reid, S., Schindler, D., Hanenberg, H., Barker, K., Hanks, S., Kalb, R., Neveling, K., Kelly, P., Seal, S., Freund, M., et al. 2007. Biallelic mutations in PALB2 cause Fanconi anemia subtype FA-N and predispose to childhood cancer. *Nat Genet* 39:162-164.
35. Vaz, F., Hanenberg, H., Schuster, B., Barker, K., Wiek, C., Erven, V., Neveling, K., Endt, D., Kesterton, I., Autore, F., et al. 2010. Mutation of the RAD51C gene in a Fanconi anemia-like disorder. *Nat Genet* 42:406-409.

36. Park, J.Y., Virts, E.L., Jankowska, A., Wiek, C., Othman, M., Chakraborty, S.C., Vance, G.H., Alkuraya, F.S., Hanenberg, H., and Andreassen, P.R. 2016. Complementation of hypersensitivity to DNA interstrand crosslinking agents demonstrates that XRCC2 is a Fanconi anaemia gene. *J Med Genet* 53:672-680.
37. Shamseldin, H.E., Elfaki, M., and Alkuraya, F.S. 2012. Exome sequencing reveals a novel Fanconi group defined by XRCC2 mutation. *J Med Genet* 49:184-186.
38. Sawyer, S.L., Tian, L., Kahkonen, M., Schwartzentruber, J., Kircher, M., and Majewski, J. 2015. Biallelic mutations in BRCA1 cause a new Fanconi anemia subtype. *Cancer Discov* 5.
39. Dong, H., Nebert, D.W., Bruford, E.A., Thompson, D.C., Joenje, H., and Vasiliou, V. 2015. Update of the human and mouse Fanconi anemia genes. *Human Genomics* 9:1-10.
40. Crossan, G.P., van der Weyden, L., Rosado, I.V., Langevin, F., Gaillard, P.H., McIntyre, R.E., Gallagher, F., Kettunen, M.I., Lewis, D.Y., Brindle, K., et al. 2011. Disruption of mouse Slx4, a regulator of structure-specific nucleases, phenocopies Fanconi anemia. *Nat Genet* 43:147-152.
41. Bakker, S.T., de Winter, J.P., and te Riele, H. 2013. Learning from a paradox: recent insights into Fanconi anaemia through studying mouse models. *Dis Model Mech* 6:40-47.
42. Bakker, S.T., de Winter, J.P., and Riele, H.t. 2013. Learning from a paradox: recent insights into Fanconi anaemia through studying mouse models. *Disease Models & Mechanisms* 6:40-47.
43. Katsuki, Y., and Takata, M. 2016. Defects in homologous recombination repair behind the human diseases: FA and HBOC. *Endocrine-Related Cancer* 23:T19-T37.
44. Knies, K., Schuster, B., Ameiziane, N., Rooimans, M., Bettecken, T., de Winter, J., and Schindler, D. 2012. Genotyping of Fanconi Anemia Patients by Whole Exome Sequencing: Advantages and Challenges. *PLoS One* 7:e52648.
45. Ishiai, M., Kitao, H., Smogorzewska, A., Tomida, J., Kinomura, A., Uchida, E., Saberi, A., Kinoshita, E., Kinoshita-Kikuta, E., Koike, T., et al. 2008. FANCI phosphorylation functions as a molecular switch to turn on the Fanconi anemia pathway. *Nat Struct Mol Biol* 15:1138-1146.
46. Nishimura, K., Ishiai, M., Horikawa, K., Fukagawa, T., Takata, M., Takisawa, H., and Kanemaki, Masato T. 2012. Mcm8 and Mcm9 Form a Complex that Functions in Homologous Recombination Repair Induced by DNA Interstrand Crosslinks. *Mol Cell* 47:511-522.

47. Seyschab, H., Friedl, R., Sun, Y., Schindler, D., Hoehn, H., Hentze, S., and Schroeder-Kurth, T. 1995. Comparative evaluation of diepoxybutane sensitivity and cell cycle blockage in the diagnosis of Fanconi anemia. *Blood* 85:2233-2237.
48. Auerbach, A.D. 1993. Fanconi anemia diagnosis and the diepoxybutane (DEB) test. *Exp Hematol* 21:731-733.
49. Kim, Y., Spitz, G.S., Veturi, U., Lach, F.P., Auerbach, A.D., and Smogorzewska, A. 2013. Regulation of multiple DNA repair pathways by the Fanconi anemia protein SLX4. *Blood* 121:54-63.
50. Ran, F.A., Hsu, P.D., Wright, J., Agarwala, V., Scott, D.A., and Zhang, F. 2013. Genome engineering using the CRISPR-Cas9 system. *Nat. Protocols* 8:2281-2308.
51. Unno, J., Itaya, A., Taoka, M., Sato, K., Tomida, J., Sakai, W., Sugawara, K., Ishiai, M., Ikura, T., Isobe, T., et al. 2014. FANCD2 Binds CtIP and Regulates DNA-End Resection during DNA Interstrand Crosslink Repair. *Cell Reports* 7:1039-1047.
52. Köntgen, F., Süss, G., Stewart, C., Steinmetz, M., and Bluethmann, H. 1993. Targeted disruption of the MHC class II Aa gene in C57BL/6 mice. *Int Immunol* 5:957-964.
53. Koentgen, F., Lin, J., Katidou, M., Chang, I., Khan, M., Watts, J., and Mombaerts, P. 2016. Exclusive transmission of the embryonic stem cell-derived genome through the mouse germline. *genesis* 54:326-333.

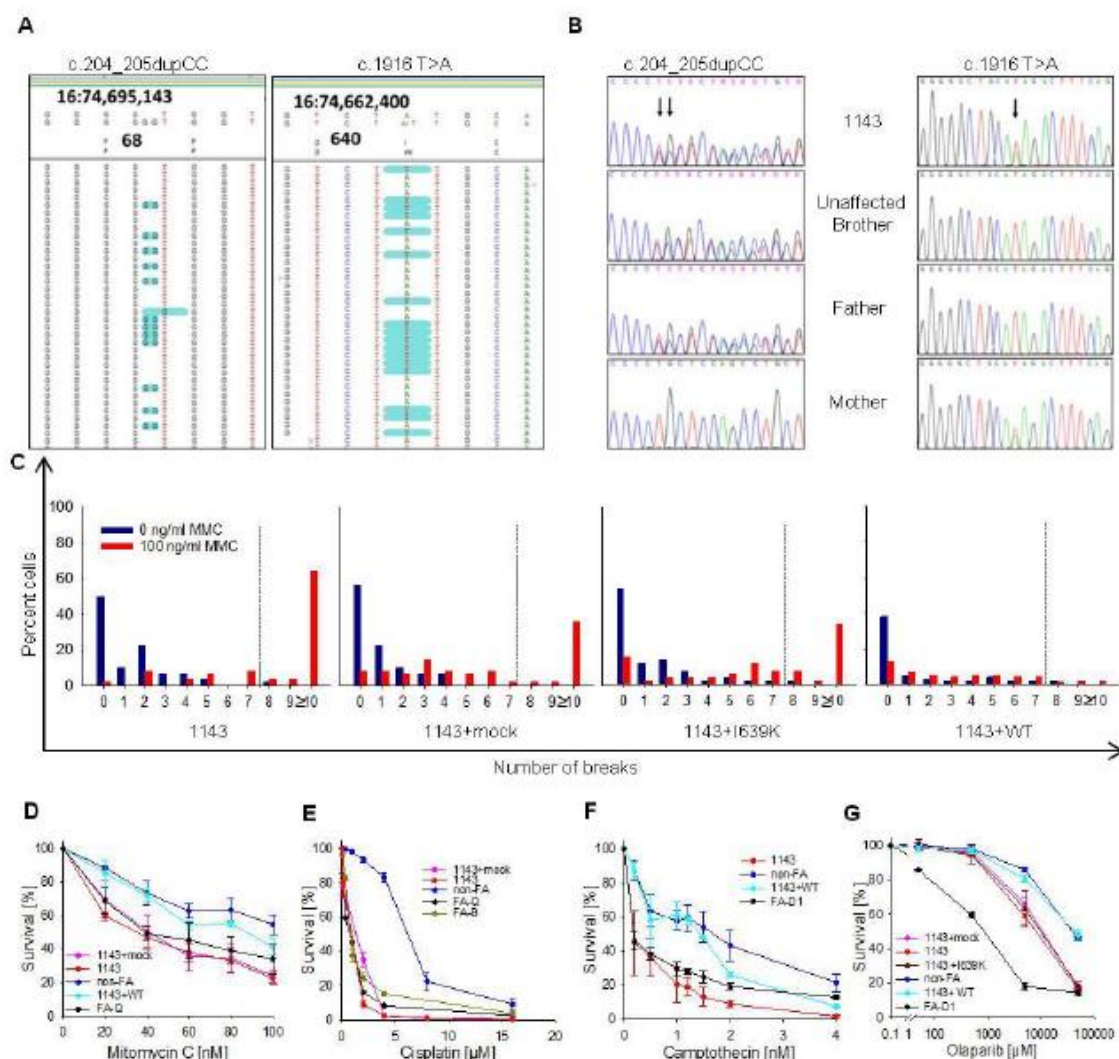


Figure 1. Identification and characterization of *RFWD3* mutations.

(A) WES data reveal two heterozygous sequence variants of the *RFWD3* gene, highlighted in green. The gene is located on the minus strand; chromosomal and amino acid positions next to the mutations are depicted.

(B) Sanger sequencing confirms both mutations in individual 1143 and familial segregation.

(C) Histograms reflecting proportions of cells with the indicated number of chromosomal breaks per metaphase, blue without, red after exposure to MMC. Dashed lines delimit high rates of *RFWD3*-mutated (1143) and transduced fibroblasts (1143+mock, 1143+I639K). 1143+WT is rescued. 50 metaphases each were scored.

(D-G) Dose-response curves of same cell lines used in (C) compared to non-FA and FA (FA-Q, FA-B or FA-D1) fibroblasts after exposure to the indicated agents and concentrations. The data represent mean \pm SEM; $N=5$.

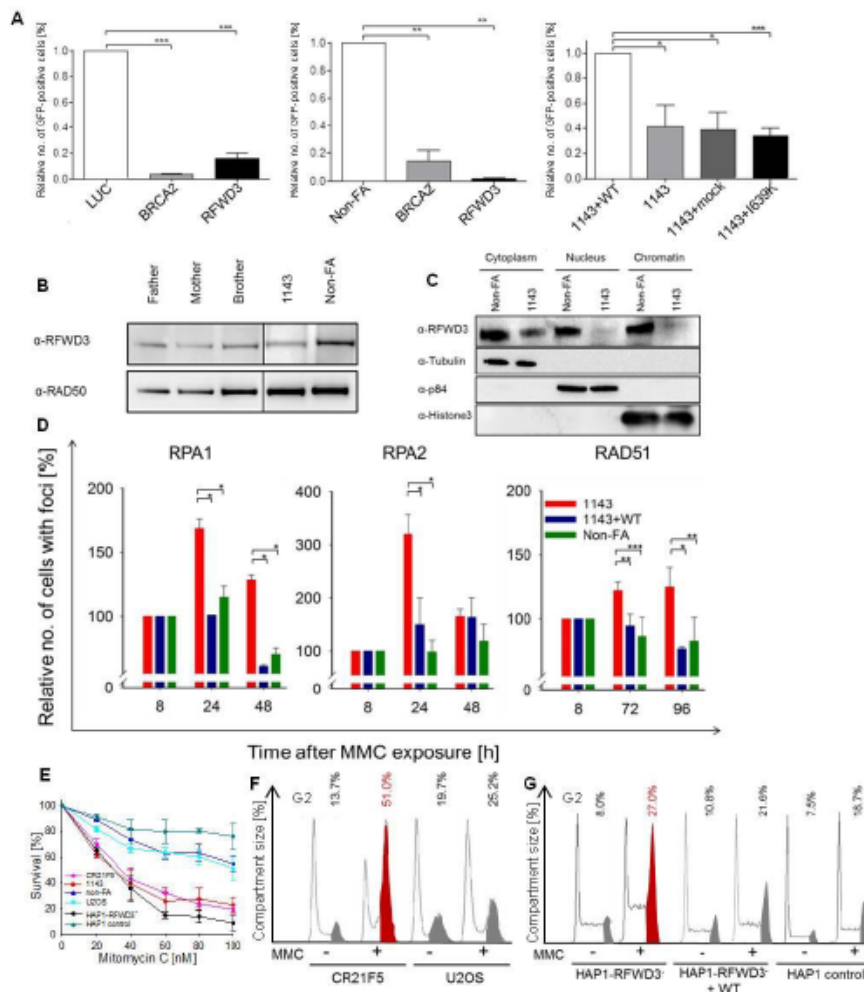


Figure 2. Involvement of RFWD3 in HR and ICL repair.

(A) Reduced HR in RFWD3-deficient human cells as signaled by the I-SceI-induced HR assay. Shown is the decrease of GFP-positive (HR-active) cells compared to controls. The left graph shows data from siRNA-transfected U2OS cells (luciferase (LUC; mock) vs. BRCA2 and RFWD3). The middle graph represents data from non-FA vs. 1143 and BRCA2/*FANCD1*-mutant fibroblasts. The right graph displays data from 1143 transduced with WT-RFWD3 vs. mock, I639K and non-transduced 1143 fibroblasts. All results are corrected for transfection rate and S-phase size.

(B) Western blot with RFWD3 antibody including lysates from 1143, her family members and non-FA fibroblasts exposed to MMC. Lanes were run on the same gel but were non-contiguous.

(C) Cell fractionation of protein lysates from non-FA and 1143 fibroblasts exposed to MMC.

(D) Proportion of RPA1, RPA2 and RAD51 foci-positive cells in 1143, 1143+WT-RFWD3 transduced and non-FA fibroblasts at different intervals after an initial 8-h pulse of MMC exposure.

(E) Dose-response curves of CRISPR clone CR21F5 vs. parental U2OS cells, HAP1-RFWD3⁻ vs. HAP1 control cells, and 1143 vs. non-FA fibroblasts exposed to MMC.

(F and G) Cell cycle analysis regarding G2-phase arrest of CRISPR clone CR21F5 vs. parental U2OS cells and of HAP1-RFWD3⁻ vs. HAP1-RFWD3⁺WT complemented and HAP1 control cells without or with exposure to MMC. Increased G2 compartment size is highlighted in red, normal size is shown in gray.

Data in (A), (D) and (E) represent mean \pm SEM; $N=3$ for siRNA experiments, otherwise $N=5$.

*** $p \leq 0.001$; ** $p \leq 0.01$; * $p < 0.05$ by unpaired, two-sided Student's T-test.

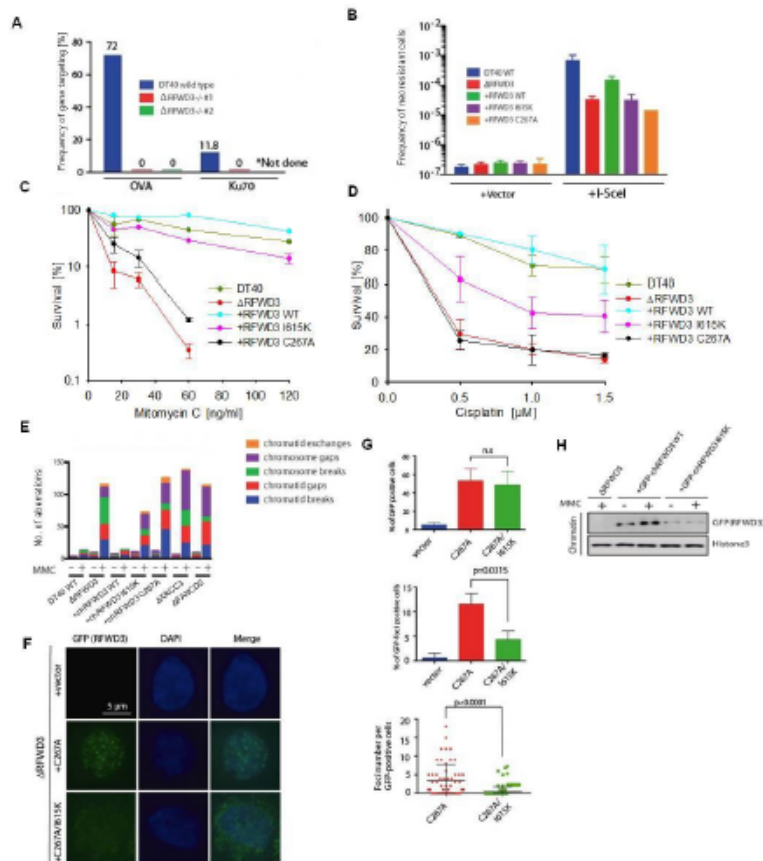


Figure 3. Functional analyses of Δ RFWD3-DT40 cells.

(A) Frequency of gene targeting at the *OVALBUMIN* (OVA) and *Ku70* loci of WT-DT40 cells (blue) and two independently generated Δ RFWD3-DT40 cell lines (#1, red and #2, green). Percentages of the targeting events relative to the number of examined clones are shown on top of each bar.

(B) Frequency of neo-resistant DT40 colonies due to HR events in the SCneo recombination substrate integrated in the OVA locus. Cells with indicated genotypes were transiently transfected with empty vector (+vector) or with vector containing I-SceI (+I-SceI) and selected in medium containing G418. After 10-14 days the number of colonies was counted.

(C and D) Dose-response curves of WT-DT40 cells vs. Δ RFWD3-DT40 cells and Δ RFWD3-DT40 cells transfected with WT-RFWD3, RFWD3-I615K or RFWD3-C267A. Cells were exposed to MMC or cisplatin.

(E) Histograms reflecting proportions of cells with the indicated number of chromosomal lesions per metaphase in WT-DT40 and mutant cells with the indicated genotypes and transfections without or with exposure to MMC. 50 cells each were scored.

(F) GFP immunofluorescence analysis of Δ RFWD3-DT40 fibroblasts transiently transfected with mock, GFP-chRFWD3-C267A or the double mutant GFP-chRFWD3-C267A/I615K after exposure to MMC.

(G) Proportion of GFP-RFWD3-positive Δ RFWD3-DT40 cells (upper panel), GFP-RFWD3 foci-positive Δ RFWD3-DT40 cells (>5, middle panel), and number of GFP-RFWD3 foci in individual GFP-RFWD3 foci-positive Δ RFWD3-DT40 cells (lower panel) after transfection with the indicated plasmids. Cells are those used in (F).

(H) Relocation of GFP-RFWD3 in Δ RFWD3-DT40 cells transfected with the indicated plasmids without and with exposure to MMC. Fractions were probed using anti-GFP and anti-histone 3 antibodies.

Data in (B-D) and (G) represent mean \pm SEM; $N=3$. *** $p \leq 0.001$; ** $p \leq 0.01$; * $p \leq 0.05$ by unpaired, two-sided Student's T-test

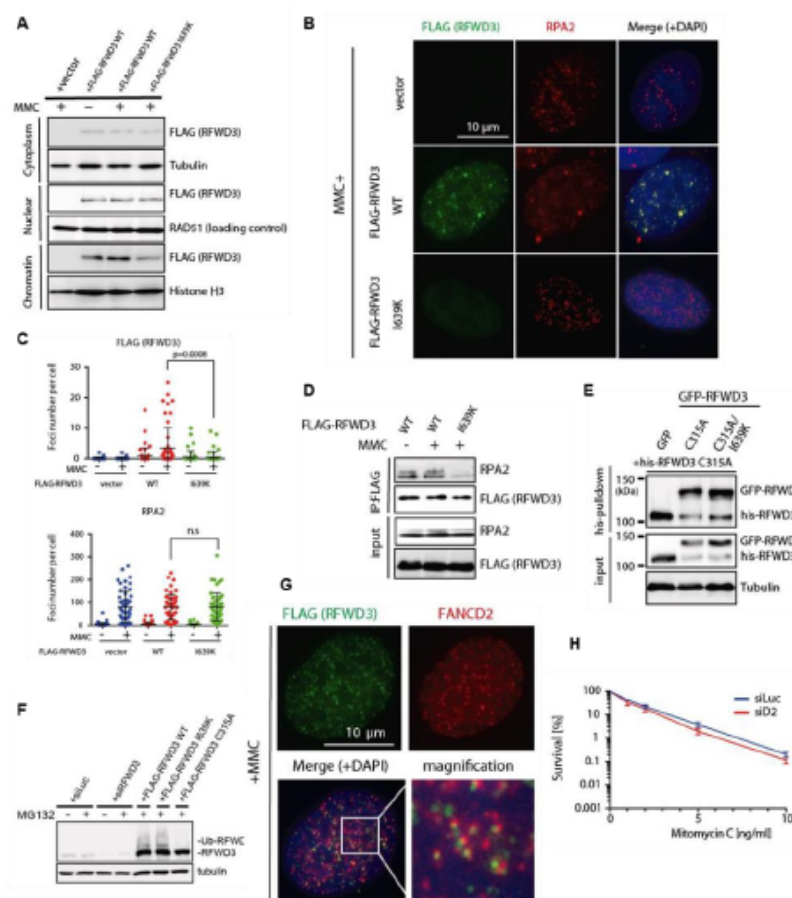


Figure 4. Interaction studies of human RFWD3.

(A) Cell fractionation shows impaired chromatin relocation of RFWD3 with the mutation in the WD40 domain when U2OS cells were transiently transfected with FLAG-WT-RFWD3 or FLAG-RFWD3-I639K and exposed to MMC as indicated.

(B) FLAG-RFWD3 immunofluorescence analysis of same cells used in (A) exposed to MMC. Anti-FLAG detected RFWD3, anti-RPA2 endogenous RPA, DAPI counterstains the nucleus.

(C) Number of FLAG-RFWD3 (upper graph) and RPA2 (lower graph) foci per nucleus without or with exposure to MMC. Cells are those used in (A). >50 cells were counted for each sample. The experiment was repeated four times. Data represent mean \pm SD. P values of WT vs. I639K were calculated using the unpaired, two-sided Student's T-test.

(D) Co-immunoprecipitation of FLAG-WT-RFWD3 or FLAG-RFWD3-I639K with RPA2 in transiently transfected U2OS cells without or with exposure to MMC.

(E) Pull-down study of GFP-RFWD3 and his-RFWD3 dimerization in U2OS cells transiently transfected with GFP, GFP-RFWD3-C315A (RING mutation) or GFP-RFWD3-C315A/I639K (double mutation). Detection was by anti-his and anti-GFP antibodies.

(F) Auto-ubiquitination of FLAG-WT-RFWD3, FLAG-RFWD3-I639K or FLAG-RFWD3-C315A in transiently transfected U2OS cells without or with exposure to the proteasome inhibitor MG132. siLuc and siRFWD3 served as negative controls. Detection was by anti-RFWD3.

(G) Colocalization of FLAG-RFWD3 and FANCD2. U2OS cells were transiently transfected with FLAG-RFWD3 and exposed to MMC (100 ng/ml for 24 h).

(H) Survival curves of RFWD3-mutated HAP1 cells transfected with siRNAs to luciferase (Luc) or FANCD2 (D2) and exposed MMC. Mean \pm SD of three independent experiments are shown. Depletion of FANCD2 and BRCA2 (control) was analyzed by immunoblotting and is shown in Supplemental Figure 4H.

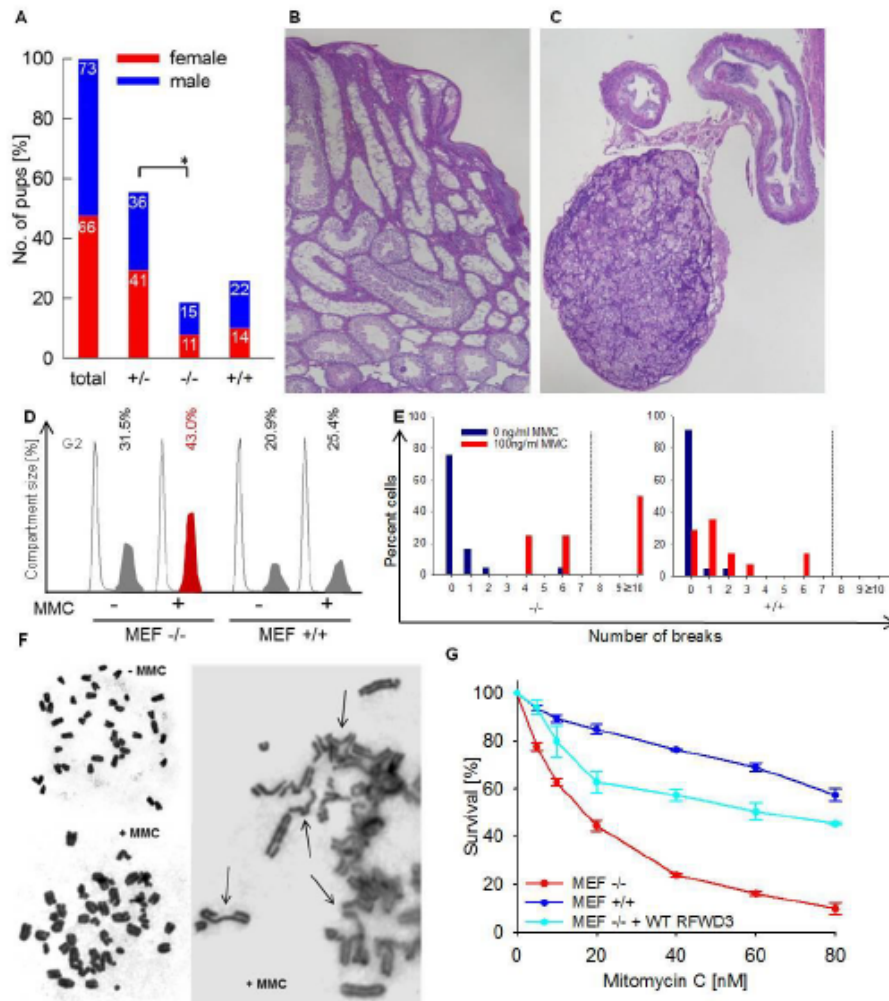


Figure 5. Characterization of an *Rfwd3*^{-/-} mouse model.

(A) Numbers and proportions of female (red) and male (blue) *Rfwd3*^{+/+}, *Rfwd3*^{-/-} and *Rfwd3*^{+/-} mouse offspring of heterozygous mating. *Rfwd3*^{-/-} pups were born at sub-Mendelian rate.

(B) Atrophic *Rfwd3*^{-/-} mouse testis shows seminiferous tubules with little active spermatogenesis and few spermatozoa. The original micrograph was taken at 40x.

(C) Atrophic *Rfwd3*^{-/-} mouse ovary demonstrates clusters of luteal cells within a delicate stroma but no follicular development. The original micrograph was taken at 40x.

(D) Cell cycle analysis examining G2-phase arrest in *Rfwd3*^{-/-} vs. *Rfwd3*^{+/+} MEFs without or with exposure to MMC. Increased G2 compartment size is highlighted in red, normal size shown in gray.

(E) Histograms reflecting proportions of cells with the indicated number of chromosomal breaks per metaphase, blue without, red after exposure to MMC, in *Rfwd3*^{-/-} and *Rfwd3*^{+/+} MEFs. 50 cells each were scored. Sensitivity is indicated by the high rate of metaphases with >7 breaks (dashed line). 50 metaphases each were scored.

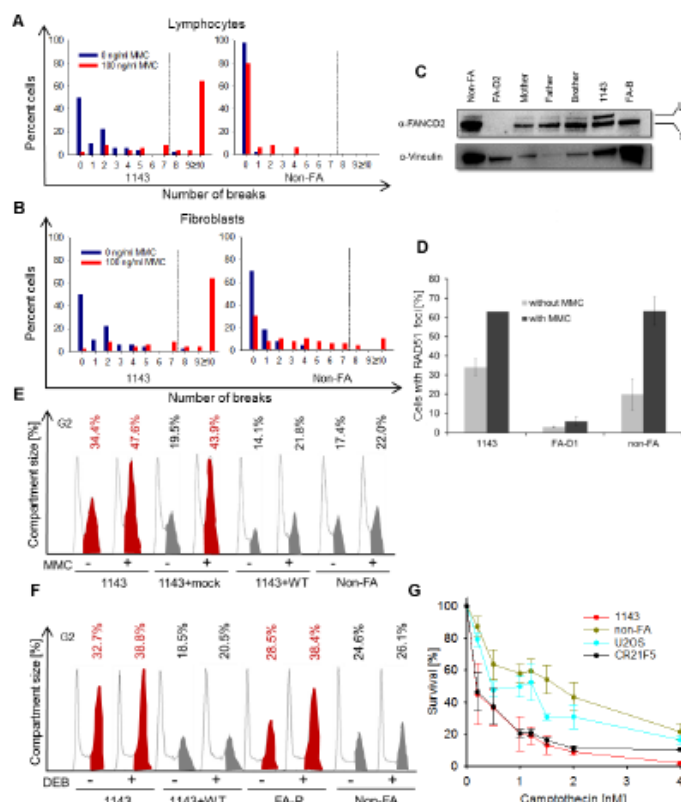
(F) Micrographs of *Rfwd3*^{-/-} MEF metaphase preparations. Unaffected cell without prior exposure to MMC (upper left image), increased chromosomal breakage after exposure to MMC (lower left image) and predominance of chromatid-type lesions and radial reunion figures (arrows, right image) after exposure to MMC.

(G) Dose-response curves of *Rfwd3*^{-/-} MEFs, *Rfwd3*^{+/+} MEFs and *Rfwd3*^{-/-} MEFs transduced with human WT-RFWD3 exposed to MMC. The data represent mean ± SEM; N=3.

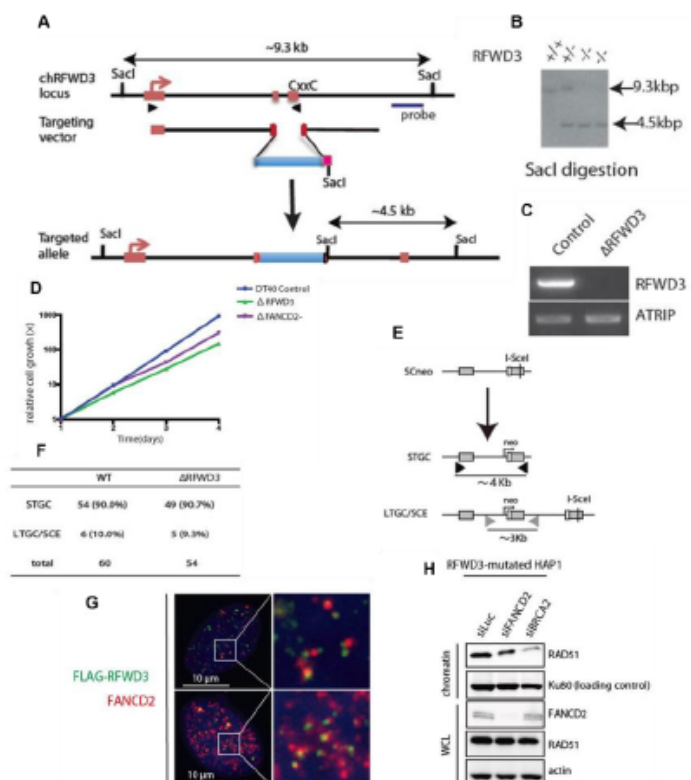
Supplemental data

Biallelic mutations in the ubiquitin ligase *RFWD3* cause Fanconi anemia

Kerstin Knies, Shojiro Inano, María J. Ramírez, Masamichi Ishiai, Jordi Surallés, Minoru Takata, and Detlev Schindler



Supplemental Figure 1. Extended FA phenotype of 1143 cells (related to Figures 1 and 2).
(A) Histograms reflecting proportions of cells with the indicated number of chromosomal breaks per metaphase from lymphocyte cultures, blue without, red after exposure to MMC. Dashed lines delimit high rates (>7). 50 metaphases each were scored.
(B) Histograms reflecting proportions of cells with the indicated number of chromosomal breaks per metaphase from fibroblast culture, blue without, red after exposure to MMC. Dashed lines delimit high rates (>7). 50 metaphases each were scored.
(C) Immunoblot analysis of FANCD2 monoubiquitination of RFWD3-mutated (1143), 1143's family members, FANCD2-mutated, FANCB-mutated and normal control lymphoblasts. Cells were exposed to 40 ng/ml MMC for 16 h.
(D) Proportion of RAD51 foci-positive nuclei in 1143, FA-D1 and non-FA fibroblasts, detected by anti-RAD51 staining without (gray) and with (black) prior exposure of cells to MMC (40 ng/ml, 16 h). Data represent mean with \pm SD. N=3.
(E) Cell-cycle analysis without or with exposure to MMC of 1143, 1143+mock, 1143+WT-RFWD3 and non-FA fibroblasts. Increased G2 compartment size of 1143 and 1143+mock cells (normal <28%) is highlighted in red, normal size is shown in gray.
(F) Cell-cycle analysis without or with exposure to MMC of 1143, 1143+WT-RFWD3, FA-P and non-FA fibroblasts. Increased G2 compartment size of 1143 and FA-P cells (normal <28%) is highlighted in red, normal size is shown in gray.
(G) Dose-response curves of CRISPR clone CR21F5 with targeted RFWD3 compared to parental U2OS, 1143 and non-FA cells, exposed to camptothecin at the indicated concentrations. Data represent mean \pm SEM; N=5.



Supplemental Figure 2. Generation and characterization of RFWD3- deficient cellular models (related to Figures 3 and 4).

(A) Partial map of the chicken *RFWD3* locus, the gene disruption vector and the configuration of the targeted allele. An inserted neo-cassette is shown in light blue, a probe for allele discrimination in dark blue. Red boxes indicate the positions of exon 1 with the translation start site, and of exons 2 and 3 that become disrupted. SacI sites and bidirectional arrows between them denote restriction fragment positions and lengths used in Supplemental Figure 2B. Arrowheads indicate the positions of primers used in Supplemental Figure 2C.

(B) Genotype determination by Southern blot analysis of WT (+/+), heterozygous (+/-) and homozygous (-/-) Δ *RFWD3*-DT40 cells. SacI-digested genomic DNA was hybridized with the probe shown in Supplemental Figure 2A.

(C) RT-PCR analysis of chicken *RFWD3* mRNA expression in control and Δ *RFWD3*-DT40 cells using the primers shown in Supplemental Figure 2A.

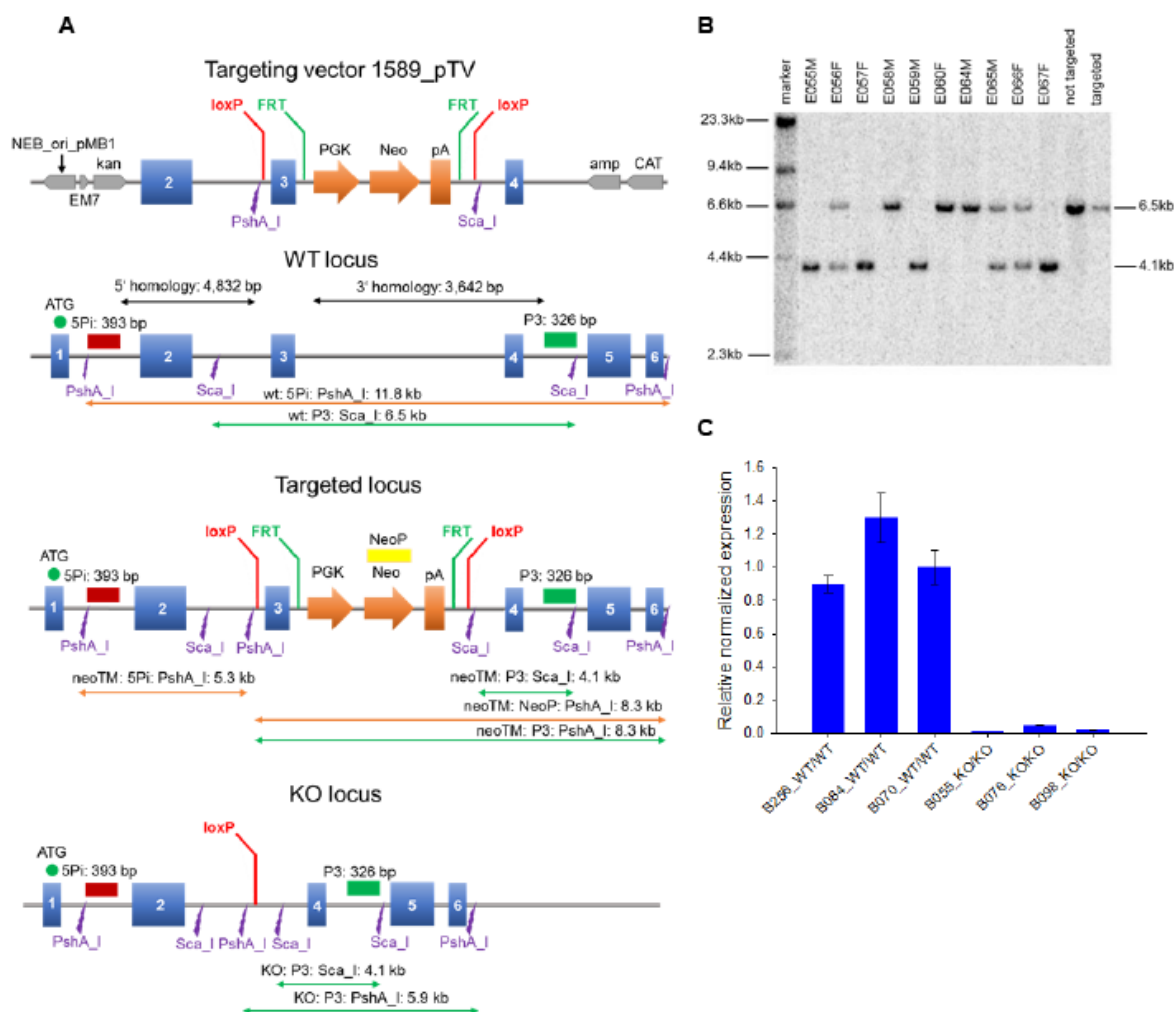
(D) Relative cell growth of WT-DT40, Δ *RFWD3*-DT40 and Δ *FANCD2*-DT40 cells over a period of four days.

(E) Structure of the SCneo construct and expected HR repair products revealing STGC (short-tract gene conversion) or LTGC/SCE (long-tract gene conversion/unequal sister chromatid exchange).

(F) Number of G418-resistant clones with STGC or LTGC/SCE events in WT-DT40 and Δ *RFWD3*-DT40 cells after transfection of I-SceI vector and selection by G418.

(G) *RFWD3*-mutant HAP1 cells were transduced with the indicated siRNAs and analyzed by immunoblotting 24 h later. Silencing of FANCD2 resulted in the loss of corresponding protein, knock-down of BRCA2 in the reduction of RAD51 on chromatin,

(H) A majority of MMC-induced FLAG-*RFWD3* and FANCD2 foci in U2OS cells co-localized or were in close proximity.



Supplemental Figure 3. Generation and characterization of *Rfwd3*^{-/-} mice (related to Figure 5).

(A) Targeting strategy. The replacement vector contains a neo-cassette (orange) flanked by FRT sites (green) which, together with exon 3, are flanked by loxP sites (red). Using 5' and 3' homology arms the vector was used to target the *Rfwd3* locus of mouse ES. After selection with G418, exon 3 and the neo-cassette were removed by Cre-mediated recombination. The FRT sites for conditional KO were not used. Blue boxes denote exons. P3 (green) 5Pi (red) and NeoP (yellow) represent Southern hybridization probes of specified sizes. PshAI and ScaI designate restriction sites (purple bolts). Bidirectional orange and green arrows display restriction fragments of indicated sizes detected by corresponding probes. **(B)** Southern blot analysis of *Rfwd3*^{-/-}, *Rfwd3*^{+/-} and *Rfwd3*^{+/+} mice. ScaI-digested genomic DNA was hybridized with the probe P3. Expected sizes: WT 6.5 kb and KO 4.1 kb. E055, 057, 059 and 067 are *Rfwd3*^{-/-}; E056, 065 and 066 are *Rfwd3*^{+/-}; E058, 060 and 064 are *Rfwd3*^{+/+}. **(C)** RT-PCR analysis of normalized relative *Rfwd3* mRNA expression in *Rfwd3*^{-/-} and *Rfwd3*^{+/+} mice. Data represent mean with \pm SD. *N*=3.

Supplemental Table 1. Statistical analysis of WES data (related to Results and Figure 1)

Number of total reads	113,599,566
Reads that passed QC	112,700,612
Reads on target	109,529,301 (97%)
Exome coverage	197x
Total number of detected variants	29,180
Reported SNPs (dbSNP Build 134)	24,675
Unknown variants in exons	3,962
Unknown variants at splice sites	666 (136 thereof at essential splice sites)
Total number of unknown variants in heterozygous condition	3,981 (including essential splice sites)
Insertions/deletions	577
Missense	2,211
Nonsense	100
Silent	982
Genes with ≥ 2 heterozygous unknown variants	385
Genes with ≥ 2 heterozygous variants, both predicted to be disease-causing	35
Genes involved in DNA repair with ≥ 2 heterozygous variants, both predicted to be disease-causing	3

Supplemental Table 2. Genes with ≥ 2 heterozygous sequence variants, both predicted to be disease-causing (related to Results and Figure 1)

LOC729737	KIAA1211
C1orf159	HGC6.3
SRRM1	CCDC146
HORMAD1	ZNF696
C2orf71/RP54	ANKRD18B
PLEKHH2	ANKRD20A2
LOC400986/ANKRD36C	ANKRD20A1
LOC100287144/USP17L10	ANKRD2
C10orf76	ZNF408/RP72
LOC100507338/PFM8	USP15
FLYWCH1	RFWD3
ROGDI	KIAA0664/CLUH
LOC400499	CBX4
ARMC5	AATK
ZNF527	PRR12
ZNF784	MCM3AP
ZNF335/MCPH10	MN1
ESX1	

Genes involved in DNA repair are marked bold. RFWD3 is highlighted in red.

Supplemental Table 3. Human genomic primer sequences (related to Methods)

Name	Sequence	Used for
RFWD3_Ex_2_F	AAGTCCATTACCAAACACTTCTGACTTAAGTA	c.204_205dupCC validation
RFWD3_Ex_2_R	CATAATTTCTAGTACAGCAATGATCACAGACT	c.204_205dupCC validation
RFWD3_Ex_3_F	AGCATTTAATGGCCTGGAGATGGGTTGA	Sanger sequencing
RFWD3_Ex_3_R	TCTACATAATTATGGCCAGTGAAGGCTCTATA	Sanger sequencing
RFWD3_Ex_4_F	CTGCTAGCTTCTCATACCTGACATATCTTAT	Sanger sequencing
RFWD3_Ex_4_R	ATATTCAGGTTGGGCATGGTGGCTC	Sanger sequencing
RFWD3_Ex_5-6_F	TACAAGTGTTCTGTAGCCCTTTTGATTGTA	Sanger sequencing
RFWD3_Ex_5-6_R	AATTATAAATAACAGTGTAAGACAGACTGCCAATG	Sanger sequencing
RFWD3_Ex_7_F	TACAGCAAAGAACGTGCATCATAGCATGAA	Sanger sequencing
RFWD3_Ex_7_R	TATAGTAGACCTCATCATAAAGTGTGTA	Sanger sequencing
RFWD3_Ex_8_F	CAGTTCTCTAGGATTGATGTTAACTTTTCATA	Sanger sequencing
RFWD3_Ex_8_R	ATCTTTGCAGCACCTGGGGTACTT	Sanger sequencing
RFWD3_Ex_9_F	TGACCAGCTGGTTCCCAAGGACTTATA	Sanger sequencing
RFWD3_Ex_9_R	AACAAAAACAGAGCTAAGGTCATCATAAC	Sanger sequencing
RFWD3_Ex_10_F	AGTGTGTTCTCAGTAAGGATTAATGATCA	Sanger sequencing
RFWD3_Ex_10_R	AACCTGGCTATACTTGTACCAGAACTCTC	Sanger sequencing
RFWD3_Ex_11_F	TCTGGAGCCGTCCGAGTTTTGGA	c.1916 T>A validation
RFWD3_Ex_11_R	ACCTCGTTAGCCTGTGAGCGGTA	c.1916 T>A validation
RFWD3_Ex_12_F	TGCATTTATGGCTTTTCCATCCAACCTAGGTT	Sanger sequencing
RFWD3_Ex_12_R	GACTCATGGAAACCAAGCAATCTCACATA	Sanger sequencing
RFWD3_Ex_13_F	GTCAGGTGTGCTGACTTTGAACAACCTT	Sanger sequencing
RFWD3_Ex_13_R	TCCTAGAATCATACTAATGCAAACAAACCATGAT	Sanger sequencing
RFWD3_Ex_c2_F	GGCCGAGGTAACCTACCGAGTCTT	cDNA Sanger sequencing
RFWD3_Ex_c2_R	AAGTCAGGCTGGGTCCTGCTCA	cDNA Sanger sequencing
RFWD3_Ex_c11_F	GGCTAACTACATCTATGCTGGACTGG	cDNA Sanger sequencing
RFWD3_Ex_c11_R	TTTTGGTCAATAGTTTGAAGTAGGTCCT	cDNA Sanger sequencing

Supplemental Table 4. Primer sequences used for RFWD3 cloning and analysis (related to Methods)

Name	Sequence	Used for
Human_Puro_for	CGAGTTGAGCGGTTCCCGGCTGG	Transduction verification
Human_Puro_rev	GTTGATTGTTCCAGACGCGTCTAGGCACC	Transduction verification
Human_I639K_for	GCTGCCCTTGGAGCCAGGGGGCTGCAAAGACTTTCAG ACAGAGAACAGCTCCCGG	Mutagenesis
Human_I639K_rev	CCGGGAGCTGTTCTGTCTGAAAGTCTTTCAGCCCC CTGGCTCCAAGGGCAGC	Mutagenesis
Human_pLVX-EF1a-IRES-puro_for	gagactagtctagaATGGCTCATGAAGCAATGGAATATGATG	Infusion cloning
Human_pLVX-EF1a-IRES-puro_rev	agaggggcgggatccTCACTCCCACTTATAGATGTGGACC	Infusion cloning
Human_pIRES_neo_for	ggcctgttaaccggtATGGCTCATGAAGCAATGGAATATGATG	Infusion cloning
Human_pIRES_neo_rev	ggatccgaattcgaaTCACTCCCACTTATAGATGTGGACC	Infusion cloning
DT40chicken_STGC_1	AACAGCTCTGGTAAGCTTGTCCAGATCGATG	Detection of STGC
DT40chicken_STGC_2	TGCTTTGCGTTCAAGCTTGGCTGCAGGTCG	Detection of STGC
DT40chicken_LTGC_1	GTGAGGAAGAGTTCTTGCAGCT	Detection of LTGC
DT40chicken_LTGC_2	CAGCGCCCGACCGAAAGGAGCGCACGACC	Detection of LTGC

Supplemental Table 5. Antibodies used in this study (related to Methods)

Name	Type of antibody	Company	Catalogue number	Used for	Dilution
Anti-FANCD2	Mouse, monoclonal	Santa Cruz Biotechnology	sc-20022	Western blotting	1:500
Anti-RAD51	Rabbit, polyclonal	abcam	ab63801	Immunofluorescence	1:800
Anti-RFWD3	Rabbit, polyclonal	abcam	ab138030	Western blotting	1:1000
Anti-Tubulin	Mouse, monoclonal	abcam	ab44928	Western blotting	1:1000
Anti-GAPDH	Rabbit, polyclonal	abcam	ab985-200	Western blotting	1:1000
Anti-p84	Mouse, monoclonal	abcam	ab487	Western blotting	1:2000
Anti-Histone H3	Rabbit, polyclonal	abcam	ab1791	Western blotting	1:600
Anti-RAD50	Mouse, monoclonal	GeneTex	GTX70228	Western blotting	1:5000
Anti-Vinculin	Rabbit, monoclonal	abcam	ab129002	Western blotting	1:10000
Anti-RPA1	Rabbit, polyclonal	Bethyl Laboratories	A300-241A	Immunofluorescence	1:1000
Anti-RPA2	Rabbit, polyclonal	Bethyl Laboratories	A300-244A	Immunofluorescence	1:1000
Alexa 594	Goat anti-rabbit igG	Life Technologies	A11072	Immunofluorescence	1:2000

Supplemental Table 6: Primer and probe sequences for mouse *Rfwd3*-targeting studies
(related to Methods)

Name	Sequence	Used for
1589_41	CTAAAGGACAGTTAAGTGCATCTAGACC	PCR fragment 1
1589_51	CTTATGGTCTCTGACTCCAAGC	PCR fragment 1
1589_42	TAAGCATTGGTAAACCGGTGACACGTGTCATAACTTCGTATAGCATACATTATACGAAG TTA TCCCAAGTGTTTGCCTGTGAGTGTAT	PCR fragment 2
1589_52	CTAAGGCGCGCCTCAGAATAAAAAACAGAAAGGGAATGCCATTACACAGG	PCR fragment 2
1589_43	CTAAAGTACTAATGATCCACCCAAGATAGTCACC	PCR fragment 3
1589_53	TAAGCATTGGTAAAAATAACAGTGCAAGGTTGGGTGG	PCR fragment 3
5Pi	CTTGTGCTGCTGCTGTTTAACTTTTATCACCAGCAGCGGAAGTGCAGCCGAAGGATA TTTTATTCTCTCTTCTGCGGGGAGGCGGGCGTGGGCAGACAGGTTAGGAACT TAACTTTGGTCCGAGCTACTAACAGGGCGAGCCTGGATACGAACCCGGGTCTGAC TGAATCCCGCGGGCTCCCGGCGACCTGTTTATTGGGGCAGCCGTCGCTCCCGCCTT CTGTGTTTATCGAAACCAAAGCTTAGCAAGGGTGGGGGGCAGAGGTGGAGTTCACGG TCTGAGGGCCGCTGACTTTTCGGGGCCATCGGACTAGCGTTTGTGCACTTAAAGAAG GGGCTCATACGAGCACGAGCCCAGGATTGGGGAACGTGTTTGTGTTTGA	Southern hybridization
P3	CCACCCAACCTTGCACTGTTATTTTGTTCAGACAGTTTGCTAGGCAGCCAGACA GGCCTTGCTTACTATCTGTTGTTTGTGTCACAGGACACATTTAGTCTACTCCCTGTT GGGGTCCCCCTCCCGCCTTTTAAACATTTTCTCGTATAAGTCAAGACTTTATATAGTTA CCTTAACAAATTGAGTGAGTATAGTCATGAGATTTATTTATAGCAGAGGTTGCCATATA AAAGGAAAGATGTTTACTTTTGTGACCAACGAATGTGCCTTTGGAAATTTATGCAA GCTATTGAAGCACCGATAAGCATGTCC	Southern hybridization
NeoP	GACTGGGCACAACAGACAATCGGCTGCTCTGATGCCGCCGTGTTCCGGCTGTCAGCG CAGG GGCGCCCGGTTCTTTTGTCAAGACCGACCTGTCCGGTGCCCTGAATGAACTGCAGGA CGAG GCAGCGCGGCTATCGTGGCTGGCCACGACGGGCGTTCCTTGCGCAGCTGTGCTCGA CGTTGT CACTGAAGCGGGAAGGGAAGTGGCTGCTATTGGGCGAAGTGCCGGGGCAGGATCTCCT GTCAT CTCACCTTGCTCCTGCCGAGAAAGTATCCATCATGGCTGATGCAATGCGGCGGCTGCA TACGC TTGATCCGGCTACCTGCCCATTCGACCACCAAGCGAAACATCGCATCGAGCGAGCAC GTAATCG GATGGAAGCCGGTCTTGTGATCAGGATGATCTGGACGAAGAGCATCAGGGGCTCGC GCCAGCC	Southern hybridization

	GAAGTGTTCGCCAGGCTCAAGGCGCGCATGCCCCGACGGCGATGATCTCGTCGTGACC CATGGCGATGCCTGCTTGCCGAATATCATGGTGGAAAATGGCCGCTTTTCTGGATTCA TCGACTGTGGCCGGCTGGGTGTGGCGGACCGCTATCAGGACATAGCGTTGGCTACCC GTGATATTGCTGAAGAGCTTGG	
Prime Time Primer 2	TGAAGCCAACATTCCAGAACA	RT-PCR
Prime Time Primer 1	CACCTTCCTCATCTTCATAGC	RT-PCR

3.2.3 THE E3 LIGASE RFWD3 PROMOTES TIMELY REMOVAL OF BOTH RPA AND RAD51 FROM DNA DAMAGE SITES TO FACILITATE HOMOLOGOUS RECOMBINATION

The E3 ligase RFWD3 promotes timely removal of both RPA and RAD51 from DNA damage sites to facilitate homologous recombination

Shojiro Inano^{1,2}, Koichi Sato^{3,7}, Yoko Katsuki¹, Wataru Kobayashi³, Hiroki Tanaka³, Kazuhiro Nakajima⁴, Shinichiro Nakada⁴, Hiroyuki Miyoshi⁵, Kerstin Knies⁶, Akifumi Takaori-Kondo², Detlev Schindler⁶, Masamichi Ishiai¹, Hitoshi Kurumizaka³, Minoru Takata^{1, 8,*}

¹Laboratory of DNA Damage Signaling, Department of Late Effects Studies, Radiation Biology Center, Kyoto University, Kyoto Japan

²Department of Hematology and Oncology, Graduate School of Medicine, Kyoto University, Kyoto, Japan

³Laboratory of Structural Biology, Graduate School of Advanced Science and Engineering, Waseda University, Tokyo, Japan

⁴Department of Bioregulation and Cellular Response, Graduate School of Medicine, Osaka University, Osaka, Japan

⁵Department of Physiology, Keio University School of Medicine, Tokyo, Japan

⁶Department of Human Genetics, Biozentrum, University of Wurzburg, Wurzburg, Germany

⁷Present address: Hubrecht Institute–KNAW & University Medical Center Utrecht, Utrecht, the Netherlands

⁸Lead contact

*Correspondence: mtakata@house.rbc.kyoto-u.ac.jp

SUMMARY

RFWD3 is a recently identified Fanconi anemia protein FANCW whose E3 ligase activity toward RPA is essential in homologous recombination (HR) repair. However, how RPA ubiquitination promotes HR remained unknown. Here we identified RAD51, the central HR protein, as another target of RFWD3. We show that RFWD3 polyubiquitinates both RPA and RAD51 *in vitro* and *in vivo*. RFWD3 inhibits persistent MMC-induced RAD51 and RPA foci by promoting VCP/p97-mediated protein dynamics and subsequent degradation. Depletion of *BRCA2* impairs RPA ubiquitination, and *RFWD3* functions with *BRCA2* in RPA foci turnover. Furthermore, MMC-induced chromatin loading of MCM8 is defective in cells with inactivated *RFWD3* or expressing a ubiquitination-deficient mutant RAD51. Collectively, our data reveal a mechanism that facilitates timely removal of RPA and RAD51 from DNA damage sites, which is crucial for progression to the late phase HR and suppression of the FA phenotype.

Keywords: Fanconi anemia, Homologous recombination, ICL repair, RFWD3, RAD51, RPA

In Brief

A novel Fanconi anemia gene FANCW/RFWD3 encodes an E3 ligase that is essential for homologous recombination repair of DNA. Inano et al. show that stepwise repair involves polyubiquitination of RPA and RAD51 and their subsequent removal from chromatin and degradation.

Highlights

- RFWD3 polyubiquitinates both RPA and RAD51 *in vitro* and *in vivo*.
- RFWD3 marks MMC-induced RPA and RAD51 foci for clearance by VCP and the proteasome.
- Defective clearance impairs HR and loading of MCM8 to chromatin.
- RFWD3 functions in RPA polyubiquitination epistatically with BRCA2.

INTRODUCTION

Cells daily incur numerous DNA lesions that threaten genome integrity. To maintain genomic integrity, cells are equipped with a myriad of mechanisms that are each specific for different types of damage. However, DNA interstrand crosslinks (ICLs) require the combined use of various modes of DNA repair, including nucleotide excision repair (NER), translesion synthesis (TLS), and homologous recombination (HR). The Fanconi anemia (FA) pathway orchestrates these DNA repair activities for ICL repair (Ceccaldi et al., 2016; Kottemann and Smogorzewska, 2013). FA is a hereditary disorder defective in ICL repair and characterized by developmental anomalies, progressive bone marrow failure, leukemia, and solid tumors (Kutler et al., 2003).

An ICL is converted to a double-strand break (DSB) by incision (termed unhooking) through the actions of a structure-specific nuclease SLX4/FANCP-XPF/FANCD1-ERCC1 complex. This is recruited in a manner dependent on the FANCD2-FANCI (D2-I) heterodimeric complex that accumulates in chromatin upon their monoubiquitination by the FA core E3 ligase complex (Ceccaldi et al., 2016; Kottemann and Smogorzewska, 2013). Importantly, a DSB generated at ICL-stalled replication forks is subsequently channeled into the HR repair pathway. Therefore, biallelic mutations in genes of the core HR machinery, such as *BRCA2/FANCD1* or *RAD51C/FANCO*, may also cause FA. More recently, *BRCA1/FANCS* and *RAD51/FANCR*, key molecules in HR, have also been identified as FA genes (Bogliolo and Surrallés, 2015; Ceccaldi et al., 2016).

The first step in HR following DSB generation during ICL repair is DNA end resection. The MRE11–RAD50–NBS1 (MRN) complex initiates resection, which is

completed by the combined actions of many DNA repair factors that are modulated by FANCD2 itself (Ceccaldi et al., 2016; Symington and Gautier, 2011). The resulting long single-stranded DNA (ssDNA) is rapidly coated with RPA, a trimeric ssDNA binding protein complex that consists of subunits RPA1 (also called RPA70), RPA2 (RPA32), and RPA3 (RPA14). The mediator BRCA2-DSS1 complex plays a major role in loading RAD51 onto RPA-bound ssDNA (Liu et al., 2010; Prakash et al., 2015; Zhao et al., 2015), resulting in RAD51 nucleoprotein filament formation. RAD51 catalyzes the critical activity in HR, i.e., the homology search and strand invasion of homologous duplex DNA, leading to the formation of a displacement loop (D-loop) recombination intermediate. The ssDNA strand displaced from the template DNA during heteroduplex DNA formation also binds RPA. Subsequently, DNA synthesis, from the 3' end of the invading strand as a primer, using a PCNA clamp and DNA polymerases (Heyer, 2015; Sebesta et al., 2013), extends the D-loop, leading to capture and annealing of the other end of the DSB (second end capture). However, it is still poorly understood how these late-phase HR processes are regulated.

RFWD3 is a RING-type E3 ligase that colocalizes with RPA in DNA-damage-induced foci. It binds to RPA2 and functions in replication checkpoints (Gong and Chen, 2011; Liu et al., 2011). It was further reported that RFWD3-mediated ubiquitination of RPA is essential for HR (Elia et al., 2015). However, the mechanisms by which RPA ubiquitination contributes to HR remain unclear. Here we show that RFWD3 ubiquitinates both RPA and RAD51 *in vitro* and *in vivo*, and increases their local turnover in DNA damage-induced foci. Ubiquitinated RPA2 and RAD51 displayed lowered ssDNA binding, and they eventually underwent proteasomal degradation. In agreement with these observations, we also found higher levels of MMC-induced RPA

and RAD51 foci that abnormally persisted in the absence of *RFWD3*. Furthermore, cells expressing ubiquitination-deficient RPA2 and RAD51 mutants displayed HR defects and higher cisplatin sensitivity. Of note, biallelic mutations in the *RFWD3* gene have been identified in a patient with FA (Knies et al. in revision).

RESULTS

Inactivation of *RFWD3* results in persistent RPA2 and RAD51 foci

To gain more insight into the *RFWD3* function in HR, $\Delta RFWD3$ cells were constructed in the HAP1 haploid human cell line using CRISPR-CAS9 (Horizon Genomics) and validated by genome sequencing (Figure S1A) and immunoblotting (Figure 1A). $\Delta RFWD3$ cells exhibited hypersensitivity to MMC, Olaparib, and Camptothecin (CPT), with milder sensitivity to gamma-ray irradiation (IR) and Hydroxyurea (HU) (Figure 1B). Importantly, reintroduction of wild type (WT) *RFWD3* reversed MMC sensitivity, whereas a RING finger domain mutant (C315A) did not, despite higher expression levels (Figure S1B). These HAP1 mutant cell lines appeared to maintain a stable DNA ploidy pattern (Figure S1B).

Next we examined how loss of *RFWD3* affects ICL repair. While $\Delta RFWD3$ cells were proficient in MMC-induced FANCD2 monoubiquitination (Figure 1A), RPA2 and RAD51 foci numbers in $\Delta RFWD3$ were drastically elevated at 16-32 hr post-MMC addition (Figure 1C and D). A similar tendency was observed after gamma-ray irradiation (IR) in U2OS cells depleted of *RFWD3*, which showed extensive colocalization of RPA2 and RAD51 (Figure S1C). Furthermore, we detected more RPA2 and RAD51 in the chromatin fraction in $\Delta RFWD3$ than in WT at 24 hr post-MMC stimulation (Figure 1E). Interestingly, the accumulated RPA2 accompanied

slower migrating species, which are probably hyperphosphorylated forms of RPA2. We also noted highly increased numbers of proximal ligation assay (PLA) signals between RPA2 and RAD51 proteins in siRFWD3-depleted MMC-stimulated U2OS cells (Figure 1F). These PLA signals might reflect the coexistence of RPA and RAD51 in HR intermediates such as D-loops, since *BRCA2* knockdown (Figure S1D) drastically diminished these signals (Figure 1F).

Prior studies have indicated that *RFWD3* is required for checkpoint signaling under replication stress (Elia et al., 2015; Gong and Chen, 2011; Liu et al., 2011). Indeed, we found that Δ *RFWD3* cells exhibited less RPA phosphorylation after HU treatment than WT (Figure S1E). However, MMC-induced phosphorylation was rather enhanced compared with control WT cells (Figure S1E). Unexpectedly, we found that expression of *RFWD3* with the RING domain mutation (C315A) restored RPA2 and Chk1 phosphorylation, as well as HU resistance, in Δ *RFWD3* cells (Figure S1F and Figure 1B). This is in sharp contrast to the situation with the ICL response. We also found that a *RFWD3* construct carrying both C315A and the FA patient-derived mutation I639K, which inhibits chromatin localization of RFWD3 (see the accompanying manuscript Knies et al. in revision), only partially reversed these defects (Figure S1F). Since Δ *RFWD3* cells treated with HU for 2 hr displayed a lower percentage of RPA foci positive cells (Figure S1G), we speculate that *RFWD3* facilitates RPA loading onto ssDNA under HU-induced stress, and subsequent ATR-Chk1 activation in a manner independent of its E3 ligase activity.

***RFWD3* promotes RPA polyubiquitination following MMC damage**

Given that *RFWD3* interacts with RPA (Gong and Chen, 2011; Liu et al., 2011), and Δ *RFWD3* cells displayed increased numbers of RPA2 foci formation after MMC

damage, we examined whether RFWD3 polyubiquitinates RPA. In cells transfected with tagged ubiquitin, we found that polyubiquitination of endogenous RPA1 and RPA2 was detectable when treated with MMC in the additional presence of proteasomal inhibitor MG132 (Figure 2A). Polyubiquitination of overexpressed RPA2 (Figure 2B) or RPA3 (Figure S2A) was also observed following combined MMC/MG132 treatment. Importantly, this was markedly suppressed by *RFWD3* depletion (Figure 2A, 2B, and S2A). RPA2 polyubiquitination was further increased when FLAG-RFWD3 WT was co-expressed (Figure 2B). This effect of *RFWD3* expression was mostly or partially abrogated by the RING domain mutation (C315A) or chromatin localization-defective mutation (I639K) (see the accompanying manuscript) (Figure 2B), respectively. The latter observation is consistent with the previous report that RPA polyubiquitination occurs in chromatin (Elia et al., 2015). These results are consistent with the possibility that *RFWD3*-dependent RPA polyubiquitination facilitates its proteasomal degradation.

ICL damage triggers RPA polyubiquitination in a manner dependent on ATR/ATM kinase

The DNA damage response (DDR) includes phosphorylation events by three major PIKK family members, ATR, ATM, and DNA-PK. To elucidate how the RFWD3 E3 ligase is activated during DDR, we tested the effects of inhibitors of ATR (VE-821), ATM (KU-55933), and DNA-PK (NU-7026) on RPA2 polyubiquitination. We found that polyubiquitination was significantly diminished by combined treatment of ATR and ATM inhibitors (Figure S2B). Since it was reported that RFWD3 Ser46 and Ser63 are phosphorylated by ATM and ATR following DNA damage (Fu et al., 2010), we introduced a *RFWD3* S46/63A mutant construct into HAP1 Δ *RFWD3* cells. We found that the mutant could not fully restore cisplatin tolerance (Figure 1B). Furthermore,

overexpressed *RFWD3* S46/63A mutant displayed decreased levels in RPA polyubiquitination (Figure 2C). These results indicated that phosphorylation of *RFWD3* S46/63 mediated by ATR/ATM kinase may be critically involved in activation of *RFWD3*.

Next, we raised a rabbit antibody against a *RFWD3* peptide containing phosphorylated Ser46 (Figure S2C and S5B). This antibody recognized MMC-induced *RFWD3* phosphorylation in *RFWD3* WT but not the S46/63A mutant by immunoblotting (Figure S2C). We found that the S46 phosphorylation was sensitive to I639K mutation (Figure S2C) or the combined treatment with ATR and ATM inhibitors (Figure S2D).

Interaction between ssDNA and ubiquitination-deficient RPA2 *in vivo*

To elucidate the functional role of RPA polyubiquitination, we constructed three types of *RPA2* ubiquitination site mutants. We focused our attention on RPA2 rather than RPA1 or RPA3 since it was shown that multiple RPA1 lysine mutations did not suppress polyubiquitination (Elia et al., 2015), and the contribution of RPA3 ubiquitination to the function of the RPA complex could be limited because of its relatively weak ubiquitination (Figure S2A and see Figure 4A below). The candidate ubiquitination residues were based on previous proteomics studies and they were replaced with Arg as follows: K37/38R (termed 2KR), K85/127/171R (3KR), and K37/38/85/127/171R (5KR) (Figure S2E). The WT and mutated his-RPA2 constructs were tested for ubiquitination by transient overexpression with *RFWD3*. We found that the 5KR mutation, but not 2KR and 3KR, largely eliminated RPA2 polyubiquitination in cells (compare lanes 2 and 3, Figure 2D).

The increased number of RPA2 foci in cells with inactivated *RFWD3* led us to

hypothesize that polyubiquitination of RPA2 reduces the amount of RPA in the chromatin fraction. To test this hypothesis, we transduced the U2OS cell line (harboring a DR-GFP reporter that is repaired to produce functional GFP by homologous recombination repair of a site-specific DSB (Prakash et al., 2015)) with lentivirus encoding FLAG-tagged RPA2-WT or -5KR under the control of a tetracycline-inducible promoter. Endogenous RPA2 was depleted by an siRNA targeting the 3' UTR, enabling us to replace endogenous RPA2 with the 5KR variant (Figure 2E). In cells expressing the FLAG-RPA2-5KR mutant, we observed modestly increased levels of RPA2 in the chromatin fraction (24 hr post-MMC) and more RPA2 foci formation (48 hr post-MMC) compared to cells expressing RPA2-WT. These results suggest that polyubiquitinated RPA tends to be removed from DNA damage sites (Figure 2E).

RAD51 is also polyubiquitinated by RFWD3 *in vivo*

Since *RFWD3* depletion also resulted in augmented numbers of RAD51 foci after ICL damage, we speculated that RAD51 might be another target of *RFWD3* ubiquitination. Indeed, we found that endogenous RAD51 in cells transfected with the his-ubiquitin construct was polyubiquitinated following MMC in a manner dependent on *RFWD3* (Figure 3A). Furthermore, we observed overexpressed his-tagged RAD51 underwent *RFWD3*-dependent ubiquitination when coexpressed with myc-tagged ubiquitin (Figure S3A). Notably, RAD51 polyubiquitination levels were increased by MMC and MG132 treatment, and decreased after siRFWD3 depletion (Figure S3A).

Previous studies reported that RAD51 has several potential candidate ubiquitination sites (Chu et al., 2015; Wagner et al., 2011): K58, K64, K107, and K156. In addition, we noticed K57 adjacent to K58 is conserved in vertebrates (Figure S3B).

To investigate these putative sites, we generated three RAD51 mutant constructs, 5KR (K57/58/64/107/156R), K58/64R, and K107/156R, and tested them for RAD51 polyubiquitination. Among these mutants, 5KR displayed the most prominent decrease in polyubiquitination levels (Figure 3B).

We then evaluated accumulation of RAD51 on damaged chromatin following MMC. FLAG-tagged siRNA-resistant RAD51-WT or -5KR was lentivirally transduced into the U2OS cell line, and expression was induced by DOX while endogenous RAD51 was depleted by siRAD51 (Figure 3C). The cells expressing RAD51-5KR showed higher levels of chromatin retention and foci formation than RAD51 at 48 hr post-MMC stimulation. These results suggest that RAD51 polyubiquitination mediated by RFWD3 promotes removal of RAD51 from DNA damage sites.

Purified RFWD3 protein polyubiquitinates RPA and RAD51 *in vitro*

To examine whether RFWD3 can directly ubiquitinate RPA or RAD51 *in vitro*, the following recombinant human proteins were purified from *E.coli*: RAD51, the trimeric RPA complex, RFWD3, UBE2T (an E2 enzyme in the FA pathway), and several other E2 proteins that are possible partners of RFWD3 (Markson et al., 2009) (Figure S4A-D). Although the RFWD3 preparation contained a ~60 kDa contaminant *E.coli* protein (Figure S4C), the RPA complex (both RPA1 and RPA2, with weaker ubiquitination on RPA3) and RAD51 were ubiquitinated to various degrees *in vitro* (Figure 4A and B) with UBE2D1 being the most efficient, suggesting that RFWD3 can use several E2 enzymes in a non-selective manner. UBE2T could not support robust polyubiquitination of the RPA subunits, but RAD51 ubiquitination occurred to some extent, with minimal enhancement upon RFWD3 addition (Figure 4B). One of the *RAD51* paralog proteins, DMC1, was modestly ubiquitinated by RFWD3 with UBE2N or UBE2D1 (Figure 4C).

We also examined the interplay between RFWD3, RPA, and ssDNA *in vitro*. We found that RFWD3 directly interacts with the RPA complex in pull-down assays (Figure S4E). This is consistent with previous reports that show DNA damage-independent RPA-RFWD3 interaction (Gong and Chen, 2011; Liu et al., 2011). We found that the interaction was significantly reduced when RPA was bound to ssDNA (Figure S4F, i), while premixed RPA-RFWD3 could be efficiently pulled down using ssDNA-beads (Figure S4F, ii). Thus, prior binding of RFWD3 with RPA might be a prerequisite for RFWD3 localization to damaged chromatin. Interestingly, the *in vitro* RPA ubiquitination efficiency was not affected in the presence of ssDNA (Figure S4G), suggesting that RPA binding with ssDNA itself does not trigger RFWD3 ubiquitination.

We also carried out ssDNA-bead pull-down experiments with *in vitro* ubiquitinated RPA or RAD51, and examined the relative amount of ubiquitination in the ssDNA-bound or -unbound fraction. The percentage of ubiquitinated RPA or RAD51 was higher in the unbound than in the bound fraction, suggesting that polyubiquitination significantly reduced the RPA and RAD51 binding with ssDNA (Figure 4D and E). This is consistent with the *in vivo* observation in MMC-treated cells that chromatin retention of RPA2 or RAD51 was higher with the ubiquitination-defective 5KR mutants than the control (Figure 2E and 3C).

RAD51 directly interacts with RFWD3

The polyubiquitination of RAD51 by RFWD3 suggests that they may physically interact. We detected an interaction between transfected FLAG-RFWD3 and endogenous RAD51 by co-immunoprecipitation (co-IP) (Figure 5A). Importantly, their interaction was modestly enhanced by MMC treatment. We further confirmed the direct interaction between RAD51 and RFWD3 with a pull-down assay using purified proteins

(Figure 5B). To fine-map the RAD51-binding site within RFWD3, we performed mammalian two-hybrid assays, and found that the N-terminal region (aa 1-278) strongly interacted with RAD51 (Figure 5C). We validated this result using co-IP and PLA assays *in vivo* (Figure 5D and Figure S5A). The co-IP of FLAG-RFWD3 and exogenous RAD51 was detectable after MMC but was almost completely abrogated by a Δ 1-278 deletion. Similar results were obtained with endogenous RAD51 in the PLA assay, though FLAG-tagged Δ 1-278 RFWD3 exhibited decreased numbers of foci, possibly due to decreased expression levels (Figure S5A). These results imply that the N-terminal region of RFWD3 is essential for RAD51 interactions *in vivo*.

The RFWD3 N-terminal region (aa 1-278) encompasses characteristic repeated sequences termed LQP-SSQ repeats (Figure S5B). We synthesized an N-terminally biotinylated peptide (LQP peptide, residues 31 to 61) containing two LQP motifs and one SQ motif that was either phosphorylated (the phospho-LQP peptide) or unphosphorylated (LQP peptide), and an AAA peptide in which both LQP motifs were replaced with three alanines (see Figure S5B for the sequence). We found that the LQP, but not the AAA, peptide modestly pulled down RAD51 from cell lysates (Figure 5E). Phosphorylation of the SQ motif (corresponding to S46) did not affect the pull-down efficiency (data not shown).

These results prompted us to construct a full-length *RFWD3* mutant with all LQP motifs replaced by triple alanines (RFWD3-LQP/AAA)(Figure S5B). We tested the RFWD3 interaction with RAD51 by co-IP, and found that the LQP/AAA mutation decreased the RFWD3-RAD51 interaction (Figure 5D). Furthermore, overexpressed FLAG-RFWD3-LQP/AAA or -S46/63A mutant proteins interacted with RPA2, whereas the I639K mutant did not (Figure S5C). RPA2 polyubiquitination by the

overexpressed LQP/AAA mutant was similar to WT *RFWD3* (Figure S5D), while RAD51 ubiquitination was mildly impaired with the LQP/AAA mutant (Figure 5F). Consistent with this, higher levels of RAD51 foci were observed in HAP1 Δ *RFWD3* cells expressing the LQP/AAA mutant relative to *RFWD3* WT (Figure 5G and Figure S1B).

VCP/p97 interacts with RPA and RAD51 to promote their local turnover following DNA damage

Our data suggest that RPA and RAD51 are removed from chromatin in an *RFWD3*-dependent manner. To clarify how this occurs, we examined whether valosin-containing protein (VCP), also known as p97 or Cdc48, is involved. VCP is a homohexameric molecular chaperone, which extracts ubiquitinated proteins from immobile cellular structures in a manner dependent on its ATPase activity, and escorts them to the 26S proteasome for their degradation. The role of VCP in eviction of chromatin-bound proteins in DDR has recently been established (Meerang et al., 2011; Vaz et al., 2013).

First, we tested whether VCP interacts with RPA2 or RAD51 in response to MMC damage. We were able to co-immunoprecipitate endogenous VCP with RPA or RAD51 from HAP1 cell extracts (Figure 6A). Both interactions were enhanced following MMC treatment, and were dependent on *RFWD3* (Figure 6A). Furthermore, depletion of VCP enhanced polyubiquitination of RPA1 and RPA2 in chromatin isolated from MMC-treated cells; this was abrogated by si*RFWD3* (Figure S6A).

To assess the effects of *RFWD3* on protein dynamics of RPA and RAD51 in DNA damage sites, we next performed Fluorescence Recovery after Photobleaching (FRAP) analysis. In each data set, we photobleached more than 50 individual foci

formed after MMC treatment of U2OS cells transiently expressing GFP-tagged RPA1 or RPA2 or expressing inducible GFP-RAD51. Examples of the MMC-induced RPA1, RPA2 and RAD51 foci are shown in Figure S6B. In line with previous studies (Galanty et al., 2012; Gibb et al., 2014), RPA1 or RPA2 in DNA damage-induced foci was highly mobile, whereas RAD51 was rather static compared to RPA, in keeping with RAD51 in nucleoprotein filaments (Essers et al., 2002; Yu et al., 2003). Strikingly, we found that knockdown of *RFWD3* drastically or mildly reduced protein turnover of RPA1 and RPA2, or RAD51, respectively (Figure 6B). Furthermore, VCP depletion reduced protein turnover of RPA2 similarly to siRFWD3 (Figure 6B). We also prepared U2OS cells stably expressing ubiquitination-deficient RPA2-5KR or RAD51-5KR variants tagged with GFP, and carried out FRAP analysis. We found that RPA2-5KR turnover was drastically reduced compared to WT RPA2, and was not affected by siRFWD3 (Figure 6B, middle panel). Knockdown of *PRP19* did not affect RPA2 turnover, which is consistent with a previous report that implicates this gene in RPA polyubiquitination via K63 linkages (Maréchal et al., 2014). Protein dynamics of the GFP-RAD51-5KR mutant were mildly reduced, as expected (Figure 6B).

Polyubiquitinated RPA and RAD51 undergo proteosomal degradation after MMC damage

Polyubiquitinated proteins removed from chromatin by p97/VCP could then be transferred to the 26S proteasome for degradation. To test whether polyubiquitination of RPA or RAD51 results in proteasomal degradation, we performed a cycloheximide (CHX) chase assay on RPA2 and RAD51 in HAP1 WT and Δ *RFWD3* cells. After a 16 hr MMC treatment, cells were cultured in the presence of CHX. During the chase period (up to 9 hr), the levels of both RPA2 and RAD51 in whole cell lysates steadily

decreased in control WT HAP1 cells, but not in $\Delta RFW3$ cells (Figure 6C). In contrast, the levels were stable, irrespective of the *RFWD3* genotype, in cells without prior MMC treatment (Figure S6C).

Ubiquitination-defective mutants of RPA2 and RAD51 display HR defects

To prove that the critical role of *RFWD3* in HR is the polyubiquitination of RPA2 and RAD51, we used U2OS cells in which endogenous RPA2 or RAD51 were replaced with the 5KR mutants as described above (Figure 2E, 3C, and S6D), and tested whether they displayed decreased HR efficiency comparable to $\Delta RFW3$ cells.

Cells expressing RPA2-5KR or RAD51-5KR showed mildly and drastically reduced HR efficiencies as measured by the DR-GFP reporter compared to the respective WT controls, respectively (Figure 6D). The mild reduction in HR by the RPA2-5KR mutant might be due to unperturbed ubiquitination on the RPA1 or RPA3 subunits. Furthermore, cells expressing these variants were cisplatin-sensitive compared to control cells (Figure S6E). Collectively, these results suggest that loss of ubiquitination of RPA2 and RAD51 may lead to defective HR in $\Delta RFW3$ cells.

We also measured the effect of a disrupted RPA2-RFW3 interaction on HR efficiency. Based on earlier studies (Elia et al., 2015; Gong and Chen, 2011), we prepared an RPA2 deletion mutant lacking residues 244-254, which was sufficient to disrupt the interaction as measured by M2H assay (not shown). Endogenous RPA2 was replaced with the RPA2 deletion, as in the experiments above (Figure S6D). As expected, HR efficiency was reduced (Figure 6D), consistent with increased levels of cisplatin sensitivity (Figure S6E). Similar defects were previously described by Elia *et al.* using RPA2 lacking residues 243-262 (Elia et al., 2015).

Of note, we purified the recombinant trimeric RPA complex with the

RPA2-5KR subunit (Figure S4A) and RAD51 with 5KR mutation to verify functionality of these mutant proteins (Figure S4B). The RPA complex stoichiometry (Figure S4A) and ssDNA binding (Figure S4H) were indistinguishable from the WT RPA complex. The purified RAD51-5KR protein showed normal levels of ATPase and strand invasion (D-loop formation) activities *in vitro* (Figure S4I), excluding the possibility that the 5KR mutation largely compromised RAD51 function.

Inactivation of *RFWD3* inhibits chromatin loading of RAD54 and MCM8

To gain insight into how *RFWD3* inactivation impairs progression of late phase HR, we examined whether chromatin recruitment of RAD54 and MCM8 occurs normally in the absence of *RFWD3*. RAD54 belongs to the SWI2/SNF2 family of dsDNA-dependent ATPase chromatin remodelers and performs important functions including both formation and disruption of RAD51 filaments, branch migration in HR, and RAD51 removal in G2 phase (Heyer et al., 2006; Mason et al., 2015; Spies et al., 2016; Wright and Heyer, 2014). MCM8 is a member of the AAA+ superfamily that is thought to work in HR downstream of RAD51 loading (Lutzmann et al., 2012; Nishimura et al., 2012) as well as in DNA end resection (Lee et al., 2015).

To detect RAD54 in cells, HAP1 and HAP1 Δ *RFWD3* cells were stably transduced with a lentivirus encoding GFP-RAD54. HAP1 Δ *RFWD3* cells displayed greatly reduced numbers of GFP-RAD54 foci (Figure 7A) and chromatin loading (Figure 7B) compared to WT cells following MMC treatment. Similarly, we found decreased chromatin loading of MCM8 in HAP1 Δ *RFWD3* (Figure 7B) or in cells treated with siRFWD3 or siVCP, consistent with our previous conclusion that *RFWD3* works in a concerted manner with *VCP* (Figure 7C). Depletion of *BRC42* in U2OS cells abrogated MMC-induced RAD51 chromatin loading as expected, and also decreased the

amount of MCM8 in chromatin (Figure S7A), as shown before using DT40 cells (Nishimura et al., 2012). These data suggest that stabilized RPA and RAD51 "locked" in recombination intermediates due to defective *RFWD3*-mediated polyubiquitination compromise progression of HR. Indeed, chromatin loading of MCM8 in response to MMC was eliminated in cells expressing the RAD51-5KR mutant compared to cells with WT RAD51 (Figure 7D).

We reasoned that the RFWD3 E3 ligase should be activated after RPA and RAD51 complete their functions. To test this possibility, we knocked down *BRCA2* to prevent the execution of RAD51 function in cells, and examined the effects on RPA1 or RPA2 polyubiquitination mediated by RFWD3. Interestingly, siBRCA2 significantly decreased levels of RPA1 or 2 polyubiquitination, accompanied by decreased RAD51 chromatin loading (Figure 2A). Moreover, in a FRAP analysis *BRCA2* depletion attenuated RPA2-GFP dynamics in MMC-induced foci, similar to *RFWD3* depletion (Figure 7F). Importantly, simultaneous depletion by siBRCA2 and siRFWD3 suggested epistasis with regard to RPA2-GFP turnover (Figure 7E). We also found that RFWD3 accumulation in chromatin and S46 phosphorylation occurred normally in siBRCA2-treated cells (Figure S7B). However, it remains unclear how BRCA2 mechanistically affects activation of RFWD3.

DISCUSSION

A previous study indicated that loss of *RFWD3* function abrogates HR (Elia et al., 2015) and an accompanying paper shows that this results in the FA phenotype in humans (Knies et al. in revision). In this study, we identified a role of RFWD3 in polyubiquitination of RPA and RAD51, their subsequent disassembly from DNA damage sites, and eventual degradation. We propose that their timely removal from

recombination intermediates after they finish their prescribed function is essential for HR repair to proceed to later steps (Figure S7C). Thus our findings indicate a molecular mechanism in the spatiotemporal regulation of the critical HR factors. An analogous process operates in other DNA repair pathways such as NER (Puumalainen et al., 2014) or NHEJ (Brown et al., 2015; Postow et al., 2008).

In sharp contrast to our results, Elia *et al.* reported that RPA polyubiquitination by RFWD3 does not lead to its degradation (Elia et al., 2015). There could be several reasons for this discrepancy. First, they used HU, 4NQO, or UV stimulation, not MMC, with different time frames in their experiments (mostly up to 2 hr post-stimulation), compared to ours (16-48 hr after MMC stimulation). Second, they did not look at RPA foci, or RPA protein levels with CHX chase, after DNA damage in the absence of *RFWD3*. Instead, they measured the amount of ubiquitinated RPA peptides following UV by a proteomic approach, and found they were not increased by pretreatment with MG132 (described in Figure S3B, the post-UV time point was not specified but probably 2 hr similar to other experiments). They may have missed the RPA degradation because of these different experimental conditions.

Regulation and activation mechanism for RFWD3 during HR repair

Prior studies have established that the RPA2-RFWD3 interaction is required for RFWD3 recruitment to DNA damage induced-RPA foci (Gong and Chen, 2011; Liu et al., 2011). In keeping with this notion, the FA patient-derived I639K mutation in the RFWD3 WD40 domain attenuated both MMC-induced RFWD3 foci (Knies et al. in revision) and the RPA2 interaction. We suggest that RFWD3 might also promote RPA loading onto chromatin as shown in Figure S1G. Our *in vitro* binding data suggest that a preformed RPA-RFWD3 complex is recruited to ssDNA, rather than RPA bound to

ssDNA recruits RFWD3. In chromatin, RFWD3 becomes phosphorylated at least on residue S46 by ATM/ATR kinases, which was abrogated by the I639K mutation. We found that the RFWD3 S46/63A double substitution diminished RPA2 and RAD51 ubiquitination and increased sensitivity to MMC, while there was no effect on the interaction of RFWD3 with RPA2. RFWD3 harbors a number of additional SQ motifs that may be involved in the activation upon phosphorylation by ATM/ATR. Thus our results support a model in which RFWD3 is recruited and enzymatically activated at the DNA damage sites depending on the interaction with RPA and subsequent multiple phosphorylations by ATM/ATR.

Interplay between RFWD3 and BRCA2

Although it remains unknown exactly at which step of HR RFWD3 acts to promote progression of ICL repair, it should be in late phase HR; logically, if RFWD3 were to act at an early phase, it would function as an anti-recombinase. Given the foci data following MMC or IR, RFWD3 does not appear to replace RPA with RAD51, which is supposed to be carried out by BRCA2 (Zelensky et al., 2014). Rather, our data suggest that *RFWD3* functions in RPA ubiquitination downstream of, and epistatically with, *BRCA2*. We speculate that RPA and RAD51 ubiquitination is under tight spatiotemporal regulation such that it only occurs in a limited context provided by *BRCA2*. For example, only polymerized RAD51 might be efficiently recognized by the N-terminal domain containing four copies of the LQP motifs. Alternatively, as a non-mutually exclusive possibility, BRCA2 activated during the DNA damage response may somehow inhibit a phosphatase or a deubiquitinase that counters RFWD3 activity.

How persistent RPA2 and RAD51 at DNA damage sites affect HR repair

Our data suggest that *RFWD3* inactivation should lead to formation of RAD51

filaments scattered with RPA (mixed filaments), which might be reflected by the increased RAD51/RPA2 foci colocalization and the PLA signal between the two proteins. If the mixed filaments were functionally compromised, this may contribute to the loss of HR activities in *ΔRFDW3* cells. Alternatively, *RFWD3* may function at the postsynaptic stage. For example, RAD51 and RPA in a D-loop may need to be removed from the 3' end of the invading ssDNA to initiate efficient DNA repair synthesis. RPA removal may also aid the annealing/capture process with the other DNA end. Further investigation will reveal how *RFWD3* recognizes RPA and RAD51 during HR repair, and how the late stages of ICL repair are coordinated. In addition to effects on RPA and RAD51, we found loss of *RFWD3* accompanied decreased chromatin loading of RAD54 and MCM8. Thus *RFWD3* may license *RAD54* or *MCM8* to carry out their tasks. Ubiquitination-defective RAD51 adversely affected chromatin MCM8 loading after MMC damage. We suggest that this could be the direct consequence of persistent accumulation of RAD51.

Conclusion

In this study, we provide evidence that an E3 ligase *RFWD3* functions in timely removal and degradation of RPA and RAD51 to allow HR progression to subsequent steps following MMC damage. These mechanisms set the framework to further elucidate the spatiotemporal regulation of critical components of HR repair, which maintains genome stability to suppress hematopoietic failure in FA and to likely prevent cancer development in humans.

EXPERIMENTAL PROCEDURES

For more details on experimental procedures, please refer to the Supplemental Experimental Procedures.

Culture of cell lines

HAP1 is a haploid human cell line derived from the male chronic myelogenous leukemia (CML) cell line KBM-7. HAP1 WT and *ΔRFWD3* cells were purchased from Horizon Genomics. HAP1 cells and derivatives were cultured in IMDM (Nacalai Tesque) supplemented with 10% fetal calf serum (GIBCO) and Penicillin/Streptomycin (Nacalai Tesque). U2OS, U2OS-DR-GFP (a kind gift from Dr Maria Jasin), and 293T cells were cultured in DMEM (Nacalai Tesque) supplemented with 10% fetal calf serum.

Cells for FRAP analysis

For RPA1-GFP or RPA2-GFP foci, U2OS cells were co-transfected with an RPA1-GFP or RPA2-GFP (WT or -5KR) expression vector along with indicated siRNAs. 24 hr later, MMC (100 ng/ml) was added and analysis was performed after an additional 24 hr. For GFP-RAD51 foci, U2OS cells expressing GFP-RAD51-WT or -5KR under a Tet-inducible promoter were transfected with indicated siRNA. 16 hr later, GFP-RAD51 expression was induced with Doxycycline (1 ng/ml) along with MMC (100 ng/ml) for 24 hr.

Author contributions

M.T., D.S., K.K., H.K., and A.T-K. conceived the study; S.I. carried out experiments with help from Y.K. and M.I.; K.S. carried out *in vitro* assays with H.K., W.K. and H.T.; K.N., S.N., and H.M. provided unpublished reagents; M.T., S.I., H.K. and K.S. wrote the paper.

ACKNOWLEDGMENTS

We would like to thank Professor James Hejna (Graduate School of Biostudies, Kyoto University) for critical reading of the manuscript; Drs Makoto Nakanishi, Yoshikazu

Johmura, Maria Jasin, Kiyoshi Miyagawa and Aziz Sancar for reagents; Dr Kazuhiro Iwai (Graduate School of Medicine, Kyoto University) for discussion; Ms Akiko Watanabe, Seiko Arai, and Fan Peng for technical or secretarial support. Radiation Biology Center is a Joint Usage Research Center supported by the Ministry of Education, Culture, Sports, Science and Technology (MEXT) of Japan. Our work is supported by JSPS KAKENHI Grant Numbers JP23114010 [to M.T.], JP26550026 [to M.T.], JP15H01738 [to M.T.], JP26281021 [to M.I.], JP25116002 [to H.K.], and JP25250023 [to H.K.], JP15H01183 [to S.N.]) and grants from The Ministry of Health, Labour and Welfare [to M.T.]. H.K. was also supported by Waseda University. The authors declare no competing financial interests.

REFERENCES

- Bogliolo, M., and Surrallés, J. (2015). Fanconi anemia: a model disease for studies on human genetics and advanced therapeutics. *Curr Opin Genet Dev* 33, 32–40.
- Brown, J.S., Lukashchuk, N., Sczaniecka-Clift, M., Britton, S., le Sage, C., Calsou, P., Beli, P., Galanty, Y., and Jackson, S.P. (2015). Neddylation promotes ubiquitylation and release of Ku from DNA-damage sites. *Cell Rep* 11, 704–714.
- Ceccaldi, R., Sarangi, P., and D'Andrea, A.D. (2016). The Fanconi anaemia pathway: new players and new functions. *Nat Rev Mol Cell Biol* 17, 337–349.
- Chu, W.K., Payne, M.J., Beli, P., Hanada, K., Choudhary, C., and Hickson, I.D. (2015). FBH1 influences DNA replication fork stability and homologous recombination through ubiquitylation of RAD51. *Nat Commun* 6, 5931.
- Elia, A.E.H., Wang, D.C., Willis, N.A., Boardman, A.P., Hajdu, I., Adeyemi, R.O., Lowry, E., Gygi, S.P., Scully, R., and Elledge, S.J. (2015). RFWD3-Dependent Ubiquitination of RPA Regulates Repair at Stalled Replication Forks. *Mol Cell* 60, 280–293.
- Essers, J., Houtsmuller, A.B., van Veelen, L., Paulusma, C., Nigg, A.L., Pastink, A., Vermeulen, W., Hoeijmakers, J.H.J., and Kanaar, R. (2002). Nuclear dynamics of RAD52 group homologous recombination proteins in response to DNA damage. *Embo J* 21, 2030–2037.
- Fu, X., Yucer, N., Liu, S., Li, M., Yi, P., Mu, J.-J., Yang, T., Chu, J., Jung, S.Y., O'Malley, B.W., et al. (2010). RFWD3-Mdm2 ubiquitin ligase complex positively regulates p53 stability in response to DNA damage. *Proc Natl Acad Sci USA* 107, 4579–4584.
- Galanty, Y., Belotserkovskaya, R., Coates, J., and Jackson, S.P. (2012). RNF4, a SUMO-targeted ubiquitin E3 ligase, promotes DNA double-strand break repair. *Genes Dev* 26, 1179–1195.

- Gibb, B., Ye, L.F., Gergoudis, S.C., Kwon, Y., Niu, H., Sung, P., and Greene, E.C. (2014). Concentration-dependent exchange of replication protein A on single-stranded DNA revealed by single-molecule imaging. *PLoS ONE* 9, e87922.
- Gong, Z., and Chen, J. (2011). E3 ligase RFWD3 participates in replication checkpoint control. *J Biol Chem* 286, 22308–22313.
- Heyer, W.-D. (2015). Regulation of Recombination and Genomic Maintenance. *Cold Spring Harb Perspect Biol* 7, a016501.
- Heyer, W.-D., Li, X., Rolfsmeier, M., and Zhang, X.-P. (2006). Rad54: the Swiss Army knife of homologous recombination? *Nucleic Acids Res* 34, 4115–4125.
- Kottemann, M.C., and Smogorzewska, A. (2013). Fanconi anaemia and the repair of Watson and Crick DNA crosslinks. *Nature* 493, 356–363.
- Kutler, D.I., Singh, B., Satagopan, J., Batish, S.D., Berwick, M., Giampietro, P.F., Hanenberg, H., and Auerbach, A.D. (2003). A 20-year perspective on the International Fanconi Anemia Registry (IFAR). *Blood* 101, 1249–1256.
- Lee, K.Y., Im, J.-S., Shibata, E., Park, J., Handa, N., Kowalczykowski, S.C., and Dutta, A. (2015). MCM8-9 complex promotes resection of double-strand break ends by MRE11-RAD50-NBS1 complex. *Nat Commun* 6, 7744.
- Liu, J., Doty, T., Gibson, B., and Heyer, W.-D. (2010). Human BRCA2 protein promotes RAD51 filament formation on RPA-covered single-stranded DNA. *Nat Struct Mol Biol* 17, 1260–1262.
- Liu, S., Chu, J., Yucer, N., Leng, M., Wang, S.-Y., Chen, B.P.C., Hittelman, W.N., and Wang, Y. (2011). RING finger and WD repeat domain 3 (RFWD3) associates with replication protein A (RPA) and facilitates RPA-mediated DNA damage response. *J Biol Chem* 286, 22314–22322.
- Lutzmann, M., Grey, C., Traver, S., Ganier, O., Maya-Mendoza, A., Ranisavljevic, N., Bernex, F., Nishiyama, A., Montel, N., Gavois, E., et al. (2012). MCM8- and

MCM9-deficient mice reveal gametogenesis defects and genome instability due to impaired homologous recombination. *Mol Cell* 47, 523–534.

Maréchal, A., Li, J.-M., Ji, X.Y., Wu, C.-S., Yazinski, S.A., Nguyen, H.D., Liu, S., Jiménez, A.E., Jin, J., and Zou, L. (2014). PRP19 Transforms into a Sensor of RPA-ssDNA after DNA Damage and Drives ATR Activation via a Ubiquitin-Mediated Circuitry. *Mol Cell* 53, 235–246.

Markson, G., Kiel, C., Hyde, R., Brown, S., Charalabous, P., Bremm, A., Semple, J., Woodsmith, J., Duley, S., Salehi-Ashtiani, K., et al. (2009). Analysis of the human E2 ubiquitin conjugating enzyme protein interaction network. *Genome Research* 19, 1905–1911.

Mason, J.M., Dusad, K., Wright, W.D., Grubb, J., Budke, B., Heyer, W.-D., Connell, P.P., Weichselbaum, R.R., and Bishop, D.K. (2015). RAD54 family translocases counter genotoxic effects of RAD51 in human tumor cells. *Nucleic Acids Res* 43, 3180–3196.

Meerang, M., Ritz, D., Paliwal, S., Garajova, Z., Bosshard, M., Mailand, N., Janscak, P., Hübscher, U., Meyer, H., and Ramadan, K. (2011). The ubiquitin-selective segregase VCP/p97 orchestrates the response to DNA double-strand breaks. *Nat Cell Biol* 13, 1376–1382.

Nishimura, K., Ishiai, M., Horikawa, K., Fukagawa, T., Takata, M., Takisawa, H., and Kanemaki, M.T. (2012). Mcm8 and Mcm9 form a complex that functions in homologous recombination repair induced by DNA interstrand crosslinks. *Mol Cell* 47, 511–522.

Postow, L., Ghenoiu, C., Woo, E.M., Krutchinsky, A.N., Chait, B.T., and Funabiki, H. (2008). Ku80 removal from DNA through double strand break-induced ubiquitylation. *J Cell Biol* 182, 467–479.

Prakash, R., Zhang, Y., Feng, W., and Jasin, M. (2015). Homologous Recombination and Human Health: The Roles of BRCA1, BRCA2, and Associated Proteins. *Cold Spring Harb Perspect Biol* 7, a016600.

- Puumalainen, M.-R., Lessel, D., Rütthemann, P., Kaczmarek, N., Bachmann, K., Ramadan, K., and Naegeli, H. (2014). Chromatin retention of DNA damage sensors DDB2 and XPC through loss of p97 segregase causes genotoxicity. *Nat Commun* 5, 3695.
- Sebesta, M., Burkovics, P., Juhasz, S., Zhang, S., Szabo, J.E., Lee, M.Y.W.T., Haracska, L., and Krejci, L. (2013). Role of PCNA and TLS polymerases in D-loop extension during homologous recombination in humans. *DNA Repair* 12, 691–698.
- Spies, J., Waizenegger, A., Barton, O., Stürder, M., Wright, W.D., Heyer, W.-D., and Löbrich, M. (2016). Nek1 Regulates Rad54 to Orchestrate Homologous Recombination and Replication Fork Stability. *Mol Cell* 62, 903–917.
- Symington, L.S., and Gautier, J. (2011). Double-strand break end resection and repair pathway choice. *Annu. Rev. Genet.* 45, 247–271.
- Vaz, B., Halder, S., and Ramadan, K. (2013). Role of p97/VCP (Cdc48) in genome stability. *Front Genet* 4, 60.
- Wagner, S.A., Beli, P., Weinert, B.T., Nielsen, M.L., Cox, J., Mann, M., and Choudhary, C. (2011). A Proteome-wide, Quantitative Survey of In Vivo Ubiquitylation Sites Reveals Widespread Regulatory Roles. *Mol Cell Proteomics* 10, M111.013284–M111.013284.
- Wright, W.D., and Heyer, W.-D. (2014). Rad54 functions as a heteroduplex DNA pump modulated by its DNA substrates and Rad51 during D loop formation. *Mol Cell* 53, 420–432.
- Yu, D.S., Sonoda, E., Takeda, S., Huang, C.L.H., Pellegrini, L., Blundell, T.L., and Venkitaraman, A.R. (2003). Dynamic control of Rad51 recombinase by self-association and interaction with BRCA2. *Mol Cell* 12, 1029–1041.
- Zelensky, A., Kanaar, R., and Wyman, C. (2014). Mediators of homologous DNA pairing. *Cold Spring Harb Perspect Biol* 6, a016451.

Zhao, W., Vaithiyalingam, S., San Filippo, J., Maranon, D.G., Jimenez-Sainz, J., Fontenay, G.V., Kwon, Y., Leung, S.G., Lu, L., Jensen, R.B., et al. (2015). Promotion of BRCA2-Dependent Homologous Recombination by DSS1 via RPA Targeting and DNA Mimicry. *Mol Cell* 59, 176–187.

Figures and Figure legends

Figure 1. HAP1 $\Delta RFWD3$ cells display increased persistence of RPA and RAD51 foci following MMC damage

- (A) Extracts prepared from HAP1 wild type (WT) and $\Delta RFWD3$ cells treated with 100 ng/ml MMC for 24 hr were immunoblotted with the indicated antibody.
- (B) Survival curves of HAP1 WT, $\Delta RFWD3$, or $\Delta RFWD3$ stably transduced with a lentivirus expressing WT or mutant *RFWD3*. Mean and SD of three independent experiments are shown.
- (C) Cells were treated with 20 ng/ml MMC for indicated durations up to 16 hr then released into fresh medium. Cells were fixed and stained with anti-RPA2 or RAD51. Each dot represents a single cell, and the mean and SD are indicated.
- (D) Representative images of RPA2 and RAD51 foci 16 hr after MMC treatment as analyzed in (C).
- (E) Levels of RPA2 and RAD51 in chromatin fraction. U2OS cells transfected with the indicated siRNAs were treated with 100 ng/ml MMC, fractionated, and blotted with the indicated antibodies. An asterisk indicates a non-specific band.
- (F) *In situ* PLA between endogenous RPA2 and RAD51 in cells depleted of *RFWD3* or *BRCA2*. U2OS cells transfected with indicated siRNAs were treated with 100 ng/ml MMC, harvested at 24 and 48 hr. Representative images are shown (below). Each dot represents a single cell, and the mean and SD are shown. See also Figure S1.

Figure 2. RPA is polyubiquitinated by RFWD3 following MMC treatment

- (A) U2OS cells simultaneously transfected with his-ubiquitin and indicated siRNA were treated with 100 ng/ml MMC for 24 hr and with the indicated doses of MG132 (μ M) for 1 hr before harvest. Cells were lysed under denaturing conditions and ubiquitinated proteins were collected by nickel resin and blotted using anti-RPA1 or RPA2 antibody. Signal intensities of the ubiquitinated RPA1 or RPA2 bands normalized to the highest value are shown below each blot.
- (B) U2OS cells transfected with myc-ubiquitin, his-RPA2, and FLAG-RFWD3 (and siRFWD3 in lane 9 and 10) were lysed in denaturing conditions. His-tagged RPA2 was purified and immunoblotted with the indicated antibodies. The ratios of

- ubiquitinated RPA2 bands (anti-myc) to the total RPA2 (anti-his) were calculated and normalized to the highest value.
- (C) 293T cells transfected with his-ubiquitin and siRFWD3 or FLAG-RFWD3 WT or a S46/63A mutant were processed as in (A), and blotted with indicated antibodies. The ratio of ubiquitinated RPA2 bands to total ubiquitinated proteins (anti-his) were quantified, normalized to the highest value, and are shown in the graph.
- (D) U2OS cells transfected with his-RPA2-WT or -KR mutants and FLAG-RFWD3 or siRFWD3 were processed as in (B) and blotted with indicated antibodies. Signal intensities of the ubiquitinated bands were normalized as in (B), and are shown with the mean and SD (n=3). The P value was calculated by Student's t-test.
- (E) Foci formation (upper panel) and chromatin retention (lower panel) of RPA2 WT or 5KR. Expression of FLAG-RPA2-WT or -5KR was induced by DOX in lentivirally transduced U2OS cells, and endogenous RPA2 was depleted by siRNA. Cells were treated with 100 ng/ml MMC for the indicated time (upper) or 24 hr (lower). Each dot represents a single cell, and the mean and SD are shown. P values were calculated by a one-way ANOVA post hoc test. See also Figure S2.

Figure 3. RFWD3 mediates RAD51 ubiquitination

- (A) Control and RFWD3-depleted 293T cells transfected with his-ubiquitin were treated with or without 100 ng/ml MMC for 24 hr, 10 μ M MG132 for 2 hr, 10 μ M PR619 (a deubiquitinase inhibitor) for 2 hr, as indicated, before harvest. Cells were lysed in denaturing conditions, diluted, and immunoprecipitated with anti-RAD51 and immunoblotted. The ratios of ubiquitinated (anti-his) to non-ubiquitinated RAD51 (anti-RAD51) normalized to the highest value are shown.
- (B) U2OS cells transfected with his-RAD51 WT or KR mutants were processed as in Figure 2D. The ratios of ubiquitinated (anti-myc) to non-ubiquitinated RAD51 (anti-his) normalized to the highest value are shown with the mean and SD (n=3). The P-value was calculated by Student's t-test.
- (C) Chromatin retention (upper panel) and foci formation (lower panel) of RAD51 WT or 5KR. Expression of siRAD51-resistant FLAG-RAD51-WT or -5KR was induced by DOX in lentivirally transduced U2OS cells, and endogenous RAD51 was depleted by siRAD51. Cells (100<) with more than 10 anti-FLAG foci were scored positive. The mean and SD are shown. P values were calculated using Student's

t-test. See also Figure S3.

Figure 4. Purified RFWD3 ubiquitinates RPA and RAD51 *in vitro*.

(A-C) Ubiquitination assay with RPA (A), RAD51 (B) or DMC1 (C). Ubiquitinated proteins were separated by SDS-PAGE, and detected by immunoblotting with indicated antibodies. Percentages of polyubiquitinated proteins (indicated, for example, as RPA1-(ub)_n) in the total amount of separated proteins were quantified, and are presented below the lanes in (A) or as bar graphs (mean and SD, n=3-5) at right in (B) and (C).

(D-E) DNA binding assay with ubiquitinated RPA (D) or RAD51 (E). A schematic diagram of the ssDNA binding assay is shown at left. RPA or RAD51 was ubiquitinated with E1, UBE2D1, RFWD3, and ubiquitin, and was incubated with ssDNA beads. Graphs represent the percentage of ubiquitinated RPA1 and RPA2 or RAD51 in the unbound and bound fractions. The mean and SD of three independent experiments are shown. See also Figure S4.

Figure 5. Physical interaction of RAD51 with the N-terminal domain of RFWD3.

(A) U2OS cells transfected with FLAG-RFWD3 were treated with or without 100 ng/ml MMC for 24 hr, and subjected to anti-RAD51 immunoprecipitation and immunoblotting.

(B) RAD51 bound to GST-tagged RFWD3 was co-pelleted with Glutathione Sepharose 4B beads, and the proteins were analyzed by SDS-PAGE with CBB staining. An asterisk indicates an impurity.

(C) Mammalian two-hybrid interaction assay between RAD51 and RFWD3 subregions. The C315A mutant was used to enhance expression levels by avoiding autoubiquitination. Luminescence signal levels were normalized to the value obtained by co-transfection of empty bait and prey vectors. FANCD2 and FANCI are included as a positive control. The domains of RFWD3 are colored according to the scheme in Figure S5B, and the expressed fragments are indicated by the amino acid number. The mean and SD values in a triplicate experiment are shown.

(D) U2OS cells co-transfected with his-RAD51 and either FLAG-RFWD3 WT or mutants were treated as in (A), and were subjected to pull-down with nickel resin. An asterisk indicates a non-specific band.

(E) Nuclear extracts were prepared from 293T cells treated as in (A), and were subjected to LQP or AAA peptide pull down. Immunoblot of bound material was

- probed by anti-RAD51, and the relative efficiency of the pull-down is shown as a graph. Sequences of LQP and AAA peptides are shown in Figure S5B.
- (D) 293T cells transfected with indicated plasmids or siRNA were treated with 100 ng/ml MMC for 24 hr and with 10 μ M MG132 for 1 hr before harvest. Cells were lysed under denaturing conditions and his-RAD51 was captured with Ni-resin and blotted with the indicated antibodies. The ratios of ubiquitinated (anti-myc) to non-ubiquitinated RAD51 (anti-his) bands normalized to the highest value are shown.
- (E) HAP1 Δ *RFWD3* cells transduced with *RFWD3* WT or LQP/AAA mutant were treated with 20 ng/ml MMC for 16 hr, and stained with anti-RAD51. Each dot represents a single cell; the mean and SD are shown. See also Figure S5.

Figure 6. RFWD3 promotes RPA2 and RAD51 foci turnover, degradation, and HR repair

- (A) HAP1 and HAP1 Δ *RFWD3* cells were treated with 20 ng/ml MMC for 16 hr and 10 μ M PR619 for 2 hr before harvest. Cell lysates were immunoprecipitated and blotted with indicated antibodies.
- (B) FRAP analysis. U2OS cells transiently transfected with the indicated siRNAs and expression constructs were exposed to 100 ng/ml MMC for 24 hr, and protein dynamics in MMC-induced foci were analyzed by FRAP. For RAD51-GFP foci FRAP, U2OS cells stably transduced with GFP-RAD51-WT or -5KR were transfected with the indicated siRNA and stimulated with DOX (1 ng/ml) and MMC (100 ng/ml) for 24 hr. The mean and SD are shown at each time point. See also Figure S6B for representative images of RPA-GFP or GFP-RAD51 foci.
- (C) HAP1 and HAP1 Δ *RFWD3* cells treated with 20 ng/ml MMC for 16 hr were chased up to 9 hr in the presence of 20 μ g/ml cycloheximide (CHX), and analyzed by immunoblotting. The ratios of RPA2-to-tubulin and RAD51-to-tubulin band intensities were normalized to those at the start of the chase. The experiments were repeated three times; the mean and SD are shown.
- (D) U2OS DR-GFP reporter cells were stably transduced with indicated RPA2 or RAD51 mutant. Expression was induced by addition of Dox, and endogenous RPA2

or RAD51 was depleted by siRNA (Figure S6D). The next day, the I-SceI expression vector was transfected, and 48 hr later the GFP-positive population was analyzed. The HR frequency was expressed as % GFP positive cells in the viable cell population. The experiments were repeated three times; the mean and SD are shown. RPA2 del, RPA2 deletion mutant lacking residues 244-254. See also Figure S6.

Figure 7. *RFWD3* and *BRCA2* act together for RPA2 turnover.

- (A) HAP1 WT or $\Delta RFWD3$ cells expressing GFP-RAD54 were treated with 20 ng/ml MMC for 16 hr, and immunostained with anti-GFP and Alexa Fluor 488 conjugated antibody. Each dot represents the number of nuclear foci in a single cell; the mean and SD are shown.
- (B) Cells in (A) were fractionated and analyzed by immunoblotting. WCL, whole cell lysates.
- (C) U2OS cells transfected with siRNAs were treated with 100 ng/ml MMC for indicated times and analyzed by immunoblotting after cell fractionation.
- (D) U2OS cells expressing Dox-inducible GFP-RAD51-WT or -5KR mutant were transfected with indicated siRNAs, stimulated with Dox and MMC (100 ng/ml) for 24 hr, and analyzed by immunoblotting with indicated antibodies.
- (E) U2OS cells transiently transfected with RPA2-GFP and indicated siRNAs were treated with 100 ng/ml MMC for 24 hr, and RPA2-GFP turnover was examined by FRAP analysis as in Figure 6B. See also Figure S7.

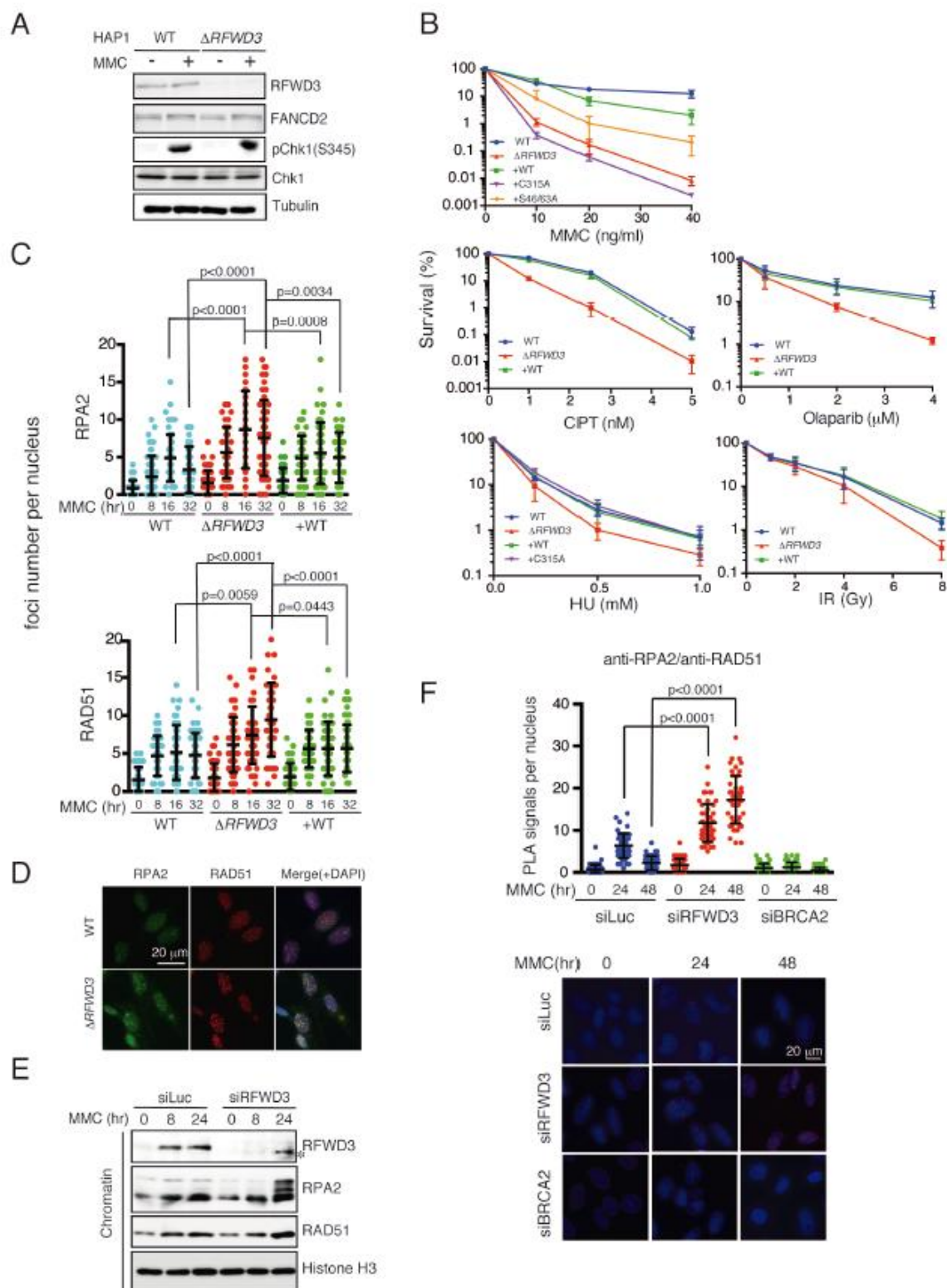
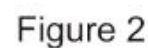


Figure 1



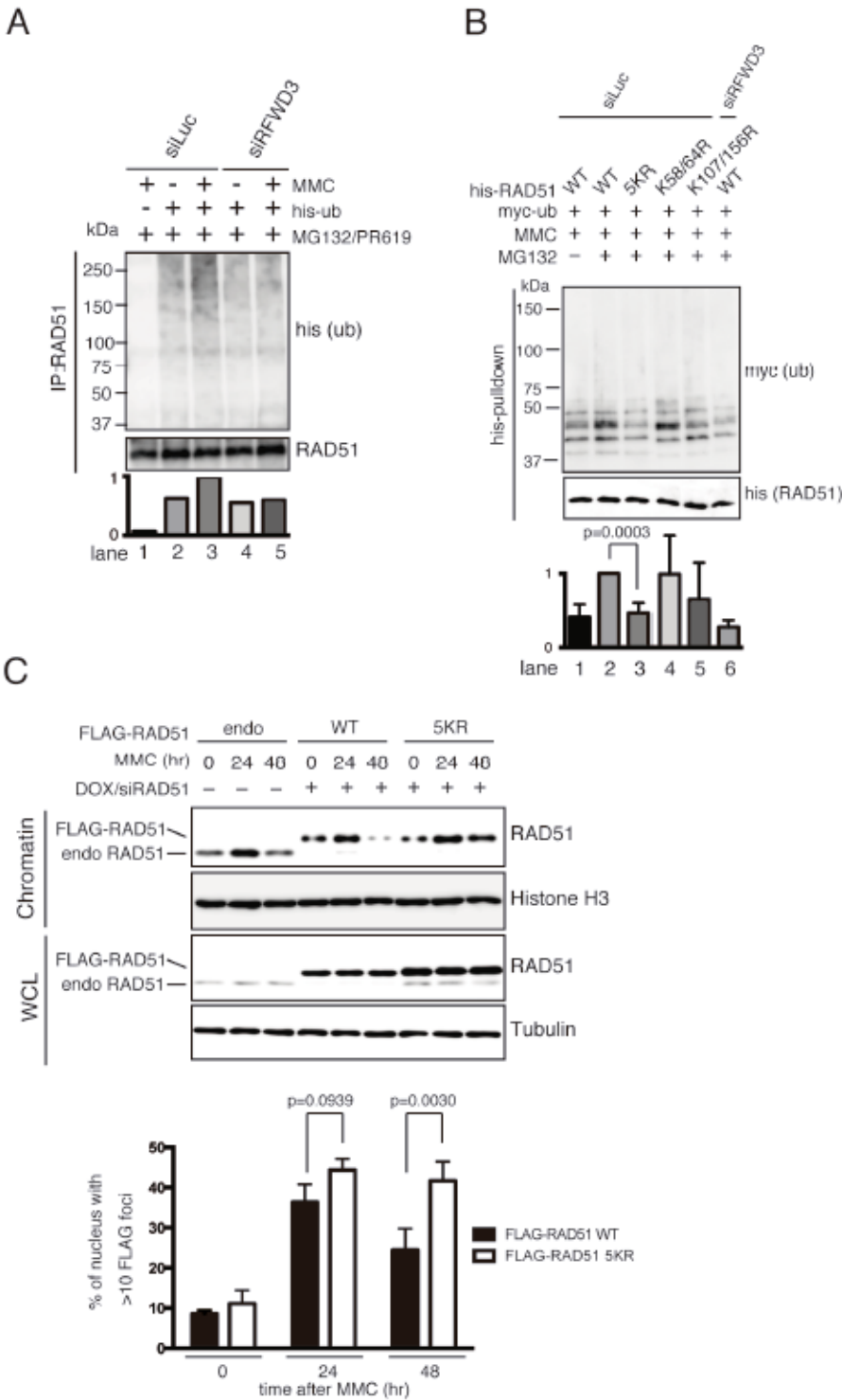


Figure 3

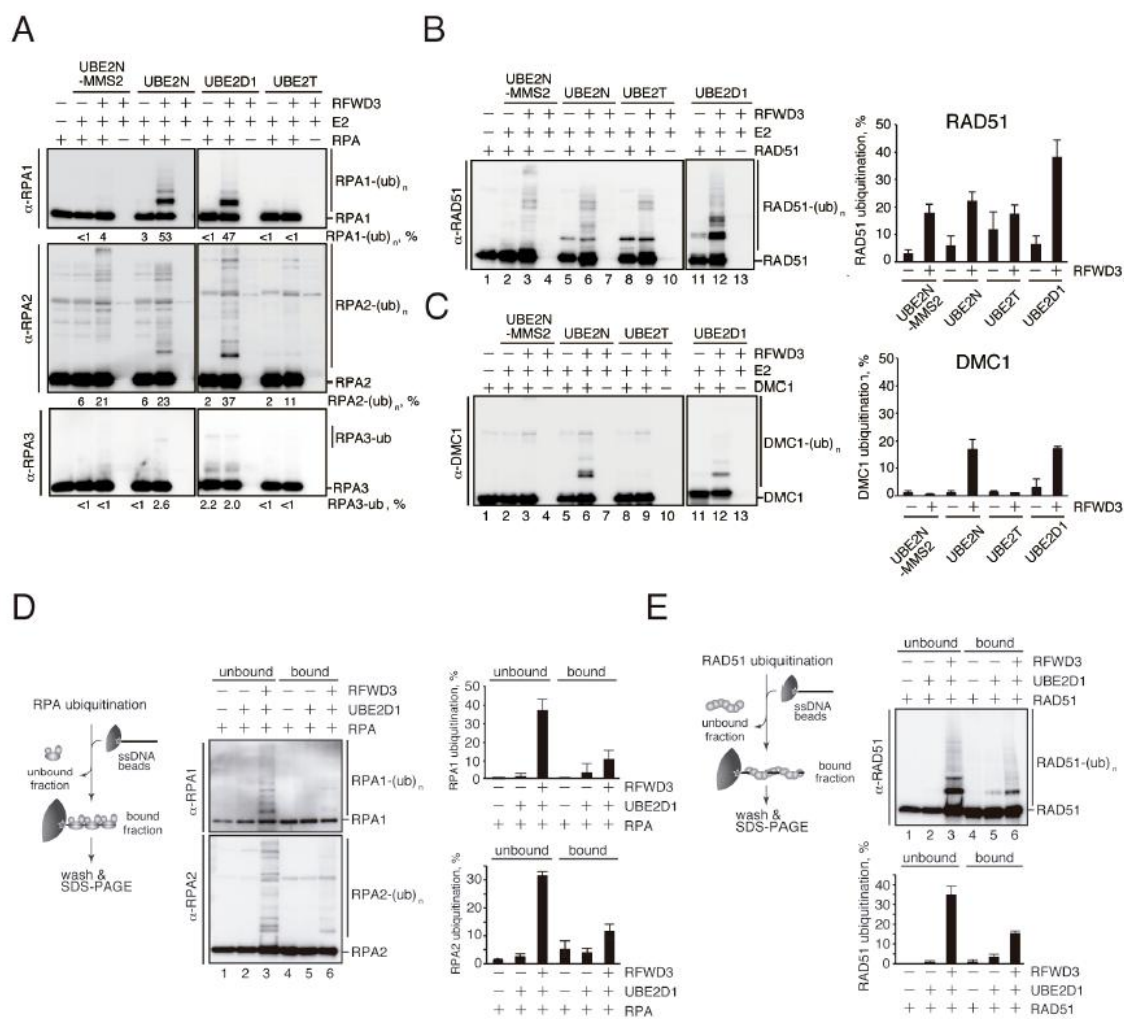


Figure 4

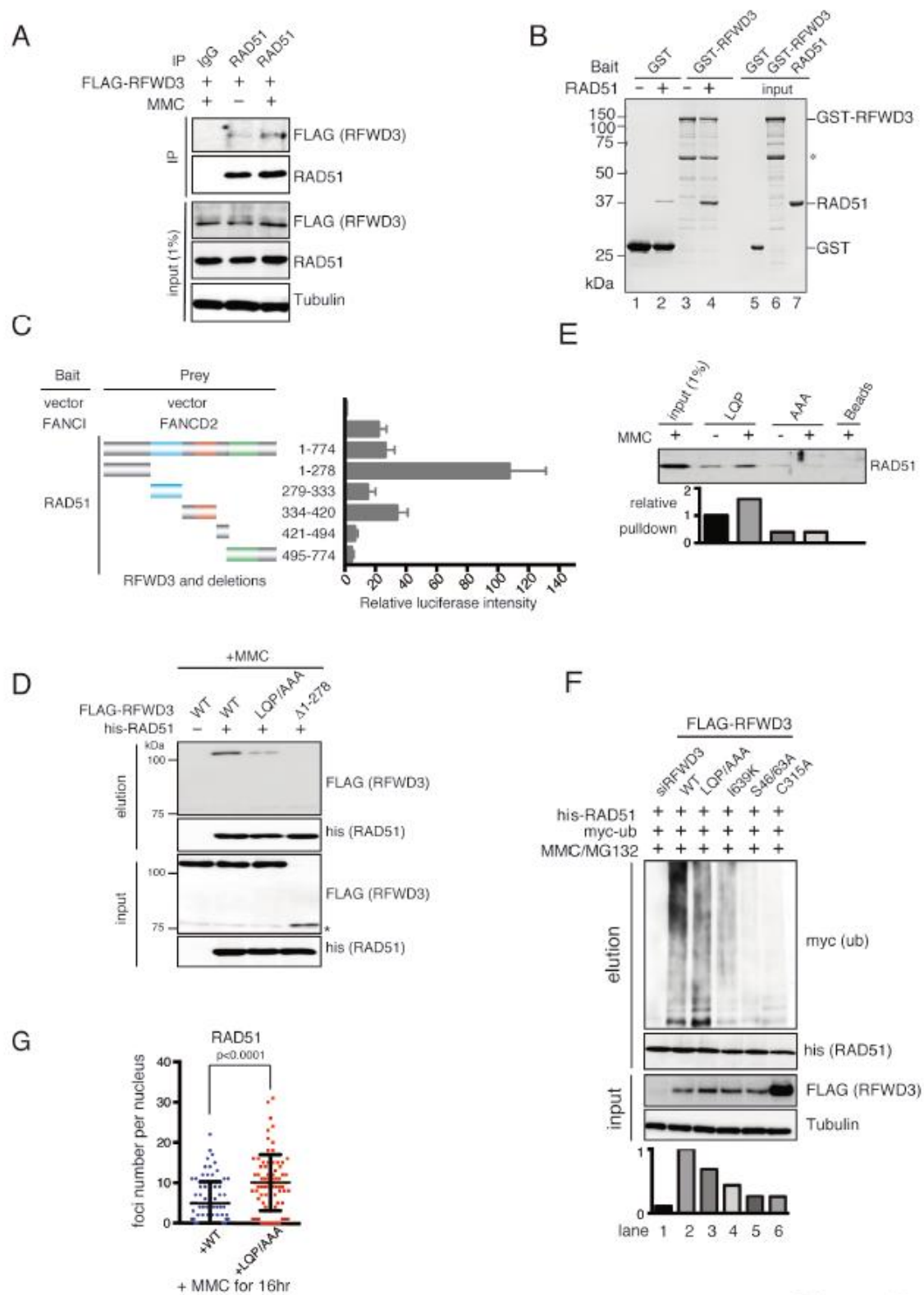
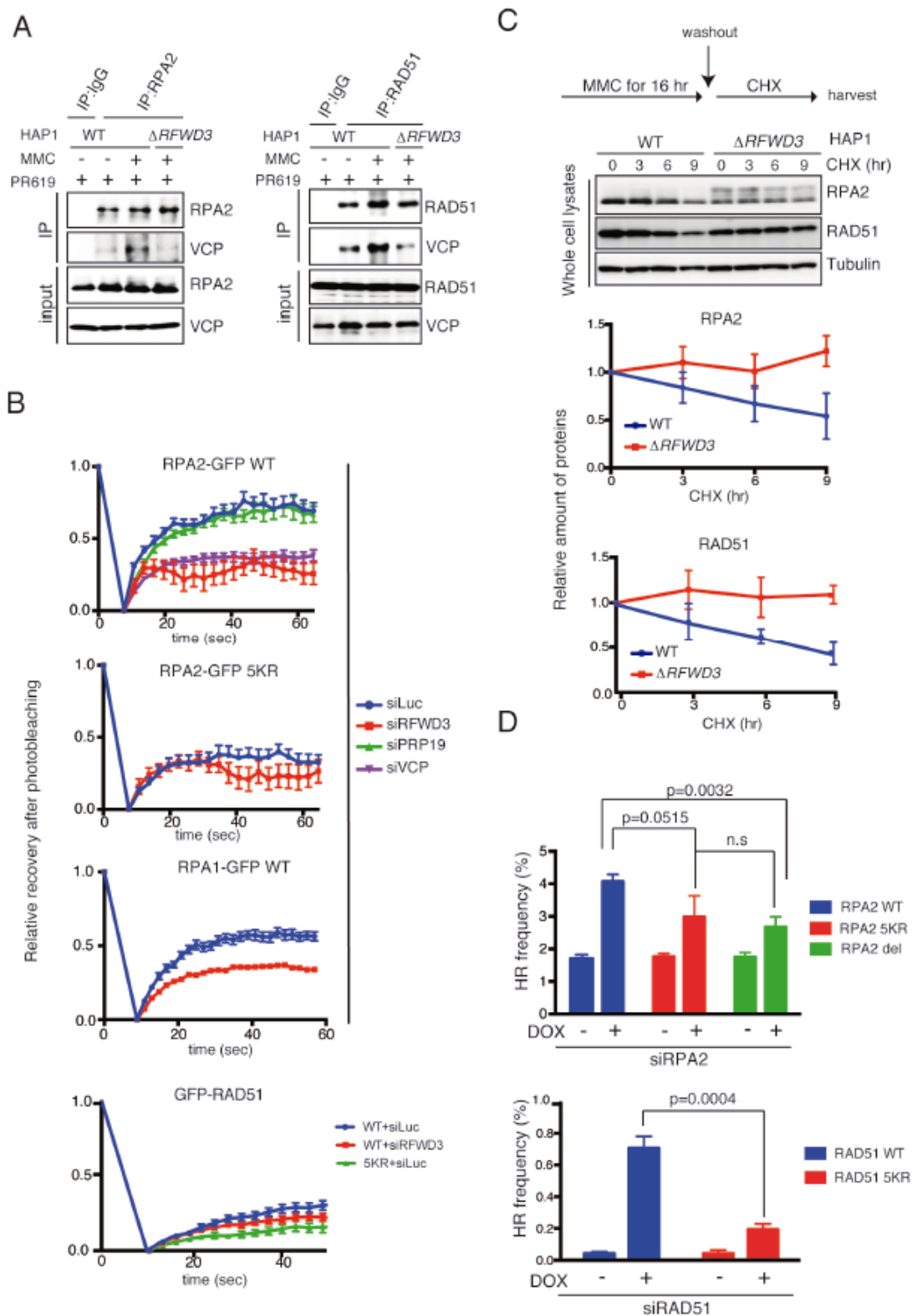


Figure 5



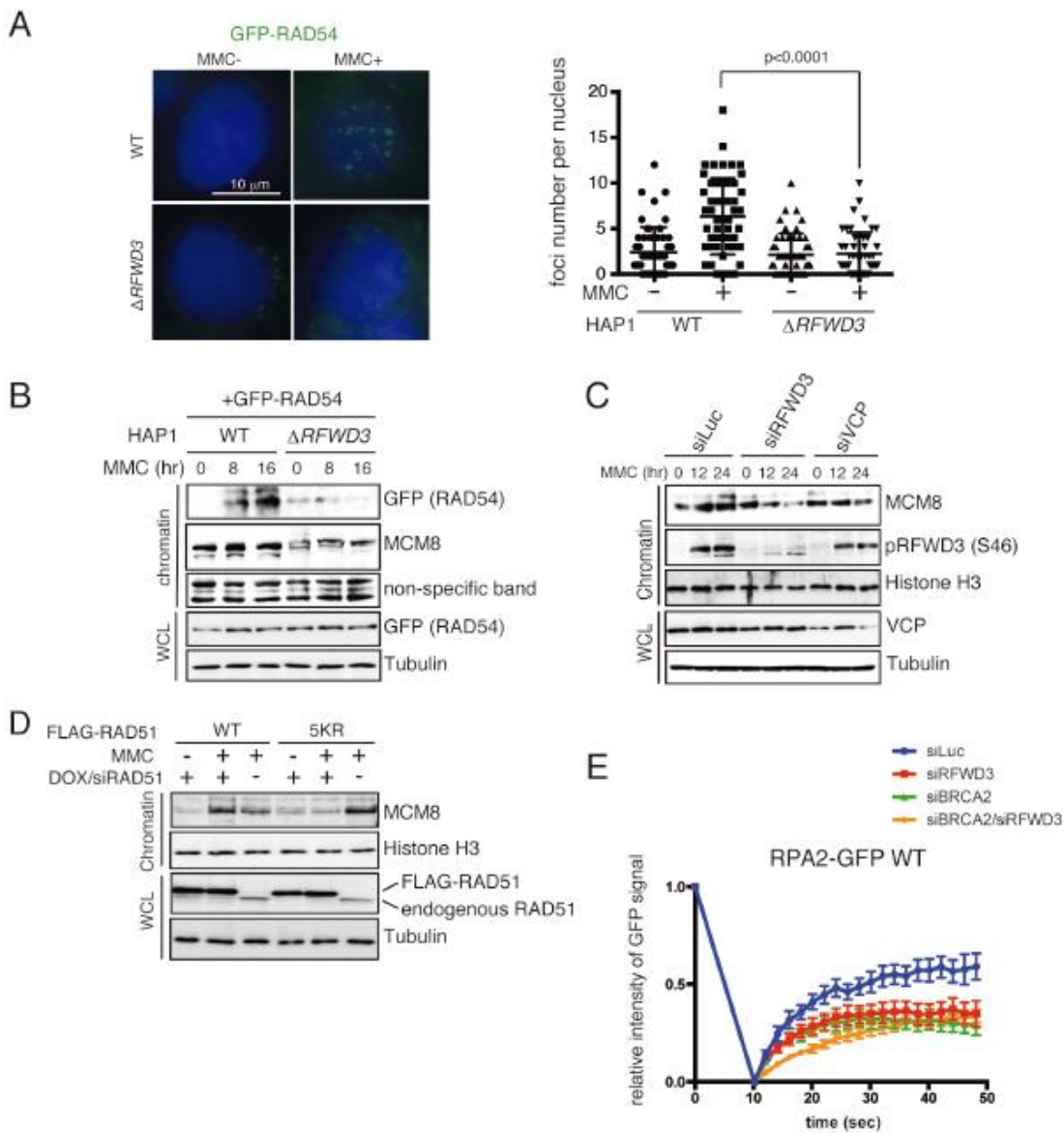


Figure 7

Supplemental Figures

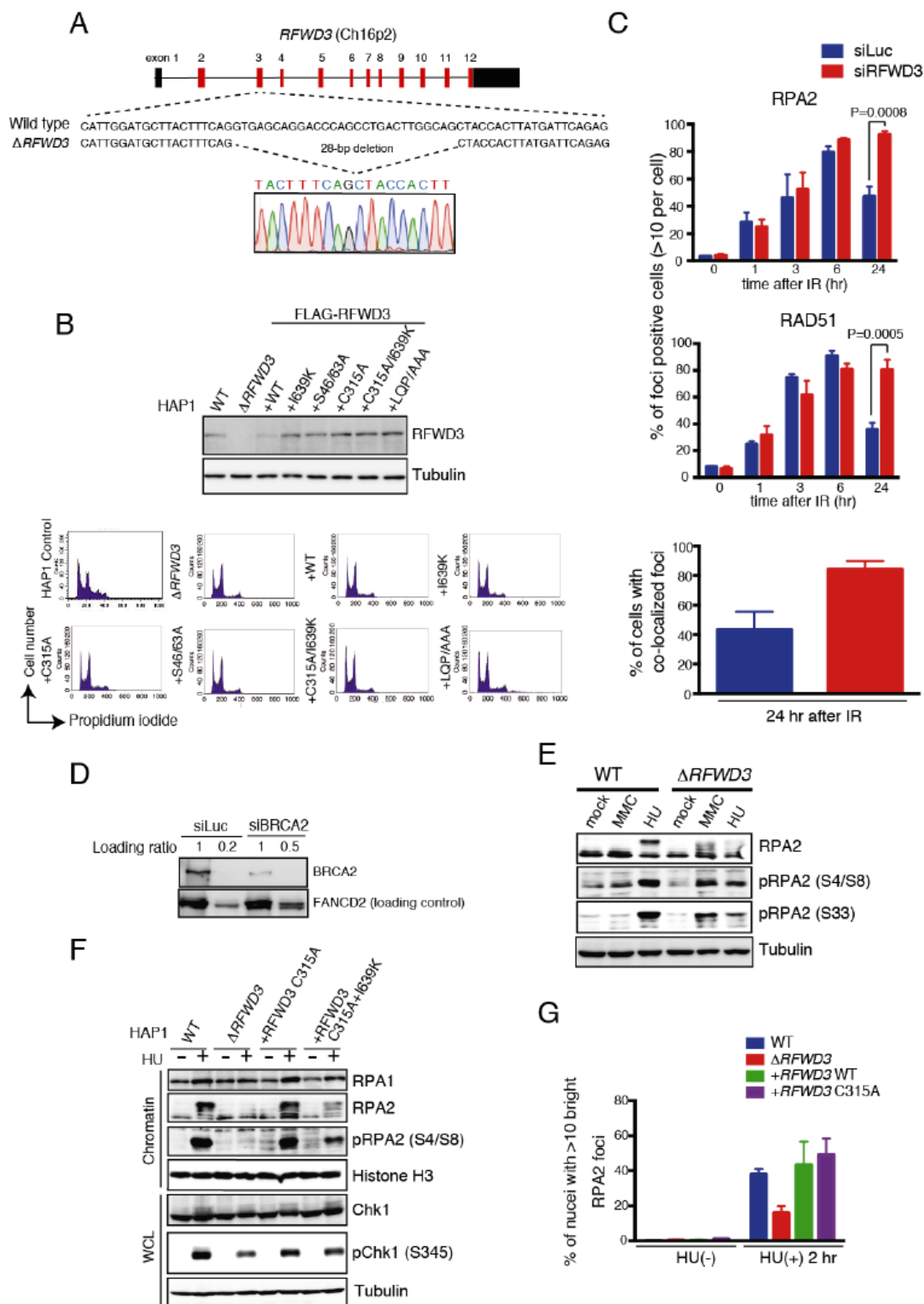


Figure S1

Figure S1. Related to Figure 1. Characterization of HAP1 $\Delta RFW3$ cells in HR repair and replication stress signaling.

- (A) Schematic illustration of the *RFWD3* knockout using the CRISPR/Cas9 system in HAP1 cells. A 28-bp deletion was introduced in exon3, resulting in a frameshift mutation (p.Q138fs46X). The deletion was validated by Sanger sequencing. The black boxes indicate untranslated regions.
- (B) Expression levels of stably transduced *RFWD3* in $\Delta RFW3$ cells were analyzed by immunoblotting (upper). HAP1 cells and derivatives fixed and stained with propidium iodide were analyzed with a FACSCalibur flow cytometer (lower).
- (C) U2OS cells were subjected to 10 Gy of gamma irradiation and permitted to recover for the indicated times before fixation and staining with anti-RAD51 or RPA2 antibodies. Cells with co-localized foci were defined as those in which RAD51 foci were positive (>10 foci per nucleus) and more than half of the RAD51 foci were co-localized with RPA2 foci. The mean and SD of three independent experiments are shown.
- (D) U2OS cells were treated with siLuc or siBRCA2, and analyzed by immunoblotting with different amounts of lysates loaded per lane.
- (E) HAP1 $\Delta RFW3$ cells were treated with 2 mM HU for 2 hr or 20 ng/ml MMC for 16 hr, and whole cell lysates were analyzed by immunoblotting.
- (F) HAP1 WT, $\Delta RFW3$, or $\Delta RFW3$ cells complemented with the indicated *RFWD3* mutants were treated with 2 mM HU for 2 hr, fractionated, and analyzed by immunoblotting. WCL, whole cell lysates.
- (G) Percentage of cells positive for RPA2 foci (>10 bright foci) in HAP1 cells (WT, $\Delta RFW3$, or $\Delta RFW3$ complemented with *RFWD3* WT or the *RFWD3* RING domain (C315A) mutant), comparing untreated cells to cells treated with 2 mM HU for 2 hr. The mean and SD of three independent experiments are shown.

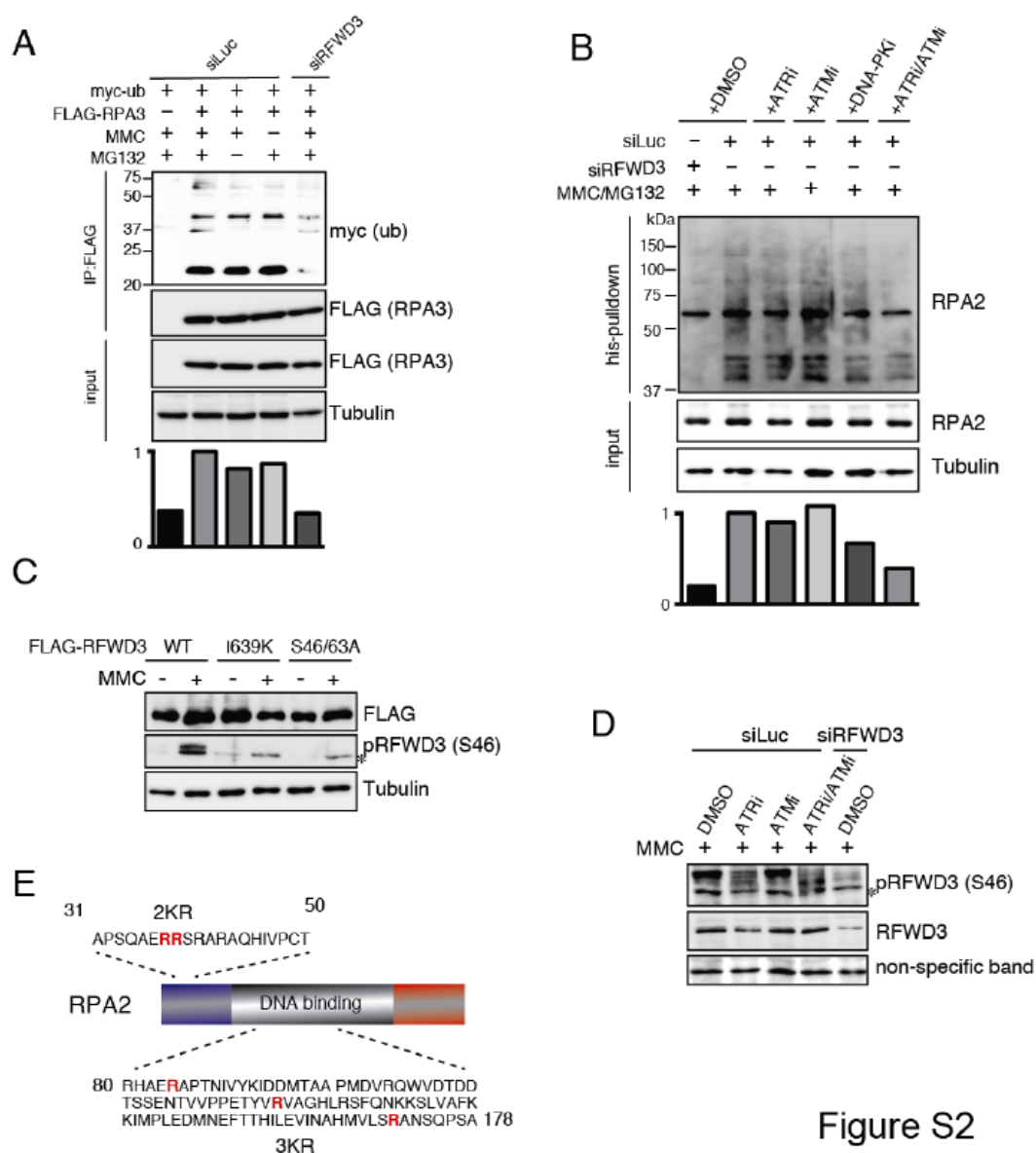


Figure S2

Figure S2. Related to Figure 2. RPA3 ubiquitination and RPA2 phosphorylation in response to

MMC damage.

- (A) U2OS cells transfected with myc-ubiquitin and FLAG-RPA3 expression vectors were treated with or without 100 ng/ml MMC for 24 hr and 10 μ M MG132 for 1 hr until harvest. Cell lysates were subjected to anti-FLAG IP and detected by immunoblotting. The ratio of ubiquitinated (anti-myc) to non-ubiquitinated RPA3 (anti-FLAG) was quantified, normalized to the highest value, and is shown beneath the immunoblots.
- (B) U2OS cells transfected with his-ubiquitin were treated as in (A). 10 μ M VE-821 (ATR inhibitor), 10 μ M KU-55933 (ATM inhibitor), or 5 μ M NU-7026 (DNA-PK inhibitor) were added simultaneously with MMC for 24 hr. Cells were lysed in denaturing conditions, and Nickel resin-bound proteins were analyzed by immunoblotting. The ratio of ubiquitinated RPA2 to non-ubiquitinated RPA2 in cell lysates was normalized to the highest value and is shown beneath the immunoblots.
- (C) U2OS cells were transfected with FLAG-RFWD3 WT or indicated mutants and treated with 100 ng/ml MMC for 24hr, and analyzed by immunoblotting. An asterisk indicates a non-specific band.
- (D) U2OS cells treated with the indicated siRNAs were subjected to 100 ng/ml MMC and the indicated inhibitors (10 mM) for 24 hr, and analyzed by immunoblotting.
- (E) Schematic illustration of RPA2 KR mutants (2KR, 3KR, and 5KR). Lysine residues in red are candidate ubiquitination sites as previously suggested, and were replaced by Arginine.

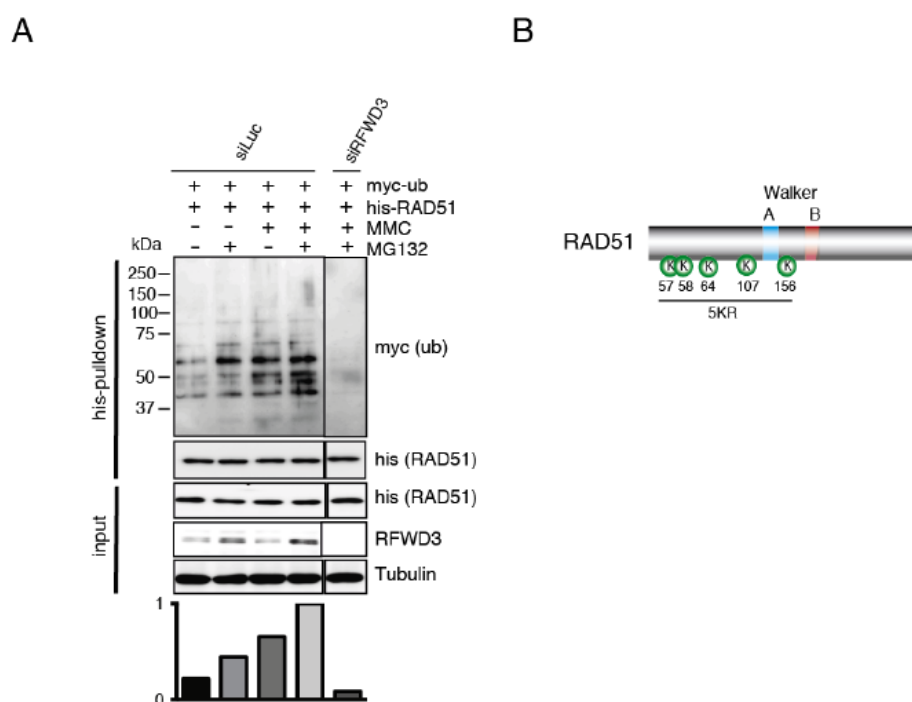


Figure S3

Figure S3. Related to Figure 3. Analysis of RFWD3-dependent polyubiquitination of RAD51.

- (A) U2OS cells transfected with indicated siRNA, his-RAD51, FLAG-RFWD3, and myc-ubiquitin WT or KR mutants were treated with 100 ng/ml MMC for 24 hr and 10 μ M MG132 for 1 hr until harvest. Cells were lysed in denaturing conditions and Nickel resin-bound materials were analyzed by immunoblotting. The ratio of ubiquitinated (anti-myc) to total RAD51 (anti-his) was normalized to the highest value and is shown beneath the immunoblots.
- (B) Schematic illustration of RAD51-KR mutation sites (5KR). Lysine residues in red are candidate ubiquitination sites as suggested by previous proteomics data, and were replaced with Arginine. K58/64R or K107/156R mutations were also generated.

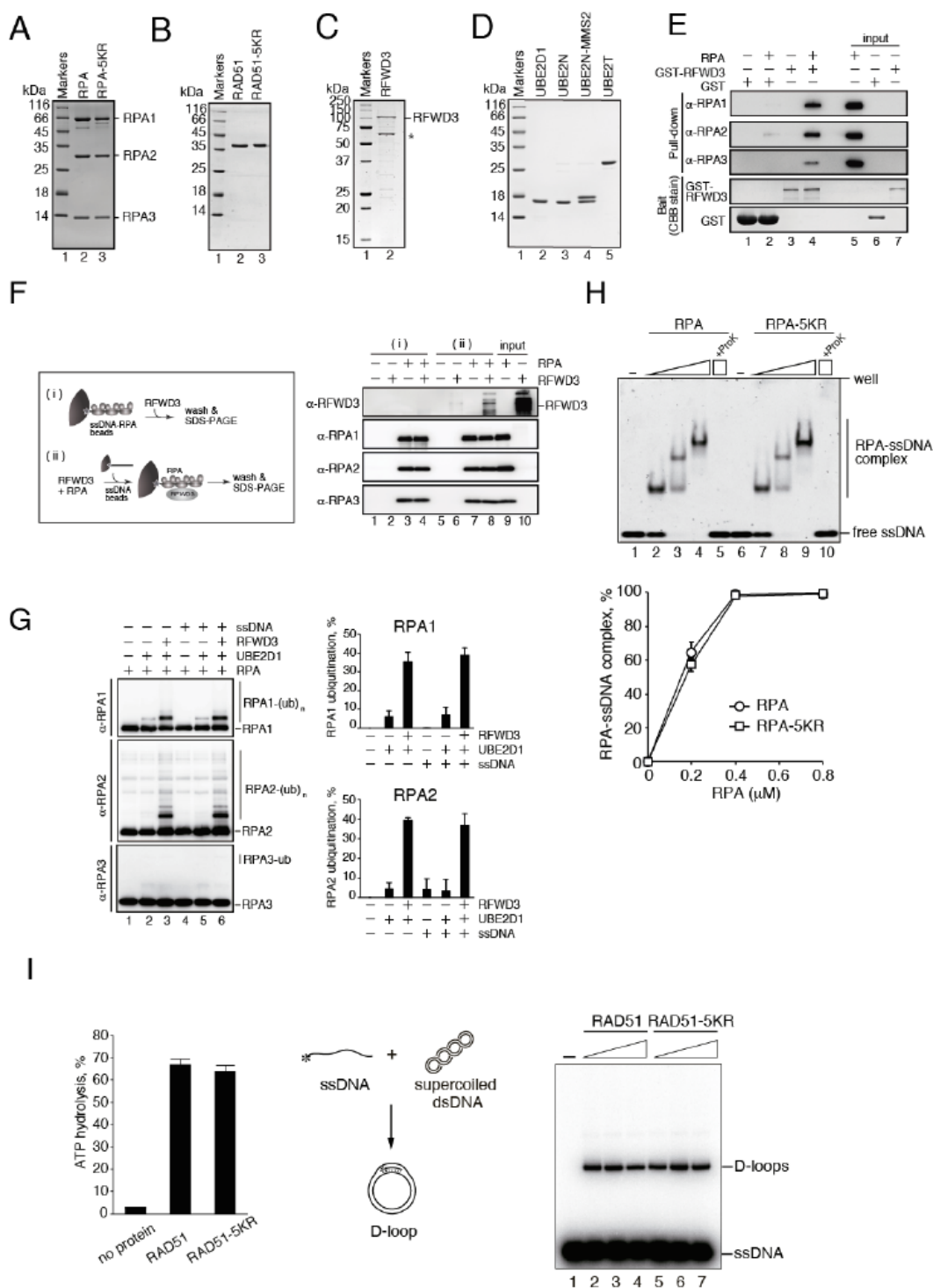


Figure S4

Figure S4. Related to Figure 4. Purification of recombinant proteins and pull-down or functional assays.

- (A) Purified human RPA, (B) RAD51 and the RAD51-5KR mutant, (C) RFWD3, and (D) UBE2D1, UBE2N, UBE2N-MMS2 complex, and UBE2T were analyzed by SDS-PAGE with Coomassie Brilliant Blue staining. Asterisk indicates an impurity.
- (E) Pull-down assay of RPA with GST-tagged RFWD3. RPA bound to GST or GST-tagged RFWD3 was co-pelleted with Glutathione Sepharose 4B beads, and the proteins were detected by immunoblotting.
- (F) Pull-down assay of RFWD3 with RPA-coated ssDNA beads (i) or RFWD3-RPA with ssDNA beads (ii). A schematic is shown at left. Pulled down proteins were detected by immunoblotting.
- (G) *In vitro* ubiquitination assay of the RPA complex with or without the addition of ssDNA. The ubiquitinated proteins were detected by immunoblotting. Percentages of polyubiquitinated species (indicated, for example, as RPA1-(ub)_n) in the total amount of RPA1 or RPA2 were determined by densitometric measurements and are presented as bar graphs (mean and SD, n=3) at right.
- (H) ssDNA binding of the RPA complex with or without the RPA2-5KR mutant was examined using the electrophoretic mobility shift assay. The percentage of shifted bands relative to the total ssDNA signal is shown in the graph beneath the blot (mean and SD, n=3 experiments).
- (I) The ATP hydrolyzing activities of RAD51 and RAD51-5KR in the presence of ssDNA were analyzed by thin layer chromatography. The average values of three independent experiments are shown, with standard deviations (left). A schematic representation of the D-loop formation assay (middle). The asterisk indicates the ³²P-labeled 5'-end of the ssDNA. A representative D-loop formation assay result (right). The protein concentrations were 0.2 μM (lanes 2 and 5), 0.4 μM (lanes 3 and 6), and 0.6 μM (lanes 4 and 7). Lane 1 indicates a negative control experiment without proteins.

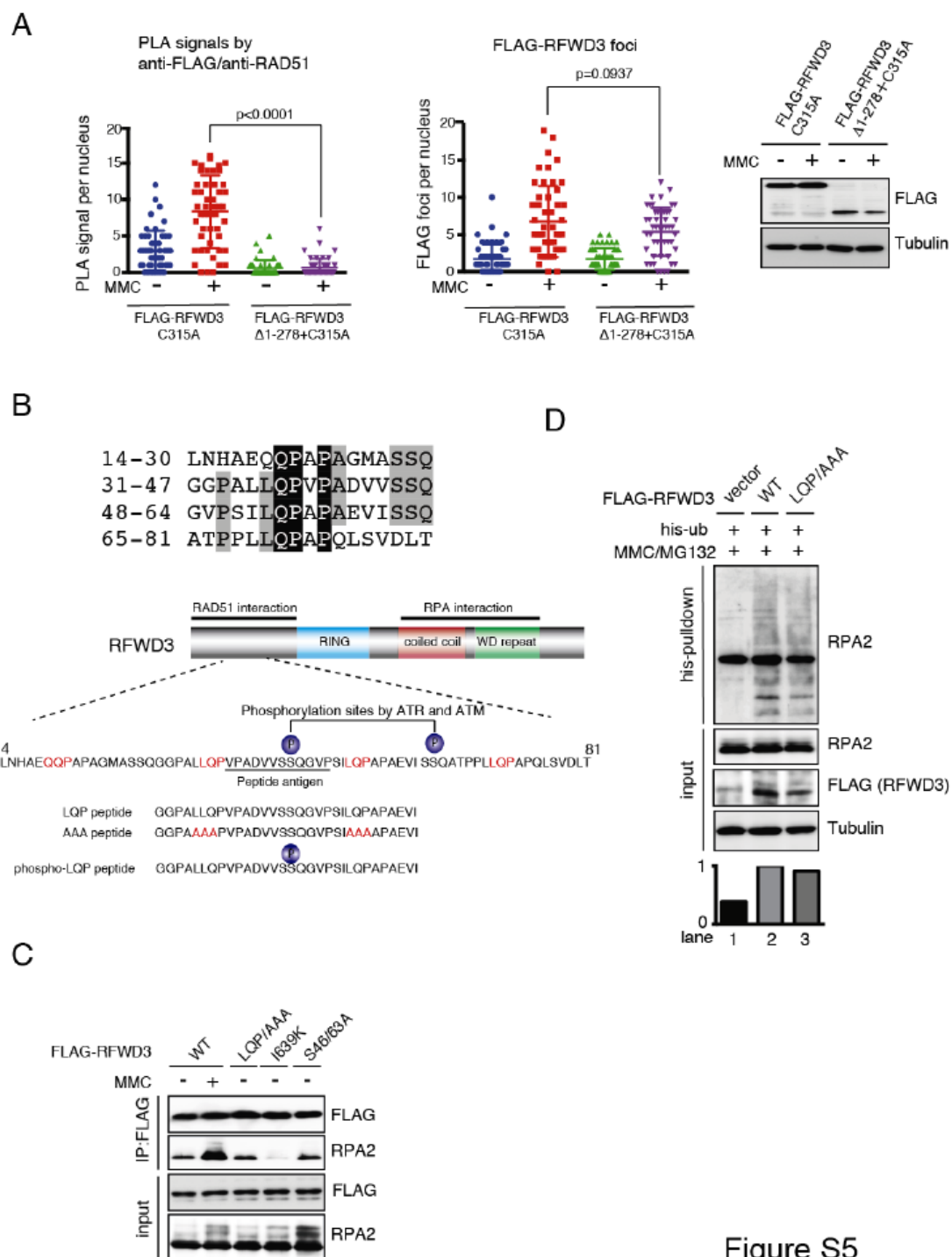


Figure S5

Figure S5. Related to Figure 5. Role of the N-terminal RFWD3 domain and the LQP motif in ubiquitination of RAD51 and RPA.

- (A) PLA signals between RAD51 and FLAG-RFWD3 WT or N-terminal deletion Δ 1-278 (left). Both RFWD3 constructs carried a RING domain mutation C315A to enhance expression levels. U2OS cells transfected with FLAG-RFWD3 C315A or Δ 1-278 + C315A were treated with 100 ng/ml MMC for 24 hr, and analyzed by PLA. Each dot represents the number of PLA signals in a single cell; the mean and SD are shown. Decreased expression levels and foci formation of RFWD3 Δ 1-278 compared to WT are shown at right. U2OS cells transfected with FLAG-RFWD3 C315A or Δ 1-278 + C315A were treated with 100 ng/ml MMC for 24 hr, and foci were analyzed using anti-FLAG antibody (left and middle), and expression was verified by immunoblotting (right).
- (B) Alignment of LQP-SSQ repeats (residue 14 to 81) and a schematic illustration of the RFWD3 domains. A section of the RFWD3 N-terminal amino acid sequence, the synthesized peptides used in Figure 5E, and the phosphorylation sites S46 and S63 are also indicated. The peptide sequence used for raising the anti-phospho-S46 antibody is underlined. The LQP motifs mutated to triple Alanines in RFWD3 LQP/AAA are indicated in red.
- (C) Co-immunoprecipitation of FLAG-RFWD3 mutants (LQP/AAA, I619K, and S46/63A) and RPA2. Lysates from 293T cells transfected with the indicated plasmid constructs were subjected to immunoprecipitation with anti-FLAG antibody, and analyzed by immunoblotting.
- (D) Comparable ubiquitination levels of RPA2 by RFWD3 WT or LQP/AAA mutant. 293T cells transfected with FLAG-RFWD3 WT or the LQP/AAA mutant, or siRNA with his-ubiquitin were treated with 100 ng/ml MMC for 24 hr and with 10 μ M MG132 for 1 hr before the harvest. Cells were lysed under denaturing conditions and ubiquitinated proteins were blotted using anti-RPA2 antibody.

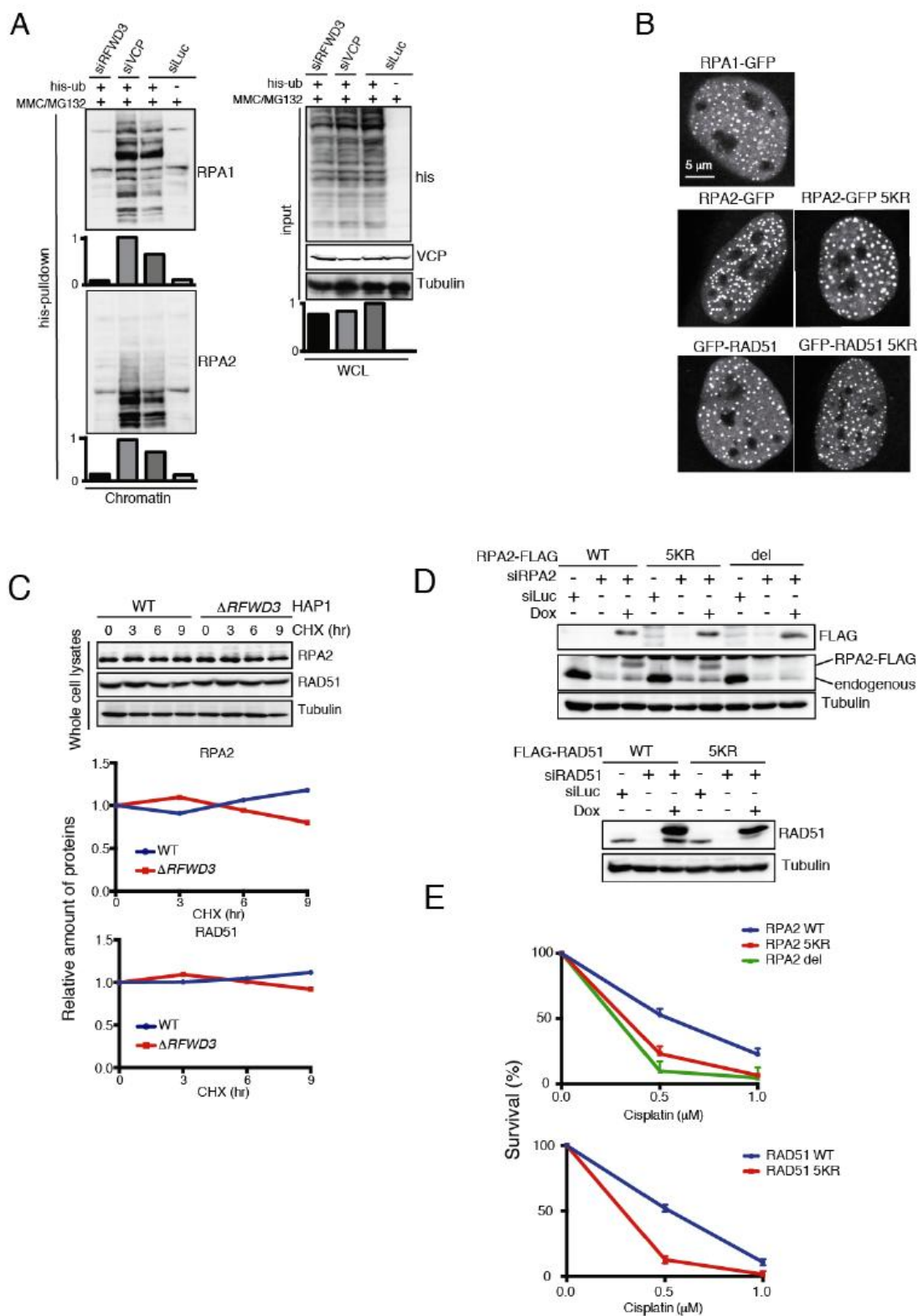


Figure S6

Figure S6. Related to Figure 6. Characterization of cells expressing ubiquitination-deficient RPA2 or RAD51 mutant proteins.

- (A) VCP mediates removal of ubiquitinated RPA2 from the chromatin fraction. 293T cells transfected with his-ubiquitin and indicated siRNAs were harvested after exposure to 100 ng/ml MMC for 24 hr, biochemically fractionated, and analyzed by immunoblotting. WCL, whole cell lysates. Ubiquitinated proteins were quantified, normalized to the highest value, and data are shown below each blot.
- (B) MMC-induced foci formation of RPA1-GFP, RPA2-GFP (WT and 5KR), or GFP-RAD51 (WT and 5KR).
- (C) Stability of RPA and RAD51 proteins in cells without MMC damage. HAP1 WT and *ΔRFWD3* cells were chased in medium containing 20 µg/ml cycloheximide for the indicated times, and analyzed by immunoblotting. The band intensity was normalized to those at the start of the chase. The experiments were repeated three times and the mean and SD are shown. See also Figure 6C.
- (D) Dox-induced expression of FLAG-RPA2 (WT, 5KR, or a deletion mutant lacking residue 244-254) or FLAG-RAD51 (WT or 5KR) in U2OS-DR-GFP cells depleted of endogenous RPA2 or RAD51 proteins by siRPA2 (targeting the 3'UTR) or siRAD51. FLAG-RAD51 was rendered insensitive to siRAD51 by synonymous mutations. Note that the RPA2 deletion (del) mutant lacking residues 244-254 was recognized by anti-FLAG but not by the anti-RPA2 that we used.
- (E) Cisplatin sensitivity of U2OS cells in which endogenous RPA2 or RAD51 were replaced with FLAG-tagged RPA2 and RAD51 with the indicated mutations. Cells were exposed to cisplatin for 24 hr at the indicated concentrations. The mean and SD of three independent experiments are shown.

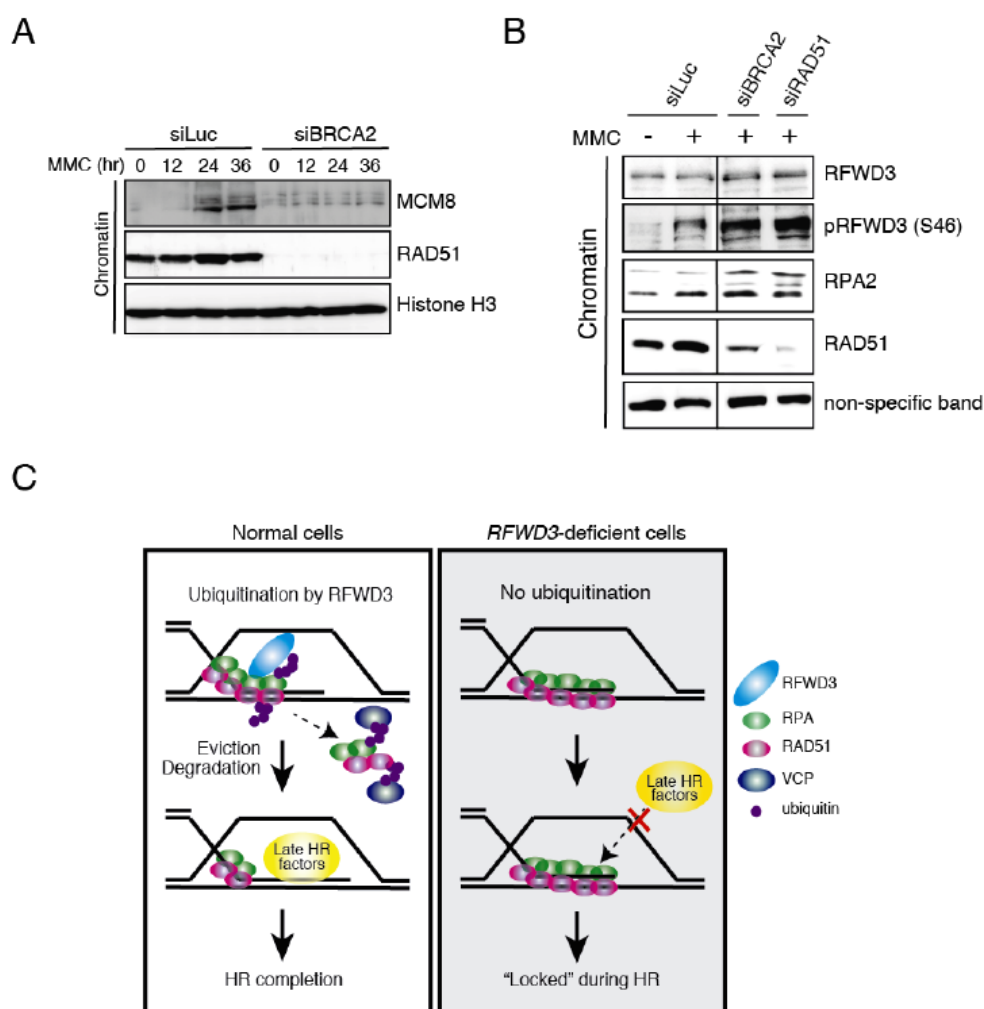


Figure S7

Figure S7. Related to Figure 7. BRCA2 depletion prevents chromatin loading of MCM8 but not RFWD3 or RFWD3 phosphorylation on S46.

- (A) BRCA2 depletion inhibits MCM8 chromatin loading upon MMC damage. U2OS cells transfected with the indicated siRNAs were harvested after exposure to 100 ng/ml MMC for the indicated times, biochemically fractionated, and analyzed by immunoblotting.
- (B) BRCA2 is not required for RFWD3 S46 phosphorylation. U2OS cells transfected with the indicated siRNAs were treated with 100 ng/ml MMC for 24 hr, and analyzed by immunoblotting after biochemical fractionation.
- (C) Model for RFWD3 mediated RPA and RAD51 ubiquitination that promotes timely removal of the proteins from recombination intermediates and degradation of RPA and RAD51 to allow HR progression to subsequent steps following MMC damage. We propose that the persistent presence of RPA and RAD51 may hinder chromatin recruitment of late-phase HR factors such as RAD54 or MCM8, resulting in a "locked" HR reaction.

Table S1. siRNAs used in this study

siRNA	sequence (5' to 3')
RFWD3#1	GGACCUACUUGCAAACUAUtt
RFWD3#2	AACUCCUGCACAUGACUGCtt
RPA2	AACAGAUUGUGAAACUAGGtt
RAD51	AGCUUCUCCAAUUUCUUCtt
VCP	ACAACUGUGAUACAAUGCGtt
BRCA2	UAAGGAACGUCAAGAGAUAt
PRP19	UGUAAGCAGUGAUCUAGUUUCAUUA
Luciferase	UCGAAGUAUUCGCGUACGtt

Table S2. Antibodies used in this study

Antigen	Host	Catalog number	Manufacturer
RFWD3	rabbit	ab138030	Abcam
pRFWD3 (S46)	rabbit	-	Custom-made
RPA1	rabbit	A300-241A	Bethyl
RPA2	rabbit	A300-244A	Bethyl
pRPA2 (S4/S8)	rabbit	A300-245A	Bethyl
pRPA2 (S33)	rabbit	A300-246A	Bethyl
RPA3	rabbit	HPA005708	Sigma
RAD51	rabbit	-	Kurumizaka lab
Chk1	mouse	sc-8408 (G-4)	Santa Cruz
pChk1 (S345)	rabbit	133D3	Cell Signaling
DDDDK tag (for cytochemistry)	mouse	M185-3L	MBL
DDDDK tag (for cytochemistry)	rabbit	PM020	MBL
FLAG (for immunoblotting)	mouse	M2	Sigma
GFP	mouse	M048-3 (1E4)	MBL
Tubulin	mouse	T5168	Sigma
Histone3	mouse	61647 (1C8B2)	Active Motif
6 x His	mouse	ab18184 (HIS.H8)	Abcam
c-Myc	mouse	sc-40 (9E10)	Santa Cruz
PCNA	mouse	sc-56 (PC10)	Santa Cruz
MCM8	goat	NB100-325	Novus
VCP	rabbit	GTX101089	GeneTex
FANCD2	rabbit	NB100-502	Novus

Table S3. Chemical inhibitors used in this study

Chemical inhibitor	Manufacturer	Catalog number	Function
MG 132	Millipore	474787	Proteasome inhibitor
PR 619	Abcam	ab144641	Deubiquitinase inhibitor
NU-7026	Sigma-Aldrich	N1537-5MG	DNA-PK inhibitor
KU-55933	Millipore	118500-10MG	ATM inhibitor
VE-821	Toronto Research Chemicals	V756700	ATR inhibitor
olaparib	Selleck Chemicals	S1060	PARP inhibitor

Supplemental Experimental Procedures

Plasmids

Human *RFWD3* (synthesized), *RAD54* (a kind gift from Dr Kiyoshi Miyagawa, University of Tokyo), and *RAD51* cDNAs were amplified and subcloned into pENTR entry vector (Invitrogen), and transferred to the expression vectors or lentiviral constructs by LR Clonase II (Invitrogen). Mutations in plasmids were generated by high-fidelity PCR using KOD-plus-neo or KOD-FX polymerases (TOYOBO) and an In-Fusion HD Cloning kit (Takara); all mutations were confirmed by Sanger sequencing. Human *RPA1* cDNA derived from U2OS, human *RPA2* cDNA in Flag-RPA2 (a kind gift from Dr Aziz Sancar, University of North Carolina, Addgene #22893) and synthesized *Ubiquitin* cDNA were amplified and subcloned into pcDNA4/HisMax C (Invitrogen) using an In-Fusion HD kit. Myc-ubiquitin constructs were previously described (Nakada et al., 2010). A long linker in the pcDNA4/HisMax C Ubiquitin was removed by PCR-based mutagenesis. Ubiquitin KR mutants were generated by PCR following a standard site-directed mutagenesis protocol using KOD-plus-neo followed by DpnI digestion and transformation into competent cells.

siRNA and plasmid transfections

siRNA duplexes were purchased from Invitrogen and are listed in the supplemental table. Transfection was carried out using Lipofectamine RNAiMAX (Invitrogen) according to the manufacturer's instructions. For plasmid transfections or co-transfection of plasmids and siRNA, Lipofectamine 3000 (Invitrogen) was used. In all siRFWD3 transfections, siRFWD3#2 was used unless stated otherwise.

Ploidy analysis

Cells at exponential growth were fixed with 70% ethanol, stained with PBS containing propidium iodide (5 µg/ml) and analyzed using a FACSCalibur flow cytometer (BD).

Colony survival assay

To measure cell survival in the presence of MMC, Cisplatin, Olaparib, CPT, or HU, an appropriate number of HAP1 cells were treated in triplicate with the indicated concentrations of the DNA damaging agents for 24 hr, except for HU (8 hr) (because of extreme toxicity with a 24 hr treatment). Cells were permitted to recover for 24 hr after treatment, and plated with serial dilutions. After 7-10 days incubation, cells were fixed with 100% ethanol, stained with 0.006% crystal violet solution (0.006% crystal violet, 25% methanol), and colonies were counted.

Immunohistochemistry and *in situ* PLA assay

Cells grown on cover glass were washed with PBS twice and fixed with PBS containing 3% paraformaldehyde, 2% sucrose, 0.5% Triton-X-100 on ice for 30 min, and then permeabilized with 0.5% Triton X-100/PBS for 5 min. After blocking with 2% BSA/PBS, staining with antibodies diluted in 2% BSA/PBS was performed for 1 hr at RT. The secondary antibodies used were Alexa Fluor 488-conjugated anti-mouse IgG or Alexa Fluor 594-conjugated anti-rabbit IgG (Molecular Probes). The experiments were repeated three times, and >50 cells were analyzed in each experiment. The *in situ* PLA assay was carried out using a DuoLink *in situ* PLA kit (Sigma) according to the manufacturer's instructions. Images were captured using a BZ-9000 fluorescence microscope (Keyence) with a Plan Apo λ 40X/NA 0.95 objective lens (Nikon). Counting of the PLA signal dots was done using Hybrid cell count software (Keyence).

Chromatin Isolation

Cells were lysed in Buffer A (10 mM HEPES, 10 mM KCl, 1.5 mM MgCl₂, 0.34 M Sucrose, 10% Glycerol, 0.1% TritonX-100, containing 1 mM DTT and 1 mM Na₃VO₄, and protease inhibitor cocktail (Roche)) on ice for 30 min; samples were then centrifuged at 1700 x g for 5 min, and remaining pellets

were washed once with Buffer A. Pellets were resuspended in Buffer B (3 mM EDTA, 0.3 mM EGTA) containing 1 mM DTT, 1 mM Na₃VO₄ and protease inhibitor cocktail, then incubated on ice for 30 min. After centrifugation at 5000 x g for 5 min, pellets were solubilized in SDS sample buffer and analyzed as the chromatin fraction.

Immunoprecipitation and blotting

Cells were washed once with PBS, lysed in NETN buffer (150 mM NaCl, 0.5 mM EDTA, 20 mM Tris-HCl pH8.0, 0.5% NP-40) supplemented with protease inhibitor cocktail, 25 unit/ml Benzonase (Millipore), 2 mM MgCl₂, and 1 mM Na₃VO₄, on ice for 30 min. Then lysates were briefly sonicated and centrifuged at 14000 rpm for 10 min. The pellet was discarded. Dynabeads Protein G (Invitrogen) was incubated with an appropriate primary antibody prior to addition to the supernatant, following the manufacturer's instructions. To capture his-tagged or FLAG-tagged proteins, cOmplete His-Tag Purification Resin (Roche) or anti-FLAG M2 Agarose Affinity Gel (Sigma) was utilized, respectively. Captured proteins were washed five times with NETN buffer and analyzed by SDS-PAGE and immunoblotting using PVDF membranes (Millipore). Detection was performed as described previously (Unno et al., 2014).

In vivo ubiquitination assay

24 hr after transfection, cells were subjected to 100 ng/ml MMC for an additional 24 hr. 10 µM MG132 was added as indicated 2 hr before sample collection. Cells were lysed in Guanidine Buffer (6 M Guanidine, 100 mM NaH₂PO₄/Na₂HPO₄, pH 8.0), or in Hot SDS Buffer at 95°C (1% SDS, 150 mM NaCl, 10 mM Tris-HCl, pH 8.0); in the latter case, samples were then diluted 10-fold with binding buffer (20 mM H₃PO₄, 300 mM NaCl, pH 8.0). After DNA fragmentation by passing through a 27G needle and sonication (Bioruptor, COSMO-BIO), lysates were incubated with Ni-resin at RT for 2 hr. Bound complexes were washed five times with washing buffer (300 mM NaCl, 20 mM H₃PO₄, pH 8.0, 5mM imidazole), and eluted in SDS sample buffer containing 200 mM imidazole. Eluted samples were analyzed by immunoblotting. For detection of endogenous RAD51 ubiquitination, 10 µM PR619, a deubiquitinase inhibitor (abcam), was added 2 hr before harvest. The band intensities of the respective ubiquitinated proteins were quantified with LAS-4000 ImageQuant TL software (GE Healthcare).

Mammalian two-hybrid analysis

Bait and prey vectors (pM and pVP16, respectively, Clontech) with indicated inserts were transfected into 293T cells in triplicate with an expression vector for *Renilla* luciferase. Cells were lysed after ~48 hr and assayed for luciferase activity using a Dual-Luciferase Reporter Assay System (Promega). Transfection efficiency was normalized by *Renilla* luciferase activity. Intensity of the interaction was expressed as luciferase activity relative to the value obtained by empty vectors. pM-FANCI and pVP16-FANCD2 were used as a positive control.

Generation of lentivirus and transduction

To complement HAP1 Δ *RFWD3* cells, lentiviral particles were prepared by cotransfecting CS II -CMV-MCS-IRES-Bsd vector, in which human *RFWD3* WT and mutant cDNAs or GFP-RAD54 were cloned, along with packaging constructs, into 293T cells using Lipofectamine 2000. Following lentivirus infection, Blastcidin S (5 µg/ml) resistant populations were selected and expanded. To produce U2OS or U2OS-DR-GFP cell lines expressing GFP-RAD51, FLAG-RAD51-WT or -5KR, and FLAG-RPA2-WT, -5KR or the deletion mutant lacking amino acid residue 244-254 under tetracycline-controlled transcriptional activation, cDNAs in the entry vector pENTR were transferred to a puromycin resistant derivative (a kind gift of Drs. Yoshikazu Johmura and Makoto Nakanishi) of CSIV-TRE-RfA-UbC-KT (Kurita et al., 2013) using LR Clonase II (Invitrogen). U2OS cells were infected with the respective lentivirus and selected with puromycin (2 µg/ml).

Peptide pull-down assay

To prepare nuclear extracts, HAP1 cells collected with a cell scraper were lysed in Buffer A as above, and chilled on ice for 30 min, then cleared by centrifugation at 1700 x g for 5 min. The remaining nuclear pellet was lysed in Buffer C (20 mM HEPES, 25% glycerol, 420 mM KCl, 1.5 mM MgCl₂, 0.2 mM EDTA, 1 mM DTT, 0.1% Triton-X-100) containing protease inhibitor cocktail and 1 mM Na₃VO₄. After incubation on ice for 30 min and centrifugation at 14000 rpm for 5 min, the supernatant was obtained as the nuclear extract. After a three-fold dilution with Buffer D (the same as Buffer C, excluding KCl), samples were incubated at 4°C overnight with Dynabeads M-280 (Streptavidin beads, Invitrogen) that had been coated with biotinylated peptides (Scrum, Inc.). After extensive washing, bound materials were analyzed by immunoblotting.

DR-GFP assay

U2OS-DR-GFP cells were transduced with lentivirus CSIV that expresses FLAG-tagged RPA2 (WT, 5KR, or the deletion lacking residues 244-254) or FLAG-RAD51 (WT or 5KR) under the Doxycycline (Dox) inducible promoter, and were selected with 2 µg/ml puromycin. The GFP-RAD51 coding sequence was rendered resistant to siRAD51 by silent mutations in the target sequence. Cells were cultured with or without 2 or 10 µg/ml Dox for 24 hr, then siRNAs targeting endogenous RPA2 or RAD51 were transfected using Lipofectamine RNAiMAX (Invitrogen) according to the manufacturer's instructions. The following day, the I-SceI expression vector was transfected using Lipofectamine 3000 (Invitrogen) and the cells were further grown for two days with or without Dox. To assess HR frequency, the GFP positive cell population was quantified with a FACSCalibur flow cytometer (Beckton-Dickinson).

Data acquisition and analysis for FRAP

FRAP was performed using a TCS SP5 II confocal microscope (Leica Microsystems), equipped with an INU incubator system for microscopes (Tokai Hit), at 37°C with 5% CO₂. After two prebleach images were obtained, a rectangular region equivalent to about one third to one fourth of the nucleus was photobleached five times with a 488 nm Argon laser at ~80% transmission, then 20 to 25 images were acquired at two sec intervals. Two or three foci per nucleus were randomly selected and more than 50 foci were analyzed per sample. Measurement of the GFP fluorescence level was carried out on ellipsoidal areas with adjustment to foci movement during experiments. The fluorescence intensity in the bleached RPA2-GFP foci was normalized to the pre-bleached signal after subtraction of the background. Data were plotted using Prism 6 software (GraphPad).

Plasmids for recombinant protein expression

The DNA fragments encoding human UBE2D1, UBE2N, and MMS2 were amplified by PCR from human HeLa Marathon-Ready cDNA (Clontech). The amplified DNA fragments encoding UBE2N and MMS2, or UBE2D1, or RFWD3 were ligated into the BamHI-SalI, or EcoRI-XhoI, or BamHI-XhoI sites of the pGEX-6P-1 vector (GE Healthcare), respectively. For the generation of the expression vector for the human RAD51-5KR mutant, the DNA fragment encoding the human *RAD51* ORF carrying the 5KR mutation was ligated into the NdeI-BamHI sites of the pET-15b vector (Novagen). For the generation of the expression vector for the human RPA-5KR mutant, the DNA fragment encoding the human *RPA2* ORF carrying the 5KR mutation was ligated into the p11d-tRPA vector (Henricksen et al., 1994), using an In-Fusion HD Cloning Kit (Takara).

Purification of recombinant proteins

Human RFWD3 was overexpressed in *Escherichia coli* BL21(DE3) Codon(+)RIL cells (Stratagene) at 16°C. The cells producing GST-tagged RFWD3 were collected by centrifugation, and were resuspended in lysis buffer (50 mM Tris-HCl (pH 8.0), 10% glycerol, 500 mM NaCl, 30 µM zinc acetate (ZnOAc), 0.1% NP-40, 1 mM phenylmethylsulfonyl fluoride, and 5 mM 2-mercaptoethanol). The cells were then disrupted by sonication, and the supernatant was separated from the cell debris by centrifugation at 27,700 x g for 30 min. The supernatant was mixed gently with Glutathione Sepharose 4B resin (3 ml; GE Healthcare) at 4°C for 1 hr. The Glutathione Sepharose 4B resin was packed into an Econo-column (Bio-Rad), and was washed with 150 ml of lysis buffer, containing 1 M NaCl. The GST-tagged RFWD3 was eluted with 50 ml of elution buffer (100 mM Tris-HCl (pH 8.8), 10% glycerol, 500 mM NaCl, 30 µM

ZnOAc, 20 mM reduced glutathione, and 5 mM 2-mercaptoethanol). The GST tag was removed from RFWD3 by digestion with PreScission protease (15 unit/mg protein; GE Healthcare) during dialysis against 4 l of dialysis buffer (20 mM Tris-HCl (pH 8.0), 10% glycerol, 150 mM NaCl, and 5 mM 2-mercaptoethanol). The protein sample was concentrated with an Amicon Ultra Centrifugal Filter Device (Millipore), and was then applied to a Superdex 200 gel filtration column (HiLoad 16/60 preparation grade; GE Healthcare) equilibrated with dialysis buffer containing 500 mM NaCl. After the purified RFWD3 was concentrated and dialyzed against 1 l of dialysis buffer, and aliquots were frozen in liquid nitrogen. Human RPA, human RPA-5KR, human RAD51, human RAD51-5KR, human DMC1, human UBE2T, and the human UBE2N-MMS2 complex were purified as described previously (Henricksen et al., 1994; Hikiba et al., 2008; Ishida et al., 2008; McKenna et al., 2001; Sato et al., 2012a; 2012b). Human UBE2D1 was prepared by the same method as that for human UBE2T.

DNA substrates

For the D-loop formation assay, a 70-mer ssDNA, 5'-CCGGT ATATT CAGCA TGGTA TGGTC GTAGG CTCTT GCTTG ATGAA AGTTA AGCTA TTAA AGGGT CAGGG-3', was used. For the ubiquitination and electrophoresis mobility shift assays, a 45-mer ssDNA, 5'-CCCAG GCCAT TACAG ATCAA TCCTG AGCAT GTTAA CCAAG CGCAG-3', and a 49-mer ssDNA, 5'-GTCCC AGGCC ATTAC AGATC AATCC TGAGC ATGTT TACCA AGCGC ATTG-3', were used. All oligonucleotides were purchased from Nihon Gene Research Laboratory, as high-pressure liquid chromatography-purified grade. DNA concentrations are expressed in moles of nucleotides.

In vitro ubiquitination assay

RPA, RAD51, or DMC1 (1 μ M) was mixed with human recombinant E1 (75 nM; Boston Biochem), an E2-conjugating protein (either UBE2D1, UBE2N, the UBE2N-MMS2 complex, or UBE2T; 4 μ M), RFWD3 (1.5 μ M), and ubiquitin (10 μ M; Boston Biochem), in the presence or absence of the 45-mer ssDNA (5 μ M), in 10 μ l of reaction buffer, containing 50 mM Tris-HCl (pH 7.5), 3% glycerol, 45 mM NaCl, 2 mM MgCl₂, 2 mM ATP, 30 μ M ZnOAc, and 0.5 mM dithiothreitol. The reaction mixtures were incubated at 37°C for 90 min, and the reactions were then stopped by the addition of 2% SDS. The reaction products were separated by 15%, 12% or 10% SDS-PAGE, and were transferred to a polyvinylidene fluoride membrane (GE Healthcare). The ubiquitinated RPA1, RPA2, RPA3, RAD51, and DMC1 proteins were detected with an anti-RPA70 antibody (1:1000; ab199240, abcam), an anti-RPA32 antibody (1:1000; A300-244A, Bethyl Laboratories, Inc.), an anti-RPA3 antibody (1:1000; HPA005708, Sigma-Aldrich), an anti-RAD51 antibody (1:1000) (Kim et al., 2005), and an anti-DMC1 antibody (1:1000; ab11054, abcam), respectively. The band intensities of the respective ubiquitinated proteins were quantified with ImageJ (for Figure 4A), or MultiGauge ver. 3.2 software (for Figure 4B-E and Figure S4G, Fujifilm).

Pull-down assays using purified proteins and ssDNA beads

RPA or RAD51 (4 μ g) was incubated with either GST (18 μ g) or GST-tagged RFWD3 (18 μ g) at 37°C for 60 min in 200 μ l of pull-down buffer, containing 20 mM Tris-HCl (pH 7.5), 10% glycerol, 150 mM NaCl, 1 mM ZnOAc, 0.02% NP-40, and 5 mM 2-mercaptoethanol. Glutathione Sepharose 4B beads (3 μ l) were added to the reaction mixtures, and were gently mixed at 23°C for 60 min. The beads were then washed twice with 1 ml pull-down buffer. RAD51 bound to the beads was analyzed by 12% SDS-PAGE with Coomassie Brilliant Blue staining. RPA1, RPA2, and RPA3 bound to the beads were analyzed by 15% SDS-PAGE, and detected with an anti-RPA70 antibody (1:1000; ab199240), an anti-RPA32 antibody (1:2000; A300-244A), and an anti-RPA3 antibody (1:1000; HPA005708), respectively. For the pull-down assay with RPA-coated ssDNA beads, RPA (3.6 μ g) was incubated with a 5'-biotinylated 80-mer poly dT ssDNA (27 μ M) conjugated to Dynabeads M-280 Streptavidin (Invitrogen) at 37°C for 15 min, in 5 μ l of reaction buffer, containing 20 mM Tris-HCl (pH 7.5), 8% glycerol, 130 mM NaCl, 0.012% NP-40, 0.6 mM ZnOAc, and 5 mM 2-mercaptoethanol. During the incubation period, the reaction mixtures were gently mixed by tapping at 3 min intervals, and RFWD3 (5 μ g) was preincubated in 50 μ l pull-down buffer at 37°C for 15 min. After the incubation, the beads were washed once with 20 μ l pull-down buffer, and were gently mixed with preincubated RFWD3 at 23°C for 30 min. For the pull-down assay with the ssDNA beads, RPA (3.6 μ g) was pre-incubated with RFWD3 (5 μ g) at 37°C for

15 min in 50 μ l pull-down buffer. A 5'-biotinylated 80-mer poly dT ssDNA conjugated to Dynabeads M-280 Streptavidin (1 μ l, 134 μ M) was added to the reaction mixtures, which were gently mixed at 23°C for 30 min. The beads were then washed twice with 200 μ l pull-down buffer, and the proteins bound to the beads were detected by immunoblotting with an anti-RFWD3 antibody (1:2000; ab138030, abcam), an anti-RPA70 antibody (1:1000; ab199240), an anti-RPA32 antibody (1:2000; A300-244A), and an anti-RPA3 (1:1000; HPA005708).

Electrophoresis mobility shift assay

The 49-mer ssDNA was mixed with 0.2, 0.4, and 0.8 μ M of wild type RPA or the RPA-5KR mutant in 10 μ l of reaction buffer, containing 23 mM Tris-HCl (pH 8.0), 64 mM NaCl, 5 mM KCl, 4.5% glycerol, 5 mM dithiothreitol and 5 μ g/ml bovine serum albumin, at 37°C for 15 min. The samples were then analyzed by 3.5% PAGE in 0.2xTBE (18 mM Tris-borate and 0.4 mM EDTA) buffer. DNAs were visualized by SYBR Gold (Invitrogen) staining.

DNA binding assay with ubiquitinated proteins

RPA or RAD51 (1 μ M) was ubiquitinated with human recombinant E1 (75 nM), UBE2D1 (4 μ M), RFWD3 (1.5 μ M), and ubiquitin (10 μ M) at 37°C for 90 min, in 20 μ l of reaction buffer, containing 50 mM Tris-HCl (pH 7.5), 3% glycerol, 45 mM NaCl, 2 mM MgCl₂, 2 mM ATP, 30 μ M ZnOAc, and 0.5 mM dithiothreitol. A 5'-biotinylated 80-mer poly dT ssDNA conjugated to Dynabeads M-280 Streptavidin (1.2 μ l, 170 μ M) was then added to the reaction mixtures, which were incubated at 37°C for 15 min. During the incubation period, the reaction mixtures were gently mixed by tapping at 3 min intervals. After the incubation, the supernatant was transferred to a new tube (unbound fraction), and the beads were then washed twice with 20 μ l of wash buffer, containing 35 mM Tris-HCl (pH 7.5), 1 mM ATP, 2.5 mM MgCl₂, 0.1% NP-40, and 1 mM dithiothreitol. The proteins bound to the beads were eluted with 10 μ l SDS-sample buffer, containing 50 mM Tris-HCl (pH 6.8), 2% SDS, 10% glycerol, and 0.7 M 2-mercaptoethanol (bound fraction). The unbound and bound fractions were separated by 12% or 15% SDS-PAGE, and the proteins were detected with anti-RPA70, anti-RPA32, or anti-RAD51 antibodies.

RAD51 ATPase assay

RAD51 or RAD51-5KR (1.5 μ M) was incubated with 5 nCi [γ -³²P]ATP in 10 μ l of reaction buffer containing 26 mM HEPES-NaOH (pH 7.5), 1 mM Tris-HCl (pH 7.5), 45 mM NaCl, 0.01 mM EDTA, 1 mM dithiothreitol, 0.6 mM 2-mercaptoethanol, 3% glycerol, 1 mM MgCl₂, 5 μ M ATP, single-strand ϕ X174 viral (+) strand DNA (20 μ M; New England Biolabs.), and 100 μ g/ml bovine serum albumin, at 37°C for 60 min. The reaction was quenched by the addition of 5 μ l of 0.5 M EDTA, and the samples were separated by thin layer chromatography on polyethyleneimine-cellulose, in a solution containing 0.5 M LiCl and 1 M formic acid. The plate was exposed to an imaging plate (Fujifilm), and the products were visualized using an FLA-7000 imaging analyzer (Fujifilm). The signal intensities of the products were quantified using MultiGauge ver. 3.2 software.

D-loop formation assay

The supercoiled dsDNA containing tandem repeats of the 5S rDNA sequence was prepared with a method avoiding irreversible denaturation by alkaline treatment of the cells (Kagawa et al., 2001). The 5'-³²P end-labeled 70-mer ssDNA (1 μ M) was incubated with RAD51 or RAD51-5KR (0-0.6 μ M) at 37°C for 10 min, in 9 μ l of reaction buffer containing 24 mM HEPES-NaOH (pH 7.5), 1 mM Tris-HCl (pH 7.5), 30 mM NaCl, 0.01 mM EDTA, 1 mM dithiothreitol, 0.4 mM 2-mercaptoethanol, 2% glycerol, 1 mM MgCl₂, 2 mM CaCl₂, 1 mM ATP, 20 mM creatine phosphate, 75 μ g/ml creatine kinase, and 100 μ g/ml bovine serum albumin. The supercoiled dsDNA (30 μ M, 1 μ l) was then added, and the reaction mixtures were further incubated at 37°C for 10 min. The reactions were stopped by addition of a 2 μ l aliquot of the stop solution, containing 0.2% SDS and 1.4 mg/ml proteinase K (Roche Applied Science). The deproteinized DNA products were separated by 1% agarose gel electrophoresis in 1x TAE buffer (40 mM Tris acetate, 1 mM EDTA). The agarose gel was dried, and was exposed to an imaging plate. The gel image was obtained using an FLA-7000 imaging analyzer.

Quantification of immunoblotting or protein gel data

For all quantification of band intensities, ImageQuant TL software (GE healthcare), MultiGauge ver. 3.2 software, or ImageJ software (<https://imagej.nih.gov/ij/>) was used.

Quantification of immunocytochemistry and PLA assays

Hybrid Cell Count software (Keyence) was used for scoring the PLA signals and most of the immunocytochemistry images, except for FLAG-RAD51 foci in Figure 3C and GFP-RAD54 foci shown in Figure 7A.

Statistical analysis

P-values were calculated by one-way ANOVA post hoc test in multiple comparisons or Student's t-test using Prism 6 (Graphpad) software.

Supplemental References

- Henricksen, L.A., Umbrecht, C.B., and Wold, M.S. (1994). Recombinant replication protein A: expression, complex formation, and functional characterization. *J Biol Chem* 269, 11121–11132.
- Hikiba, J., Hirota, K., Kagawa, W., Ikawa, S., Kinebuchi, T., Sakane, I., Takizawa, Y., Yokoyama, S., Mandon-Pépin, B., Nicolas, A., et al. (2008). Structural and functional analyses of the DMC1-M200V polymorphism found in the human population. *Nucleic Acids Res* 36, 4181–4190.
- Ishida, T., Takizawa, Y., Sakane, I., and Kurumizaka, H. (2008). The Lys313 residue of the human Rad51 protein negatively regulates the strand-exchange activity. *Genes Cells* 13, 91–103.
- Kagawa, W., Kurumizaka, H., Ikawa, S., Yokoyama, S., and Shibata, T. (2001). Homologous pairing promoted by the human Rad52 protein. *J Biol Chem* 276, 35201–35208.
- Kim, J.-S., Krasieva, T.B., Kurumizaka, H., Chen, D.J., Taylor, A.M.R., and Yokomori, K. (2005). Independent and sequential recruitment of NHEJ and HR factors to DNA damage sites in mammalian cells. *J Cell Biol* 170, 341–347.
- Kurita, R., Suda, N., Sudo, K., Miharada, K., Hiroshima, T., Miyoshi, H., Tani, K., and Nakamura, Y. (2013). Establishment of immortalized human erythroid progenitor cell lines able to produce enucleated red blood cells. *PLoS ONE* 8, e59890.
- McKenna, S., Spyropoulos, L., Moraes, T., Pastushok, L., Ptak, C., Xiao, W., and Ellison, M.J. (2001). Noncovalent interaction between ubiquitin and the human DNA repair protein Mms2 is required for Ubc13-mediated polyubiquitination. *J Biol Chem* 276, 40120–40126.
- Nakada, S., Tai, I., Panier, S., Al-Hakim, A., Iemura, S.-I., Juang, Y.-C., O'Donnell, L., Kumakubo, A., Munro, M., Sicheri, F., et al. (2010). Non-canonical inhibition of DNA damage-dependent ubiquitination by OTUB1. *Nature* 466, 941–946.
- Sato, K., Ishiai, M., Toda, K., Furukoshi, S., Osakabe, A., Tachiwana, H., Takizawa, Y., Kagawa, W., Kitao, H., Dohmae, N., et al. (2012a). Histone chaperone activity of Fanconi anemia proteins, FANCD2 and FANCI, is required for DNA crosslink repair. *EMBO J* 31, 3524–3536.
- Sato, K., Toda, K., Ishiai, M., Takata, M., and Kurumizaka, H. (2012b). DNA robustly stimulates FANCD2 monoubiquitylation in the complex with FANCI. *Nucleic Acids Res* 40, 4553–4561.

Unno, J., Itaya, A., Taoka, M., Sato, K., Tomida, J., Sakai, W., Sugawara, K., Ishiai, M., Ikura, T., Isobe, T., et al. (2014). FANCD2 binds CtIP and regulates DNA-end resection during DNA interstrand crosslink repair. *Cell Rep* 7, 1039–1047.

4 DISKUSSION

4.1 WHOLE EXOME SEQUENCING ALS SCHLÜSSELTECHNOLOGIE IN DER FA-KOMPLEMENTATIONSGRUPPENBESTIMMUNG

In den letzten Jahren hielt NGS, insbesondere das WES, Einzug in die Mutationssuche bei Patienten mit Erkrankungen ungeklärter, genetischer Ursache. So konnten wir bereits 2012 bei einem Patienten Mutationen in *FANCDQ* mittels WES nachweisen (siehe 3.2.1). Durch eine vereinfachte Anwendung in Form von Benchtop-Geräten und reduzierten Kosten erwogen wir, NGS bzw. WES auch in der Routinediagnostik zum Einsatz zu bringen.

Dazu wurde von uns im Rahmen dieser Arbeit, eine Evaluierung von WES für die FA-Diagnostik durchgeführt. (Knies et al., 2012) Nach der Zuordnung von fünf Patienten zu den Komplementationsgruppen FA-D1, FA-D2, FA-G und FA-J und FA-P, überzeugte diese Methode in der FA-Diagnostik in unserem Labor. (Knies et al., 2012; Schuster et al., 2013). Zudem bietet WES die Möglichkeit neue FA-Gene zu entdecken und somit das Verständnis um den FA/BRCA-Signalweg zu verbessern. Hierauf soll in Abschnitt 4.2 näher eingegangen werden.

Wichtig war bei der Etablierung der Methode vor allem die strategische Auswertung der Datenmenge. Nach der Anreicherung und Sequenzierung der verschiedenen Patienten gDNAs bei unterschiedlichen Service-Providern, wurden die Daten mit Hilfe der NextGENe Software von Softgenetics align und ausgewertet. Zunächst beschränkte sich die Auswertung auf alle bekannten FA-Gene und mögliche Kandidatengene, wie *FAAP20*, *FAAP100*, *FAAP24*, *MHF1* und *MHF2*. Diese sind bereits als ein Teil des FA-Signalwegs bekannt, jedoch wurde bisher noch kein FA-Patient mit Mutationen in einem dieser Gene gefunden. Nach Ausschluss bekannter Polymorphismen, die bereits in der dbSNP Datenbank von *NCBI (National Center for Biotechnology Information)* gelistet waren, erfolgte die Analyse von heterozygoten oder homozygoten Varianten, basierend auf dem familiären Hintergrund der Patienten. Dennoch gab es verschiedene Hindernisse und Herausforderungen, die bei der Auswertung der Daten der o.g. Patienten auffielen und bewältigt werden mussten. Diese werden im Folgenden diskutiert.

Allen voran steht die Abdeckung der einzelnen Exons. Hier zeigten sich deutliche Unterschiede, nicht nur in Abhängigkeit von GC-reichen Bereichen oder polyA- oder polyT-Stretches, sondern auch aufgrund einer erhöhten Fehlerrate bei der Detektion der richtigen Base an der richtigen Stelle. Verschiedene Studien zeigen, dass eine

Abdeckung von 30- bis 40-fach ausreichend ist, um die meisten Exons vollständig abzudecken und eine eindeutige Aussage bezüglich vorhandener Varianten treffen zu können. (Lohmann and Klein, 2014; Majewski et al., 2011) Im Durchschnitt lag die Abdeckung unserer fünf publizierten WES-Analysen bei 58x. Für die FA-Gene betrug sie bei den gleichen Exomen 40x. Obwohl dies prinzipiell ausreichend ist, beobachteten wir bei einzelnen Exons eine geringere Abdeckung, wie z. B. bei *FANCE* Exon 1. *FANCE* Exon 1 hat einen hohen GC-Gehalt und lies sich unabhängig der Anreicherungstechnik und der Sequenzierplattform nie ausreichend bzw. gar nicht abdecken. Hier war es nötig, die Abdeckung auf 100-fach zu erhöhen, um eine minimale Abdeckung dieser Exons von mindestens 10 Reads zu erreichen.

Ein Problem stellt auch die Speicherung der großen Datenmengen dar, die beim WES generiert werden. Nach der Sequenzierung sind die Daten in *FASTQ Files* enthalten, die nach dem Alignment in das sog. *Sequence Alignment/Map (SAM)* Format umgewandelt werden. Diese werden wiederum komprimiert und im sog. *Binary Sequence Alignment/Map (BAM)* Format gespeichert, das die Dateigröße um ein drei- bis vierfaches reduziert, dennoch aber einige Gigabyte groß ist. Das kleinstmögliche Speicherformat ist das sog. *Variants call format (VCF)*, welches nur noch die nach der Analyse detektierten Varianten enthält und nicht größer als 100 Megabyte (MB) ist. Es ist jedoch ratsam, die *FASTQ* oder *BAM* Dateien zu speichern, da bei einer erneuten Analyse so auf die Rohdaten zurückgegriffen werden kann. Eine nochmalige Betrachtung der Daten kann vor allem dann wichtig sein, wenn *copy number variations (CNV)* oder mitochondriale DNA untersucht werden sollen. Außerdem könnten in der Zwischenzeit andere Gene oder vorherige Kandidatengene als neue krankheitsassoziierte Gene identifiziert werden, wie es bspw. für FA auch im Rahmen dieser Arbeit erfolgte. Eine Kompression der NGS-Daten geht meist mit einem Verlust an Informationen einher. Daher ist es wichtig ein Format zu wählen, das ein Mindestmaß an Daten enthält. Das beinhaltet vor allem die Position der Variante und deren Abdeckung. Ein vielversprechendes, neues Format ist das sog. *challenge-response authentication mechanism* Format (CRAM). Es ist um 38-55 % kleiner als eine *BAM* Datei und wurde u. a. auch für das *1000 Genomes project* verwendet. In den letzten Jahren sind neben kleineren Dateiformaten auch neue Speichermöglichkeiten aufgekommen, wie bspw. die Cloud. Sie ist eine kostengünstige, leicht bedienbare und kommerziell angebotene Speicherplattform. Trotz der Nutzung von großen Konsortien wie dem *International Cancer Genome Consortium (ICGC)* ist der Gebrauch aus ethischen und legalen Gründen abzuwägen. (Lelieveld et al., 2016) Daten des NGS sind sensible und sehr persönliche Informationen des jeweiligen Patienten. Anhand ihrer Auswertung ist, trotz einer Pseudo- oder Anonymisierung, eine genaue Zuordnung zu einer bestimmten Person möglich. Da es sich bei der Cloud um ein

Internet-basiertes Speichermedium handelt, muss man berücksichtigen, dass diese Daten Hacker-Angriffen ausgesetzt sein können. Des Weiteren ist auch bei der Cloud keine 100 %ige Garantie vor einem Datenverlust gegeben. Die große Menge an generierten NGS-Daten wird daher zukünftig ein Speicherplatzproblem darstellen, das nur mit der Entwicklung von neuen und kleineren Dateiformaten zu bewältigen sein wird. Da es sich bei den WES-Daten um medizinische Daten handelt, müssen diese normalerweise, wie andere Patientendaten auch, für mindestens 10 Jahre aufgehoben werden. Diese Vorschrift wurde jedoch für Exomdaten bereits gelockert, sodass hier eine Aufbewahrungspflicht von lediglich 2 Jahren besteht. (Rehm et al., 2013; Weiss et al., 2013)

Eine weitere Herausforderung ist die Interpretation der entdeckten Varianten. Hierbei gilt es nicht nur zu beurteilen, ob eine Variante die normale Gen- bzw. Proteinfunktion beeinträchtigt, sondern auch, ob das veränderte Gen überhaupt eine Relevanz für die Pathogenese einer Krankheit hat. Mit Hilfe von großen Datenbanken wie das *Exome Aggregation Consortium* (ExAC, <http://exac.broadinstitute.org/>), welches zurzeit mehr als 60.000 Varianten mendelscher Erkrankungen beinhaltet, ist eine Beurteilung vereinfacht worden. In Bezug auf FA ist auch ein Abgleich mit dem *International Fanconi Anemia Registry* (IFAR) bzw. der *Fanconi Anemia Mutation Database* der Rockefeller Universität (<http://www.rockefeller.edu/fanconi/mutate/>) zu empfehlen. Sie enthält alle bisher in FA-Genen detektierten und veröffentlichten Varianten (5363 Varianten, Stand Februar 2017). Dennoch gibt das keine Garantie vor falsch-positiven oder falsch-negativen Befunden. Zudem geben *in silico* Vorhersageprogramme nur eine Prognose für die entdeckte Variante, jedoch aber keine 100 %ige Sicherheit. Es ist daher ratsam, mehrere verschiedene *in silico* Tools zu nutzen und die verschiedenen Aussagen zu vergleichen. Des Weiteren sollte der Abgleich der entdeckten Variante mit dem Vorhersageprogramms auf verschiedenen Ebenen stattfinden. Auf DNA-Ebene (z. B. <http://www.mutationtaster.org/>), als auch auf Proteinebene (z. B. <http://genetics.bwh.harvard.edu/pph2/>). Projekt 3 in Knies et al. beschreibt solch einen Fall, eines schwer zu interpretierenden Ergebnisses. Es wurden neben der als pathogen definierten Mutation c.7890_7891insAA in *FANCD1* drei weitere Varianten in der Exomanalyse detektiert. Laut den o. g. Vorhersageprogrammen war jedoch nur die als *single nucleotide polymorphism* (SNP) gelistete Variante c.7795G>A ebenfalls pathogen. Das Problem stellt der an dieser Position gelistete SNP dar. Dieser beinhaltet eine drei-Basenpaar-Deletion von c.7795_7797. In unserem Fall ist jedoch nur die erste Position dieses SNPs von einem Basenaustausch betroffen. Somit wurde fälschlicherweise dieser Basenaustausch als SNP gelistet und erst durch sorgfältige Nachanalyse als pathogene Variante detektiert. Es ist von Vorteil, bei nur einer

bestätigten, heterozygoten pathogenen Variante auch gelistete SNPs im gleichen Gen näher zu betrachten und diese mittels *in silico* Programmen zu bewerten. Außerdem sollte stets die neuste Version der dbSNP Datenbank zur Exomanalyse verwendet werden, bestenfalls in Kombination mit *minor allele frequencies* und Daten aus dem *1000 Genomes project*. (Knies et al., 2012)

Zudem erschweren vorhandene Pseudogene eine Variantenbeurteilung erheblich. Pseudogene entstehen durch Duplikation einzelner Gensegmente oder durch Retrotransposons. Sie haben eine hohe Übereinstimmung in der Sequenzabfolge, werden jedoch nicht transkribiert und sind daher funktionslos. (Khurana et al., 2010) Durch die kurze Readlänge (< 300 bp) beim WES, kann es zu fehlerhaften Alignments mit den Pseudogenen kommen, die dann als falsch-positive Varianten detektiert werden. Bei der Analyse der o. g. WES-Daten fielen immer wieder gleiche Gene mit einer deutlich erhöhten Anzahl an Varianten im Vergleich zu den anderen Genen auf. Nach genauerer Recherche war festzustellen, dass diese Gene wie bspw. *CDC27*, *MUC* oder *NBPF* eine hohe Anzahl an gelisteten Pseudogenen aufwiesen. In Bezug auf FA-Gene ist bisher nur das Vorhandensein von Pseudogenen bei *FANCD2* bekannt. Aktuell sind in der Pseudogendatenbank (Build 83) fünf Pseudogene für *FANCD2* bestimmt. Dabei handelt es sich um *PGOHUM00000299338* (*FANCD2P1*), *PGOHUM00000299341* (*FANCD2P2*), *PGOHUM00000299342* (*FANCD2P3*), *PGOHUM00000305819* (*FANCD2P4*) sowie *PGOHUM00000305820* (*FANCD2P5*). Rost et al. (persönliche Kommunikation) konnte zeigen, dass *FANCD2P5* mit *FANCD2P3* und *FANCD2P4* mit *FANCD2P2* identisch sind. Somit ergeben sich drei Pseudogene für *FANCD2* (*FANCD2P1*, *FANCD2P2* und *FANCD2P3*). Diese Daten erweitern die Analysen von Kalb et al. aus dem Jahr 2007. (Kalb et al., 2007) Es empfiehlt sich bei einer detektierten Variante in *FANCD2*, diese mit Vorsicht zu beurteilen und auf jeden Fall mittels Sanger Sequenzierung, am besten auf cDNA Ebene, zu validieren. Des Weiteren helfen längere Readlängen (300-800 bp), wie sie beim Roche454 oder den Pacific Bioscience Geräten generiert werden, Pseudogene in der Analyse von WES-Daten zu umgehen.

Nebenbefunde stellen ein weiteres Problem beim WES dar. Bei einer gezielten Panel-Analyse werden ausschließlich krankheitsassoziierte Gene und evtl. damit zusammenhängende Kandidatengene analysiert. Bei WES ist das anders. Da das gesamte Exom eines Patienten betrachtet wird, ergeben sich neben dem mit der untersuchten Krankheit, auch Varianten in Genen, die für andere Krankheiten ursächlich sein können. Man unterscheidet zwischen verschiedenen Kategorien von Nebenbefunden: nicht-behandelbare Erkrankungen im Kindesalter, nicht-behandelbare Erkrankungen im Erwachsenenalter, behandelbare Erkrankungen im Erwachsenenalter

und Anlageträgerschaft für eine Erkrankung. (Bishop et al., 2017) Neben einer zielgerichteten, bioinformatischen Auswertung der Daten, ist auch die individuelle Absprache mit dem Patienten notwendig. Nimmt man FA als Beispiel, sollten zunächst nur, die mit FA assoziierten Gene und Kandidatengene untersucht werden. Da ein Teil der FA-Gene auch mit familiär bedingten Brust- und Eierstockkrebs in Verbindung gebracht wird (siehe 1.3.1), sollten monoallelische Varianten in diesen Genen notiert und auch auf ihre Pathogenität hin untersucht werden. Findet sich in den bereits bekannten FA-Genen und den Kandidatengenen keine krankheitsauslösende Veränderung, ermöglicht die Exomanalyse nach neuen FA-Genen zu screenen. Hier steigt auch die Gefahr für Nebenbefunde. Konsortien wie das *American College of Medical Genetics and Genomics* (ACMG) oder die *American Society of Human Genetics*, haben in den letzten Jahren immer wieder Empfehlungen zum Umgang mit Nebenbefunden herausgegeben. Darüber hinaus aktualisiert das ACMG jährlich eine Liste mit Genen, deren mutierte Genprodukte zu schweren, hoch penetranten Erkrankungen führen können und als Nebenbefunde mitgeteilt werden sollten. Dabei ist zu beachten, dass nur bekannte pathogene (*known pathogen*, KP) oder als pathogen vorhergesagte (*expected pathogen*, EP) Varianten als Nebenbefunde angegeben und dem Patienten mitgeteilt werden sollen. Die aktuelle Liste umfasst 59 Gene, die vornehmlich mit Krankheiten wie verschiedene Krebsarten oder Kardiomyopathien assoziiert sind, deren Ursprung monogenisch ist. Die Kriterien zur Aufnahme eines Gens in diese Liste sind klar definiert: Es muss sich um eine schwere, lebensbedrohliche Erkrankung handeln, die eine hohe Penetranz aufweist und dennoch mit spezifischen Untersuchungen und Vorsorgen zu vermeiden oder behandelbar ist. Auf dieser Liste befinden sich auch die beiden FA-Gene *BRCA1* (*FANCS*) und *BRCA2* (*FANCD1*), die wie bereits erwähnt, bei monoallelischer Mutation zu familiär bedingtem Brust- und Eierstockkrebs führen können. (Kalia et al., 2016) Das Problem der Nebenbefunde wird sich mit WGS noch weiter verstärken, da sich die Anzahl an detektierten Varianten durch die Anreicherung der Introns deutlich erhöhen wird. Letztlich liegt die Entscheidung über eine Mitteilung von Nebenbefunden ausschließlich beim Patienten selbst. Eine Zustimmung über deren Mitteilung sollte bereits vor der Analyse erfolgen, zumal im Anschluss eine humangenetische Beratung zur Bewertung des Risikos unbedingt erfolgen sollte.

Trotz der diskutierten Probleme, die sich im Rahmen von WES ergeben können, eignet sich diese Methode sehr gut zur Genotypisierung von FA-Patienten. Oft durchlaufen Patienten mit seltenen Erkrankungen, wie bspw. auch bei FA, eine Odyssee an Untersuchungen, da nicht jeder Arzt mit dem heterogenen klinischen Phänotyp vertraut ist. WES erleichtert in diesem Fall die Zuordnung eines Patienten zu einer bestimmten Krankheit in einer kurzen Zeitspanne und mit einer genauen Mutationsanalyse. Generell

ist die Zuordnung der Komplementationsgruppe für die Patienten ein weiteres Puzzlestück in der Gesamtheit ihrer Erkrankung. Besonders bei Mutationen in Genen wie *FANCD1*, *FANCN* oder auch *FANCS* wird sich ein intensiviertes Vorsorgeprogramm auf Grund der erhöhten Krebsdisposition anschließen, die dem Patienten eine schnellere und gezieltere Behandlung ermöglicht.

Auch wenn in Zukunft WGS günstiger und schneller durchzuführen sein wird, ist WES für FA durchaus ausreichend. Es bietet die gleichzeitige Abdeckung aller bisher bekannten FA-Gene und möglicher Kandidatengene. Etwa 85 % aller bisher bekannten Mutationen liegen in Exons bzw. an Exongrenzen und Spleißstellen, sodass WGS nur einen geringen Teil an neuen Mutationen beitragen könnte – sog. tief intronische Mutationen. Dabei besteht nur ca. 1 % des menschlichen Genoms aus Protein-codierenden Genen. (Majewski et al., 2011) Weitere Möglichkeiten des NGS sind die Transkriptom-Sequenzierung und die gezielte Anreicherung der FA-Gene mittels sog. Panelsequenzierung. Die Vorteile der Transkriptom-Analyse liegen in ihren niedrigen Kosten, der Analyse von kodierenden Bereichen und der Identifikation von großen Deletionen und Insertionen. Dennoch hat auch sie ihre Limitierung, die vor allem in der Vorbereitung der RNA und der Umschreibung in cDNA liegt. Aufgrund der Expression instabiler Transkripte, kann es zu Fehlern kommen, die sich letztlich als falsch-positive oder falsch-negative Ergebnisse in der Auswertung zeigen. Bei der gezielten Anreicherung der FA-Gene und möglicher Kandidatengene mit Hilfe der Paneldiagnostik, ist meist mit einer hohen Abdeckung der einzelnen Bereiche zu rechnen und die Anzahl an Nebenbefunden reduziert sich dadurch erheblich. Dennoch bietet eine gezielte Anreicherung der FA-Gene nicht die Möglichkeit neue FA-Gene, außerhalb der angereicherten Kandidatengene, zu finden.

Für die Anwendung von WES in der FA-Routinediagnostik sollten zunächst die o. g. Probleme gelöst werden. Zudem müssen Standardprotokolle für die Sequenzierung als auch die Auswertung etabliert werden. Hinzu kommen die nötigen Einverständniserklärungen der Patienten, auch in Bezug auf Nebenbefunde und die Möglichkeit der Forschung zur Entdeckung neuer FA-Gene mit Hilfe von WES. Des Weiteren wird in naher Zukunft auch eine Abklärung mit der Krankenkasse bzw. dem Kostenträger nötig sein, damit WES in der FA-Routinediagnostik in den Leistungskatalog aufgenommen werden kann.

4.2 DIE ENTDECKUNG NEUER FANCONI ANÄMIE GENE UND DEREN CHARAKTERISIERUNG IM RAHMEN DES FA/BRCA-SIGNALWEGS

4.2.1 DIE STRUKTUR-SPEZIFISCHE ENDONUKLEASE XPF

Innerhalb der letzten 5 Jahre wurden sechs FA-Gene mit Hilfe von NGS, insbesondere WES gefunden. (Ameziane et al., 2015; Bluteau et al., 2016; Bogliolo et al., 2013; Hira et al., 2015; Sawyer et al., 2015; Shamseldin et al., 2012; Wang et al., 2015) Zu diesen Genen konnten bis heute wenige FA-Patienten zugeordnet werden, womit sie zu den seltenen Komplementationsgruppen zählen. Doch gerade hierfür eignet sich die Mutationssuche mittels WES sehr gut, da es keine Kenntnisse über die molekularen Funktionen und Interaktionen im FA/BRCA-Signalweg voraussetzt.

XPF war bereits vorher als krankheitsverursachendes Gen von XP Subtyp F beschrieben worden und auch im Zusammenhang mit Segmentaler Progerie (XFE) bekannt. (Niedernhofer et al., 2006; Sijbers et al., 1996) Das Mutationsspektrum für diese beiden Krankheiten war jedoch sehr speziell und lies keine Rückschlüsse auf einen Zusammenhang mit FA zu. Dennoch erregte das Ergebnis der WES-Analyse eines zuvor nicht zugeordneten FA-Patienten unsere Aufmerksamkeit, nachdem sich zwei compound-heterozygote Mutationen in *XPF* fanden. Somit konnte im Jahr 2013 *XPF* als das sechzehnte FA-Gen identifiziert und näher charakterisiert werden. (Bogliolo et al., 2013)

Unsere genetischen, biochemischen und funktionalen Studien, die bereits bekannte Mutationen in *ERCC4* berücksichtigten, konnten zeigen, dass abhängig von der Mutation, drei unterschiedliche Krankheiten aus einem mutierten *XPF*-Gen hervorgehen können. Im Gegensatz zu XP, deren XP-F Patienten meist einen milden Phänotyp aufweisen und hauptsächlich an einer Photosensitivität der Haut leiden, weisen XPF-Patienten mit FA die klassischen Merkmale wie hämatologische Auffälligkeiten und Knochenmarkversagen auf. (Gregg et al., 2011) Die Zellen der XP-Patienten zeigen keinen erhöhten G2-Phase Arrest nach MMC-Zugabe, reagieren jedoch sensitiv auf UV-Strahlen. Sie haben ein vermindertes Level an nukleärem XPF-Protein, das in einer reduzierten NER-Aktivität resultiert. Dennoch reicht der Anteil an nukleärem XPF-Protein aus, um interstrangquervernetzungs-spezifische Reparaturfunktionen aufrechtzuerhalten und einen Zellzyklusarrest und Chromosomenbrüche zu vermeiden. Dies ist gegensätzlich zu den FA-Q Patienten, die eine ausreichende NER-Aktivität besitzen, jedoch keine Interstrangquervernetzungen auflösen können. Das segmentale Progerie-Syndrom manifestiert sich sowohl durch Kennzeichen von XP als auch von FA. Die Zellen haben einen sehr geringen Anteil an nukleärem XPF-Protein, wodurch weder NER noch die

Reparatur von Interstrangquervernetzungen möglich ist. Bis heute wurde nur ein Patient für XFE beschrieben, der auch im klinischen Phänotyp eine Mischung aus FA und XP zeigt. Er hat eine erhöhte Photosensitivität sowie Anämie und auch auf zellulärer Ebene lässt sich die Kombination aus den beiden anderen Erkrankungen erkennen. Die Zellen sind sowohl sensitiv gegenüber UV-Strahlen als auch gegenüber DNA-quervernetzenden Substanzen. (Niedernhofer et al., 2006) Zeitgleich mit der Entdeckung von *XPF* als FA-Gen, wurde von Kashiyama et al. eine Patientin mit Mutationen in *ERCC4* beschrieben, die klinische Merkmale für sowohl XP, FA als auch Cockayne Syndrom (CS) zeigt. Neben einer erhöhten UV-Sensitivität zeigen ihre Zellen ebenfalls eine erhöhte Sensitivität gegenüber MMC und daraus resultierende erhöhte Chromosomenbruchraten. Interessanterweise sind die beschriebenen Mutationen bisher nur mit XP und CS in Verbindung gebracht worden und reflektieren keine der Mutationen der beiden bei Bogliolo et al. beschriebenen FA-Q Patienten. In beiden Arbeiten ist die verminderte Endonukleaseaktivität von XPF in Bezug auf FA untersucht und obwohl sich das Mutationsspektrum der drei Patienten unterscheidet, ist bei allen eine verminderte Endonukleaseaktivität zu beobachten. In Bogliolo et al. resultiert diese aus den Mutationen, die direkt in der Nuklease-Domäne des Proteins lokalisiert sind. Bei Kashiyama ergibt sie sich aus der gestörten Interaktion mit TFIIH. (Bogliolo et al., 2013; Kashiyama et al., 2013) Einen ähnlichen Fall wie für *XPF*, kennt man von *XPD*, der Komplementationsgruppe D von Xeroderma Pigmentosum. Unterschiedliche Mutationen in diesem Gen können ebenfalls zu drei verschiedenen Erkrankungen führen: XP, CS oder Trichothiodystrophie. (Cleaver et al., 2009)

Zudem ist XPF auf Grund seiner Funktion als Endonuklease sehr interessant im Kontext des FA/BRCA-Signalwegs. Die bisher beschriebenen FA-Gene sind entweder in der Schadenserkennung oder der DNA-Reparatur mittels HR oder TLS beteiligt. XPF und sein Interaktionspartner ERCC1 bilden zusammen eine Endonukleaseeinheit, deren Funktion im FA/BRCA-Signalweg die eigentliche Schadensbehebung darstellt. Im Rahmen vieler Studien hat man herausgefunden, dass XPF an verschiedenen DNA-Reparaturmechanismen beteiligt ist. (Manandhar et al., 2015) Je nach Reparaturweg schneidet die Endonuklease 5' oder 3' des DNA-Schadens. Bei NER erfolgt der Einschnitt 5' der geschädigten DNA-Stelle. (Mu et al., 1996; Sijbers et al., 1996) Findet die Reparatur mittels NHEJ statt, entfernt ERCC1-XPF die 3' non-homologen Enden der DSB innerhalb des alternativen-NHEJ Wegs. (Bennardo et al., 2008) In Bezug auf FA ist die Beteiligung an der ICL Schadenbeseitigung jedoch am wichtigsten. Vergleichbar mit NER erfolgt der Einschnitt der DNA 5' der Interstrangquervernetzung. Im Anschluss wird mittels seines Interaktionspartners *SLX4/FANCP* entweder die HR oder TLS eingeleitet. (Kuraoka et al., 2000) Trotz seiner

vielfältigen Funktion innerhalb verschiedenster Reparaturmechanismen, ist XPF ein Schlüsselprotein im FA/BRCA-Signalweg, da es durch seine Nukleaseaktivität die eigentliche DNA-Schadensreparatur erst einleitet.

Auf Grund seiner Zugehörigkeit zu den sog. „*downstream*“ Genen des FA/BRCA-Signalwegs, war *XPF* ein potenzielles Kandidatengen für familiär bedingten Brust- und Eierstockkrebs, so wie es auch bei *FANCN*, *FANCO* und *FANCD1* der Fall war. Jedoch bestätigen verschiedene Studien, dass der Anteil an monoallelischen Mutationen unter den betroffenen Familien mit Brust- und Eierstockkrebs sehr klein bis vernachlässigbar ist. Somit kann *XPF* als kausales Gen für die erbliche Variante dieser Erkrankungen ausgeschlossen werden. (Kohlhase et al., 2014; Osorio et al., 2013) Des Weiteren scheint *XPF* in der embryonalen Entwicklung eine wichtige Rolle zu spielen, da bisher kein Patient beschrieben wurde, der eine homozygote oder compound-heterozygote Nullmutation trägt. (Kashiyama et al., 2013) Im Gegensatz dazu konnte von Lehmann et al. mit Hilfe des CRISPR/Cas9 Systems eine stabile humane Fibroblastenzelllinie mit einer *XPF*-Defizienz hergestellt werden. (Lehmann et al., 2017) Es handelt sich hierbei jedoch um ein *in vitro* Experiment. So ist davon auszugehen, dass *XPF in vivo* weitere Aufgaben bzw. Interaktionen übernimmt, welche für das Überleben eines Organismus von großer Bedeutung zu sein scheinen. Zukünftige Studien werden nötig sein, um dieses Phänomen aufzuklären und zu testen, ob andere Endonukleasen wie Mus81/Eme1, SLX4/SLX1 oder FAN1 die Aufgaben im Fall einer *XPF*-Defizienz übernehmen können. (Lehmann et al., 2017)

4.2.2 DIE E3-UBIQUITIN LIGASE RFWD3

Mit Hilfe von WES wurde neben *XPF/FANCD1* auch das neueste FA-Gen, die RING-Typ E3-Ubiquitin Ligase *RFWD3*, alias *FANCD3*, identifiziert. (siehe 3.2.2) Ubiquitinierung, als eine Form der post-translationalen Modifikation, wurde im Zusammenhang mit DNA-Reparatur bereits häufig beschrieben. (Schwertman et al., 2016) Der Prozess der Ubiquitinierung ist durch drei Enzyme geregelt: das Ubiquitin-aktivierende Enzym (E1), das Ubiquitin-konjugierende Enzym (E2) und die Ubiquitin-Protein-Ligase (E3). (Hershko and Ciechanover, 1998) Zudem gibt es verschiedene Formen der Ubiquitinierung: Monoubiquitinierung wie bei *FANCD2/FANCD1*, Multiubiquitinierung an verschiedenen Lysinen des selben Zielproteins oder Polyubiquitinierung, wobei mehrere Ubiquitin-Moleküle in Form einer Kette an ein Lysin des Zielproteins angehängt werden. (Boisvert and Howlett, 2014) Darüber hinaus ist Ubiquitin in der Lage Polymere bzw. Ubiquitinketten zu bilden, die an acht verschiedenen Bindungsstellen entstehen können. Jedes siebte Lysin innerhalb von Ubiquitin (K6, K11, K27, K29, K33, K48 und K63) sowie das amino-terminale Methionin kann als Ubiquitin-Akzeptor dienen. (Komander, 2009; Komander and Rape, 2012) Diese interne Ubiquitinierung reguliert Protein-Protein-Interaktionen oder gibt das Signal für den proteasomalen Abbau. Die Ubiquitinierung an K11 und K48 bspw. dient als Markierung für den Abbau mittels des Proteasoms. Für eine Signaltransduktion bei DSBs wird hingegen K63 bevorzugt ubiquitiniert. (Elia et al., 2015a) Die unterschiedliche Funktion ist durch die strukturellen Gegebenheiten der polyubiquitinierten Lysine gegeben. (Komander, 2009) Im menschlichen Genom wurden bisher zwei E1-, ca. 40 E2- und > 600 E3-Enzyme charakterisiert. (Deshaies and Joazeiro, 2009)

Fehlerhafte oder fehlende Ubiquitinierung konnte bereits mit verschiedenen Erkrankungen assoziiert werden. So führen Mutationen in der Ubiquitinligase *PARKIN* zu einer bestimmten Form der Parkinson Erkrankung. (Shimura et al., 2000) Außerdem wurden Mutationen in der E3 Ligase *CULLIN7* mit der autosomal-rezessiven Wachstumsstörung 3M-Syndrom in Verbindung gebracht. (Huber et al., 2005) Ein weiteres Beispiel ist *BRCA1*, bei dem Mutationen in der RING-Domäne häufig in Brust- und Eierstockkrebs resultieren. (Maxwell and Domchek, 2012) Neben *BRCA1/FANCD3*, gibt es auch weitere Gene im FA-Signalweg (bspw. *FANCD1*, *FANCD2*, *UBE2T*, *FANCL*) die auf Grund einer fehlenden oder fehlerhaften Ubiquitinierung zu FA führen. (Dorsman et al., 2007; Hira et al., 2015; Meetei et al., 2003a; Rickman et al., 2015; Sims et al., 2007; Smogorzewska et al., 2007; Timmers et al., 2001; Virts et al., 2015)

Unsere Studie zeigt, dass biallelische Mutationen in *RFWD3* zu einer fehlerhaften DNA-Reparatur führen und in einem FA-Phänotyp resultieren. Bei den

compound-heterozygoten Mutationen unserer Patientin ist vor allem die Missense-Mutation c.1916 T>A (p.I639K) von Interesse, da die Duplikation von zwei Cytosinen an der Stelle c.204_205 zu einem vorzeitigen Abbau des Proteins führt (*nonsense-mediated decay*, NMD). Die Missense-Mutation ist in der WD40-Domäne am C-terminalen Ende des Proteins lokalisiert und verhindert dadurch Protein-Protein-Interaktionen, insbesondere mit RPA2 (*replication protein A2*) und eine Relokalisation von RFWD3 ans Chromatin. (Gong and Chen, 2011; Liu et al., 2011) Inano *et al.* untersuchte auf der Basis, der von uns gefundenen Missense-Mutation in *RFWD3* die Interaktion von RPA (vor allem RPA1 und RPA2) und RFWD3 näher. Dies geschah im Wesentlichen in einer etablierten Modellzelllinie, DT40 Zellen von *Gallus gallus*. Dabei stellten sie fest, dass RFWD3 und RPA einen Komplex bilden, der an ssDNA bindet. Dies steht im Gegensatz zu der Hypothese, dass RPA erst an ssDNA bindet und im Anschluss RFWD3 rekrutiert. (Gong and Chen, 2011; Liu et al., 2011) Erst kürzlich wurde von Elia *et al.*, in einem FA-unabhängigen Kontext, die Funktion von RFWD3 und RPA näher charakterisiert. Hierbei ist vor allem die Ubiquitinierung von RPA mittels RFWD3 hervorzuheben. (Elia et al., 2015b) Diese Interaktion ist bei der von uns beschriebenen Patientin gestört. Die Daten von Inano *et al.* stellen zudem einen Widerspruch zu Elia et al. dar. Anhand von untersuchten RPA-Foci 16-48 Stunden nach einem induzierten DNA-Schaden mittels MMC, konnten Inano *et al.* einen Abbau von polyubiquitinierten RPA feststellen, wohingegen Elia et al. diesen Abbau nicht beobachten konnten. (siehe 3.2.3) RPA ist neben RAD51, einer der Hauptkomponenten der Homologen Rekombination (HR), da es einzelsträngige DNA (ssDNA) stabilisiert, indem es sich an sie anlagert und somit einen Abbau verhindert (siehe 1.3.2.4 B).

Es stellte sich die Frage, ob RFWD3 - als ein Interaktionspartner von RPA - ebenfalls ein Teil der HR ist und welche Rolle es in diesem wichtigen Reparaturweg einnimmt. In den letzten zwei Jahren wurden einige Gene, die Bestandteil der HR sind, als FA-Gene identifiziert (bspw. *RAD51*, *BRCA1* oder *XRCC2*). (Ameziane et al., 2015; Park et al., 2016; Sawyer et al., 2015; Wang et al., 2015) Insgesamt kann man bis heute sieben FA-Gene zählen, die in verschiedenen Bereichen der HR involviert sind. *RAD51*, *RAD51C* und *XRCC2* sind vor allem an der Stranginvasion, D-Loop Bildung und der Auflösung der Holliday Junctions beteiligt, wohingegen RFWD3 eine frühere Rolle in der HR einzunehmen scheint, indem es ssDNA markiert. Die persistierenden RPA1-, RPA2- und *RAD51*-Foci in Patienten- und Δ RFWD3 DT40 Zellen geben einen weiteren Hinweis darauf, dass RFWD3 nicht nur mit RPA interagiert, sondern auch mit *RAD51*, dem Schlüsselprotein der HR. Diese Hypothese konnte vor allem die Gruppe um Inano *et al.* mit ihrer biochemischen Charakterisierung von RFWD3 in Bezug auf FA untermauern. *RAD51* wird ebenfalls von RFWD3 ubiquitiniert und damit für einen Abbau markiert. Für

diesen Mechanismus gibt es zwei mögliche Erklärungen: 1) Bei einer fehlenden Ubiquitinierung bilden RAD51 und RPA Filamente aus, woraus eine fehlerhafte HR resultieren könnte. 2) RPA und RAD51 müssen aus einer D-Loop Struktur am 3'-Ende der ssDNA entfernt werden, um ein Fortschreiten der DNA-Reparatur zu gewährleisten. Hierbei könnte RFWD3 die entscheidende Rolle spielen. Anhand der Foci-Daten, scheint RFWD3 RPA nicht durch RAD51 an ssDNA zu ersetzen. Dies ist mit Hilfe von BRCA2 reguliert. (Zelensky et al., 2014) Es scheint, als ob *RFWD3 downstream* von und epistatisch mit *BRCA2* interagiert. Die Daten erlauben die Hypothese, dass die Ubiquitinierung von RPA und RAD51 sowohl räumlich als auch zeitlich streng durch BRCA2 geregelt ist. So gehen Inano et al. davon aus, dass das aktivierte BRCA2-Protein während der DNA-Schadensantwort eine Phosphatase oder Deubiquitinase inhibiert, die die Aktivität von RFWD3 mindern könnten. (Inano et al. 2017, in revision, Molecular Cell)

An der Anzahl der Gene lässt sich erkennen, dass der FA/BRCA-Signalweg stark mit der HR verwoben ist. Dennoch wurden die meisten dieser Gene erst in den letzten Jahren als FA-Gene identifiziert. Mit Hilfe von WES konnte jedoch auch der geringe Anteil an Patienten mit Mutationen in diesen Genen zugeordnet werden. Außerdem weisen Patienten mit Defekten in den HR-Genen oft hypomorphe Mutationen auf. Dies könnte einen Hinweis darauf sein, dass andere Mutationen bereits embryonal lethal sind. Des Weiteren sind die meisten dieser Gene auch mit verschiedenen Krebserkrankungen, insbesondere erblichem Brust- und Eierstockkrebs, assoziiert. (Katsuki and Takata, 2016) Dennoch zeigen biallelische Mutationen in diesen Genen erstaunlicherweise kaum ein erhöhtes Krebsrisiko im Kindesalter oder eine verstärkte Neigung zu AML für FA-Patienten. Eine Ausnahme stellen hierbei *BRCA2* und *PALB2* dar. (Howlett et al., 2002; Reid et al., 2007) Aufgrund der reduzierten Penetranz der p.I639K Mutation in *RFWD3*, zeigt unsere Patientin bisher ebenfalls keine Tumorgenese. Dies ist vergleichbar mit Patienten der Komplementationsgruppe FA-O, FA-U, FA-R und FA-S. (Ameziane et al., 2015; Park et al., 2016; Sawyer et al., 2015; Shamseldin et al., 2012; Vaz et al., 2010) Es ist daher davon auszugehen, dass vor allem *BRCA2* und sein Interaktionspartner *PALB2* die verstärkte Neigung zu bösartigen Tumoren begünstigt, da sich das bei den anderen „*downstream*“ Genen nicht beobachten lässt. Interessanterweise konnte die Gruppe um Chung et al. einen SNP (rs4888262) in *RFWD3* mit einem erhöhten Risiko für Stammzell-basierten Hodenkrebs assoziieren. (Chung et al., 2013) Eine weitere Studie brachte den gleichen SNP mit einem erhöhten Risiko für Multiples Myelom in Verbindung. (Mitchell et al., 2016) Beide Studien könnten einen Hinweis für eine erhöhte Krebsdisposition bei *RFWD3* Mutationen geben, obgleich es sich nicht um Krebsarten handelt, die typischerweise bei FA auftreten. Es ist daher abzuwarten, was die kommende

Entwicklung unserer Patientin zeigt und ob weitere FA-Patienten gefunden werden, die der Komplementationgruppe FA-W zugeordnet werden können.

Mittels verschiedener Zellsysteme und einem weiteren *in vivo* Modell, der Maus, konnten wir zeigen, dass die E3-Ligase RFWD3 ein Bestandteil der HR ist und damit erheblich zum Verständnis des FA/BRCA-Signalwegs beiträgt. Weitere Studien werden nötig sein, um den exakten Mechanismus der Ubiquitinierung von RPA und RAD51 mittels RFWD3 aufzuklären. Dabei ist auch zu prüfen, ob es weitere Interaktoren gibt, die an diesem Prozess beteiligt sind. Außerdem ist es interessant zu untersuchen, ob die Deubiquitinase UCHL3, die für die Deubiquitinierung von RAD51 und der damit verbundenen Interaktion mit BRCA2 verantwortlich ist, auch RPA in Rahmen der HR deubiquitiniert. Damit würde UCHL3 den Gegenspieler von RFWD3 darstellen. Dies würde die o. g. These von Inano *et al.* untermauern, dass BRCA2 eine Phosphatase oder Deubiquitinase inhibiert, die die Aktivität von RFWD3 mindern könnten. Ferner ist *UCHL3* in meinen Augen ein potenzielles FA-Kandidatengen, das sich durch seine Interaktion mit RAD51 und dem bereits beschriebenen Zusammenhang mit Brustkrebs auszeichnet. (Luo et al., 2016)

5 REFERENZEN

AgoulNIK, A.I., Lu, B., Zhu, Q., Truong, C., Ty, M.T., Arango, N., Chada, K.K., and Bishop, C.E. (2002). A novel gene, Pog, is necessary for primordial germ cell proliferation in the mouse and underlies the germ cell deficient mutation, gcd. *Hum Mol Genet* 11, 3047-3053.

Alter, B.P. (2014). Fanconi anemia and the development of leukemia. *Best Pract Res Clin Haematol* 27, 214-221.

Alter BP, K.G. (1993-2015). Alter BP, and Kupfer G (1993–2015) Fanconi Anemia. In: Pagon RA, Adam MP, Ardinger HH, Wallace SE, Amemiya A, Bean LJH, Bird TD, Dolan CR, Fong CT, Smith RJH, Stephens K, editors. *GeneReviews®* [Internet]. Seattle (WA): University of Washington, Seattle. Available From [HTTP://WWW.NCBI.NLM.NIH.GOV/BOOKS/NBK1401/](http://www.ncbi.nlm.nih.gov/books/NBK1401/) Access date February 7, 2013.

Ameziane, N., May, P., Haitjema, A., van de Vrugt, H.J., van Rossum-Fikkert, S.E., Ristic, D., Williams, G.J., Balk, J., Rockx, D., Li, H., *et al.* (2015). A novel Fanconi anaemia subtype associated with a dominant-negative mutation in RAD51. *Nat Commun* 6.

Ameziane, N., Sie, D., Dentre, S., Ariyurek, Y., Kerkhoven, L., Joenje, H., Dorsman, J.C., Ylstra, B., Gille, J.J., Sistermans, E.A., *et al.* (2012). Diagnosis of fanconi anemia: mutation analysis by next-generation sequencing. *Anemia* 2012, 132856.

Apostolou S, Whitmore S A, Crawford J, Lennon G, Sutherland G R, Callen D F, Ianzano L, Savino M, D'Apolito M, Notarangelo A, *et al.* (1996). Positional cloning of the Fanconi anaemia group A gene. The Fanconi anaemia/breast cancer consortium. *Nat Genet* 14, 324-328.

Atanassov, B.S., Barrett, J.C., and Davis, B.J. (2005). Homozygous germ line mutation in exon 27 of murine Brca2 disrupts the Fancd2-Brca2 pathway in the homologous recombination-mediated DNA interstrand cross-links' repair but does not affect meiosis. *Genes, chromosomes & cancer* 44, 429-437.

Auerbach, A.D. (2009). Fanconi anemia and its diagnosis. *Mutat Res* 668, 4-10.

Bakker, S.T., de Winter, J.P., and te Riele, H. (2013). Learning from a paradox: recent insights into Fanconi anaemia through studying mouse models. *Dis Model Mech* 6, 40-47.

Bakker, S.T., Vrugt, H.J., Rooimans, M.A., Oostra, A.B., Steltenpool, J., and Delzenne-Goette, E. (2009). Fancm-deficient mice reveal unique features of Fanconi anemia complementation group M. *Hum Mol Genet* 18.

Bakker, S.T., Vrugt, H.J., Visser, J.A., Delzenne-Goette, E., Wal, A., and Berns, M.A. (2012). Fancf-deficient mice are prone to develop ovarian tumours. *J Pathol* 226.

Bamshad, M.J., Ng, S.B., Bigham, A.W., Tabor, H.K., Emond, M.J., Nickerson, D.A., and Shendure, J. (2011). Exome sequencing as a tool for Mendelian disease gene discovery. *Nat Rev Genet* 12, 745-755.

- Barber, L.J., Youds, J.L., Ward, J.D., McIlwraith, M.J., O'Neil, N.J., Petalcorin, M.I., Martin, J.S., Collis, S.J., Cantor, S.B., Auclair, M., *et al.* (2008). RTEL1 maintains genomic stability by suppressing homologous recombination. *Cell* 135, 261-271.
- Bennardo, N., Cheng, A., Huang, N., and Stark, J.M. (2008). Alternative-NHEJ is a mechanistically distinct pathway of mammalian chromosome break repair. *PLoS Genet* 4, e1000110.
- Bernstein, C., Prasad, A.R., Nfonsam, V., and Bernstein, H. (2013). DNA Damage, DNA Repair and Cancer.
- Bishop, C.L., Strong, K.A., and Dimmock, D.P. (2017). Choices of incidental findings of individuals undergoing genome wide sequencing, a single center's experience. *Clinical genetics* 91, 137-140.
- Bluteau, D., Masliah-Planchon, J., Clairmont, C., Rousseau, A., Ceccaldi, R., Dubois d'Enghien, C., Bluteau, O., Cucuini, W., Gachet, S., Peffault de Latour, R., *et al.* (2016). Biallelic inactivation of REV7 is associated with Fanconi anemia. *J Clin Invest* 126, 3580-3584.
- Bogliolo, M., Schuster, B., Stoepker, C., Derkunt, B., Su, Y., and Raams, A. (2013). Mutations in ERCC4, encoding the DNA-repair endonuclease XPF, cause Fanconi anemia. *Am J Hum Genet* 92.
- Bogliolo, M., and Surrallés, J. (2015). Fanconi anemia: a model disease for studies on human genetics and advanced therapeutics. *Current Opinion in Genetics & Development* 33, 32-40.
- Boisvert, R.A., and Howlett, N.G. (2014). The Fanconi anemia ID2 complex: dueling axes at the crossroads. *Cell Cycle* 13, 2999-3015.
- Bowne, S.J., Humphries, M.M., Sullivan, L.S., Kenna, P.F., Tam, L.C., Kiang, A.S., Campbell, M., Weinstock, G.M., Koboldt, D.C., Ding, L., *et al.* (2011). A dominant mutation in RPE65 identified by whole-exome sequencing causes retinitis pigmentosa with choroidal involvement. *Eur J Hum Genet* 19, 1074-1081.
- Brett, M., McPherson, J., Zang, Z.J., Lai, A., Tan, E.S., Ng, I., Ong, L.C., Cham, B., Tan, P., Rozen, S., *et al.* (2014). Massively parallel sequencing of patients with intellectual disability, congenital anomalies and/or autism spectrum disorders with a targeted gene panel. *PLoS One* 9, e93409.
- Callen, E., Casado, J.A., Tischkowitz, M.D., Bueren, J.A., Creus, A., Marcos, R., Dasi, A., Estella, J.M., Munoz, A., Ortega, J.J., *et al.* (2005). A common founder mutation in FANCA underlies the world's highest prevalence of Fanconi anemia in Gypsy families from Spain. *Blood* 105, 1946-1949.
- Callen, E., and Surrallés, J. (2004). Telomere dysfunction in genome instability syndromes. *Mutat Res* 567, 85-104.
- Chen, M., Tomkins, D.J., Auerbach, W., McKerlie, C., Youssoufian, H., Liu, L., Gan, O., Carreau, M., Auerbach, A., Groves, T., *et al.* (1996). Inactivation of Fac in mice produces inducible chromosomal instability and reduced fertility reminiscent of Fanconi anaemia. *Nat Genet* 12, 448-451.
- Cheng, N.C., Vrugt, H.J., Valk, M.A., Oostra, A.B., Krimpenfort, P., and de, V.Y. (2000). Mice with a targeted disruption of the Fanconi anemia homolog Fanca. *Hum Mol Genet* 9.

- Chung, C.C., Kanetsky, P.A., Wang, Z., Hildebrandt, M.A.T., Koster, R., Skotheim, R.I., Kratz, C.P., Turnbull, C., Cortessis, V.K., Bakken, A.C., *et al.* (2013). Meta-analysis identifies four new loci associated with testicular germ cell tumor. *Nature genetics* 45, 680-685.
- Ciccina, A., and Elledge, S.J. (2010). The DNA damage response: making it safe to play with knives. *Mol Cell* 40, 179-204.
- Clarke, A.A., Philpott, N.J., Gordon-Smith, E.C., and Rutherford, T.R. (1997). The sensitivity of Fanconi anaemia group C cells to apoptosis induced by mitomycin C is due to oxygen radical generation, not DNA crosslinking. *Br J Haematol* 96, 240-247.
- Cleaver, J.E., Lam, E.T., and Revet, I. (2009). Disorders of nucleotide excision repair: the genetic and molecular basis of heterogeneity. *Nat Rev Genet* 10, 756-768.
- Cohn, M.A., Kowal, P., Yang, K., Haas, W., Huang, T.T., Gygi, S.P., and D'Andrea, A.D. (2007). A UAF1-containing multisubunit protein complex regulates the Fanconi anemia pathway. *Mol Cell* 28, 786-797.
- Collis, S.J., Ciccina, A., Deans, A.J., Horejsi, Z., Martin, J.S., Maslen, S.L., Skehel, J.M., Elledge, S.J., West, S.C., and Boulton, S.J. (2008). FANCM and FAAP24 function in ATR-mediated checkpoint signaling independently of the fanconi anemia core complex. *Mol Cell* 32, 313-324.
- Crossan, G.P., van der Weyden, L., Rosado, I.V., Langevin, F., Gaillard, P.H., McIntyre, R.E., Gallagher, F., Kettunen, M.I., Lewis, D.Y., Brindle, K., *et al.* (2011). Disruption of mouse Slx4, a regulator of structure-specific nucleases, phenocopies Fanconi anemia. *Nat Genet* 43, 147-152.
- Cumming, R.C., Lightfoot, J., Beard, K., Youssoufian, H., O'Brien, P.J., and Buchwald, M. (2001). Fanconi anemia group C protein prevents apoptosis in hematopoietic cells through redox regulation of GSTP1. *Nat Med* 7, 814-820.
- de Winter, J.P., Waisfisz, Q., Rooimans, M.A., van Berkel, C.G., Bosnoyan-Collins, L., Alon, N., Carreau, M., Bender, O., Demuth, I., Schindler, D., *et al.* (1998). The Fanconi anaemia group G gene FANCG is identical with XRCC9. *Nat Genet* 20, 281-283.
- Deans, B., Griffin, C.S., Maconochie, M., and Thacker, J. (2000). Xrcc2 is required for genetic stability, embryonic neurogenesis and viability in mice. *EMBO J* 19, 6675-6685.
- Deshaies, R.J., and Joazeiro, C.A. (2009). RING domain E3 ubiquitin ligases. *Annu Rev Biochem* 78, 399-434.
- Dong, H., Nebert, D.W., Bruford, E.A., Thompson, D.C., Joenje, H., and Vasiliou, V. (2015). Update of the human and mouse Fanconi anemia genes. *Hum Genomics* 9, 1-10.
- Dorsman, J.C., Levitus, M., Rockx, D., Rooimans, M.A., Oostra, A.B., Haitjema, A., Bakker, S.T., Steltenpool, J., Schuler, D., Mohan, S., *et al.* (2007). Identification of the Fanconi anemia complementation group I gene, FANCI. *Cell Oncol* 29, 211-218.
- Douwel, D.K., Boonen, R.A.C.M., Long, D.T., Szypowska, A.A., Räsche, M., Walter, J.C., and Knipscheer, P. (2014). XPF-ERCC1 acts in unhooking DNA interstrand crosslinks in cooperation with FANCD2 and FANCP/SLX4. *Molecular cell* 54, 460-471.

- Du, W., Adam, Z., Rani, R., Zhang, X., and Pang, Q. (2008). Oxidative stress in Fanconi anemia hematopoiesis and disease progression. *Antioxidants & redox signaling* 10, 1909-1921.
- Dutrillaux, B., Aurias, A., Dutrillaux, A.M., Burriot, D., and Prieur, M. (1982). The cell cycle of lymphocytes in Fanconi anemia. *Human genetics* 62, 327-332.
- Elia, A.E., Boardman, A.P., Wang, D.C., Huttlin, E.L., Everley, R.A., Dephoure, N., Zhou, C., Koren, I., Gygi, S.P., and Elledge, S.J. (2015a). Quantitative Proteomic Atlas of Ubiquitination and Acetylation in the DNA Damage Response. *Mol Cell* 59, 867-881.
- Elia, Andrew E.H., Wang, David C., Willis, Nicholas A., Boardman, Alexander P., Hajdu, I., Adeyemi, Richard O., Lowry, E., Gygi, Steven P., Scully, R., and Elledge, Stephen J. (2015b). RFWD3-Dependent Ubiquitination of RPA Regulates Repair at Stalled Replication Forks. *Mol Cell* 60, 280-293.
- Fanconi, G. (1927). Familiäre infantile perniziösaartige Anämie (perniziöses Blutbild und Konstitution). In *Jahrbuch für Kinderheilkunde und physische Erziehung* (Wien), pp. 257-280.
- Freie, B., Li, X., Ciccone, S.L., Nawa, K., Cooper, S., Vogelweid, C., Schantz, L., Haneline, L.S., Orazi, A., Broxmeyer, H.E., *et al.* (2003). Fanconi anemia type C and p53 cooperate in apoptosis and tumorigenesis. *Blood* 102, 4146-4152.
- Fu, C., Begum, K., and Overbeek, P.A. (2016). Primary Ovarian Insufficiency Induced by Fanconi Anemia E Mutation in a Mouse Model. *PLoS ONE* 11, e0144285.
- Fullwood, M.J., Wei, C.-L., Liu, E.T., and Ruan, Y. (2009). Next-generation DNA sequencing of paired-end tags (PET) for transcriptome and genome analyses. *Genome research* 19, 521-532.
- Garaycoechea, J.I., and Patel, K.J. (2014). Why does the bone marrow fail in Fanconi anemia? *Blood* 123.
- Garcia-Higuera, I., Taniguchi, T., Ganesan, S., Meyn, M.S., Timmers, C., Hejna, J., Grompe, M., and D'Andrea, A.D. (2001). Interaction of the Fanconi anemia proteins and BRCA1 in a common pathway. *Mol Cell* 7, 249-262.
- Gille, J.J., Floor, K., Kerkhoven, L., Ameziane, N., Joenje, H., and Winter, J.P. (2012). Diagnosis of Fanconi anemia: mutation analysis by multiplex ligation-dependent probe amplification and PCR-based Sanger sequencing. *Anemia* 2012.
- Gluckman, E., Broxmeyer, H.A., Auerbach, A.D., Friedman, H.S., Douglas, G.W., Devergie, A., Esperou, H., Thierry, D., Socie, G., Lehn, P., *et al.* (1989). Hematopoietic reconstitution in a patient with Fanconi's anemia by means of umbilical-cord blood from an HLA-identical sibling. *The New England journal of medicine* 321, 1174-1178.
- Godthelp, B.C., Wiegant, W.W., Waisfisz, Q., Medhurst, A.L., Arwert, F., Joenje, H., and Zdzienicka, M.Z. (2006). Inducibility of nuclear Rad51 foci after DNA damage distinguishes all Fanconi anemia complementation groups from D1/BRCA2. *Mutat Res* 594, 39-48.
- Gong, Z., and Chen, J. (2011). E3 Ligase RFWD3 Participates in Replication Checkpoint Control. *J Biol Chem* 286, 22308-22313.

- Gottlieb, T.M., and Jackson, S.P. (1993). The DNA-dependent protein kinase: requirement for DNA ends and association with Ku antigen. *Cell* 72, 131-142.
- Gregg, S.Q., Robinson, A.R., and Niedernhofer, L.J. (2011). Physiological consequences of defects in ERCC1-XPF DNA repair endonuclease. *DNA repair* 10, 781-791.
- Haber, J.E. (2000). Partners and pathways repairing a double-strand break. *Trends in genetics : TIG* 16, 259-264.
- Hakem, R., Pompa, J.L., and Mak, T.W. (1998). Developmental studies of Brca1 and Brca2 knock-out mice. *J Mammary Gland Biol Neoplasia* 3.
- Hanenberg, H., Batish, S.D., Pollok, K.E., Vieten, L., Verlander, P.C., Leurs, C., Cooper, R.J., Gottsche, K., Haneline, L., Clapp, D.W., *et al.* (2002). Phenotypic correction of primary Fanconi anemia T cells with retroviral vectors as a diagnostic tool. *Experimental hematology* 30, 410-420.
- Hartlerode, A.J., and Scully, R. (2009). Mechanisms of double-strand break repair in somatic mammalian cells. *The Biochemical journal* 423, 157-168.
- Hershko, A., and Ciechanover, A. (1998). THE UBIQUITIN SYSTEM. *Annu Rev Biochem* 67, 425-479.
- Hira, A., Yabe, H., Yoshida, K., Okuno, Y., Shiraishi, Y., Chiba, K., Tanaka, H., Miyano, S., Nakamura, J., Kojima, S., *et al.* (2013). Variant ALDH2 is associated with accelerated progression of bone marrow failure in Japanese Fanconi anemia patients. *Blood* 122, 3206-3209.
- Hira, A., Yoshida, K., Sato, K., Okuno, Y., Shiraishi, Y., Chiba, K., Tanaka, H., Miyano, S., Shimamoto, A., Tahara, H., *et al.* (2015). Mutations in the Gene Encoding the E2 Conjugating Enzyme UBE2T Cause Fanconi Anemia. *The American Journal of Human Genetics* 96, 1001-1007.
- Houghtaling, S., Granville, L., Akkari, Y., Torimaru, Y., Olson, S., Finegold, M., and Grompe, M. (2005). Heterozygosity for p53 (Trp53+/-) accelerates epithelial tumor formation in fanconi anemia complementation group D2 (Fancd2) knockout mice. *Cancer research* 65, 85-91.
- Houghtaling, S., Timmers, C., Noll, M., Finegold, M.J., Jones, S.N., Meyn, M.S., and Grompe, M. (2003). Epithelial cancer in Fanconi anemia complementation group D2 (Fancd2) knockout mice. *Genes Dev* 17, 2021-2035.
- Howlett, N.G., Taniguchi, T., Olson, S., Cox, B., Waisfisz, Q., De Die-Smulders, C., Persky, N., Grompe, M., Joenje, H., Pals, G., *et al.* (2002). Biallelic inactivation of BRCA2 in Fanconi anemia. *Science* 297, 606-609.
- Huang, Y., Leung, J.W., Lowery, M., Matsushita, N., Wang, Y., Shen, X., Huong, D., Takata, M., Chen, J., and Li, L. (2014). Modularized functions of the Fanconi anemia core complex. *Cell reports* 7, 1849-1857.
- Huber, C., Dias-Santagata, D., Glaser, A., O'Sullivan, J., Brauner, R., Wu, K., Xu, X., Pearce, K., Wang, R., Uziel, M.L.G., *et al.* (2005). Identification of mutations in CUL7 in 3-M syndrome. *Nat Genet* 37, 1119-1124.

- Joenje, H., Arwert, F., Eriksson, A.W., de Koning, H., and Oostra, A.B. (1981). Oxygen-dependence of chromosomal aberrations in Fanconi's anaemia. *Nature* 290, 142-143.
- Kalb, R., Duerr, M., Wagner, M., Herterich, S., Gross, M., Digweed, M., Joenje, H., Hoehn, H., and Schindler, D. (2004). Lack of sensitivity of primary Fanconi's anemia fibroblasts to UV and ionizing radiation. *Radiation research* 161, 318-325.
- Kalb, R., Neveling, K., Hoehn, H., Schneider, H., Linka, Y., Batish, S.D., Hunt, C., Berwick, M., Callen, E., Surralles, J., *et al.* (2007). Hypomorphic mutations in the gene encoding a key Fanconi anemia protein, FANCD2, sustain a significant group of FA-D2 patients with severe phenotype. *Am J Hum Genet* 80, 895-910.
- Kalia, S.S., Adelman, K., Bale, S.J., Chung, W.K., Eng, C., Evans, J.P., Herman, G.E., Hufnagel, S.B., Klein, T.E., Korf, B.R., *et al.* (2016). Recommendations for reporting of secondary findings in clinical exome and genome sequencing, 2016 update (ACMG SF v2.0): a policy statement of the American College of Medical Genetics and Genomics. *Genetics in medicine : official journal of the American College of Medical Genetics*.
- Kashiyama, K., Nakazawa, Y., Pilz, Daniela T., Guo, C., Shimada, M., Sasaki, K., Fawcett, H., Wing, Jonathan F., Lewin, Susan O., Carr, L., *et al.* (2013). Malfunction of Nuclease ERCC1-XPF Results in Diverse Clinical Manifestations and Causes Cockayne Syndrome, Xeroderma Pigmentosum, and Fanconi Anemia. *American journal of human genetics* 92, 807-819.
- Kato, Y., Alavattam, K.G., Sin, H.-S., Meetei, A.R., Pang, Q., Andreassen, P.R., and Namekawa, S.H. (2015). FANCB is essential in the male germline and regulates H3K9 methylation on the sex chromosomes during meiosis. *Human molecular genetics* 24, 5234-5249.
- Katsuki, Y., and Takata, M. (2016). Defects in homologous recombination repair behind the human diseases: FA and HBOC. *Endocrine-Related Cancer* 23, T19-T37.
- Khurana, E., Lam, H.Y., Cheng, C., Carriero, N., Cayting, P., and Gerstein, M.B. (2010). Segmental duplications in the human genome reveal details of pseudogene formation. *Nucleic Acids Res* 38, 6997-7007.
- Kim, Y., Lach, F.P., Desetty, R., Hanenberg, H., Auerbach, A.D., and Smogorzewska, A. (2011). Mutations of the SLX4 gene in Fanconi anemia. *Nat Genet* 43, 142-146.
- Kitao, H., and Takata, M. (2011). Fanconi anemia: a disorder defective in the DNA damage response. *International journal of hematology* 93, 417-424.
- Knies, K., Schuster, B., Ameziane, N., Rooimans, M., Bettecken, T., de Winter, J., and Schindler, D. (2012). Genotyping of Fanconi Anemia Patients by Whole Exome Sequencing: Advantages and Challenges. *PLoS One* 7, e52648.
- Kohlhase, S., Bogdanova, N.V., Schürmann, P., Bermisheva, M., Khusnutdinova, E., Antonenkova, N., Park-Simon, T.-W., Hillemanns, P., Meyer, A., Christiansen, H., *et al.* (2014). Mutation Analysis of the ERCC4/FANCD1 Gene in Hereditary Breast Cancer. *PLOS ONE* 9, e85334.
- Komander, D. (2009). The emerging complexity of protein ubiquitination. *Biochemical Society Transactions* 37, 937-953.
- Komander, D., and Rape, M. (2012). The ubiquitin code. *Annu Rev Biochem* 81, 203-229.

Kubbies, M., Schindler, D., Hoehn, H., Schinzel, A., and Rabinovitch, P.S. (1985). Endogenous blockage and delay of the chromosome cycle despite normal recruitment and growth phase explain poor proliferation and frequent edomitosis in Fanconi anemia cells. *American journal of human genetics* 37, 1022-1030.

Kuraoka, I., Kobertz, W.R., Ariza, R.R., Biggerstaff, M., Essigmann, J.M., and Wood, R.D. (2000). Repair of an interstrand DNA cross-link initiated by ERCC1-XPF repair/recombination nuclease. *J Biol Chem* 275, 26632-26636.

Kutler, D.I., Auerbach, A.D., Satagopan, J., Giampietro, P.F., Batish, S.D., Huvos, A.G., Goberdhan, A., Shah, J.P., and Singh, B. (2003). High incidence of head and neck squamous cell carcinoma in patients with Fanconi anemia. *Archives of otolaryngology--head & neck surgery* 129, 106-112.

Kuznetsov, S., Pellegrini, M., Shuda, K., Fernandez-Capetillo, O., Liu, Y., Martin, B.K., Burkett, S., Southon, E., Pati, D., Tessarollo, L., *et al.* (2007). RAD51C deficiency in mice results in early prophase I arrest in males and sister chromatid separation at metaphase II in females. *J Cell Biol* 176, 581-592.

Langevin, F., Crossan, G.P., Rosado, I.V., Arends, M.J., and Patel, K.J. (2011). Fancd2 counteracts the toxic effects of naturally produced aldehydes in mice. *Nature* 475, 53-58.

Lehmann, J., Seebode, C., Smolorz, S., Schubert, S., and Emmert, S. (2017). XPF knockout via CRISPR/Cas9 reveals that ERCC1 is retained in the cytoplasm without its heterodimer partner XPF. *Cellular and Molecular Life Sciences*, 1-14.

Lelieveld, S.H., Veltman, J.A., and Gilissen, C. (2016). Novel bioinformatic developments for exome sequencing. *Human genetics* 135, 603-614.

Levitus, M., Waisfisz, Q., Godthelp, B.C., de Vries, Y., Hussain, S., Wiegant, W.W., Elghalbzouri-Maghrani, E., Steltenpool, J., Rooimans, M.A., Pals, G., *et al.* (2005). The DNA helicase BRIP1 is defective in Fanconi anemia complementation group J. *Nat Genet* 37, 934-935.

Levran, O., Attwooll, C., Henry, R.T., Milton, K.L., Neveling, K., Rio, P., Batish, S.D., Kalb, R., Velleuer, E., Barral, S., *et al.* (2005). The BRCA1-interacting helicase BRIP1 is deficient in Fanconi anemia. *Nat Genet* 37, 931-933.

Lieber, M.R., Ma, Y., Pannicke, U., and Schwarz, K. (2003). Mechanism and regulation of human non-homologous DNA end-joining. *Nat Rev Mol Cell Biol* 4, 712-720.

Lim, D.S., and Hasty, P. (1996). A mutation in mouse rad51 results in an early embryonic lethal that is suppressed by a mutation in p53. *Mol Cell Biol* 16, 7133-7143.

Lim, E.T., Würtz, P., Havulinna, A.S., Palta, P., Tukiainen, T., Rehnström, K., Esko, T., Mägi, R., Inouye, M., Lappalainen, T., *et al.* (2014). Distribution and Medical Impact of Loss-of-Function Variants in the Finnish Founder Population. *PLoS genetics* 10, e1004494.

Liu, S., Chu, J., Yucer, N., Leng, M., Wang, S.-Y., Chen, B.P.C., Hittelman, W.N., and Wang, Y. (2011). RING Finger and WD Repeat Domain 3 (RFWD3) Associates with Replication Protein A (RPA) and Facilitates RPA-mediated DNA Damage Response. *J Biol Chem* 286, 22314-22322.

- Liu, T., Ghosal, G., Yuan, J., Chen, J., and Huang, J. (2010). FAN1 Acts with FANCI-FANCD2 to Promote DNA Interstrand Cross-Link Repair. *Science* 329, 693-696.
- Lobitz, S., and Velleuer, E. (2006). Guido Fanconi (1892-1979): a jack of all trades. *Nat Rev Cancer* 6, 893-898.
- Lohmann, K., and Klein, C. (2014). Next Generation Sequencing and the Future of Genetic Diagnosis. *Neurotherapeutics* 11, 699-707.
- Luo, K., Li, L., Li, Y., Wu, C., Yin, Y., Chen, Y., Deng, M., Nowsheen, S., Yuan, J., and Lou, Z. (2016). A phosphorylation–deubiquitination cascade regulates the BRCA2–RAD51 axis in homologous recombination. *Genes & development* 30, 2581-2595.
- Machida, Y.J., Machida, Y., Chen, Y., Gurtan, A.M., Kupfer, G.M., and D'Andrea, A.D. (2006). UBE2T is the E2 in the Fanconi anemia pathway and undergoes negative autoregulation. *Mol Cell* 23.
- Majewski, J., Schwartzentruber, J., Lalonde, E., Montpetit, A., and Jabado, N. (2011). What can exome sequencing do for you? *Journal of medical genetics* 48, 580-589.
- Mamrak, N.E., Shimamura, A., and Howlett, N.G. (2016). Recent discoveries in the molecular pathogenesis of the inherited bone marrow failure syndrome Fanconi anemia. *Blood reviews*.
- Manandhar, M., Boulware, K.S., and Wood, R.D. (2015). The ERCC1 and ERCC4 (XPF) genes and gene products. *Gene* 569, 153-161.
- Mardis, E.R. (2008). The impact of next-generation sequencing technology on genetics. *Trends in genetics : TIG* 24, 133-141.
- Margulies, M., Egholm, M., Altman, W.E., Attiya, S., Bader, J.S., Bemben, L.A., Berka, J., Braverman, M.S., Chen, Y.J., Chen, Z., *et al.* (2005). Genome sequencing in microfabricated high-density picolitre reactors. *Nature* 437, 376-380.
- Matsuzaki, K., Borel, V., Adelman, C.A., Schindler, D., and Boulton, S.J. (2015). FANCI suppresses microsatellite instability and lymphomagenesis independent of the Fanconi anemia pathway. *Genes Dev* 29, 2532-2546.
- Maxwell, K.N., and Domchek, S.M. (2012). Cancer treatment according to BRCA1 and BRCA2 mutations. *Nature reviews. Clinical oncology* 9, 520-528.
- McAllister, K.A., Houle, C.D., Malphurs, J., Ward, T., Collins, N.K., Gersch, W., Wharey, L., Seely, J.C., Betz, L., Bennett, L.M., *et al.* (2006). Spontaneous and irradiation-induced tumor susceptibility in BRCA2 germline mutant mice and cooperative effects with a p53 germline mutation. *Toxicologic pathology* 34, 187-198.
- McVey, M., and Lee, S.E. (2008). MMEJ repair of double-strand breaks (director's cut): deleted sequences and alternative endings. *Trends in genetics : TIG* 24, 529-538.
- Meetei, A.R., de Winter, J.P., Medhurst, A.L., Wallisch, M., Waisfisz, Q., van de Vrugt, H.J., Oostra, A.B., Yan, Z., Ling, C., Bishop, C.E., *et al.* (2003a). A novel ubiquitin ligase is deficient in Fanconi anemia. *Nat Genet* 35, 165-170.

- Meetei, A.R., Levitus, M., Xue, Y., Medhurst, A.L., Zwaan, M., Ling, C., Rooimans, M.A., Bier, P., Hoatlin, M., Pals, G., *et al.* (2004). X-linked inheritance of Fanconi anemia complementation group B. *Nat Genet* 36, 1219-1224.
- Meetei, A.R., Medhurst, A.L., Ling, C., Xue, Y., Singh, T.R., Bier, P., Steltenpool, J., Stone, S., Dokal, I., Mathew, C.G., *et al.* (2005). A human ortholog of archaeal DNA repair protein Hef is defective in Fanconi anemia complementation group M. *Nat Genet* 37, 958-963.
- Meetei, A.R., Sechi, S., Wallisch, M., Yang, D., Young, M.K., Joenje, H., Hoatlin, M.E., and Wang, W. (2003b). A multiprotein nuclear complex connects Fanconi anemia and Bloom syndrome. *Mol Cell Biol* 23, 3417-3426.
- Mitchell, J.S., Li, N., Weinhold, N., Försti, A., Ali, M., van Duin, M., Thorleifsson, G., Johnson, D.C., Chen, B., Halvarsson, B.-M., *et al.* (2016). Genome-wide association study identifies multiple susceptibility loci for multiple myeloma. *Nature Communications* 7, 12050.
- Motycka, T.A., Bessho, T., Post, S.M., Sung, P., and Tomkinson, A.E. (2004). Physical and functional interaction between the XPF/ERCC1 endonuclease and hRad52. *J Biol Chem* 279, 13634-13639.
- Mu, D., Hsu, D.S., and Sancar, A. (1996). Reaction mechanism of human DNA repair excision nuclease. *J Biol Chem* 271, 8285-8294.
- Muller, A., and Fishel, R. (2002). Mismatch repair and the hereditary non-polyposis colorectal cancer syndrome (HNPCC). *Cancer investigation* 20, 102-109.
- Murai, J., Yang, K., Dejsuphong, D., Hirota, K., Takeda, S., and D'Andrea, A.D. (2011). The USP1/UAF1 complex promotes double-strand break repair through homologous recombination. *Mol Cell Biol* 31, 2462-2469.
- Neitzel, H., Kühl, J.-S., Gerlach, A., Ebell, W., and Tönnies, H. (2007). Clonal Chromosomal Aberrations in Bone Marrow Cells of Fanconi Anemia Patients: Results and Implications. In *Fanconi Anemia. A Paradigmatic Disease for the Understanding of Cancer and Aging.*, M. Schmid, ed. (Basel: Karger), pp. 79-94.
- Neveling, K., Endt, D., Hoehn, H., and Schindler, D. (2009). Genotype-phenotype correlations in Fanconi anemia. *Mutation Research/Fundamental and Molecular Mechanisms of Mutagenesis* 668, 73-91.
- Ng, S.B., Buckingham, K.J., Lee, C., Bigham, A.W., Tabor, H.K., Dent, K.M., Huff, C.D., Shannon, P.T., Jabs, E.W., Nickerson, D.A., *et al.* (2010). Exome sequencing identifies the cause of a mendelian disorder. *Nat Genet* 42, 30-35.
- Niedernhofer, L.J., Garinis, G.A., Raams, A., Lalai, A.S., Robinson, A.R., Appeldoorn, E., Odijk, H., Oostendorp, R., Ahmad, A., van Leeuwen, W., *et al.* (2006). A new progeroid syndrome reveals that genotoxic stress suppresses the somatotroph axis. *Nature* 444, 1038-1043.
- Nijman, S.M., Huang, T.T., Dirac, A.M., Brummelkamp, T.R., Kerkhoven, R.M., D'Andrea, A.D., and Bernards, R. (2005). The deubiquitinating enzyme USP1 regulates the Fanconi anemia pathway. *Mol Cell* 17, 331-339.

- Noda, T., Takahashi, A., Kondo, N., Mori, E., Okamoto, N., Nakagawa, Y., Ohnishi, K., Zdzienicka, M.Z., Thompson, L.H., Helleday, T., *et al.* (2011). Repair pathways independent of the Fanconi anemia nuclear core complex play a predominant role in mitigating formaldehyde-induced DNA damage. *Biochem Biophys Res Commun* 404, 206-210.
- Oostra, A.B., Nieuwint, A.W.M., Joenje, H., and de Winter, J.P. (2012). Diagnosis of Fanconi Anemia: Chromosomal Breakage Analysis. *Anemia* 2012, 238731.
- Osorio, A., Bogliolo, M., Fernández, V., Barroso, A., de la Hoya, M., Caldés, T., Lasa, A., Ramón y Cajal, T., Santamariña, M., Vega, A., *et al.* (2013). Evaluation of Rare Variants in the New Fanconi Anemia Gene ERCC4 (FANCC) as Familial Breast/Ovarian Cancer Susceptibility Alleles. *Human mutation* 34, 1615-1618.
- Pagano, G., Talamanca, A.A., Castello, G., d'Ischia, M., Pallardo, F.V., Petrovic, S., Porto, B., Tiano, L., and Zatterale, A. (2013). From clinical description, to in vitro and animal studies, and backward to patients: oxidative stress and mitochondrial dysfunction in Fanconi anemia. *Free radical biology & medicine* 58, 118-125.
- Pang, Q., Keeble, W., Christianson, T.A., Faulkner, G.R., and Bagby, G.C. (2001). FANCC interacts with Hsp70 to protect hematopoietic cells from IFN-gamma/TNF-alpha-mediated cytotoxicity. *EMBO J* 20, 4478-4489.
- Park, J.Y., Virts, E.L., Jankowska, A., Wiek, C., Othman, M., Chakraborty, S.C., Vance, G.H., Alkuraya, F.S., Hanenberg, H., and Andreassen, P.R. (2016). Complementation of hypersensitivity to DNA interstrand crosslinking agents demonstrates that XRCC2 is a Fanconi anaemia gene. *J Med Genet* 53, 672-680.
- Parmar, K., D'Andrea, A., and Niedernhofer, L.J. (2009). Mouse models of Fanconi anemia. *Mutation research* 668, 133-140.
- Pettan-Brewer, C., Morton, J., Cullen, S., Enns, L., Kehrl, K.R.M., Sidorova, J., Goh, J., Coil, R., and Ladiges, W.C. (2012). Tumor growth is suppressed in mice expressing a truncated XRCC1 protein. *American journal of cancer research* 2, 168-177.
- Rajendra, E., Oestergaard, V.H., Langevin, F., Wang, M., Dornan, G.L., Patel, K.J., and Passmore, L.A. (2014). The genetic and biochemical basis of FANCD2 monoubiquitination. *Mol Cell* 54, 858-869.
- Rantakari, P., Nikkila, J., Jokela, H., Ola, R., Pylkas, K., Lagerbohm, H., Sainio, K., Poutanen, M., and Winqvist, R. (2010). Inactivation of Palb2 gene leads to mesoderm differentiation defect and early embryonic lethality in mice. *Hum Mol Genet* 19, 3021-3029.
- Rehm, H.L., Bale, S.J., Bayrak-Toydemir, P., Berg, J.S., Brown, K.K., Deignan, J.L., Friez, M.J., Funke, B.H., Hegde, M.R., Lyon, E., *et al.* (2013). ACMG clinical laboratory standards for next-generation sequencing. *Genetics in medicine : official journal of the American College of Medical Genetics* 15, 733-747.
- Reid, S., Schindler, D., Hanenberg, H., Barker, K., Hanks, S., Kalb, R., Neveling, K., Kelly, P., Seal, S., Freund, M., *et al.* (2007). Biallelic mutations in PALB2 cause Fanconi anemia subtype FA-N and predispose to childhood cancer. *Nat Genet* 39, 162-164.
- Rickman, K.A., Lach, F.P., Abhyankar, A., Donovan, F.X., Sanborn, E.M., Kennedy, J.A., Sougnez, C., Gabriel, S.B., Elemento, O., Chandrasekharappa, S.C., *et al.* (2015). Deficiency of UBE2T, the

E2 Ubiquitin Ligase Necessary for FANCD2 and FANCI Ubiquitination, Causes FA-T Subtype of Fanconi Anemia. *Cell reports* 12, 35-41.

Rosenberg, P.S., Greene, M.H., and Alter, B.P. (2003). Cancer incidence in persons with Fanconi anemia. *Blood* 101, 822-826.

Rosenberg, P.S., Tamary, H., and Alter, B.P. (2011). How high are carrier frequencies of rare recessive syndromes? Contemporary estimates for Fanconi Anemia in the United States and Israel. *American journal of medical genetics. Part A* 155A, 1877-1883.

Sawyer, S.L., Tian, L., Kahkonen, M., Schwartzentruber, J., Kircher, M., University of Washington Centre for Mendelian, G., Consortium, F.C., Majewski, J., Dymment, D.A., Innes, A.M., *et al.* (2015). Biallelic mutations in BRCA1 cause a new Fanconi anemia subtype. *Cancer Discov* 5, 135-142.

Schindler, D., Endt, D., and Neveling, K. (2012). Fanconi Anemia. In *Encyclopedia of Cancer*, M. Schwab, ed. (Springer).

Schindler, D., and Hoehn, H. (1988). Fanconi anemia mutation causes cellular susceptibility to ambient oxygen. *Am J Hum Genet* 43, 429-435.

Schroeder, T.M., Anschutz, F., and Knopp, A. (1964). [Spontaneous chromosome aberrations in familial panmyelopathy]. *Humangenetik* 1, 194-196.

Schuster, B., Knies, K., Stoepker, C., Velleuer, E., Friedl, R., Gottwald-Muhlhauser, B., de Winter, J.P., and Schindler, D. (2013). Whole exome sequencing reveals uncommon mutations in the recently identified Fanconi anemia gene SLX4/FANCP. *Hum Mutat* 34, 93-96.

Schwertman, P., Bekker-Jensen, S., and Mailand, N. (2016). Regulation of DNA double-strand break repair by ubiquitin and ubiquitin-like modifiers. *Nat Rev Mol Cell Biol* 17, 379-394.

Seyschab, H., Friedl, R., Sun, Y., Schindler, D., Hoehn, H., Hentze, S., and Schroeder-Kurth, T. (1995). Comparative evaluation of diepoxybutane sensitivity and cell cycle blockage in the diagnosis of Fanconi anemia. *Blood* 85, 2233-2237.

Shamseldin, H.E., Elfaki, M., and Alkuraya, F.S. (2012). Exome sequencing reveals a novel Fanconi group defined by XRCC2 mutation. *J Med Genet* 49, 184-186.

Sharma, S., Helchowski, C.M., and Canman, C.E. (2013). The roles of DNA polymerase zeta and the Y family DNA polymerases in promoting or preventing genome instability. *Mutat Res* 743-744, 97-110.

Shimamura, A. (2006). Inherited Bone Marrow Failure Syndromes: Molecular Features. *ASH Education Program Book 2006*, 63-71.

Shimamura, A., Montes de Oca, R., Svenson, J.L., Haining, N., Moreau, L.A., Nathan, D.G., and D'Andrea, A.D. (2002). A novel diagnostic screen for defects in the Fanconi anemia pathway. *Blood* 100, 4649-4654.

Shimura, H., Hattori, N., Kubo, S., Mizuno, Y., Asakawa, S., Minoshima, S., Shimizu, N., Iwai, K., Chiba, T., Tanaka, K., *et al.* (2000). Familial Parkinson disease gene product, parkin, is a ubiquitin-protein ligase. *Nat Genet* 25, 302-305.

Sijbers, A.M., de Laat, W.L., Ariza, R.R., Biggerstaff, M., Wei, Y.-F., Moggs, J.G., Carter, K.C., Shell, B.K., Evans, E., de Jong, M.C., *et al.* (1996). Xeroderma Pigmentosum Group F Caused by a Defect in a Structure-Specific DNA Repair Endonuclease. *Cell* 86, 811-822.

Sims, A.E., Spiteri, E., Sims, R.J., 3rd, Arita, A.G., Lach, F.P., Landers, T., Wurm, M., Freund, M., Neveling, K., Hanenberg, H., *et al.* (2007). FANCI is a second monoubiquitinated member of the Fanconi anemia pathway. *Nat Struct Mol Biol* 14, 564-567.

Singh, T.R., Bakker, S.T., Agarwal, S., Jansen, M., Grassman, E., Godthelp, B.C., Ali, A.M., Du, C.H., Rooimans, M.A., Fan, Q., *et al.* (2009). Impaired FANCD2 monoubiquitination and hypersensitivity to camptothecin uniquely characterize Fanconi anemia complementation group M. *Blood* 114, 174-180.

Smogorzewska, A., Matsuoka, S., Vinciguerra, P., McDonald, E.R., 3rd, Hurov, K.E., Luo, J., Ballif, B.A., Gygi, S.P., Hofmann, K., D'Andrea, A.D., *et al.* (2007). Identification of the FANCI protein, a monoubiquitinated FANCD2 paralog required for DNA repair. *Cell* 129, 289-301.

Stauffer, M.E., and Chazin, W.J. (2004). Structural mechanisms of DNA replication, repair, and recombination. *J Biol Chem* 279, 30915-30918.

Stoepker, C., Hain, K., Schuster, B., Hilhorst-Hofstee, Y., Rooimans, M.A., Steltenpool, J., Oostra, A.B., Eirich, K., Korthof, E.T., Nieuwint, A.W., *et al.* (2011). SLX4, a coordinator of structure-specific endonucleases, is mutated in a new Fanconi anemia subtype. *Nat Genet* 43, 138-141.

Strathdee, C.A., Duncan, A.M., and Buchwald, M. (1992a). Evidence for at least four Fanconi anaemia genes including FACC on chromosome 9. *Nat Genet* 1, 196-198.

Strathdee, C.A., Gavish, H., Shannon, W.R., and Buchwald, M. (1992b). Cloning of cDNAs for Fanconi's anaemia by functional complementation. *Nature* 356.

Suzuki, A., de la Pompa, J.L., Hakem, R., Elia, A., Yoshida, R., Mo, R., Nishina, H., Chuang, T., Wakeham, A., Itie, A., *et al.* (1997). Brca2 is required for embryonic cellular proliferation in the mouse. *Genes Dev* 11, 1242-1252.

Swuec, P., and Costa, A. (2016). DNA replication and inter-strand crosslink repair: Symmetric activation of dimeric nanomachines? *Biophysical chemistry*.

Swuec, P., Renault, L., Borg, A., Shah, F., Murphy, V.J., van Twest, S., Snijders, B., Deans, A.J., and Costa, A. (2016). The FA Core Complex Contains a Homo-dimeric Catalytic Module for the Symmetric Mono-ubiquitination of FANCI-FANCD2. *Cell reports*.

Tian, M., Shinkura, R., Shinkura, N., and Alt, F.W. (2004). Growth Retardation, Early Death, and DNA Repair Defects in Mice Deficient for the Nucleotide Excision Repair Enzyme XPF. *Molecular and cellular biology* 24, 1200-1205.

Timmers, C., Taniguchi, T., Hejna, J., Reifsteck, C., Lucas, L., Bruun, D., Thayer, M., Cox, B., Olson, S., D'Andrea, A.D., *et al.* (2001). Positional cloning of a novel Fanconi anemia gene, FANCD2. *Mol Cell* 7, 241-248.

Tischkowitz, M.D., and Hodgson, S.V. (2003). Fanconi anaemia. *J Med Genet* 40, 1-10.

Trujillo, J.P., Mina, L.B., Pujol, R., Bogliolo, M., Andrieux, J., Holder, M., Schuster, B., Schindler, D., and Surrallès, J. (2012). On the role of FAN1 in Fanconi anemia, Vol 120.

Trujillo, J.P., and Surrallès, J. (2015). Savior siblings and Fanconi anemia: analysis of success rates from the family's perspective. *Genetics in medicine : official journal of the American College of Medical Genetics* 17, 935-938.

Uehlinger, E. (1929). Konstitutionelle Infantile (Perniciosaartige) Anämie. *Klinische Wochenschrift* 8, 1501-1503.

van Twest, S., Murphy, V.J., Hodson, C., Tan, W., Swuec, P., O'Rourke, J.J., Heierhorst, J., Crismani, W., and Deans, A.J. (2016). Mechanism of Ubiquitination and Deubiquitination in the Fanconi Anemia Pathway. *Mol Cell*.

Vaz, F., Hanenberg, H., Schuster, B., Barker, K., Wiek, C., Erven, V., Neveling, K., Endt, D., Kesterton, I., Autore, F., *et al.* (2010). Mutation of the RAD51C gene in a Fanconi anemia-like disorder. *Nat Genet* 42, 406-409.

Virts, E.L., Jankowska, A., Mackay, C., Glaas, M.F., Wiek, C., Kelich, S.L., Lottmann, N., Kennedy, F.M., Marchal, C., Lehnert, E., *et al.* (2015). AluY-mediated germline deletion, duplication and somatic stem cell reversion in UBE2T defines a new subtype of Fanconi anemia. *Hum Mol Genet* 24, 5093-5108.

Wang, A.T., Kim, T., Wagner, J.E., Conti, B.A., Lach, F.P., and Huang, A.L. (2015). A dominant mutation in human RAD51 reveals its function in DNA interstrand crosslink repair independent of homologous recombination. *Mol Cell* 59.

Watanabe, N., Mii, S., Asai, N., Asai, M., Niimi, K., Ushida, K., Kato, T., Enomoto, A., Ishii, H., Takahashi, M., *et al.* (2013). The REV7 subunit of DNA polymerase zeta is essential for primordial germ cell maintenance in the mouse. *J Biol Chem* 288, 10459-10471.

Weiss, M.M., Van der Zwaag, B., Jongbloed, J.D., Vogel, M.J., Bruggenwirth, H.T., Lekanne Deprez, R.H., Mook, O., Ruivenkamp, C.A., van Slegtenhorst, M.A., van den Wijngaard, A., *et al.* (2013). Best practice guidelines for the use of next-generation sequencing applications in genome diagnostics: a national collaborative study of Dutch genome diagnostic laboratories. *Hum Mutat* 34, 1313-1321.

Williams, R.S., and Tainer, J.A. (2007). Learning our ABCs: Rad50 directs MRN repair functions via adenylate kinase activity from the conserved ATP binding cassette. *Mol Cell* 25, 789-791.

Williams, S.A., Wilson, J.B., Clark, A.P., Mitson-Salazar, A., Tomashevski, A., Ananth, S., Glazer, P.M., Semmes, O.J., Bale, A.E., Jones, N.J., *et al.* (2011). Functional and physical interaction between the mismatch repair and FA-BRCA pathways. *Hum Mol Genet* 20, 4395-4410.

Winter, J.P., Leveille, F., Berkel, C.G., Rooimans, M.A., Der, W.L., and Steltenpool, J. (2000a). Isolation of a cDNA representing the Fanconi anemia complementation group E gene. *Am J Hum Genet* 67.

Winter, J.P., Rooimans, M.A., Der, W.L., Berkel, C.G., Alon, N., and Bosnoyan-Collins, L. (2000b). The Fanconi anaemia gene FANCF encodes a novel protein with homology to ROM. *Nat Genet* 24.

Xia, B., Dorsman, J.C., Ameziane, N., de Vries, Y., Rooimans, M.A., Sheng, Q., Pals, G., Errami, A., Gluckman, E., Llera, J., *et al.* (2007). Fanconi anemia is associated with a defect in the BRCA2 partner PALB2. *Nat Genet* 39, 159-161.

Yabe, M., Yabe, H., Morimoto, T., Fukumura, A., Ohtsubo, K., Koike, T., Yoshida, K., Ogawa, S., Ito, E., Okuno, Y., *et al.* (2016). The phenotype and clinical course of Japanese Fanconi Anaemia infants is influenced by patient, but not maternal ALDH2 genotype. *Br J Haematol* 175, 457-461.

Yang, Y., Kuang, Y., Montes, O.R., Hays, T., Moreau, L., and Lu, N. (2001). Targeted disruption of the murine Fanconi anemia gene, *Fancg/Xrcc9*. *Blood* 98.

Zakrzewski, S., and Sperling, K. (1980). Genetic heterogeneity of Fanconi's anemia demonstrated by somatic cell hybrids. *Human genetics* 56, 81-84.

Zelensky, A., Kanaar, R., and Wyman, C. (2014). Mediators of homologous DNA pairing. *Cold Spring Harb Perspect Biol* 6, a016451.

Zuchner, S., Dallman, J., Wen, R., Beecham, G., Naj, A., Farooq, A., Kohli, M.A., Whitehead, P.L., Hulme, W., Konidari, I., *et al.* (2011). Whole-exome sequencing links a variant in *DHDDS* to retinitis pigmentosa. *Am J Hum Genet* 88, 201-206.

6 ANHANG

I. LISTE DER ABKÜRZUNGEN

A	Adenin
ACMG	<i>American College of Medical Genetics and Genomics</i>
AML	Akute myeloische Leukämie
ALL	Akute lymphatische Leukämie
Alt-EJ	alternatives End-joining
AT	Ataxia Teleangiectasia
ATM	<i>Ataxia Telangiectasia Mutated</i>
ATR	<i>Ataxia Telangiectasia and Rad3 related</i>
BAM	<i>Binary sequence alignment/map</i>
BLM	Bloom Syndrom, <i>RecQ helicase-like</i>
BMF	<i>Bone marrow failure</i> (Knochenmarkversagen)
bp	Basenpaar(e)
BRAFT	Komplex aus BLM, RPA, FA und Topo III alpha
BRCA1/2	<i>Breast cancer susceptibility gene 1/2</i>
BRIP1	<i>BRCA1 interacting protein C-terminal helicase 1</i>
bzw.	beziehungsweise
C	Cytosin
cDNA	<i>Complementary DNA</i>
CDC27	<i>Cell division cycle 27 homolog (S. cerevisiae)</i>
cNHEJ	<i>Classical Non-homologous-end-joining</i>
CNV	<i>Copy number variation</i>
Co-IP	Co-Immunopräzipitation
CRAM	<i>Challenge-response authentication mechanism</i>
CRISPR	<i>Clustered regularly interspaced short palindromic repeats</i>
CS	Cockayne Syndrom
CtBP	<i>C-terminal binding protein</i>
CtIP	<i>CtBP-interacting protein</i>
DBA	Diamond-Blackfan Anämie
dbSNP	<i>Single nucleotide polymorphism database</i>
DEB	Diepoxybutan
dHJs	<i>Double Holliday junctions</i>
DNA	<i>Desoxyribonucleic acid</i>
DSB	Doppelstrangbruch
EME1	<i>Essential meiotic endonuclease 1 homolog (S. cerevisiae)</i>
EP	<i>Expected pathogen</i>

ERCC1	<i>Excision repair cross-complementing rodent repair deficiency, complementation group 1</i>
ExAC	<i>Exome Aggregation Consortium</i>
EXO1	Exonuklease 1
FA	Fanconi Anämie
FAN1	<i>Fanconi anemia associated nuclease 1</i>
FAAP	Fanconi Anämie assoziiertes Protein
G	Guanin
gDNA	Genomische DNA
GEN1	<i>Holliday Junction 5' Flap Endonuclease</i>
HEF	<i>Helicase-associated endonuclease for fork-structured DNA</i>
HR	Homologe Rekombination
HRR	Homologe Rekombinationsreparatur
HES1	<i>Hairy and enhancer of split-1</i>
HLA	<i>Human leukocyte antigen</i>
HNPCC	Hereditäres non-polypöses kolorektales Karzinom
ICGC	<i>International Cancer Genome Consortium</i>
ICL	<i>Interstrand crosslink</i> (Interstrang-Quervernetzung)
ID	Komplex bestehend aus FANCI und FANCD2
IFAR	<i>International Fanconi Anemia Registry</i>
INF	Interferon
IPS	Induzierte pluripotente Stammzelle
KP	<i>Known pathogen</i>
Lof	<i>Loss of function</i>
MB	Megabyte
MDS	Myelodysplastisches Syndrom
MEF	<i>Mouse embryonic fibroblasts</i>
MHF1/2	<i>FANCM-interacting histone fold protein 1/2</i>
MLH1/3	mutL Homolog 1/3
MLPA	<i>Multiplex Ligation-dependent Probe Amplification</i>
MMC	Mitomycin C
MMEJ	<i>Microhomology-mediated end-joining</i>
MRN	Komplex bestehend aus MRE11, RAD50 und NBS1
MSH2/3	mutS Homolog 2/3
MUC	<i>Mucin gene, oligomeric mucus/gel-forming</i>
MUS81	<i>MUS81 endonuclease homolog (S. cerevisiae)</i>
NBPF	<i>Neuroblastoma Breakpoint Family</i>
NBS	Nijmegen-Breakage-Syndrom
NCBI	<i>National Center for Biotechnology Information</i>
NER	Nucleotidexzisionsreparatur
NGS	<i>Next Generation Sequencing</i>

NHEJ	<i>Non-homologous-end-joining</i>
PALB2	<i>Partner and localizer of BRCA2</i>
PCNA	<i>Proliferating-cell-nuclear-antigen</i>
PHD	<i>Plant homeodomain</i>
PKC	<i>Proteinkinase C</i>
PMS2	<i>Postmeiotic segregation increased 2</i>
Pol	<i>Polymerase</i>
POLD	<i>Polymerase delta</i>
RAD51	<i>RAD51 Homolog (S. cerevisiae), RecA-like protein</i>
RAD51C	<i>RAD51 Homolog C (S. cerevisiae), RAD51L2</i>
RAD52	<i>RAD52 Homolog (S. cerevisiae)</i>
REV1	<i>REV1 Polymerase</i>
RFC	<i>Replication factor C</i>
RFWD3	<i>Ring Finger and WD Repeat Domain 3</i>
RNA	<i>Ribonucleic acid</i>
ROI	<i>Region of interest</i>
ROS	<i>Reaktive Sauerstoffspezies</i>
RPA	<i>Replication protein A</i>
RTEL1	<i>Regulator of telomere elongation helicase 1</i>
SAM	<i>Sequence alignment/map</i>
SDSA	<i>Synthesis-dependent strand annealing</i>
SLX1	<i>SLX1 structure-specific endonuclease subunit homolog (S. cerevisiae)</i>
SLX4	<i>SLX4 structure-specific endonuclease subunit homolog (S. cerevisiae)</i>
SNP	<i>Single nucleotide polymorphism</i>
SSA	<i>Single-strand annealing</i>
ssDNA	<i>single-stranded DNA (Einzelsträngige DNA)</i>
T	<i>Thymin</i>
TAR	<i>Thrombocytopenia-Absent Radius Syndrome</i>
TLS	<i>Translasionssynthese</i>
TNF	<i>Tumornekrosefaktor</i>
TOPOIII	<i>Topoisomerase III</i>
TWIST1	<i>Twist-related protein 1</i>
UAF1	<i>USP1 associated factor 1</i>
UBE2T	<i>Ubiquitin Conjugating Enzyme E2 T</i>
UBZ	<i>Ubiquitin-binding zinc finger domain</i>
UCHL3	<i>Ubiquitin Carboxyl-Terminal Esterase L3</i>
USP1	<i>Ubiquitin specific peptidase 1</i>
UV	<i>Ultraviolett (Strahlung)</i>
VCF	<i>Variants call format</i>
WES	<i>Whole Exome Sequencing</i>
WGS	<i>Whole Genome Sequencing</i>

WT	Wildtyp
XFE	<i>ERCC4 associated progeroid syndrome, segmental progeria</i>
XLf	<i>XRCC4-like factor</i>
XP	Xeroderma pigmentosum
XPd	Xeroderma pigmentosum, Komplementationsgruppe D
XPf	Xeroderma pigmentosum, Komplementationsgruppe F
XRCC4	<i>X-ray repair cross-complementing protein 4</i>

II. EIGENE VERÖFFENTLICHUNGEN

- Genotyping of Fanconi Anemia Patients by Whole Exome Sequencing: Advantages and Challenges

Kerstin Knies*, Beatrice Schuster*, Najim Ameziane, Martin Rooimans, Thomas Bettecken, Johan de Winter, Detlev Schindler

PLoS ONE. 2012;7(12):e52648. doi: 10.1371/journal.pone.0052648. Epub 2012 Dec 20.

*geteilte Erstautorschaft

- Whole Exome Sequencing reveals novel mutations in the recently identified Fanconi anemia gene *SLX4/FANCP*

Beatrice Schuster*, **Kerstin Knies***, Chantal Stoepker, Eunike Velleuer, Richard Friedl, Birgit Mühlhäuser- Gottwald, Johan P de Winter, Detlev Schindler

HUM MUTAT. 2013 Jan;34(1):93-6. doi: 10.1002/humu.22221. Epub 2012 Oct 16

*geteilte Erstautorschaft

- Mutations in *ERCC4*, encoding the DNA-repair endonuclease XPF, cause Fanconi anemia.

Massimo Bogliolo, Beatrice Schuster, Chantal Stoepker, Burak Derkunt, Yan Su, Anja Raams, Juan P Trujillo, Jordi Minguillón, Maria J Ramírez, Roser Pujol, José A Casado, Rocío Baños, Paula Rio, **Kerstin Knies**, Sheila Zúñiga, Javier Benítez, Juan A Bueren, Nicolaas G Jaspers, Orlando D Schärer, Johan P de Winter, Detlev Schindler, Jordi Surrallés

AM J HUM GENET. 2013 May 2;92(5):800-6. doi: 10.1016/j.ajhg.2013.04.002. Epub 2013 Apr 25.

- Biallelic Mutations in the Ubiquitin Ligase *RFWD3* cause Fanconi Anemia

Kerstin Knies, Shojiro Inano, Maria J Ramírez, Masamichi Ishiai, Jordi Surrallés, Minoru Takata, Detlev Schindler

JCI. 2017, in revision

- The E3 Ligase RFWD3 promotes timely removal of both RPA and RAD51 from DNA damage sites to facilitate homologous recombination

Shojiro Inano, Koichi Sato, Yoko Katsuki, Wataru Kobayashi, Hiroki Tanaka, Kazuhiro Nakajima, Shinichiro Nakada, Hiroyuki Miyoshi, **Kerstin Knies**, Akifumi Takaori-Kondo, Detlev Schindler, Masamichi Ishiai, Hitoshi Kurumizaka, Minoru Takata

MOLCELL. 2017, in revision

III. EIGENE BEITRÄGE ZU DEN ENTHALTENEN VERÖFFENTLICHUNGEN

Die folgenden Seiten enthalten die Unterschriften aller Co-Autoren der enthaltenen Veröffentlichungen. Leider ist Johan P. de Winter bereits verstorben, sodass von ihm keine Unterschrift mehr zu bekommen war.


Persönlicher Beitrag zur nachfolgenden Publikation

**Genotyping of Fanconi Anemia Patients by Whole Exome
Sequencing:**
Advantages and Challenges

Knies K, Schuster B, Ameziane N, Rooimans M, Bettecken T, de Winter J, Schindler D.

Plos One, 2012

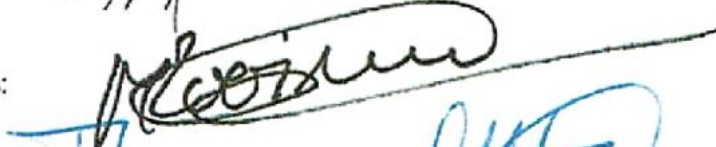
Kerstin Knies evaluated the bioinformatic pipeline, analyzed the data, did validation experiments and wrote the manuscript.

B. Schuster: 

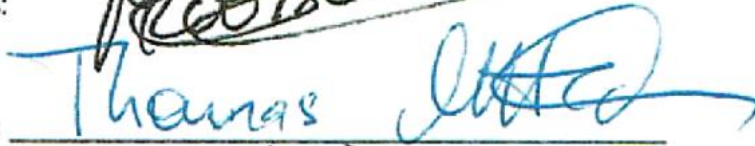
N. Ameziane:



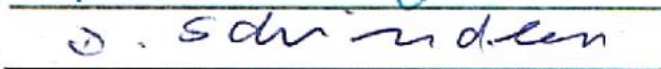
M. Rooimans:



T. Bettecken:



D. Schindler:



Persönlicher Beitrag zur nachfolgenden Publikation

Whole Exome Sequencing Reveals Uncommon Mutations in the Recently Identified Fanconi Anemia Gene SLX4/FANCP

Schuster B, Knies K, Stoepker C, Velleuer E., Friedl R., Gottwald-Mühlhauser B., de Winter JP, Schindler D

Human Mutation, 2012

Kerstin Knies analyzed the WES data, did validation experiments and wrote the manuscript

B.Schuster: B. Schuster

C. Stoepker: C. Stoepker

E. Velleuer: E. Velleuer

R. Friedl: R. Friedl

B. Gottwald-Mühlhauser: B. Gottwald-Mühlhauser

D. Schindler: D. Schindler

Persönlicher Beitrag zur nachfolgenden Publikation

Mutations in ERCC4, encoding the DNA-repair endonuclease XPF, cause Fanconi anemia.

Bogliolo M, Schuster B, Stoepker C, Derkunt B, Su Y, Raams A, Trujillo JP, Minguillón J, Ramírez MJ, Pujol R, Casado JA, Baños R, Rio P, Knies K, Zúñiga S, Benítez J, Bueren JA, Jaspers NG, Schärer OD, de Winter JP, Schindler D, Surrallés J

American Journal of Human Genetics, 2013

Kerstin Knies performed experiments like Western Blotting and Co-Immunoprecipitation. She also was involved in proofreading the manuscript.

M. Bogliolo:



B. Schuster:



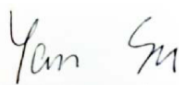
C. Stoepker:



B. Derkunt:



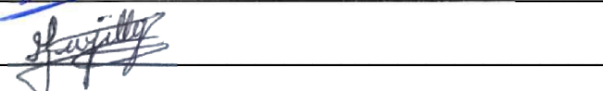
Y. Su:



A. Raams:



J. Trujillo:



J. Minguillón:



M. Ramirez:

R. Pujol:

J. Casado:

R. Baños:

P. Rio:

S. Zúñiga:

J. Benitez:

J. Bueren:

G. Jaspers:

O. Schärer:

D. Schindler:

J. Surrallés:

Persönlicher Beitrag zur nachfolgenden Publikation

Biallelic mutations in the ubiquitin ligase RFWD3 cause Fanconi anemia

Knies K., Inano S., Ramirez MJ, Ishiai M., Surrallés J., Takata M., Schindler D.

Journal of Clinical Investigation, in review

Kerstin Knies discovered and characterized the disease causing mutations by analyzing the WES data. She designed and performed all experiments with patient cell lines, CRISPR, HAP1 and MEF cell lines. Finally she prepared the figures and wrote the draft.

S. Inano: S. Inano
M. Ramirez: ~~M. Ramirez~~
M. Ishiai: Masquiché Ishiai
J. Surrallés: ~~J. Surrallés~~
M. Takata: M. Takata
D. Schindler: D. Schindler

Persönlicher Beitrag zur nachfolgenden Publikation

The E3 Ligase RFWD3 promotes timely removal of both RPA and RAD51 from DNA damage sites to facilitate homologous recombination

Inano S., Sato K., Katsuki Y., Kobayashi W., Tanaka H., Nakajima K., Nakada S., Miyoshi H., Knies K., Takaori-Kondo A., Schindler D., Ishiai M., Kurumizaka H., Takata M.,

Molecular Cell, in revision

Kerstin Knies war an der Konzeption dieser Studie beteiligt, die auf der Basis der Entdeckung von RFWD3 als FA-Gen beruht.

S. Inano: Shyiro Inano
 K. Sato: Keichi Sato
 Y. Katsuki: YOKO KATSUKI
 W. Kobayashi: Wataru Kobayashi
 H. Tanaka: Hiroki Tanaka
 K. Nakajima: Kazuhiro Nakajima
 S. Nakada: Satoshi Nakada
 H. Miyoshi: Hiroyuki Miyoshi
 A. Takaori-Kondo: Akifumi Takaori-Kondo
 D. Schindler: D. Schindler
 M. Ishiai: Masahiko Ishiai
 H. Kurumizaka: Hiroshi Kurumizaka
 M. Takata: M. Takata

IV. LEBENSLAUF

_____PERSÖNLICHE ANGABEN

Kerstin Knies

geb. 02.02.1985 in Würzburg



_____AKADEMISCHER WERDEGANG

Seit April 2011	Promotion am Institut für Humangenetik der bayerischen Julius-Maximilians-Universität Würzburg Dissertationsthema: „Neue Fanconi-Anämie-Gene als Wächter des Genoms“
Feb. 2011	Abschluss des Studiums als Diplombiologin an der bayerischen Julius-Maximilians-Universität Würzburg (Note: sehr gut) Diplomarbeit am Institut für Pharmakologie/Toxikologie mit dem Thema: „Untersuchung der Rolle des Ca ²⁺ -Haushalts von Herzmuskelzellen für ihre kontraktile Funktion bei genetischen Kardiomyopathien“
Okt. 2005 - Jan. 2011	Studium der Biologie an der bayerischen Julius-Maximilians-Universität Würzburg Schwerpunkte: Mikrobiologie, Humangenetik und Pharmakologie/Toxikologie

_____PREISE & AUSZEICHNUNGEN

Okt. 2013	Ehrendauszeichnung zur Entdeckung eines neuen Fanconi-Anämie-Gens durch die Dt. Fanconi Anämie Hilfe FARF Discovery Award, Ehrendauszeichnung zur Entdeckung eines neuen Fanconi Anämie Gene
-----------	---

BERUFSERFAHRUNG & PRAKTIKA

Seit April 2011	Wissenschaftliche Mitarbeiterin am Institut für Humangenetik der bayerischen Julius-Maximilians- Universität Würzburg
Juli 2010 – Dez. 2010	Wissenschaftliche Hilfskraft am Institut für Pharmakologie der bayerischen Julius-Maximilians-Universität Würzburg
Mai 2008 – Juni 2008	6-wöchiges Fortgeschrittenenpraktikum im MVZ für Laboratoriumsmedizin und Mikrobiologie Würzburg Weitere diverse studienrelevante Praktika
Mai 2005 – Juni 2005	Pflegerpraktikum am orthopädischen Lehrkrankenhaus König-Ludwig-Haus der bayerischen Julius-Maximilians-Universität Würzburg
Juli 2002	Sozialpraktikum im Zentrum für Körperbehinderte, Würzburg

SCHULISCHER WERDEGANG

Sept. 1995 – Juni 2004	Städt. Mozart- und Schönborngymnasium Würzburg mit Abschluss Abitur (Note: 1,8)
Sept. 1991 – Juli 1995	Grundschule Stadtmitte Würzburg

KONFERENZEN & FORTBILDUNGEN

Okt. 2015	GSLs Symposium „EUREKA“, Würzburg, Deutschland
Okt. 2014	GSLs Symposium „EUREKA“, Würzburg, Deutschland
März 2014	GfH Konferenz, Essen, Deutschland, mit Posterpräsentation
März 2013	GfH Konferenz Dresden, Deutschland, mit Posterpräsentation
Okt. 2012	GSLs Symposium „EPOS“, Würzburg, Deutschland
Sept. 2012	Next Generation Sequencing Symposium, Medizinische Hochschule Hannover, Deutschland
Juni 2012	ESHG Konferenz Nürnberg, Deutschland, mit Posterpräsentation
Okt. 2011	Teilnahme am Fanconi Anämie Familientreffen in Gersfeld, Deutschland

Juni 2011 EMBL Master Kurs „Target Enrichment and Next Generation Sequencing“, Heidelberg, Deutschland

_____SONSTIGES

Fremdsprachen: Englisch sehr gut (in Wort und Schrift)
 Französisch gut - sehr gut (in Wort und Schrift)
 Arabisch Grundkenntnisse (VHS-Kurs)

Interessen: Sport als Ausgleich, Reisen, Lesen

Gerbrunn,

.....

V. DANKSAGUNG

Zunächst möchte ich mich bei Herrn Prof. Dr. Thomas Haaf bedanken, der es mir ermöglicht hat an seinem Institut zu promovieren und diese Arbeit anzufertigen.

Des Weiteren danke ich meinem Erstkorrektor und Doktorvater Herrn Prof. Dr. Detlev Schindler, für die Bereitstellung des Themas, sowie der Korrekturübernahme und Hilfestellung während der Zeit meiner Dissertation.

Herrn Prof. Dr. Thomas Dandekar gilt ebenfalls mein Dank, für die Übernahme der Zweitkorrektur.

Ein herzlicher Dank geht auch an Frau Prof. Dr. Schröder-Kurth und Herrn Prof. Dr. Höhn. Während unserer Seminare am Freitag, haben Sie stets konstruktive Kritik geübt und mich motiviert. Zudem konnte ich durch die Finanzierung aus dem Schröder-Kurth Fonds das RFWD3-Mausmodell generieren lassen, welches einen großen Beitrag zu meiner Arbeit geleistet hat.

Vielen Dank auch an Dr. Reinhard Kalb, der trotz der kurzen Zeit, die wir uns kennen, mich immer unterstützt und oft wertvolle Tipps gegeben hat.

Außerdem möchte ich herzlich der ganzen Arbeitsgruppe Schindler danken, für die immerwährende Unterstützung, gegenseitigen wissenschaftlichen und nicht-wissenschaftlichen Austausch und die daraus entstandenen Freundschaften. Ihr seid spitze, bleibt so wie ihr seid!

An unsere Kooperationspartner in Japan und Spanien richte ich ebenfalls meinen Dank. Vor allem Inano Shojiro und Prof. Dr. Minoru Takata möchte ich danken, dass sie es mir erlaubten, die noch unveröffentlichten biochemischen Daten für die Diskussion um RFWD3 zu nutzen.

Ein ganz besonderer Dank gilt auch meinem Freund Michael Popp, der mich in diesen Jahren immer unterstützt und motiviert hat. Danke, dass ich immer auf Dich zählen konnte!

Mein innigster Dank geht jedoch an meine Eltern. Ich danke Euch von ganzem Herzen für Eure finanzielle und moralische Unterstützung während meiner ganzen Studienzeit und auch jetzt in den letzten Jahren. Vor allem Du - Mama - hast mich immer wieder motiviert durchzuhalten und mich über das ein oder andere Tief hinweggebracht, sodass ich diese Arbeit zu Ende bringen konnte. Ihr seid toll und ich bin dankbar und stolz Eure Tochter zu sein.